Paragenetic History of the Ordovician Trenton Group Carbonates, Southwestern Ontario

by

Ian M. Colquhoun, B.Sc.

A Thesis
submitted to the
Department of Geological Sciences
in partial fulfillment of the requirements
for the degree of
Master of Science

January 1991
Brock University
St. Catharines, Ontario

Abstract

Geochemical examination of the rock matrix and cements from core material extracted from four oil wells within southwestern Ontario suggest various stages of diagenetic alteration and preservation of the Trenton Group carbonates. The geochemical compositions of Middle Ordovician (LMC) brachiopods reflect the physicochemical water conditions of the ambient depositional environment. The sediments appear to have been altered in the presence of mixed waters during burial in a relatively open diagenetic microenvironment. Conodont CAI determination suggests that the maturation levels of the Trenton Group carbonates are low and proceeded at temperatures of about 30 - 50 °C within the shallow burial environment.

The Trenton Group carbonates are characterized by two distinct stages of dolomitization which proceeded at elevated temperatures. Pre-existing fracture patterns, and block faulting controlled the initial dolomitization of the precursor carbonate matrix. Dolomitization progressed in the presence of warm fluids (60 - 75°C) with physicochemical conditions characteristic of a progressively depleted basinal water. The matrix is mostly Idiotopic-S and Idiotopic-E dolomite, with Xenotopic-A dolomite dominating the matrix where fractures occur. The second stage of dolomitization involved hydrothermal basinal fluid(s) with temperatures of about 60 - 70°C. These are the postulated source for the saddle dolomite and blocky calcite cements occurring in pore space and fractures. Rock porosity was partly occluded by Idiotopic-E type dolomite. Late stage saddle dolomite, calcite, anhydrite, pyrite, marcasite and minor sphalerite and celestite cements effectively fill any remaining porosity within specific horizons. Based on cathode luminescence, precipitation of the different diagenetic phases probably proceeded in open diagenetic systems from chemically homogeneous fluids. Ultraviolet fluorescence of

the matrix and cements demonstrated that hydrocarbons were present during the earliest formation of saddle dolomite.

Oxygen isotope values of -7.6 to -8.5 ‰ (PDB), and carbon isotope values of - 0.5 and -3.0 ‰ (PDB) from the latest stage dog-tooth calcite cement suggest that meteoric water was introduced into the system during their formation. This is estimated to have occurred at temperatures of about 25 - 40°C.

Specific facies associations within the Trenton Group carbonates exhibit good hydrocarbon generating potential based on organic carbon preservation (1-3.5%). Thermal maturation and Lopatin burial-history evaluations suggest that hydrocarbons were generated within the Trenton Group carbonates some time after 300 Ma .

Progressively depleted vanadium trends measured from hydrocarbon samples within southwestern Ontario suggests its potential use as a hydrocarbon migration indicator on local (within an oilfield) and on regional scales.

Acknowledgements

I am indebted to Telesis Oil and Gas Ltd. for funding this research, through a grant to Professor Uwe Brand, and for kindly making information relative to this research freely available. I also wish to acknowledge funding of part of this thesis through equipment grants, from NSERC (0043282) and URIF (BR11-001) and NSERC Operating grant A7961 to Dr. Uwe Brand.

I am especially grateful to my supervisor, Professor Uwe Brand, for his professional contributions to this thesis. I would also like to thank him for the thorough education that he has provided.

I would like to extend gratitude to Allan R. Phillips (Kerr-McGee Corporation) and Steven A. Colquhoun (Telesis Oil and Gas Ltd.) for the experience of working with them on the preparation of the B. A. Liberty Memorial Core Workshop, Cores of the Trenton-Black River, for the Ontario Petroleum Institute Annual Meeting held in November of 1989. This professional co-operation led to the development of the subsurface facies analysis presented in this thesis. I also appreciate the help given me by the staff, and the interest in my work expressed by the management, of Telesis Oil and Gas Ltd.

Thanks is extended to the Ministry of Natural Resources in London Ontario, particularly Terry Carter, for the co-operation and use of their facilities, and to Professor Anita Harris (Case Western University) for providing the type-Ordovician conodont samples.

At Brock University, Professor M. Manocha of the Department of Biological Sciences generously allowed me use of the ultraviolet fluorescence microscope. From the Department of Geological Sciences, special thanks to William Parkins for help and advice with the conodont extractions, and Professor Jaan Terasmae for use of the facilities in the Palynology Laboratory. Departmental technicians Candace Kramer and

Mike Lozon are thanked for special efforts and assistance above their normal duties.

I also acknowledge my parents who have supported me both morally and financially over the years.

Finally, the most important of all the people in my life to date has been the friendship and love given to me from Maria Goulbourne. We have come a long way together. I thank you for being there for me time after time and for the unselfish love that has grown over the last two years.

Table of Contents

Table of Contents Page No.

Table of Contents Page No.

Table of Contents Page No.

List of Figures

List of Figures **Page No.**

List of Figures

List of Tables

List of Plates

Introduction

The Trenton Group (Mid-Ordovician) carbonates of the Michigan Basin have been the subject of recent re-evaluation. Taylor and Sibley (1986) proposed that three distinct dolomite types occur within the Trenton Group of the Michigan Basin. They recognized (1) a 'cap' dolomite in the upper portions of the Trenton, (2) a 'fracture- related' dolomite at the perimeter of the basin, and (3) a 'regional' dolomite at the southwestern and western edges of the basin.

This study investigates the lower Paleozoic rocks located beneath Essex and Kent Counties, more specifically within Mersea and Romney Townships of southwestern Ontario (Figure 1). Core from four oil wells of the Consumers' Gas Company Ltd. et al., the 33821 Mersea 3-12-I well and the 33823 Mersea 1-12-A well from the Hillman oil pool, the 34151 Mersea 7-18-VIII well from the Goldsmith oil pool, and the 34160 Romney 5-8-II well from the North Wheatly East oil pool were chosen. The stratigraphic units examined include the Cobourg and the Sherman Fall formations of the Trenton Group (good to moderate pay zones in all wells are delineated). The Kirkfield Formation of the Trenton Group, and the Coboconk Formation and Gull River Formation of the Black River Group were also studied from the 33821 Mersea 3-12-I well.

The objectives of the study are:

1) To determine the paragenetic sequence of events, using a) light microscopy to evaluate the relative timing of the diagenetic events, document the various textures of alteration, and compositional (textural and chemical) changes within the rocks and cements; b) cathode luminescence to evaluate the degree of compositional homogeneity of the diagenetic carbonate cements to determine the relative chemical composition of the fluids which were responsible for their precipitation; c)

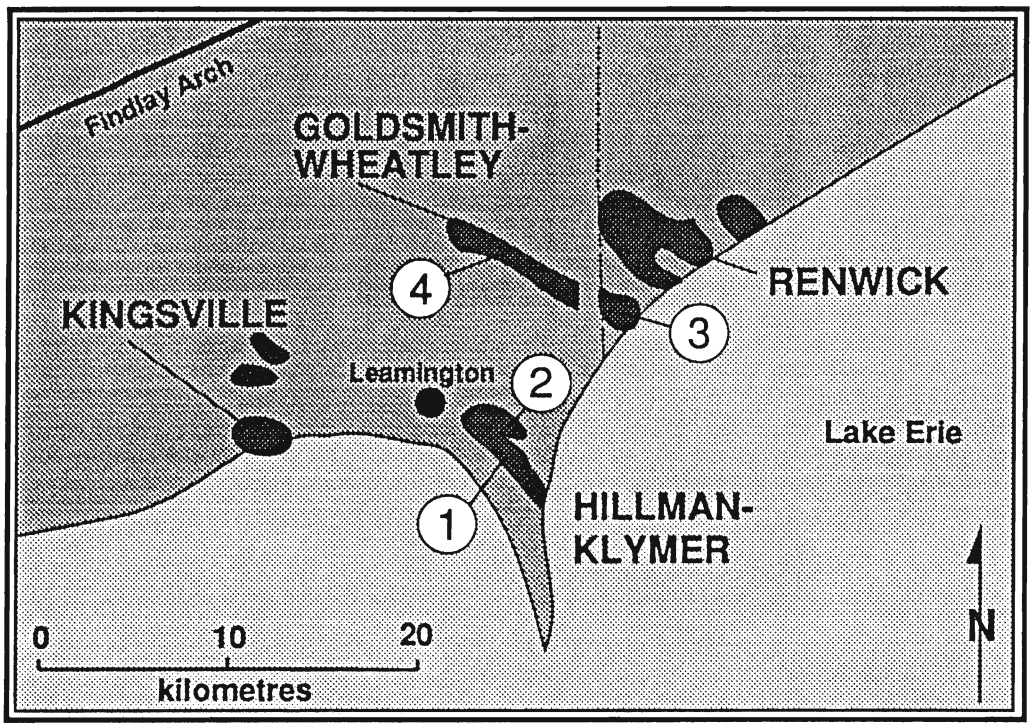

1. 33823 Mersea 1-12-A
2. 33821 Mersea 3-12-I
3. 34160 Romney 5-8-II
4. 34151 Mersea 7-18-VIII

Figure 1: Location Map of the four wells studied within southwestern Ontario. The 33823 Mersea 1-12-A well and the 33821 Mersea 3-12-I well are from the Hillman-Klymer oilfield within Mersea township. The 34151 Mersea 7-18-VIII well is located in the northwest portion of the Goldsmith-Wheatly oilfield, and the 34160 Romney 5-8-II well is from the southeastern portion of the Goldsmith-Wheatly oilfield (north Wheatly east) located within Romney township.

ultraviolet fluorescence to estimate the timing of hydrocarbon emplacement in the various diagenetic carbonate phases.

2) Geochemical analysis of the carbonate components was used to explore trends of the various trace elements (Ca, Mg, Sr, Na, Mn, Fe, V, Ni, Pb, Zn and Cu) in the rocks to document the process of limestone diagenesis, dolomitization, and the paragenesis of the saddle dolomite and calcite cements. By utilizing the appropriate partition coefficients for Sr, it is possible to calculate the composition of the fluids responsible for limestone diagenesis, dolomitization, and cement precipitation.

3) The oxygen and carbon isotopic compositions of the limestones, dolomites and diagenetic carbonate cements were determined to confirm the paragenetic sequence of diagenetic alteration with respect to timing, isotopic composition and temperature of the diagenetic fluids.

4) Trace element analysis, and oxygen and deuterium isotope analysis of the formation waters (brines) provided insight into the nature and type of water that presently exists within the Trenton-Black River reservoirs and its role within the paragenetic history of the diagenetic rocks and cements.

5) The thermal maturation of the various diagenetic carbonate reservoir rocks was determined by extracting conodonts from the various diagenetic lithologies and determining their colour alteration index. The conodonts proved to be useful maturation indicators of the rocks above and below the payzones.

6) Organic carbon and Leco sulphur elemental analysis of the various lithology types established the relative hydrocarbon-generating potential of the rocks throughout the study area. The Lopatin Basin Modeling technique in conjunction with the thermal maturation provide an evaluation of the hydrocarbon generating potential of Trenton and Black River Group limestones and dolomites.

7) Ni and V trends in the rocks and cements, and hydrocarbons from eighteen wells in southwestern Ontario were evaluated as potential tracers of hydrocarbons.

History of Oil and Gas Discovery:

Pre-Hillman Discoveries

Ordovician dolomites of the Trenton and Black River groups of the Michigan Basin have been prolific oil and gas producers since the late 1800's. Figure 2 is a compilation of all the Ordovician aged oil and gas producing fields discovered to date. Bownocker (1903) documented North America's first oil and gas discoveries which started on the northern flanks of the Findlay-Kankakee Arch in Indiana and Ohio in 1884. Oil production since then, nearly 500 million barrels, has been produced from linear, highly dolomitized reservoirs around the Bowling Green fault zone (Keith, 1985). Part of the Lima-Indiana field is in a linear structure which is similar to the other linear trends of the Albion-Scipio (discovered in 1957) and Stoney Point (discovered in 1982) oil fields.

The first linear Trenton reservoir in Ontario was drilled in 1917 in Dover township. The Dover field is also an elongated, east-west trending, dolomitized reservoir located within a synclinal sag (Burgess, 1960). However, the first commercial Trenton oil was discovered in 1936 which came from the Deerfield oil pool located in Monroe county, Dundee township, Michigan. This oil field is located along the Lucas-Monroe monocline which is an extension of the Bowling Green fault zone.

The Northville field was the next Trenton oil field to be discovered in 1954. This reservoir was unique in that it produced oil and gas from Dundee (Devonian), Salina-Niagarian (Silurian) and Trenton-Black River rocks (Ordovician). Trenton-Black River production came from dolomitized and fractured limestones located on the east flank of the Northville fault structure (Landes, 1970). It was this discovery of linear, fault/fractured,

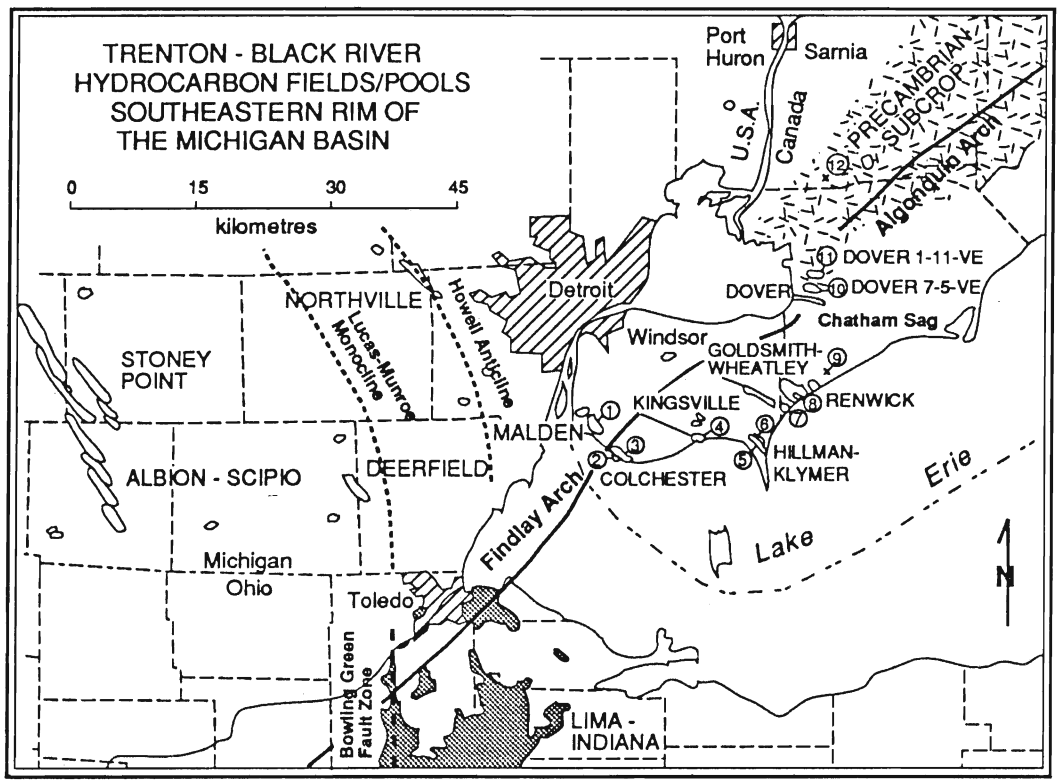

Figure 2: Map of Ordovician-aged hydrocarbon pools within southeastern Michigan basin. (modified from Phillips et al., 1989).

structurally bound, and dolomitized units which lead to the discovery of the Albion-Scipio field in 1957.

Essex County/Hillman Discoveries

Essex County was the site for the first commercial natural gas field as early as 1889 from Silurian age rocks (Sanford, 1961). The Colchester oil field produced from the Cobourg and Sherman Fall formations, which form a porous bioclastic limestone succession. Subsequent production, in more recently drilled wells, has been from dolomitized zones within the Cobourg and Sherman Fall formations. These hydrocarbons possibly originated in the Manitoulin Formation source rocks and migrated at depth along fractures into the Cobourg and Sherman Fall formations (Sanford, 1961). The hydrocarbons were trapped stratigraphically within the flanks of a synclinal structure within dolomitized rocks bounded by limestones of the Cobourg and argillaceous and bioclastic limestones of the Sherman Fall Formation.

Until 1960, only three commercially producing wells were drilled in Ordovician rocks (Sanford, 1961). Marginal yields and showings of both oil and gas from mid-Ordovician rocks were found at widely separated localities throughout southwestern Ontario. Since 1981, Ordovician reservoirs have contributed 2% to the cumulative production of hydrocarbons in southwestern Ontario since recovery started in 1863. (Powell et al., 1984).

Sanford (1961) suggested exploration for oil within the Trenton Group carbonates that exhibited thinner (<120 m) and cleaner (without a high argillaceous content) lateral facies changes extending to the north and south of the central part of the Michigan Basin. He further suggested that many stratigraphic and sedimentologic traps exist within the areas of Essex and Kent Counties because the Findlay Arch passes through both

counties. In these areas he postulated that higher degrees of deformation have taken place producing tectonically inclined reservoirs.

Sanford (1961) documented that Ordovician rocks on the limbs of synclines are the predominant hydrocarbon bearing structure. Subsequent work by Sanford et al., (1985) suggested that fault block readjustment of the dolomitized rocks provided the structural control for the origin and subsequent development of southwestern Ontario's hydrocarbon traps.

The discovery of subsequent producing wells came from recognizing the linear trend of the reservoir, the top of the Trenton sag above producing wells, and the adopted NW-SE trending line from known producers. The synclinal sag structure became known as the "Golden Gulch" to explorationists working in Michigan and southwestern Ontario.

In the late 1950's and early 1960's, discoveries were made at Colchester, Malden and Kingsville. A total of nine oil and/or gas fields have been discovered within the Trenton and Black River groups in southwestern Ontario. Since 1960, five of these fields have been active; the Hepworth gas field, Dover gas and oil field, Picton gas field, Acton gas field, and the Colchester oil field, all within Essex County. The Colchester oil field in Colchester South Township, Essex County, was discovered in 1959 within the Trenton Group. Since 1982, the most significant oil fields discovered in southwestern Ontario are the Dover 7-5-VE (1982), Hillman (1983), Wheatly (1983) and Renwick (1987). In Michigan, the Stoney Point oil pool was discovered in 1983, just 8 km east of the Albion Scipio pool, primarily on the basis of soil-gas geochemistry.

Essex County produced the largest amount of Ontario's oil, 40,892.8 m^3 in 1987, mainly from the Hillman oil pool. By the end of 1988, the Hillman pool in Essex county and the Dover 7-5-VE pool were the largest Ordovician producers with more than 63,000 m^3 (398,000 bbl) of oil from a total of 19 active wells (Carter and Campbell, 1989).

Background- General Geology

The Ordovician carbonate shelf formed in response to Middle to Upper Ordovician seas that transgressed across the pre-Shadow Lake unconformable surface around 434 million years ago (Gale et al., 1979). An extensive carbonate complex developed with the onlapping of the seas onto the proto-North American continent (Figure 3). Ordovician carbonates lie unconformably on Upper Cambrian clastics and carbonates throughout southwestern Ontario (Cooper, 1978), and lie directly on Precambrian rock in the northeast part of southern Ontario. On this irregular Precambrian surface sedimentary facies patterns developed that were markedly different than those further offshore on the carbonate ramp (Phillips et al., 1989). Therefore, time equivalent sediments studied in the subsurface exhibit different facies patterns and sedimentologic relationships than those observed from surface exposures. This has resulted in correlation problems throughout southwestern Ontario.

Many workers have studied the Ordovician outcrop belt of southern Ontario. These studies include detailed mapping of the biostratigraphic units by Ludvigsen, (1978), and detailed lithostratigraphy by Liberty, (1969), Liberty and Bolton, (1971), Winder and Sandford, (1972), and Brett and Brookfield, (1988). Radiometric dating of the units was done by Gale et al., (1979). A compilation of some of these authors work is presented in Figure 4. The subsurface rocks of southwestern Ontario are correlated with the outcrop belt (Sanford, 1961) soon after the discovery of oil at Colchester, and is still used today by exploration geologists (eg. Phillips et al., 1989, Table 1).

Paleoenvironment of Trenton-Black River sediments

The Middle Ordovician (Caradocian) limestones of southwestern Ontario have been interpreted on the basis of outcrop studies. It was

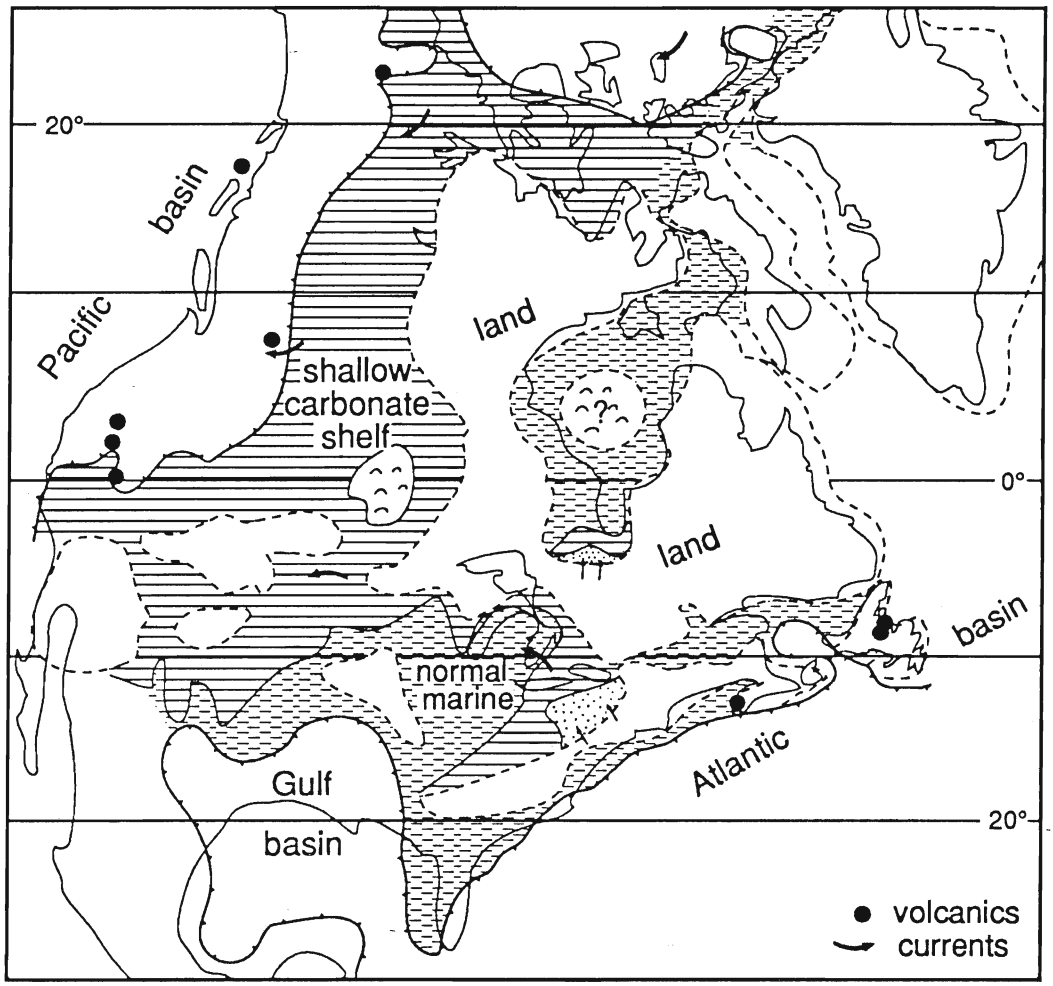

Figure 3: Projected outline of late Caradocian Ordovician shelf around the proto-North American continent (modified after Cooper, 1978).

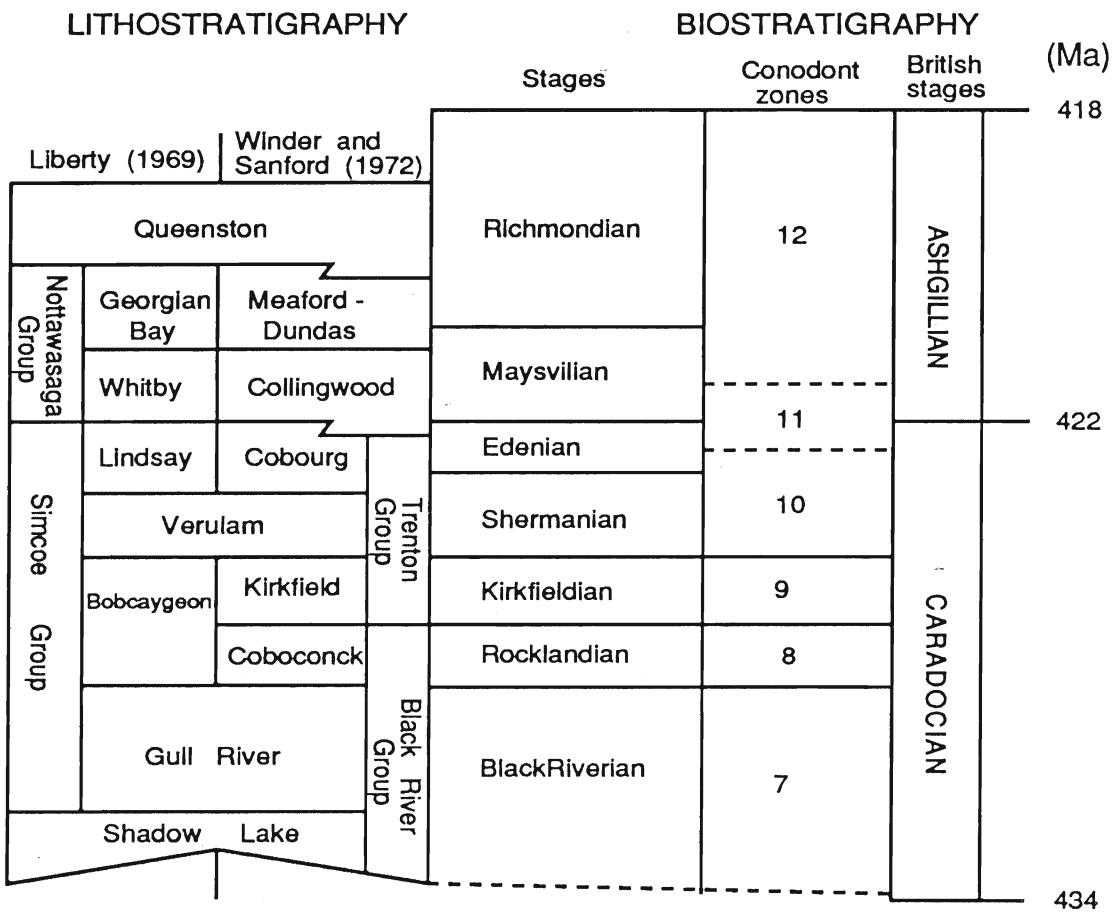

Figure 4: Stratigraphic chart used for comparison of rock units in outcrop to the subsurface in southwestern Ontario (modified from Kobluk and Brookfield, 1982). Biostratigraphic zones compiled by Ludwigsen (1978), conodont zones compiled by Sweet and Bergstrom (1976), and the radiometric dating compiled from Gale et al., (1979).

proposed that these sediments were generated during the development of the Appalachian foreland basin (Brookfield and Brett, 1988). The depositional sequences represent deepening-upwards cycles of shallow marine sedimentation. Glacio-eustatic sea-level changes are postulated to have controlled some aspects of carbonate sedimentation on the Ordovician shelf (Brookfield and Brett, 1988). The sediments are described as a series of crinoidal limestone and marlstone belts extending out from the shallow basin edge, whereby the facies patterns are the result of a storm-dominated, shallow crinoidal ramp (Kobluk and Brookfield, 1982). The shallow crinoidal ramp of amalgamated grainstones adjacent to the shoreline, grades seaward into the subtidal slope which is dominated by interbedded wackestones and mudstones (Kobluk and Brookfield, 1982; Figure 5). Potential modern analogues for these Ordovician environments are the Arabian shelf of the Persian Gulf, and the Sahul shelf of northern Australia (Brookfield and Brett, 1988).

Descriptions of the lithofacies observed from core examined in this study are summarized in Appendix I.

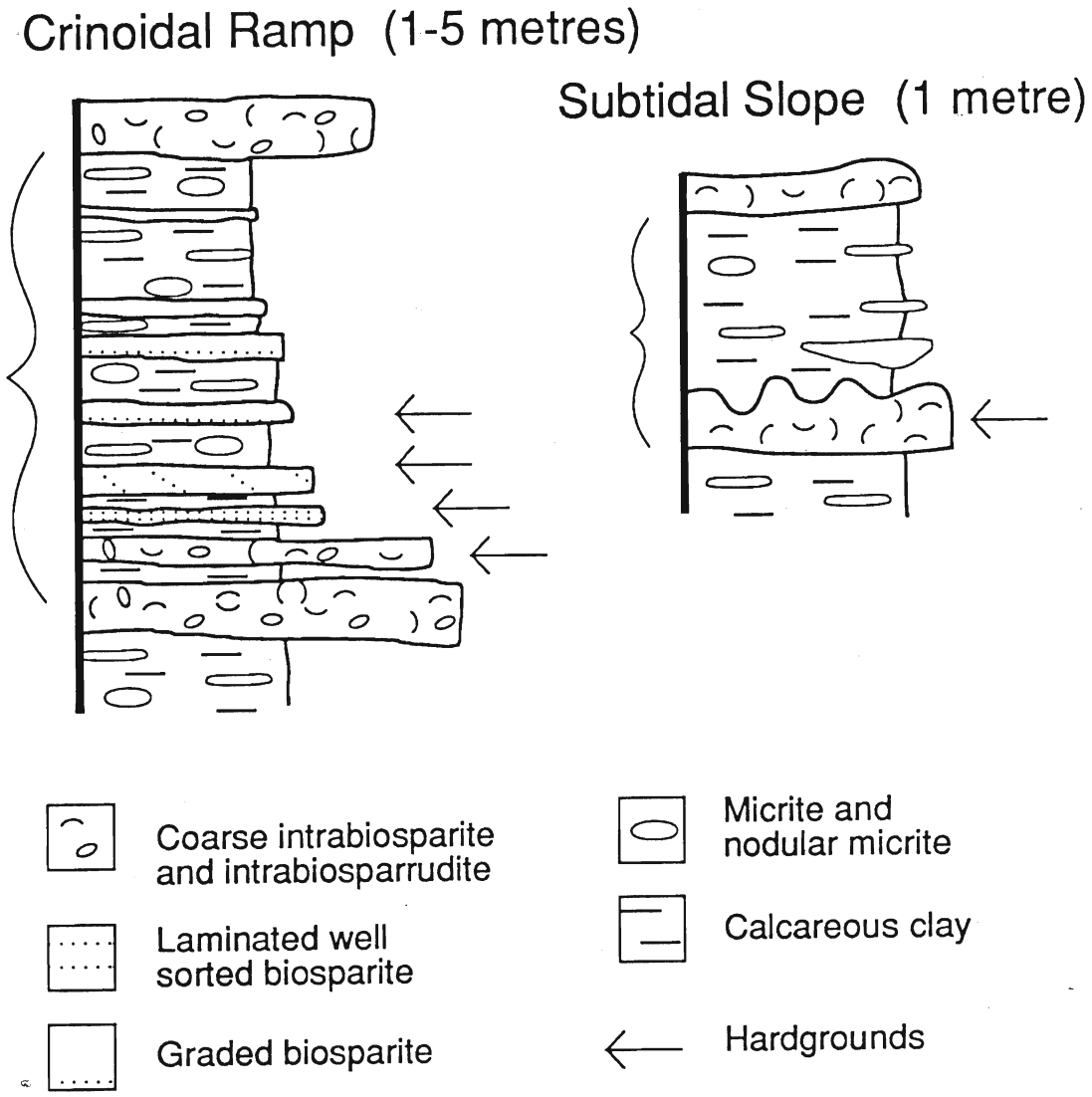

Figure 5: Idealized stratigraphic sections of crinoidal ramp and subtidal slope depositional cycles from typical Trenton carbonates outcropping in the Peterborough to Lake Simcoe areas, southern Ontario (modified from Kobluk and Brookfield, 1982).

Structural Review of the Michigan Basin in southwestern Ontario

The Michigan Basin is approximately 300 km wide and covers about 7.1 x 10^4 km^2 (Figure 6; McCrossan, 1973). Wold et al. (1981) determined a maximum sediment thickness of about 4.5 km at the centre of the basin. The progressive thickening of the sediments, evident on isopachs along with the presence of deeper water facies near the centre of the basin, indicates that basin subsidence was concomitant with sedimentation.

The basin overlies a failed arm of the Proterozoic Keweenawan Rift System (DeRito et al., 1983) which is interpreted to be the result of a hot spot to the north of the basin (Wallace, 1981). This rift system contains mafic volcanics overlain by sandstones. The continuous and layered nature of these sediments suggests that the rift was subsiding as it was being filled (Zhu and Brown, 1986). The rift forms a half ellipse through Lake Superior below the Michigan Basin and Lake Erie (Figure 7). This crustal rifting occurred at approximately 1.3 - 0.6 Ga (Wallace, 1981).

The Algonquin and Findlay Arches, separated by the Chatham sag, divide the Ontario Paleozoic succession into two parts. One extends westward and northward into the Michigan Basin, while the other extends southward and eastward into the Appalachian Basin (Brigham, 1971). The regional dip of Ontario strata into these basins is approximately 6-9 m/km (Winder and Sandford, 1972).

Much controversy exists over the age of the structures flanking the Michigan Basin. It has been agreed over the years that the Algonquin Arch was a positive feature during Paleozoic time. Sanford and Quillian (1959) established through isopach maps that the transgressive overlap of the Upper Cambrian units onto the arch indicates its presence in late Cambrian time. However, Sutterlin and Brigham (1967) provided evidence of an earlier age, Precambrian, based on the progressive thinning of the

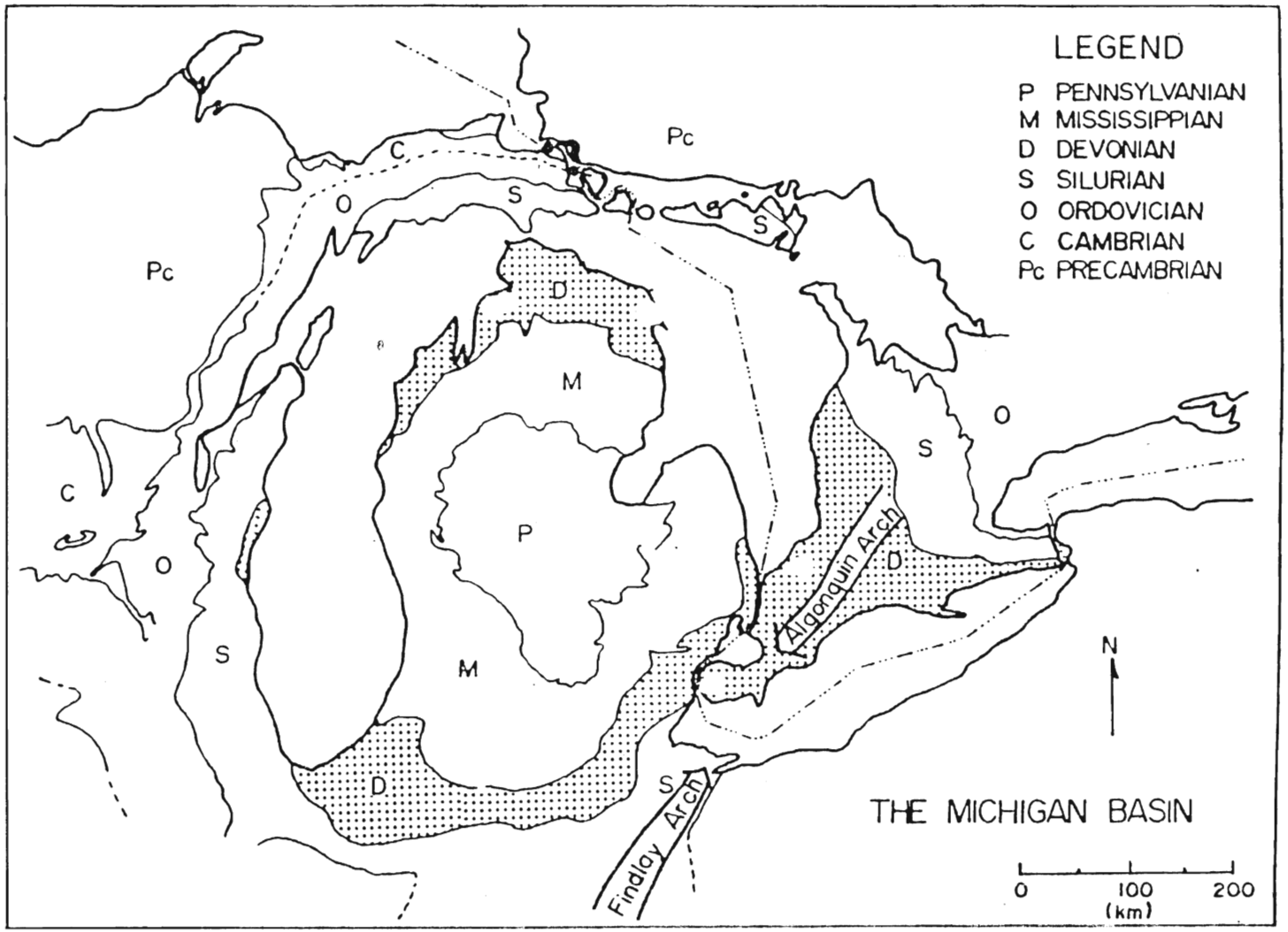

Figure 6: Geologic map of the Michigan Basin illustrating the distribution of sediments which make up its subcircular nature (from Sleep, 1982).

Figure 7: The Keweenawan rift, which has been delineated by high Bouger gravity anomalies as a result of infilling by dense Keweenawan igneous rock (from Wallace, 1981).

Upper Cambrian rocks over local Precambrian highs; highs representing previous erosional features prior to deposition. The lack of lower Ordovician rocks in southwestern Ontario and eastern Michigan represents an intense erosional event at the end of Prairie du Chien time (Cohee, 1945, 1947; Brigham, 1971).

The Findlay Arch developed during Cincinnatian time (Pirtle, 1932). Based on offlap of Upper Cambrian units, lack of Lower Ordovician and Upper Cambrian units in northeast Ohio and southeast Michigan, and absence of Cambrian and Lower Ordovician rocks in southwestern Ontario, Cohee (1948) inferred that the Findlay Arch was present during late Cambrian time. Lockett (1947) correlated the Findlay Arch to the Algonquin Arch. This was disputed by Sanford (1961) who established through isopach maps and lithologic data that the Findlay Arch was not a prominant feature until late Ordovician (possibly late Trentonian) time. Calvert (1964) suggested that the Findlay Arch must have formed during post-Ordovician time by the westward migration of the north central Ohio Arch.

The Chatham Sag was considered to act as a breach in the older Findlay-Algonquin Arches due to the subsidence of the adjacent Michigan and Appalachian Basins (Lockett, 1947). Sanford (1961) proposed that the arches were not tectonically related and that the Chatham Sag was a faulted basement block along which the Findlay Arch became activated. The slight thickening of Middle Ordovician sediments provides minor evidence of an early development of the Sag, but apparent thickening of the units did not occur again until the late Devonian or early Mississippian time.

During the Tippecanoe transgression from 460 - 410 Ma, the Michigan and Illinois Basins received sediments during the Taconic Orogeny resulting in a uniform thickness of shale and limestone from the Michigan to the Appalachian Basin. This was interpreted to be the result

of the simultaneous yoking of the two basins (Quinlan and Beaumont, 1984). From 420 - 410 Ma a broad regional barrier or pinnacle reef sequence of carbonates developed and totally surrounded the clastic deposits in the Michigan Basin. This event was coincident with the independent subsidence of the Michigan Basin (Quinlan and Beaumont, 1984).

A possible mechanism for subsidence of the Michigan Basin could be thermal contraction (Jarvis and Mackenzie, 1980), or phase change which involves mantle diapirs rising to the MOHO causing the conversion of the lower crustal meta-stable gabbroic rocks to eclogite (Joyner, 1967; Haxby et al., 1976; Jerome, 1988). As the Mantle cooled by conduction, the Michigan Basin subsided under the load of the more dense eclogite. This explanation by Quinlan and Beaumont (1984) was preferred over the load-thrusting model which has been used to explain the subsidence of the nearby Appalachian Basin and the neighboring Illinois Basin.

Structural lineaments within the Michigan Basin such as the Howell Anticline, Lucas-Monroe Monocline, Albion-Scipio trend are thought to be fault controlled and associated with Precambrian basement rocks (Ells, 1967; Fisher, 1969; Sanford et al., 1984, 1985).

LANDSAT imagery studies (Prouty, 1976, 1980, 1984; Sanford et al., 1984, 1985) suggest that the dominant NW-SE and NE-SW trending folds and faults and persistent joint patterns are related to shear faulting during the formation of the Appalachian Mountains. Other theories which include fault block tectonics (Fisher, 1983; Sanford et al., 1984, 1985) and deep seated faulting during progressive development of the Keweenawan rift. The rift system is interpreted as the mid-Michigan gravity high (Chase and Gilmer, 1973). A review of the structural patterns and features throughout the Paleozoic sequences suggests that the fault and fracture pattern is best explained by wrench movement of basement blocks. This

process is believed to have been accentuated towards the late Paleozoic but was initiated during the late Ordovician (c.f. Lizotte, 1962; Ells, 1962).

Structural similarities recognized in Michigan Basin Hydrocarbon Reservoirs

The largest hydrocarbon accumulation is found in Michigan and is known as the Albion-Scipio field located within Hillsdale, Jackson and Calhoun Counties. The trend is composite, made up of en echelon bands trending N30-35°W (Ells, 1962). The Albion-Scipio trend lacks a gravity signature and lies west of and parallel to the major Bouger gravity anomaly that is indicative of the Precambrian Keewenawas Rift Zone. However, a circular depression follows the middle of the belt as a series of irregular sinks that demonstrates relief over 16 to 33 m in places (Ells, 1962; Shaw, 1975). These authors illustrated that this depression is expressed on isopach maps of Silurian and Devonian strata and correlate with the producing zones which immediately underlie the central depression.

The Northville-Howell fields have a characteristic fracture-related structural trend of N45°W (Ells, 1962; Lizotte, 1962). Second order fractures are also related to these fields which extend northward into Oakland County from the southern part of Northville. Again several narrow en echelon morphological features, in this case anticlines trending northwest-southeast, are found extending through parts of Wayne, Washtenaw, and Oakland Counties. The steeper northeast flank of the asymmetrical anticlines demonstrate structural relief on the Trenton surface (> 100 m) less than 1/2 km apart (Amoruso, 1957). However, in the northern extension of the Northville trend, the southwest flank is the steeper side of the structure and shows northwest plunging anticlines with only 30 m of closure and no faulting. Ells (1962) demonstrated that the

Howell structure is faulted with vertical displacement as much as 300 m. Steep dips persist on the southwest flank and is reflected by Ordovician, Silurian, Devonian, and Mississippian units throughout the Northville-Howell structure. Isopachs of the Lower Silurian and Cincinnatian strata demonstrate thinning to be coincident with the Trenton structure which implies that movement occurred as early as Late Ordovician (Lizotte, 1962).

The Lucas-Monroe trend is a north-south structural trend in Washtenaw County intersected by a N45°W trend, along which the small Freedom field lies (Ells, 1962). This area is southwest of the Northville and Howell anticlines (see Figure 2). Structural relief of nearly 200 m is expressed by all the Devonian formations (Ells, 1962). This provides evidence that the fault-related anticlinal structure was active up until latest Devonian time.

In each field the reservoir development is related to fracture systems oriented northwest-southeast and north-south. This structural feature is seen in the south and east flanks of the Michigan Basin, a reticulate system over the Findlay Arch in which there was the development of secondary porosity due to the dolomitization of the reservoir rock. The northwest trends have been attributed to the result of wrench faulting associated with the Pennsylvanian Appalachian orogeny, overprinting the major Middle Paleozoic fault and fracture patterns within southern Michigan and are suggested to have taken place up to the latest Paleozoic. A structural contour map of the Middle Devonian Traverse limestone in the Michigan Basin demonstrates that the northwest fracture trends extend northwards and is present throughout the entire Michigan Basin (see Fisher, 1969).

All the oil fields within the southern and southeastern portion of the Michigan Basin contain occurrences of high temperature dolomitization with associated MVT features and mineralization.

Theoretical Background and Considerations

Carbonate Geochemistry

Carbonate sediments deposited in the marine environment are aragonite (A), high-magnesium calcite (HMC), and low-magnesium calcite (LMC). These carbonate phases differ with respect to their crystal morphology and chemistry. Brand and Veizer (1980) stated that these original carbonate phases can be precipitated in inorganic chemical equilibrium with the ambient sea water.

The precipitation or dissolution of $CaCO_3$ in a carbonate system (Bathurst, 1975) occurs as follows;

$$CaCO_3 + H_2O + CO_2 = Ca(HCO_3)_2 \quad (1)$$

Various chemical equilibria are involved in the simplified dissolution-reprecipitation process defined above. Brand and Veizer (1980) found that various trace and minor elements (Mg, Sr, Mn, Fe, Na, Zn) substitute to various degrees for Ca in the $CaCO_3$ lattice. The substitution can occur in the following forms: 1) diadochic, 2) interstitial, 3) adsorption for unsatisfied charges, or 4) filling in vacancies derived by lattice defects (Brand and Veizer, 1980). Carbonate diagenesis occurs during exposure of carbonate minerals to meteoric waters or with admixtures of sea water. This is reflected in the differences in the chemistry between the original and altered carbonate sediment, and attests to the complex nature of the water system responsible for the diagenetic products (Brand and Veizer, 1980). Brand and Veizer (1980) further established that chemical concentrations in carbonates are controlled by the water/rock ratio. This alteration proceeds within diagenetic microenvironments which is influenced by partly closed or open systems of alteration (Pingitore, 1976). An exchange of trace and minor elements occur during interaction of interstitial pore waters and the metastable carbonate phases (A, HMC), and subsequent reprecipitation as diagenetic LMC (dLMC). Veizer (1977) stated that localized reaction zones

on solid-liquid interfaces provide for continuous elemental exchange between the pore waters and the recrystallization sites.

In diagenetic systems with high rock/water ratios, the chemistry of the water is the rate and concentration limiting factor. Conversely, in diagenetic systems with a low rock/water ratio, the chemistry of the dissolving carbonate phase is the limiting factor.

Elemental partitioning applies to both organically and inorganically precipitated carbonates (A, HMC, LMC, dLMC, and dolomite) in the marine and diagenetic environments (Brand and Veizer, 1980; Land, 1980). The partition coefficient (k) is defined at low activities (Brand and Veizer, 1980) by the following equation:

$$k = (m_t/m_c)_s \,/\, (m_t/m_c)_l \qquad (2)$$

In the above equation, t stands for the trace or minor element, c is the carrier or major element, s is the solid phase, l is the liquid phase, m is the moles of the trace and carrier elements (after McIntire, 1963).

Veizer (1977) stated that diagenetic equilibration is a time-limited process where further alteration after formation of the stable phase is of considerably small possibility. Strontium and Mn are useful diagenetic indicators due to their widely divergent partition coefficients (Brand and Veizer, 1980). With progressive diagenesis there is an enrichment in Fe, Mn, Mg, and Zn with a concomitant depletion in Na and Sr (Brand and Veizer, 1980; Veizer, 1977).

The transformation of the original metastable carbonate components (A, HMC) and matrix into dLMC involves textural alteration as well as chemical alteration (Brand and Veizer, 1980). Textural diagenesis is the concomitant occlusion of pore space in the sediments due to compaction and cementation of the carbonate precursor. This process is controlled within proposed reaction zones, described by Katz and Matthews (1977), Pingitore (1976), and Veizer (1977). Brand and Veizer (1980) described "Partly Closed Reaction Zones" which derive their dissolved ions from both

the dissolving metastable phase and the surrounding bulk aquifer water. Brand and Veizer (1980) further described a mechanism known as the "Messenger Film", similar to "thin film" by Kinsman (1969), which acts as a medium for transferring textural and chemical 'information' from the dissolving carbonate phase to the precipitating carbonate phase.

Stable Isotope Geochemistry

Our oceans represent large homogeneous reservoirs because of the very short mixing time of circulating oceanic waters. Although the isotopic composition of ocean may have varied through geological time and have undergone large excursions, the variations will be registered by the precipitating sediments (Odin, 1982); specifically by the oxygen and carbon elements whose isotopic composition is recorded by carbonates (Odin, 1982). Since the time constant of oceanic mixing is less than 1000 years for oxygen and carbon (Broecker, 1979), the isotopic changes and its dissolved elements are expected to be spatially synchronous (Odin, 1982).

Isotopic Variations of Geological Relevance

Carbon isotopic variations

Carbon isotope values reflect changes in the ^{13}C content of the aqueous carbonate reservoir from which the carbonates precipitate (Anderson and Arthur, 1983). There are two main causes for this change: (1) a modification of the volume of one part of the exchangeable CO_2 reservoir, such as an increase or decrease in the continental biomass; since this is an extra-oceanic modification, the change occurs equally everywhere and the $\partial^{13}C$ must change everywhere in the same direction; (2) a change in the residence time of the deep-water masses whereby a longer residence time favours the conversion through oxidation of ^{13}C depleted carbon from marine organic matter to dissolved bicarbonate; the longer the residence time, the lighter the $\partial^{13}C$ (Odin, 1982). Temperature

has relatively little effect on the $\partial^{13}C$ concentration of marine carbonates (Anderson and Arthur, 1983).

For surface waters, the exchange between dissolved CO_2 and the air varies according to latitude, such that the ratio $^{13}C/^{12}C$ of the dissolved CO_2 decreases from equatorial to high latitudes (Odin, 1982). In the vicinity of continents, runoff brings waters enriched with respect to ^{12}C in the form of organic matter, which can influence the $^{13}C/^{12}C$ ratio of the mixed sea-waters (Odin, 1982).

Variations in the $^{13}C/^{12}C$ ratio in the carbonates within coastal sabkha-type environments include: (1) local changes in the composition of the aqueous carbon reservoir under the influence of ^{13}C-depleted organic carbon; (2) phytoplankton and algal photosynthetic activities; and (3) exchange with the atmospheric carbon dioxide reservoir (Fritz et al., 1988). The most important factors affecting the carbon isotope compositions would be related to photosynthetic and associated production and decomposition of organic matter, since they preferentially use isotopically light carbon. This results in ^{13}C enrichments in the dissolved inorganic carbon (DIC) of near surface waters (Fritz et al., 1988).

Therefore, a shift in the $\partial^{13}C$ in carbonates towards slightly negative values would indicate either the input of depleted carbon from oxidized organic matter, or that the carbonates did not form in the near-surface environment but represent slightly deeper water facies.

Oxygen isotopic variations

The $^{18}O/^{16}O$ variations of marine carbonates reflect the temperature and the $^{18}O/^{16}O$ ratio of the water in which they precipitated (Veizer, 1983). Both temperature and sea-water $^{18}O/^{16}O$ ratio vary with climate. Atmospheric water vapour is depleted in the heavier isotope relative to the sea-water from which it evaporates (Epstein and Mayeda, 1953; Dansgaard, 1964). Conversely, condensation from a limited amount of

vapour results in enriched condensate and a residual vapour depleted in the heavier isotope relative to the initial vapour.

It stands to reason that with any ice-cap building or any increase in the amount of ice, water extracted from the ocean will be depleted in the heavier isotope while the remaining ocean water becomes isotopically heavier. This ^{18}O enrichment should be reflected in marine carbonates. As the temperature of precipitation of carbonates decreases, the $\partial^{18}O$ generally increases (Odin, 1982). Thus, heavy oxygen isotope ratios indicate a cold climate, while temperature increases and ice-cap melting will be reflected by enrichments in ^{16}O.

Use of stable isotopes in the analysis of ancient carbonates

Factors that control the ^{18}O composition of carbonates in the ancient environment are: (1) temperature; (2) $\partial^{18}O$ of the water in which the carbonate was precipitated; and (3) diagenetic changes, which include, (a) the stability of the original carbonate phase; (b) openness of the diagenetic system; (c) differences in the chemical and isotopic composition of the depositional and diagenetic water; and (d) burial depth (O'Shea et al., 1988).

The isotopic composition of carbonate rocks show a trend towards depleted $\partial^{18}O$ values with increasing geologic age (Degens and Epstein, 1964; Perry, 1967; Fritz, 1971; Perry and Tan, 1972; Veizer and Hoefs, 1976; Brand and Veizer, 1981; Brand, 1982). These trends have been interpreted to represent the variations in the oxygen isotopic composition of ancient waters (Perry, 1967; Fritz, 1971; Perry and Tan, 1972; Veizer, 1977), or caused by the increasing post-depositional equilibration of the carbonate sediment with interstitial meteoric waters (Dickson and Coleman, 1980). The latter case attributes this variation to be due to higher temperatures of the ancient oceans (Knauth and Epstein, 1976). The utilization of stable isotopic compositions in the study of dolomites is

limited due to the inability to precipitate dolomite at low temperatures in laboratory experiments (cf. Carpenter, 1980; Land, 1980). Estimation of the equilibrium fractionation of oxygen isotopes between dolomite - water and dolomite - calcite at these low temperatures is not known, however estimates of these fractionation factors can be obtained through extrapolation of the oxygen isotopic compositions from high temperature synthesis studies (Northrop and Clayton, 1966; O'Neil et al., 1969; Matthews and Katz, 1977). Land (1980) demonstrated that the $\partial^{18}O$ composition of ancient dolomites are not those obtained during dolomitization, but are the result of varying degrees of burial diagenesis and neomorphism. Therefore the implicit use of oxygen isotope ratios must be interpreted with some caution.

Dolomitization

The alteration of calcium carbonate to dolomite can be expressed (Carpenter, 1980) as follows:

$$2CaCO_3 + Mg^{2+} = Ca,Mg(CO_3)_2 + Ca^{2+} \qquad (3)$$

Dolomitization follows similar chemical and textural alteration processes as described for the diagenetic alteration of the carbonate precursor. As dolomitization proceeds there are enrichments in the Mn and Fe contents of the rock. With dedolomitization there is usually a respective depletion in Fe, due to Fe quenching, and an enrichment in Mn, evidenced by the typical luminescence in zoned dolomites due to Mn activation (Fairchild, 1983). Land (1980) reported that dolomitization of a carbonate leads to an enrichment in Mg, and depletions in Sr, and Na. The decrease in Sr concentration is related to the increasing substitution of Fe for Ca, and particularly Mg into the dolomite lattice (Veizer, 1977).

Burial Compaction Model

Compaction of fine-grained sediments during burial dolomitization involves the progressive expulsion of pore waters from shale masses which are underlain or bordered by thick shelf-carbonate sequences (Morrow, 1982a). The burial compaction model has been supported by a study of Mattes and Mountjoy (1980) who also considered the previous work by Folk and Land (1975), and Friedman (1980). They identified four main criteria that address the kinetics of dolomitization during deep burial:

1) with deep burial, dolomite reaction rate increases rapidly,

2) with increasing temperature, the hydration of Mg^{2+} may be progressively removed so incorporation takes place in the crystal lattice more easily,

3) subsurface hydraulic flow can maintain chemical stability, eliminate mass balance restrictions and enhance formation of massive dolomite through dynamic recharge and continued solute supply, and,

4) permeability barriers may be counteracted by rate considerations and increased reaction time.

Some problems still exist when considering the sources and volumes of Mg^{2+} required for dolomitization. About 5.5×10^3 moles of Mg^{2+} are required to dolomitize 1 cm^3 of calcite at 10% porosity (Morrow, 1982b). This requires 32 cm^3 of shale, compacted from 70% porosity to 2% porosity to provide this amount of Mg-rich water (Morrow, 1982b). This assumes that all of the water passes through the carbonate, when in reality more than half of the water from compacting shales is lost vertically upward upon deposition (Morrow, 1982b).

The burial compaction model best explains the modification of pre-existing porosity of the carbonate precursor. Also, a number of sources for Mg^{2+} ions must be considered when applying this model to large and extensive dolomite units.

Sabhka and Coorong Models

Sabhka type dolomitization is always associated with the formation of evaporites. This model refers to dolomite that forms in areas with seasonal or rare flood recharge whereby seawater moves landward through the sediments to replace groundwater lost by capillary evaporation at or near the sabhka surface, hence "evaporative pumping" (MacKenzie et al, 1980). Dolomitization proceeds with a constant flux of magnesium ions, which in turn releases calcium ions for anhydrite (gypsum) formation, and the equilibrium reaction leads to a decrease in the Mg:Ca ratio of the interstitial fluids (MacKenzie et al., 1980).

In contrast, Coorong type dolomites are not associated with evaporites. Muir et al. (1980) interpreted the lack of evaporite minerals or evaporite casts in ancient dolomites not to mean that concentrated brines were never present, but that the evaporites may have been precipitated during the summer months, and flushed out during the winter by a reflux mechanism. They further noted that the dissolution and destruction of the evaporites is a penecontemporaneous diagenetic process, and not the result of deep burial diagenesis. This conclusion is also supported by the work of Friedman (1980) and Dunham and Olsen (1980). They suggested that the flux of dense brines came from adjacent, or stratigraphically subjacent, hypersaline environment, which lead to the formation of replacement dolomite (Dunham and Olsen, 1980; Friedman, 1980).

Mixed-Water Model

Hanshaw et al (1971) documented the first large-scale system of deep burial dolomitization under the influence of fresh groundwater in the confined Tertiary carbonate aquifer of Florida. Since then many authors have emphasized that active groundwater circulation aids in supplying marine-derived Mg^{2+} ions for dolomitization (Morrow, 1982b). Authors such as Land (1973), Dunham and Olsen (1980), and Choquette and Steinen

(1980) have argued that many ancient platform dolomites, which lack evaporites and are depleted in trace elements and heavy isotopes, formed in a similar manner (Morrow, 1982a). Land (1980) stated that these quantitative interpretations of absolute isotopic or trace element values are tenuous due to their respective distribution coefficients, fractionation factors, and the multiple crystallization events that occur in partly closed systems. Overall the qualitative interpretation of regional or stratigraphic parameters, such as elemental covariances, seems to be quite useful in determining the mode of alteration. Slow precipitation rates favour dolomitization of the precursor carbonates (Morrow, 1982b). This model successfully explains many ancient dolomite sequences.

Pressure Solution Model

Various authors (e.g., Logan and Semeniuk, 1975; Wanless, 1979) documented pressure solution along solution seams and stylolites as a major process of dolomitization (Morrow, 1982b). The source of Mg^{2+} ions (Wanless, 1979) is attributed to the cannibalization of Mg^{2+} from pre-existing magnesium calcite during pressure solution (Morrow, 1982b). Mattes and Mountjoy (1980) postulated that pressure solution was only one of three major modes of dolomitization during deep burial diagenesis of the Miette build-up of Jasper National Park, Alberta. This mode of dolomitization does not explain large lateral extents of dolomite because high-magnesium calcite is usually converted to low-magnesium calcite before burial, and preservation occurs outside of the stylolitized zones. Thus, more than one source for the Mg^{2+} ions is required to provide multiple stages of dolomitization within the deep-burial diagenetic environment (Mattes and Mountjoy, 1980).

Hydrothermal or Saddle Dolomite

The term used to describe the saddle-shaped texture was pearl dolomite by Dana (1837). The first significant documentation of the saddle-shaped variety of dolomite was by Tschermak (1884). Later it was reported to occur with sphalerite at Joplin, Missouri (Dana, 1892). In the past, many authors reported on the occurrence of dolomite but none having the characteristic curved faces, cleavage and undulatory extinction of the saddle variety. Recently this form of dolomite has been referred to as saddle-shaped dolomite (Dunsmore, 1973), baroque dolomite (Folk and Asserto, 1974), hydrothermal dolomite (Goldberg and Bogoch, 1978), and Xenotopic-C dolomite (Gregg and Sibley, 1984).

Saddle dolomite has been associated with epigenetic mineralization such as sulphates (Choquette, 1971), sulphides (Beales, 1971; Choquette, 1971; Folk and Asserto, 1974; Mathis, 1978; Radke, 1978) and fluorite (Chouquette, 1971; Mathis, 1978; Radke, 1978). Occurrence of saddle dolomite within breccia (Beales, 1971), fractures (Beales, 1971; Choquette, 1971; Folk and Asserto, 1974; Mathis, 1978; Radke, 1978), and stylolites (Beales, 1971; Mathis, 1978; Radke, 1978) has been well documented. The saddle dolomite variety has also been documented to be associated with hydrocarbons (Mathis, 1978).

Saddle dolomite lines pore space and vugs associated with dolomitic host rocks. Beales (1971) and Choquette (1971) proposed that the formation of saddle dolomite occurs at elevated temperatures (50°C - 130°C) in saline, epigenetic waters of neutral pH and moderate to highly reducing conditions. Folk and Asserto, (1974) suggested that saddle dolomite forms at early stages within a marine environment diluted by meteoric waters, whereas Friedman and Radke (1979) proposed that it is characteristic of a hypersaline carbonate environment. Radke and Mathis (1980) found saddle dolomite to commonly occur in association with tectonically induced fractures and faults that unequivocally suggest an

epigenetic origin. They also concluded that the formation of saddle dolomite was favoured under the following conditions:

1) temperatures above 60 °C,

2) sulphate-reducing conditions, and

3) pyroelectric effects under fluctuating temperature conditions that result in selective ion adsorption at different sites on the crystal surface.

Machel (1987) provided evidence that the thermochemical sulphate reduction process may be representative of other processes that control the rate and abundance of saddle dolomite formation in the presence of increasing carbonate alkalinity. Gregg (1983) demonstrated experimentally that saddle dolomite did not need to form within sulphate-reducing conditions or by pyroelectric effects under fluctuating temperature conditions. He concluded that saddle dolomite was a useful paleotemperature indicator as originally proposed by Radke and Mathis (1980).

The works by Machel and Mountjoy (1986) and Hardie (1987) summarized the formation of dolomite. It is thermodynamically favoured in solutions of low Ca^{2+}/Mg^{2+} ratios, low Ca^{2+}/CO_3^{2-} ratios, and high temperatures under both low and high salinities. Under the appropriate kinetic and thermodynamic conditions, three environments have been characterized to be chemically conducive to the formation of dolomite (Machel and Mountjoy, 1986): (1) environments of any salinity above both the thermodynamic and kinetic saturation with respect to dolomite; (2) alkaline environments such as those under the influence of bacterial reduction or fermentation processes, or those with a high input of alkaline continental waters; (3) environments with temperatures that exceed 50 °C, such as subsurface and hydrothermal environments.

Dedolomite

Dedolomite is known as the replacement of dolomite by calcite (originally described by Von Marlot, 1847; Radke, 1978). Shearman et al. (1961) recognized dedolomite and proposed the following criteria for its identification:

1) the occurrence of relics of incompletely replaced dolomite crystals,
2) the presence of pseudomorphs of calcite, and
3) the occurrence of palimpest textures in which rhombic zones of ferric oxide or grain boundaries of the earlier dolomite crystals remain as ghosts in the generation of calcite.

De Groot (1967), using an experimental approach, found that the dedolomite texture takes place by the incongruent dissolution of dolomite at low $_pCO_2$ and is enhanced in the presence of:

1) waters with initially high Ca/Mg ratios,
2) high flow rates of water through dolomite,
3) temperatures of less than 50°C, and
4) pCO_2 of less than 0.5 atmospheres.

The reaction for the dedolomitization process (originally from Von Marlot, 1847 found in Radke, 1978), is the following:

$$Ca,Mg(CO_3)_2 + CaSO_4 * 2H_2O \text{ —— } 2CaCO_3 + MgSO_4 + 2H_2O \qquad (4)$$

Radke (1978) suggested that dedolomitization is a near-surface weathering process which is related to unconformities, either ancient or modern (originally proposed by Schmidt, 1965; de Groot, 1967; Evamy, 1967; Friedman and Sanders, 1967; Goldberg, 1967; Braun and Friedman, 1970; and Moore, 1975).

Budai et al. (1984) pointed out that dedolomite can form during burial diagenesis (Mattavelli et al., 1969), contact metamorphism (Wood and Armstrong, 1975), and occur in freshwater zones along faults (Longman and Mench, 1978) or schizohaline environments (Magaritz and Kafri, 1981).

Thermal Maturation

Conodont Colour Alteration Studies

Conodonts are tooth-like microfossils ranging in size from 0.1 to 4 mm (Clarke et al., 1981). They can be cones, bars, blades and platforms and are essentially composed of concentric layers of carbonate apatite [$Ca_5Na_{0.14}(PO_4)_{3.01}$ $(CO_3)_{0.16}F_{0.73}(H_20)_{0.85}$], that approach the mineral francolite (Epstein et al., 1977). The basal part of the conodont is laminated and contains higher concentrations of organic matter than the denticles. It is essentially this area of the conodont that changes colour with thermal maturation.

Field and laboratory studies by Epstein et al., (1977) showed that colour alteration in conodonts is due to increasing burial temperatures and the duration of heating the organic constituents. This was established using long-term, high-temperature runs, with and without water in both open and closed systems. The open system was subject to air, while the closed system operated under confined pressures (1 kb) of argon and methane. The experimental results were then plotted using the Arrhenius equation and extrapolated into geologic time and higher temperatures. The results corresponded very well with their field collections and they were able to demonstrate the same sequence of colour changes from yellow (amber) to black. A total of 5 colour changes monitor the progressive alteration of the trace amounts of organic matter within the conodont with increased thermal alteration (Epstein et al., 1977). Rejebian et al., (1987) re-established the CAI indices within the ranges from 5-8 as a function of textures due to regional metamorphism, contact metamorphism and hydrothermal alteration.

Limitations with the CAI determination

1) Colour changes will vary in different host-rock lithologies (Epstein et al., 1977) such as black platy carbonates interbedded with black slate and light grey carbonates which were only 100 m apart).

2) The size, shape and maturity of individual conodonts. The larger thicker or adult elements were darker than the thin, delicate or juvenile elements (Epstein et al., 1977).

3) The difficulty to calculate precise burial temperatures using the Arrhenius curve for CAI values of 1.5 (Legall et al., 1981). They stated that the critical time/temperature zone for CAI 1.5 was too difficultto examine ($>10^7$ years but $<3 \times 10^8$ years). This has been compensated by their proposal of an acritarch alteration index (AAI) (see Legall et al., 1981).

4) Conodonts with CAI's between 6 - 8 cannot be used to asses precise temperatures of hydrothermally altered rocks but may serve as useful indicators of potential mineralization (Rejebian et al., 1987).

Host rock Maturation

The thermal maturation history of the source rock is the most important factor in the origin of petroleum. Diagenesis has been characterized as the process of biological, physical, and chemical alteration of the organic matter prior to the pronounced effects of temperature. During diagenesis a complex mixture of geo- and biopolymers and monomers undergo a series of low temperature reactions that result in the formation of hydrocarbon-like materials through the loss of oxygen, nitrogen and sulphur, which cover the temperature range from the surface to 50 °C (Hunt, 1979).

Catagenesis describes the process by which organic matter is altered due to the effect of increasing temperature and where a linear increase in temperature causes a logarithmic increase in the reaction rate for

petroleum formation (Hunt, 1979). This increase in temperature is also responsible for the increasing solubility of some organic compounds in the sediment-derived fluids, thereby increasing their ability to migrate (Hunt, 1979). Catagenesis is defined as ranging from 50 °C to 200 °C, whereby higher temperatures are considered to represent metamorphism, during which all organic matter is ultimately converted to methane and graphite (Hunt, 1979).

Evaluation of Hydrocarbon Potential

Gehman (1962) was the first to suggest that carbonates are effective oil source rocks at lower total organic carbon contents than shales. He further substantiated that the ratio of hydrocarbons to the total organic matter was about four times greater in limestones than in shales. Hunt (1967, 1979) and Tissot and Weldt (1978) suggested that fine-grained carbonate rocks can generate more hydrocarbon for the same amount of organic matter then organic shales; they further suggested that as little as 0.3 weight percent of organic carbon may be needed. Carbonates can yield large quantities of oil because these rocks contain mainly amorphous organic carbon derived from algae, whereas shales always contain recycled organic carbon from the continents, along with woody and coaly materials, which yield very little petroleum (Hunt, 1979). However, further evaluation of the organic carbon content of carbonate rocks lead to the contention that it would take a minimum of 1-1.5 percent organic carbon, because most carbonate rocks also contain some recycled organic carbon which is carbonized and cannot produce petroleum (Hunt, 1979).

Jacobsen et al., (1988) recognized two distinct types of Ordovician oils: (1) oils sourced from *Gloeocapsamorpha prisca*, a non-photosynthetic, prokaryotic micro-organism, and (2) oils sourced from amorphous organic matter in argillaceous rocks. The former oils are concentrated within shale laminae of open-marine carbonate rocks and generally have high

generative potential. The latter types have lower generative potential. It has been determined that the Ordovician oils found within the Trenton-Black River fields of Ontario and the Lima-Indiana field of Ohio have non-G.*Prisca* type oil characteristics and their geochemical attributes can be related to the Collingwood Shale of southwestern Ontario (Powell et al., 1984) and the Point Pleasant Formation (the Collingwood Shale equivalent) of Ohio (Cole et al., 1987).

Powell et al., (1984) estimated that middle Ordovician and Cambrian hydrocarbons within southwestern Ontario represent one distinctive family and cannot be distinguished based on their geochemical signatures. The Collingwood Member of the Lindsay Formation is recognized as the only high quality Ordovician source rock and is mature throughout southwestern Ontario. Total organic carbon is as high as 11.0 percent which represents good to excellent hydrocarbon yield (Powell et al., 1984). Detailed studies by Churcher (1985) and Russel and Telford (1983) reported total organic carbon contents (TOC's) from 2 % up to 5 - 10 % from Ontario exposures of the Collingwood Shale member, a possible petroleum source bed and oil shale.

High concentrations of organics are commonly seen as black organic matter within stylolitic partings in limestones. The two dominant types of kerogen found within most sedimentary rocks are the sapropelic and humic varieties (Hunt, 1979). In a detailed study of the Paleozoic rocks of the middle Volga region (Rodionova and Chetverikova, 1962), humic kerogen predominates in the nearshore marine clay-silt-sandstone facies in the presence of oxygen, and the sapropelic kerogen predominated in the deep water, low energy clay and clay-carbonate sediments with little to no oxygen. The gradation and predominance of the kerogen types was attributed to variable contributions by continental and marine derived organic matter (Hunt, 1979).

Geoporphyrins

The foundation of modern organic geochemistry began with Treibs' (1936) suggestion that sedimentary metalloporphyrins were derived from biological pigments. He had suggested that metal complexes of etioporphyrins (ETIO) are derived from haem, and the desoxophylloerythroetioporphyrins (DPEP) are derived from chlorophyll. Recent reviews suggest that both the ETIO and DPEP porphyrins are derived primarily from chlorophylls (Baker and Louda, 1986; Filby and Van Berkel, 1987), although a haem origin for some ETIO porphyrins has been recently re-introduced by Bonnet et al., (1987) and Chicarelli et al., (1987). Boreham et al., (1989) found that the ETIO porphyrins may have more than one primary source. Their study of the abundance of ETIO porphyrins in two distinct oil shales of Albian and early Tertiary age suggested that ETIO porphyrins containing 28-31 carbon atoms were derived mainly from chlorophyll, whereas the C_{32} ETIO porphyrin was probably derived mainly from haem.

Petroleum porphyrins also contain these porphyrin skeletons. Extensive studies by Treibs (1936) proved their biological origin and related them to the chlorophyll or hemin molecules. Hodgson (1967), Baker (1969), and Blumer (1965, 1973) identified them in a number of sediments and crude oils and established a wide distribution of these geochemical fossils (Tissot and Weldt, 1978). The major type of fossil porphyrins (Tissot and Weldt, 1978) are desoxophylloerythoetioporphyrin (DPEP), which contains an isocyclic ring in addition to the four pyrrole rings, and mesoetioporphyrin or etioporphyrin III without the isocyclic ring. These fossil porphyrins are either metal-free or mostly chelated with nickel or vanadyl (VO; Figure 8).

The transformation of chlorophyll, or hemin, likely starts during sedimentation or early diagenesis (Tissot and Weldt, 1978). Magnesium and iron are lost at an early stage and a re-chelation with vanadyl or

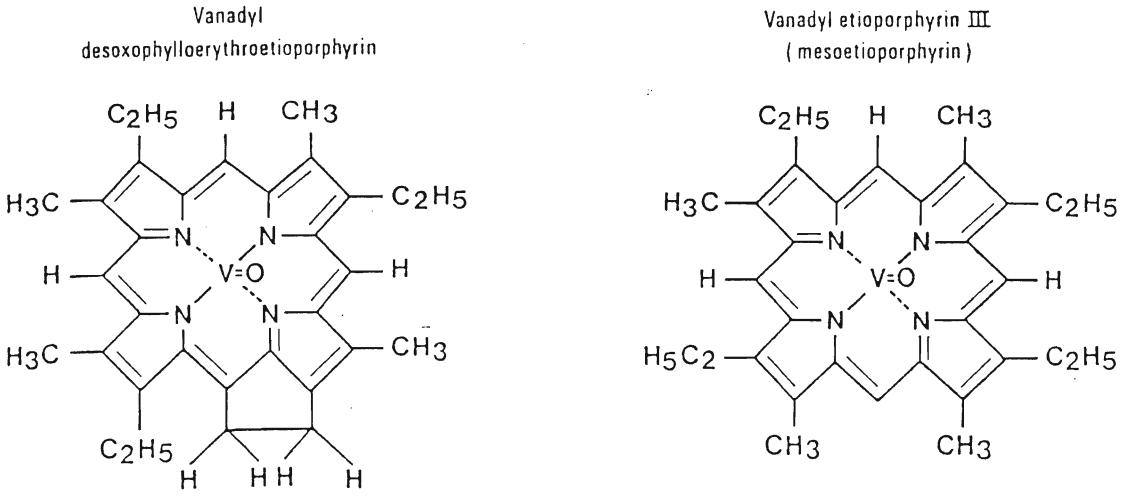

Figure 8: Examples of the geoporphyrins found in ancient sediments and crude oils as presented in Tissolt and Weldt (1978, Fig. II.3.18). The DPEP porphyrin structure, on the left, is converted into the ETIO porphyrin structure, on the right, during catagenesis.

nickel may stablize the molecule and insure its preservation. Reduction of the vinyl and carbonyl groups takes place at a later stage where decarboxylation of the carboxylic acids leads to the formation of the petroporphyrins (Tissot and Weldt, 1978). Casagrande and Hodgson (1976) suggested that the homologous series of the chain lengths, in near surface sediment from the Black Sea, are generated during early stages of diagenesis.

The relative proportions of the DPEP and ETIO porphyrins in oils and extracts depend on the thermal maturity of the organic matter in the sediments (Barwise and Park, 1983; Louda and Baker, 1981; Mackenzie et al., 1980). The decrease in the ratio occurs with increasing thermal maturity due to the formation of ETIO porphyrins from DPEP porphyrins by cleavage of the isocyclic ring (Corwin, 1960). Barwise and Roberts (1984) suggested that both DPEP and ETIO porphyrins are formed during early diagenesis, and the decrease in the ratio with maturity is caused by several distinct but interdependant mechanisms; mainly due to the more rapid decomposition of the DPEP porphyrin. However, (Barwise, 1987) suggested that the decrease in the DPEP/ETIO ratio was mainly due to the generation of the ETIO porphyrin from kerogen.

The findings of Sundararaman et al. (1988) suggest that the changes in the ETIO vanadylporphyrins are due to the dilution of pre-existing DPEP vanadylporphyrins by ETIO vanadylporphyrins released from kerogen during catagenesis. By employing a quantitative expression of the change in the vanadylporphyrin distribution during maturation, called the Porphyrin Maturity Parameter, they were able to provide a basis for determining the onset of petroleum generation (Sundararaman et al., 1988).

Application to Hydrocarbon Geochemistry

Chlorophyll is the only porphyrin that is synthesized into significant amounts of organic matter by living organisms (Hunt, 1979). As chlorophyll is subjected to diagenetic processes at increasingly greater depths, it loses the phytol chain, and the green chlorins become red porphyrins, which gradually form an increasingly wide spectrum of hydrocarbon derivatives (Hunt, 1979). The relatively simple hydrocarbon pattern of algae becomes increasingly complex with burial and diagenesis. With increasing temperatures, thermal and catalytic cracking reactions break down the organic matrix (kerogen) and produce hundreds of hydrocarbons that will mix with the original biogenic mixture (Hunt, 1979). Ancient sediments may contain thousands of porphyrins derived from the chlorophyll molecule (Hunt, 1979).

The presence and distribution of petroporphyrins is attributed to the conversion of the desoxophylloerythroetioporphyrin (DPEP) to the mesoetioporphyrin (ETIO) during decarboxylation with thermal maturation. Incorporation of nickel and vanadium in the porphyrin structure takes place during early diagenesis (Tissot and Welte, 1978). In contrast, Mg and Fe combine with oxygen and nitrogen compounds in the porphyrin structure, and are lost during diagenesis. At the same time a re-chelating (combine) with nickel, and at higher temperatures with vanadyl (VO), stabilizes the molecule and leads to its preservation (Tissot and Welte, 1978).

The source for the nickel and vanadium would be the hydrocarbon source rock. It has been suggested that the amount of nickel and vanadium concentrated in organic matter of sedimentary rocks is dependant on two factors: (1) preservation of the tetrapyrroles (sourced from algae in the subaqueous environment), and (2) persistence of an open sediment system (Lewan and Maynard, 1982). They further suggested that diffusion of dissolved materials from an overlying water body into the

interstitial waters of a sediment column is critical to maintaining a viable source of vanadium and nickel. Enrichment of vanadium or nickel in the organic matter of a sedimentary rock suggests that within its environment of deposition, algae derived organic matter encountered anaeorbic conditions in its preservation, or burial histories and sedimentation rates were slow enough to insure the persistence of an open sediment system (Lewan and Maynard, 1982).

Since the distribution coefficient of Ni and V for the interaction of liquids, such as hydrocarbons, with various carbonate mineral phases is not known it is difficult to quantify changes during catagenesis and hydrocarbon generation. A quantification of this process may lead to an understanding of the distribution of these elements during catagenesis and provide an estimate on the timing and evolution of hydrocarbon generation and migration.

Analytical Techniques

Part 1: Petrographic Analyses

Diagenetic features include dolomitization, dedolomitization, saddle dolomite formation, and calcite cementation. A paragenetic sequence was constructed from these relationships using a variety of petrographic analyses.

Light Microscopy

Forty-six thin sections from the 33821 Mersea 3-12-I core, 26 thin sections from the 33823 Mersea 1-12-A core, 60 thin sections from the 34160 Romney 5-8-II, and 40 thin sections from the 34151 Mersea 7-18-VIII were used to evaluate the paragenetic diagenetic sequence (Appendix II). These slides were etched with 2 % HCl before immersion in the staining solution of Alizarin Red-S and potassium ferrocyanide. Stains allow for the differentiation between the different carbonate minerals (calcite and dolomite) and determination of relative amounts of iron within the individual grains (Lindholm and Finkelman, 1972).

Cathodoluminescence

A total of 50 thin sections from all four of the cored wells were prepared for cathode luminescence analysis. The analysis of the thin sections requires them to be prepared to a thickness of 50 microns, as well as to be left unstained and uncovered.

Cathodoluminescence analysis was performed on a Nuclide ELM-2B luminoscope. The operating conditions of the luminoscope for viewing dolomite in 50 micron thick thin sections, were the following:

1) vacuum pressure between 70-80 millitorrs,
2) beam current maintained at approximately 0.5 mA,
3) high voltage maintained within 12-15 KV.

Ultraviolet Fluorescence

A total of 50, thirty micron thick and uncovered sections, were prepared for ultraviolet fluorescence (U/V) analysis to determine the presence and/or absence of hydrocarbon in fluid inclusions within the various carbonate phases.

Ultraviolet fluorescence was performed using a Leitz Diaplan light microscope equipped with the ultraviolet lamp in the reflected light mode. Both green and red filters were employed to establish the brightest spectrum of fluorescence of the hydrocarbons present within each sample.

Part 2: Geochemical Analyses

Rock and Cement Trace Element Determination

A total of 506 rock matrix and cement samples were prepared for trace element determination. Of these samples, 323 were dolomite rock matrix, 29 were limestone rock matrix, 24 were shale matrix, 68 were saddle dolomite cement, 58 were calcite cement, and 4 were brachiopods. All of the samples were manually separated, cements and brachiopods were cleaned of surface impurities, crushed and then dried in preparation for digestion. The dolomite matrix and saddle dolomite cement samples of 0.025, 0.05 and 0.10 g were dissolved in 6, 12, and 24 mL of 2 % (v/v) HNO_3, respectively, and the limestone matrix and calcite cement samples of 0.01, 0.025, 0.05 and 0.10 g were dissolved in 2, 4, 8, and 16 mL of 2 % (v/v) HNO_3, respectively. After 2 - 2.5 hours of leaching, the samples were filtered through ashless papers (Whatman #40). Deionized water was added to the solution making the final volume 50 mL.

In order to determine the insoluble residue (IR), each filter paper with the IR was put into a Vitrocel crucible and ashed in a muffle furnace at 800 °C for 1 hour. Each crucible was weighed before (without IR) and after (with IR) firing. The weight of the soluble fraction was obtained by subtracting the weight of the IR from the initial weight of the sample.

The major (Ca), minor (Sr, Mg), and trace (Fe, Mn, Na and Cu), elements were analyzed on a Varion SpectrAA-400P Atomic Absorption Spectrometer (AAS) by flame analysis. The trace elements Pb, Zn, Ni and V were analyzed on the GTA-96A Graphite Furnace of the AAS. The concentration of each element was determined by using the Standard Curve Method. This method involves preparing standard solutions which span the optimum working range of the AAS for the element to be analyzed. Ten thousand ppm La was added to Ca and Mg sample solutions to suppress interelement interference, and 2000 ppm K was added to solutions to prevent ionization during the analysis of Sr. The concentration of each element was calculated to 100 percent carbonate basis (IR free) using the formula, (Appendix III);

$$\text{ppm of element in rock} = \frac{\text{original dissolution volume} * Y * Z}{\text{(initial weight-insoluble residue)}}$$

in which Y is the extra dilution (if necessary), and Z is the AAS concentration.

Accuracy of the analysis was determined using International Standards - NBS 634, and NBS 636. Reported accuracy for all major and minor elements for the NBS standards is reported in Appendix IIIb. Precision of the analytical procedures was determined by running duplicates of samples at various stages of the analytical process. Average precision of analyses based on duplicate determination was: Ca (5.9), Mg (8.5), Sr (14.2), Fe (15.5), Mn (4.4) and Na (19.2) relative percent (Appendix IIIb).

Since Cu, Pb and Zn were at and/or below the detection limit, in most cases, the accuracy could not be reproduced to within 50 relative percent. Due to this problem the elemental concentrations of Cu, Pb, and Zn have been excluded from further discussion. Ni and V concentrations were not

reproducible to within 25 relative percent in most cases, due to very low concentrations.

Shale Trace Element Determination

A total of 24 shale matrix samples were also prepared for trace element determination. The procedure for shales was followed:

1) Dry crushed powder at 150 °C for 3 hours,
2) Cool in a dessicator,
3) Weight out 0.200 g of sample into a teflon beaker,
4) Add 20 mL of concentrated HF acid,
5) Add 8 mL of concentrated Perchloric acid,
6) Heat on hot plate at 2.0 - 2.5,
7) Repeat steps 1 - 6 until dissolved,
8) Add 20 mL 2 % (v/v) HNO_3,
9) Pour into 50 mL volumetric and top with deionized water.

The analytical determination of the trace element composition of the shales was calculated back to 100 % whole rock with no insoluble residue. The trace element values for the shales are reported in ppm (Appendix IV).

Brine and Oil Trace Element Determination

A total of 18 hydrocarbon and brine samples were collected from the wellheads of currently producing wells of the Hillman Oilfield. Thirteen hydrocarbon and brine samples were taken from the Hillman/Klymer Oilfields, 2 samples from the Renwick Oilfield, and 3 samples from the Goldsmith/Wheatly Oilfields.

Preparation of the hydrocarbons and the brine samples for analytical analysis required that the two phases be manually separated. This was accomplished by pipetting the single liquid phase from the sample bottle, centrifuging for 10 minutes by increasing the speeds to allow further

separation, and filtering each phase through Watman No. 1 filter paper. Once the sample was separated each component was transferred to a (aqua reqia cleaned) glass sample bottle, labelled and sealed.

The brine samples were diluted to appropriate concentrations in order to analyze for all of the major, minor and trace elements. The various trace element determinations (cations only) were carried out similar to that for the carbonate rock matrix and cement samples. The final elemental concentrations of the brine samples were calculated by subtracting the chemistry of the flowline drilling fluid (blank) from the observed elemental concentrations of the brines. The adjusted elemental concentrations are reported in ppm and (Appendix V).

Precision of the analytical analysis was tested using duplicates. All major and minor cation concentrations of the brines were reproducible to within 10 relative percent.

Hydrocarbons may contain high values for many of trace and minor elements and the preparation of the samples for trace element determination was followed:

1) Determine the specific gravity of the liquid hydrocarbons by weighting out a known volume and calculating its weight to volume ratio,

2) Weight out close to 0.500 g of liquid hydrocarbon into a teflon beaker by using either properly cleaned (aqua regia) glass pipettes or using disposable pipettes for each sample,

3) Add 50 mL of Di-isobutyl ketone (DIBK) organic solvent.

Due to the high organic content of the hydrocarbon samples, only the trace elements Ni and V were determined using the furnace capability of the AAS and are reported in ppm in Appendix VI. Actual trace element composition of the hydrocarbons followed the listed recipe:

1) 1 / Sp. gr. (g/mL) * weight (g) = volume (mL) of sample used

2) Volume of sample (mL) + 50 ml of dilutent = total volume

3) % hydrocarbon = volume of hydrocarbon / total volume

4) Dilution Factor = 100 % / % hydrocarbon

5) True elemental concentration = dilution factor * conc. determined from AAS absorbance reading

Reproducibility for both Ni and V concentrations of the hydrocarbon samples was within 15 relative percent.

Organic Carbon and Leco Sulphur Determination

A total of 150 rock samples were selected for organic carbon and sulphur elemental analysis. Twenty-six dolomite and 5 limestone rock samples taken from the 33821 Mersea 3-12-I well covering 85 m, 18 dolomite and 4 limestone rock samples from the 33823 Mersea 1-12-A well covering 55 m, 8 dolomite rock samples from the 34151 Mersea 7-18-VIII well covering 37 m, and 13 dolomite rock samples from the 34160 Romney 5-8-II well covering 60 m. The sampling interval was chosen to evaluate every lithology.

A secondary part of this study required the sampling and analysis of core from two other wells. They were sampled at a more detailed scale to evaluate the changing C and S concentrations at the interfacies level. The first was the 34428 Romney 6-206-I well, which represents the Trenton Group. A total of 37 samples covered 30 m of limestone was selected resulting in a sampling interval of approximately 0.75 m. The Black River Group was represented by the core from the Row Ram #7 Dover 3-12-VE well. Thirty-nine samples of limestone were selected covering 35 m resulting in a sampling interval of approximately 0.75 - 0.80 m.

Detection limits for both Total Organic Carbon and Total Sulphur results were within 0.01 % (Appendix VII).

Part 3: Isotope Analyses

Rock and Cement Stable Isotope Determination

A total of 135 rock/mineral samples were selected for stable isotope analysis. From the core of the 33821 Mersea 3-12-I well, a total of 24 dolomite matrix samples, 7 limestone matrix samples, 4 saddle dolomite cement samples, 10 calcite cement samples, and 3 brachiopod samples were selected. From the core of the 33823 Mersea 1-12-A well, a total of 18 dolomite matrix samples, 2 limestone matrix samples, 7 saddle dolomite cement samples, and 4 calcite cement samples were selected. From the core of the 34151 Mersea 7-18-VIII well, a total of 10 dolomite matrix samples, 5 saddle dolomite cement samples, and 7 calcite cement samples were selected. From the core of the 34160 Romney 5-8-II well, a total of 14 dolomite matrix samples, 9 saddle dolomite cement samples, 9 calcite cement samples, and 2 brachiopods samples were selected. Co-occurring saddle dolomite and calcite cements were extracted to evaluate the variability in the progressive precipitation processes responsible for the diagenetic carbonate cements.

The samples were analyzed for their oxygen and carbon isotopes on a V.G. Micromass® 903 mass spectrometer (University of Waterloo isotope lab). A minimum of 5 mg of powdered sample is reacted with 100 % phosphoric acid at 25 °C for 30 minutes. The isotopic ratios are expressed in (∂) notation relative to PDB in permil (‰). Average accuracy and reproducibility compared to the recommended values for NBS 20 (Solnhofen Limestone) were better than 0.2 ‰, and all samples were corrected for ^{17}O (Appendix VIII).

Oxygen and Deuterium Determination of the Brines

Stable isotope determination was performed on a total of 18 formation waters (brines) which were located within the immediate study

area. Collection of the brine samples was covered in the trace element methodology section.

Fifty mL aliquots of each brine sample were prepared similar to the procedure outlined in the trace element section. The brines were sealed in polyethylene containers and shipped to the University of Waterloo for analysis.

The $^{18}O/^{16}O$ determination and $^{2}H/H$ determination of the brine samples were performed on a VG 903 mass-spectrometer and a VG 602D mass-spectrometer respectively, according to the procedures outlined in Fritz et al., (1986), and McNutt et al., (1987). The overall average reproducibility was better than 0.2 ‰ for both analyses (Appendix V).

Part 4: Thermal Maturation Analysis

A total of 40 rock samples of approximately 1 kg each were collected from cores of the four oil producing wells. Fifteen samples were taken from the 33821 Mersea 3-12-I well, seven rock samples from the 33823 Mersea 1-12-A well, thirteen samples from the 34160 Romney 5-8-II well, and 5 samples from the 34151 Mersea 5-18-VIII well. The crushed rocks were placed in plastic buckets with a 15% solution of acetic acid and left to dissolve for up to 5 days before changing the solution. This process was repeated for approximately 2 1/2 months before enough rock had dissolved and sufficient sediment was collected for conodonts extraction. The sediments were washed in a 150 mesh sieve, then dried, and the heavy and light fractions separated using tetrabromoethane. The conodonts were picked by hand from the heavy fraction under a binocular microscope.

Petrographic Analyses: Results and Discussion
Part 1: Light Microscopy

Lithological variations, diagenetic features, and relationships to evaluate the timing of hydrocarbons were observed. Mineralized fractures and secondary diagenetic textures and fabrics were also studied. Logs with the number and location of the thin sections within each well are presented in Appendix II.

Discussion of Dolomite Textures

The classification scheme for dolomite textures of Gregg and Sibley (1984), (Figure 9) is followed in this study, except the term saddle dolomite is used in place of Xenotopic-C dolomite (Gregg and Sibley, 1984).

There is little evidence of the original sediment/rock type due to the pervasive dolomitization and associated mineralization. The original bioclastic limestone is preserved in a 15 m interval (see core log for 33821 Mersea 3-12-I). It is neomorphosed and in most cases partially dolomitized (Plate 1). The bioclasts include fragments of brachiopods and crinoid ossicles. The dolomite and limestone matrices are argillaceous.

Dolomite Matrix

Idiotopic-S and Idiotopic-E dolomite are the most abundant types of dolomite present in the groundmass, but as suggested by the prefix, idio, the origins are not well understood. Gregg and Sibley (1984) suggested that these types of dolomite are formed below the CRT by near-surface processes, according to their experimental results. They further suggested that a critical roughening temperature (CRT) exists for dolomite, between 50°C and 100°C, above which anhedral dolomite crystals form. Gregg and Sibley (1984) found that idiotopic dolomite texture can exist above the CRT, because crystal faces become stabilized either adjacent to pore space

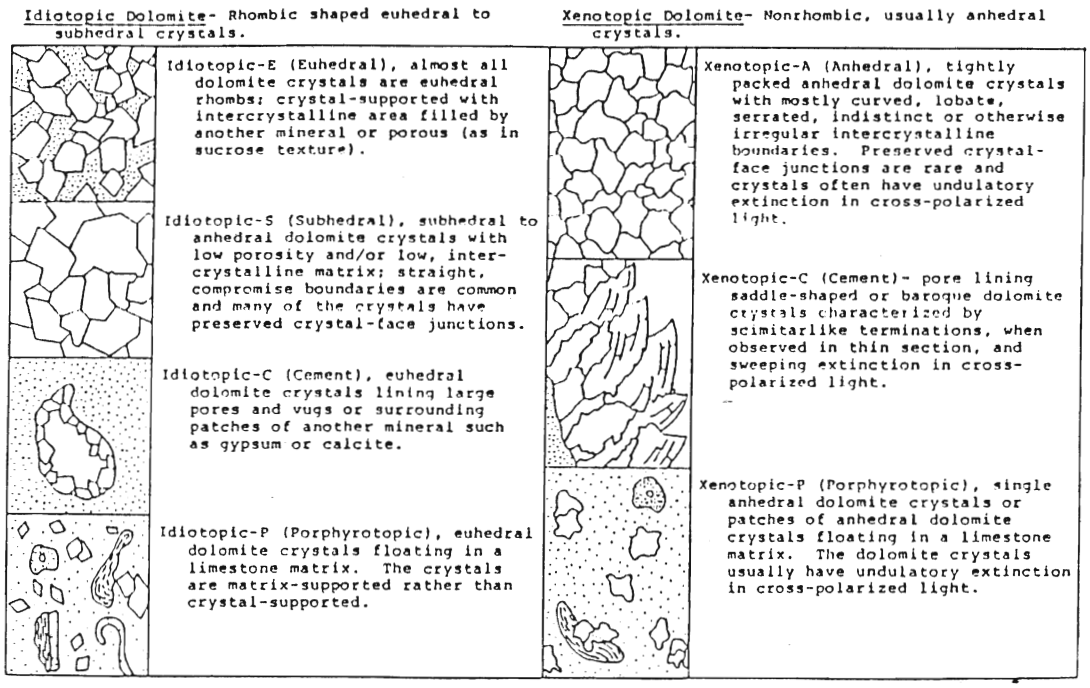

Figure 9: Classification scheme used for dolomite textures (Gregg and Sibley, 1984; Fig. 6).

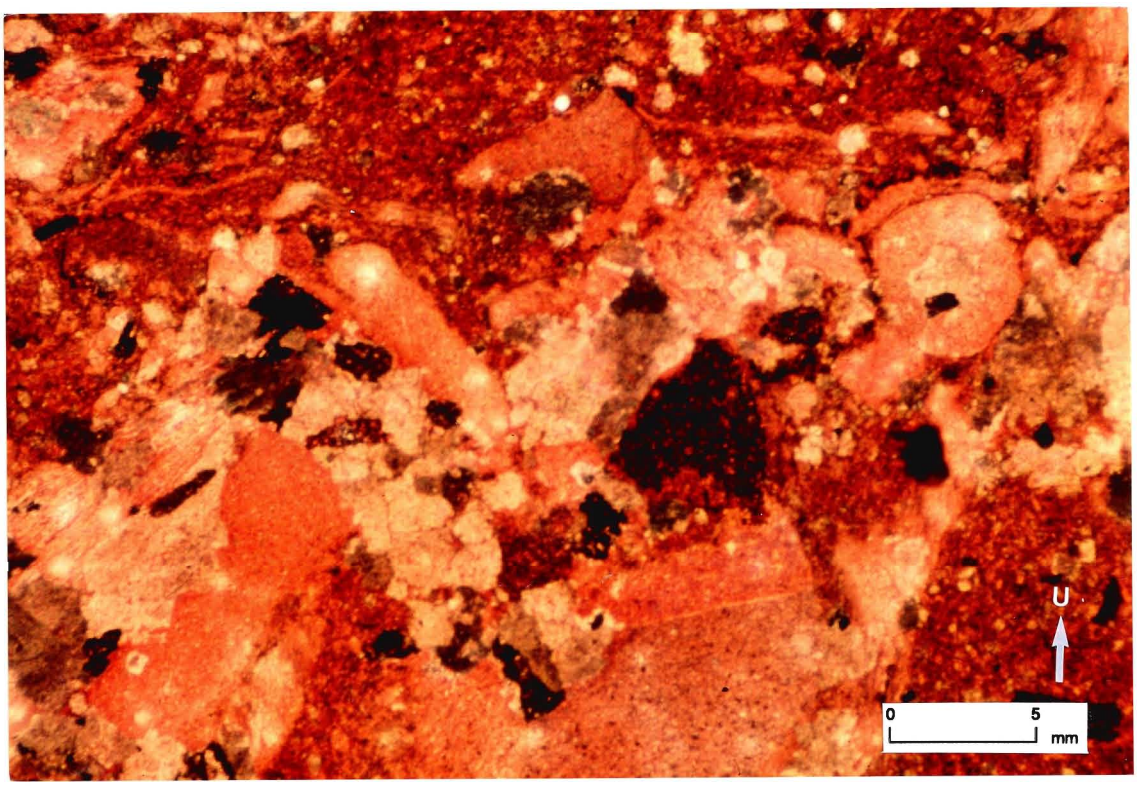

Plate 1: Photomicrograph of stained thin section under plane light shows dolomitization of calcarenitic limestone (wackestone). Dolomite rhombs occur interstitial to bioclastic material within the matrix. Bioclasts are mainly brachiopod and crinoid plate fragments. (U = up direction in core).

or during growth by impurities such as organic material or clay minerals. The next most common dolomite texture, Xenotopic-A dolomite, occurs as direct replacement of limestone adjacent to fractures. It is pervasive within the matrix where extensive fracturing and solution breccia occurs within the rock. Xenotopic-A dolomite mimics the morphology and optical characteristics of saddle dolomite.

Idiotopic-S Dolomite

A typical occurrence of Idiotopic-S dolomite is illustrated in Plate 2. Idiotopic-S dolomite is present within limestones that exhibit early stages of neomorphism. This photomicrograph was taken from a dolomitized lithology within the 'preserved' limestone sequence of the 33821 Mersea 3-12-I well.

Textural relationships of the Idiotopic-S dolomite are the following:

1) variable grain size (0.1-2.2 mm, average grain size of 0.4 mm) from thin section to thin section, and more importantly, variable grain size within the same thin section;

2) gradation between the Idiotopic-S dolomite and Idiotopic-E dolomite texture, and some occurrences that exhibit interlaminations of the two distinct textures;

3) gradation between the Idiotopic-S and Xenotopic-A dolomite, and some occurrences where the Idiotopic-S dolomite encloses the Xenotopic-A dolomite;

4) staining of the sections documented zonation within individual grains; multiple zonation within dolomite rhombs that occur within some calcite cements;

5) irregular patches of saddle dolomite and calcite cement;

6) fracture filling within Xenotopic-A dolomite groundmass; and,

7) cavities are lined by argillaceous material.

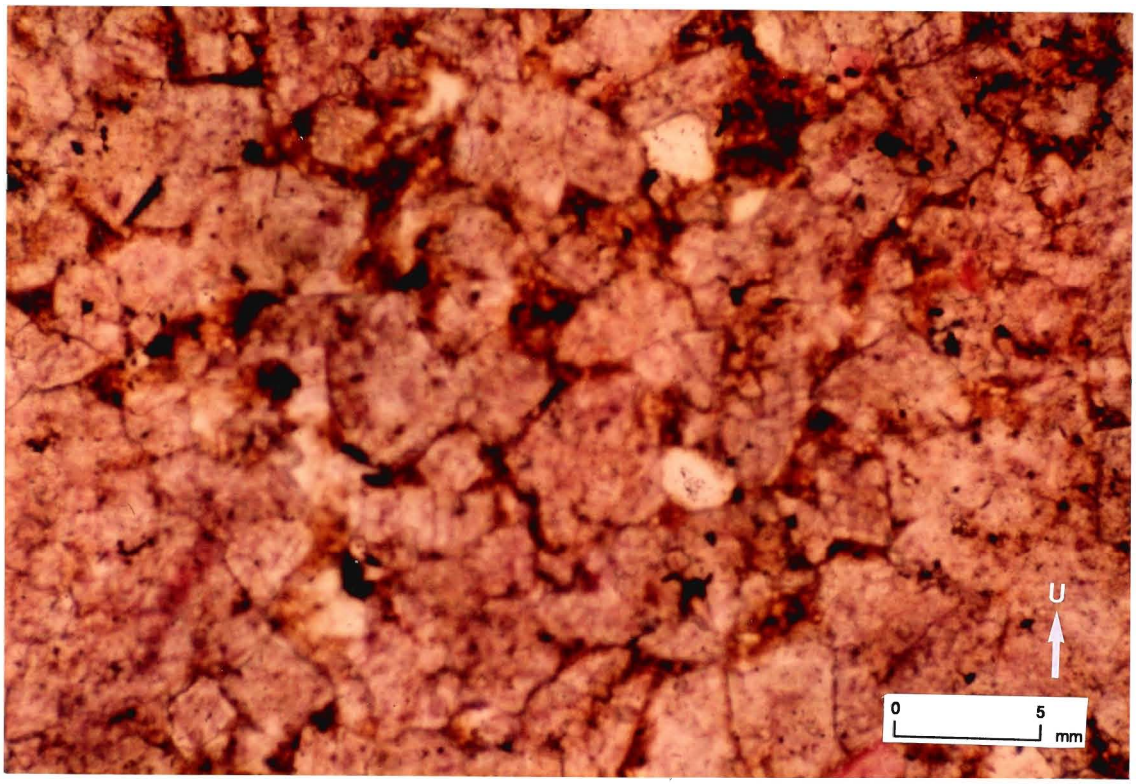

Plate 2: Photomicrograph of stained thin section under polarized light of Idiotopic-S type dolomite. Intercrystalline porosity, stained with bitumen, is typical of this form of dolomite. (U = up direction in core).

Porosity is low in these dolomites. They appear to lack permeability since bitumen can only be found in minor quantities staining crystal faces within isolated areas. Crystal faces in Idiotopic-S dolomite contain minor bitumen where these dolomites occur adjacent to stylolites and microstylolites.

Idiotopic-E Dolomite

Idiotopic-E dolomite has the characteristics outlined in Figure 9 (Gregg and Sibley, 1984) except for some subhedral grains that occur in the groundmass. Generally, intercrystalline porosity is high, or it is decreased by finely crystalline material suspected of being very fine crystals of Idiotopic-E dolomite.

Typical occurrences of the Idiotopic-E dolomite texture are presented in Plates 3 and 4. These photomicrographs demonstrate the variable grain size of the Idiotopic-E dolomite.

Idiotopic-E dolomite exhibits the following textures:

1) variable grain size (0.2-1.0 mm, average grain size of 0.25 mm);

2) gradational with Idiotopic-S dolomite; some occurrences exhibiting interlaminations of the two textures;

3) gradation of Idiotopic-E dolomite with Xenotopic-A dolomite; in some cases Idiotopic-E dolomite encloses Xenotopic-A dolomite;

4) associated with other dolomite types and/or occurs between grain boundaries of other dolomites;

5) staining of the sections shows zonation within individual grains; multiple zonation due to dedolomitization;

6) occurs as single crystals within matrix of coarsely crystalline calcite; and

7) occurs within stylolite seams containing argillaceous material, minor quartz, variable porosity, and variable amounts of bitumen; most cases exhibit bitumen stained crystal faces and grain boundaries.

Plate 3: Photomicrograph of stained thin section under polarized light of Idiotopic-E dolomite. Gradation from porous Idiotopic-E dolomite to finer-grained Idiotopic-S dolomite. Permeability and porosity are well developed. Blue epoxy shows secondary porosity (U = up direction in core).

Plate 4: Photomicrograph of stained thin section under polarized light of porous, permeable, and coarse-grained Idiotopic-E dolomite. Blue epoxy shows secondary porosity. (U = up direction in core).

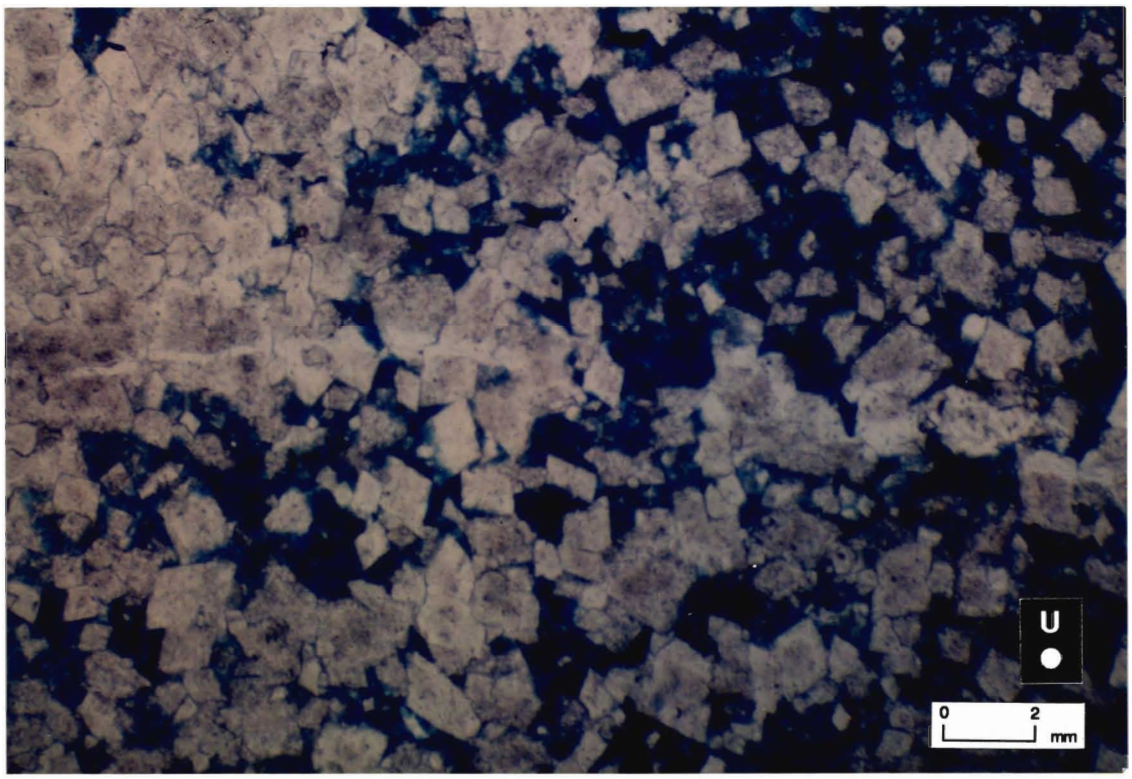
U
0
2
mm

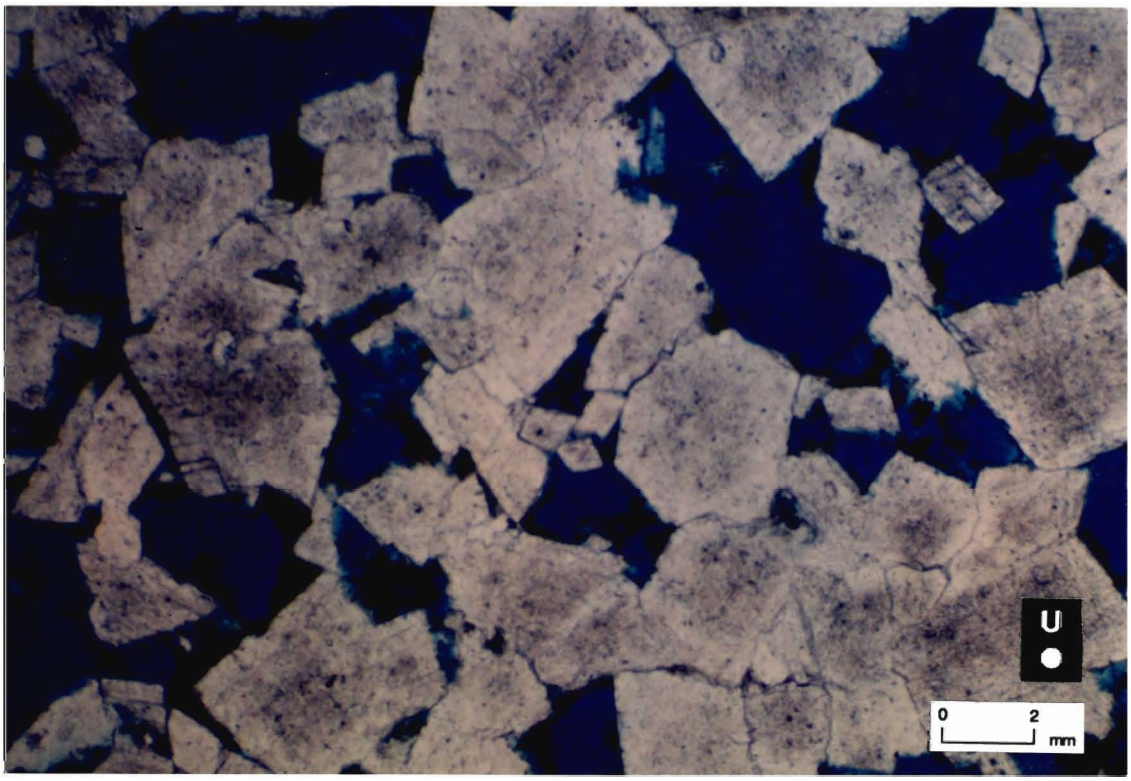
U
0
2
mm

Idiotopic-E dolomites are generally porous and contain the highest porosity (5 to 10 %). The areas where bitumen is clearly visible are characterized by stylolite seams that contain Idiotopic-E dolomite. Large amounts of hydrocarbons in the intercrystalline porosity suggests that permeability was high in these zones.

Xenotopic-A dolomite

Xenotopic-A dolomite exhibits the criteria outlined in Figure 9 (Gregg and Sibley, 1984), except for occurrences of some curved crystal faces and undulatory extinction within isolated areas of the groundmass. A typical occurrence of Xenotopic-A type dolomite is presented in Plate 5.

Xenotopic-A dolomite exhibits the following textures:

1) variable grain size (0.1-1.5 mm, average grain size of 0.5 mm);

2) gradation of Xenotopic-A into Idiotopic-S dolomite; in some cases it is enclosed by Idiotopic-S dolomite;

3) occurrences of Idiotopic-E dolomite as seams within the Xenotopic-A dolomite groundmass;

4) patches of Xenotopic-A dolomite within Idiotopic-E dolomite groundmass;

5) Idiotopic-E dolomite crystals along grain boundaries of the Xenotopic-A dolomite crystals;

6) euhedral dolomite crystal inclusions exhibiting corroded rims, possible dedolomitization feature; and,

7) zonation of individual grains, possible dedolomitization textures.

In some cases Xenotopic-A dolomite is found with argillaceous material, and has bitumen stained crystal faces. Porosity is generally low, 1-3% maximum, with relatively low permeability.

Saddle Dolomite

The fracture- and vug-filling dolomite possess textures indicative of saddle dolomite (Plate 6). Physical and optical features include the characteristic 'spear-head' morphology, curved crystal faces, and undulatory extinction.

Saddle dolomite exhibits the following textures:

1) variable grain size (0.2-3.2 mm, average grain size of 1.5 mm);

2) replacement feature, clearly developed as a cement partially to completely filling vugs;

3) exhibiting vague to more distinct zonation of individual grains;

4) associated with bitumen; and,

5) occurring as a fracture lining containing anhydrite, pyrite and calcite cement.

The presence of saddle dolomite, in significant amounts within all the wells, suggests that the rocks have been subjected to high temperatures under burial diagenesis.

Dedolomite

Dedolomite is easily confused with coarsely crystalline calcite cement that formed subsequent to the dolomite. Typical zonation and corrosion of many dolomite rhombs with the subsequent formation of calcite cement is apparent in many thin sections. The predominant form of dedolomite found within the rocks occurs as illustrated in Plate 7. Plate 7 demonstrates the replacement of saddle dolomite crystals to calcite with the complete infilling of calcite cement within the centre of the large vug.

Silica

Silicification is quite common within the dolomitized portions of the Sherman Fall Formation. One example includes a distinct laminae of chert (fracture filling) which cuts perpendicular to the bedding (Plate 8). The

Plate 5: Photomicrograph of stained thin section under plane light of Xenotopic-A dolomite. Coarse-grained xenotopic dolomite crystals show rare development of intracrystalline porosity. This high temperature dolomite is characterized by anhedral crystal morphology which mimics the spear-head morphology of saddle dolomite. (U = up direction in core).

Plate 6: Photomicrograph of stained section under plane light of coarse-grained, euhedral saddle dolomite cement (white; extinguishing grey) lining a large vug filled with equant blocky calcite cement (red). (CV = centre of vug; U = up direction in core).

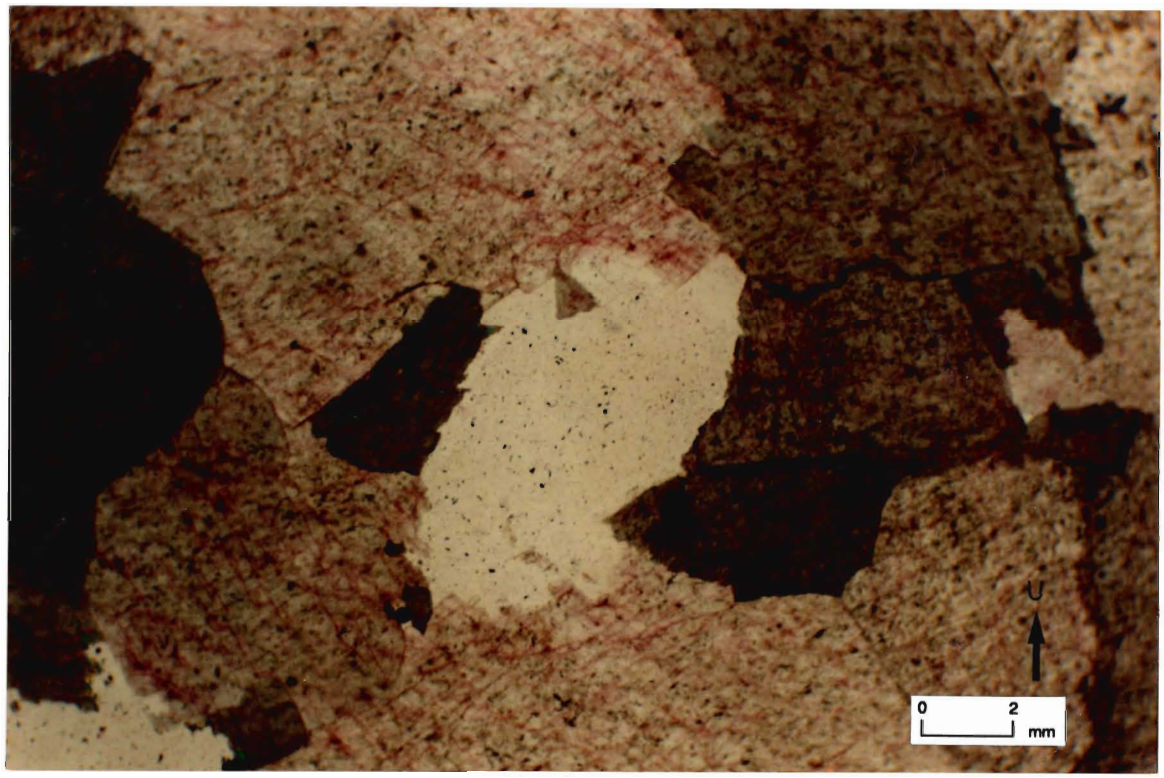
U
0
2
mm

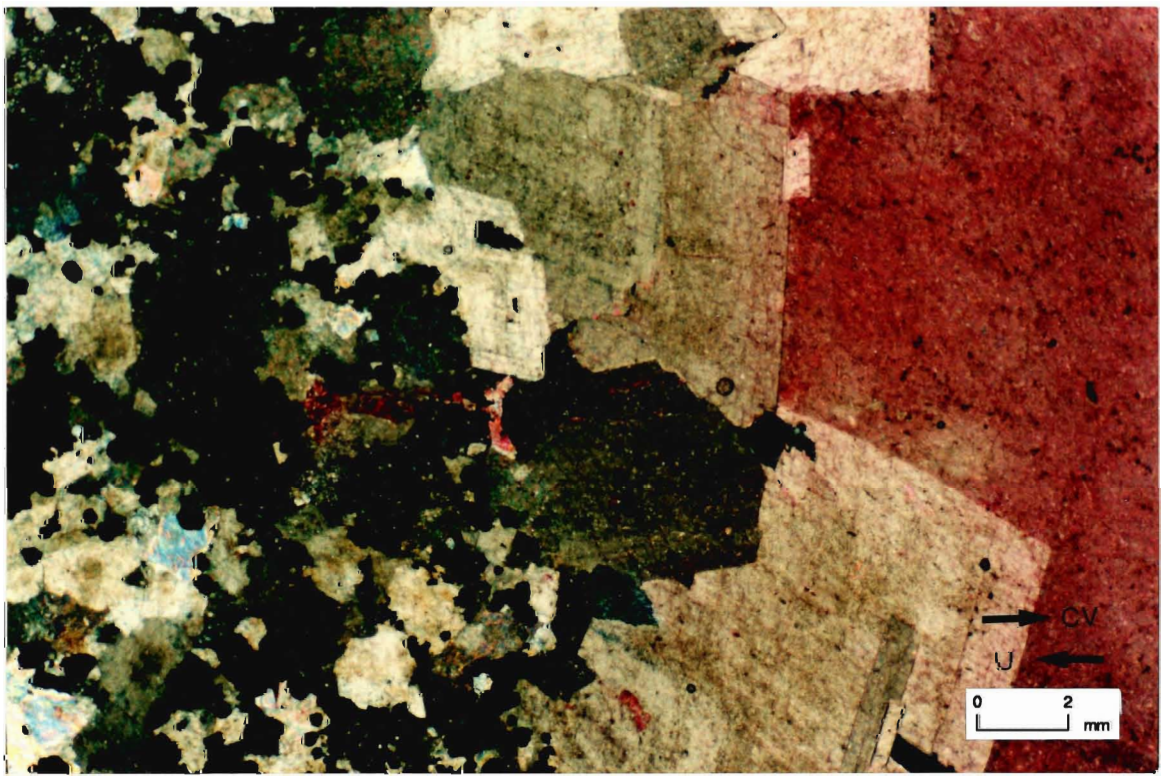
CV
U
0
2
mm

Plate 7: Photomicrograph of stained thin section under plane light illustrating dedolomitization of saddle dolomite cement. Saddle dolomite crystals are typically zoned and replaced by calcite cement (red). (CV = centre of vug; U = up direction coming out of page).

Plate 8: Photomicrograph of stained thin section under plane light shows fracture filling by high temperature chert. The coarse quartz grains are increase in size toward the centre of the vug.
(U = up direction in core).

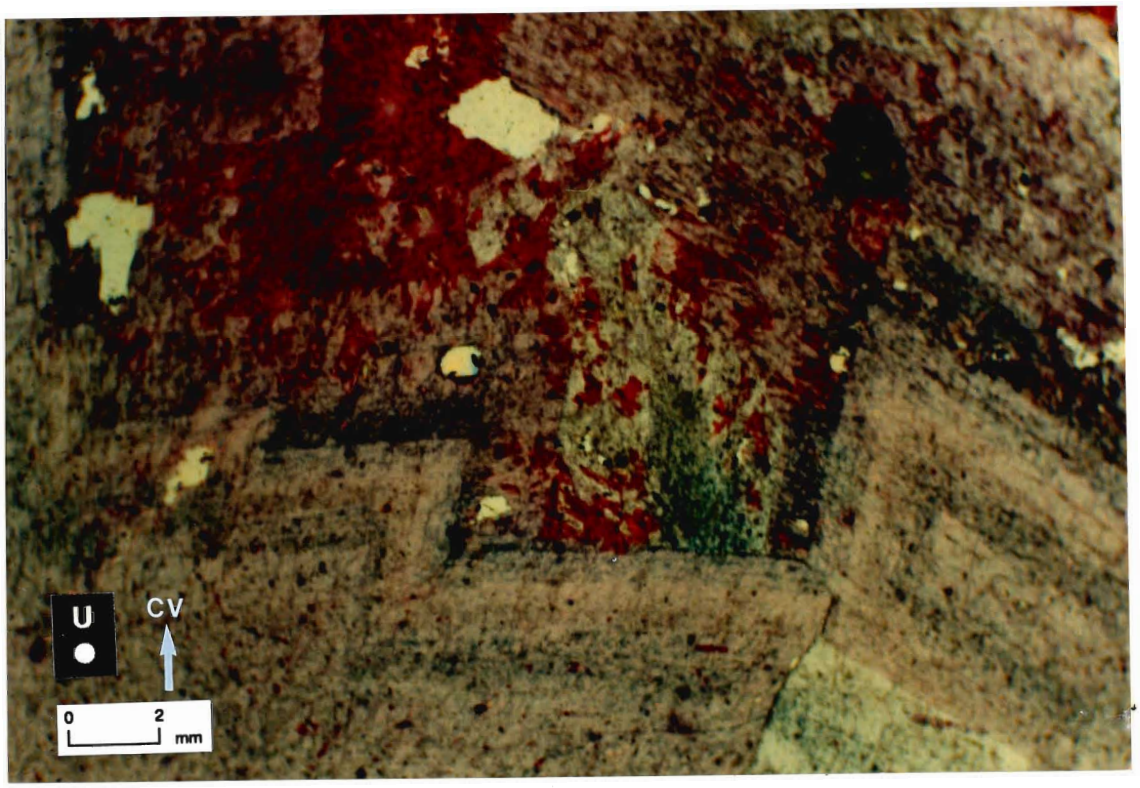
U
CV
0
2
mm

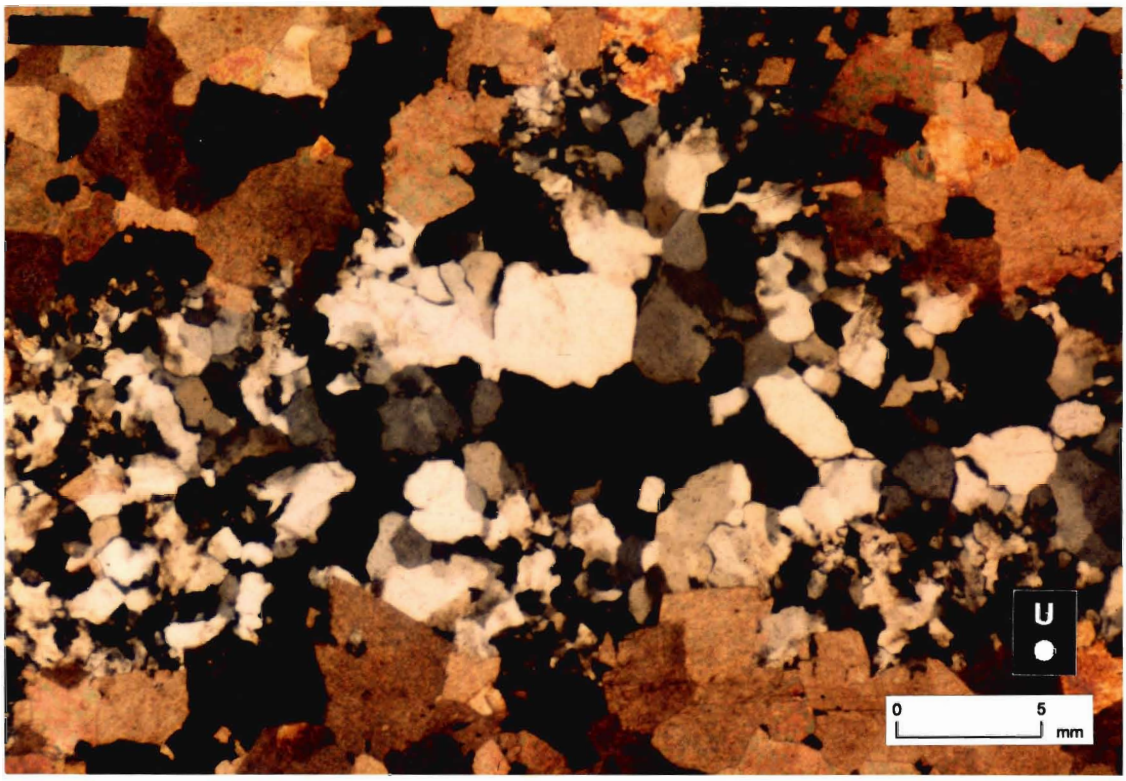
U
0
5
mm

upper sections of the wells show some occurrences of silica, but it occurs mainly as small (0.1-0.3 mm), rounded to subrounded grains of quartz whose origin may be detrital.

The silicification occurs as:

1) replacement of bioclastic material in the form of spherulitic quartz,

2) irregular shaped patches of spherulitic quartz either as finely crystalline (< 0.1 mm) or slightly coarser crystalline (0.1-0.2 mm),

3) laminae of chert replacing extensive areas of the rock, whose average grain size is 0.3 mm, and

4) within stylolitized seams and areas of argillaceous material.

The mode of emplacement and the timing of the silicification is not clear. Other important features include a partially filled cavity of chert containing remnants of dolomite, dedolomite and possibly anhydrite laths. These occurrences suggest that silicification took place after dolomitization of the rock matrix, and before saddle dolomite cementation and dedolomitization.

Stylolites

Stylolitization of the rocks occurred after the dolomitization of the rock matrix. Evidence of stylolitization during and after dolomite formation is noted by the predominence the Idiotopic-E dolomite within the pressure solution seams. Saddle dolomite has been observed within fractures extending away from stylolite seams. This suggests that the timing for the formation of saddle dolomite cement may be equivalent to the pressure solution process.

Pyrite and Anhydrite

Pyrite occurs extensively at the top of the 33821 Mersea 3-12-A well in the Cobourg Formation. The average grain size of the pyrite crystals is 0.3 mm. The pyrite replaces many of the microfossils (mainly

Plate 9a: Photomicrograph of stained thin section under polarized light of pyritized phosphate nodules, that occur between the top of the Cobourg and the overlying Collingwood Formations. Contact is sharp between the dolomitized Cobourg (white to clear) and the Collingwood Formation shales (light brown).
(U = up direction in core).

Plate 9b: Photomicrograph of stained thin section under polarized light of microfossils just below the contact of the Cobourg Formation. Microfossils are dominantly conodonts (phosphatic lag).
(U = up direction in core).

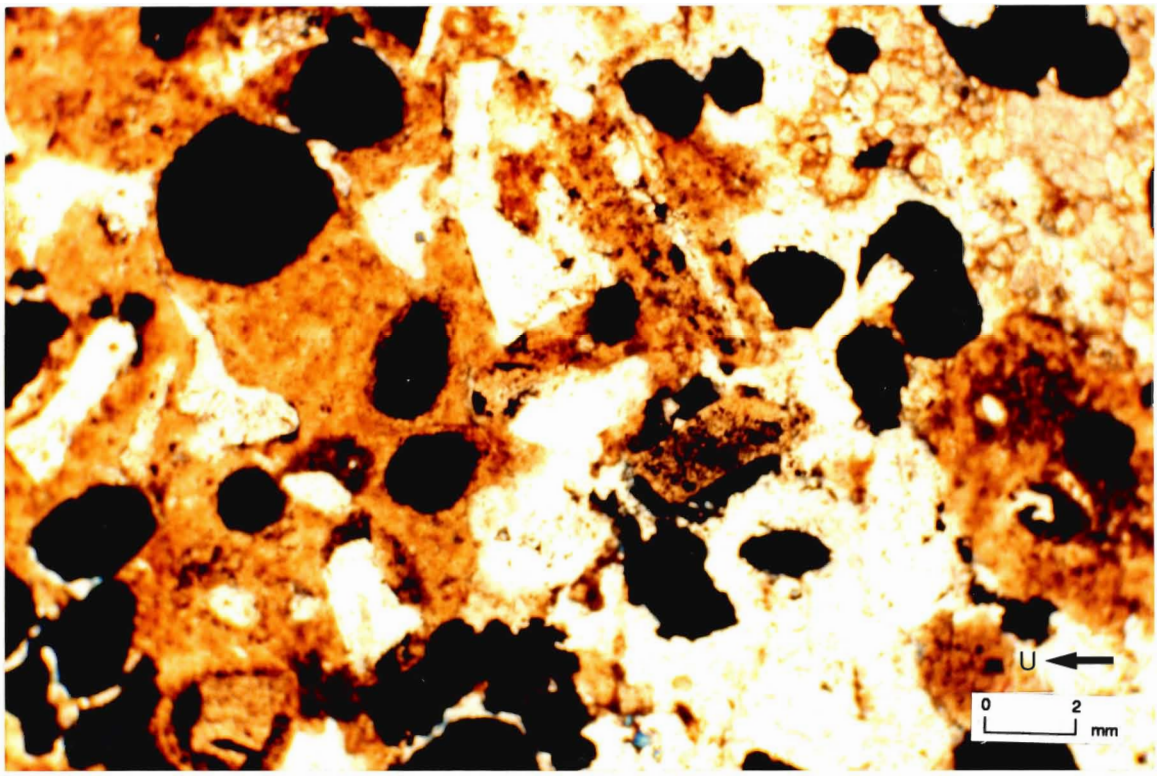
U
0
2
mm

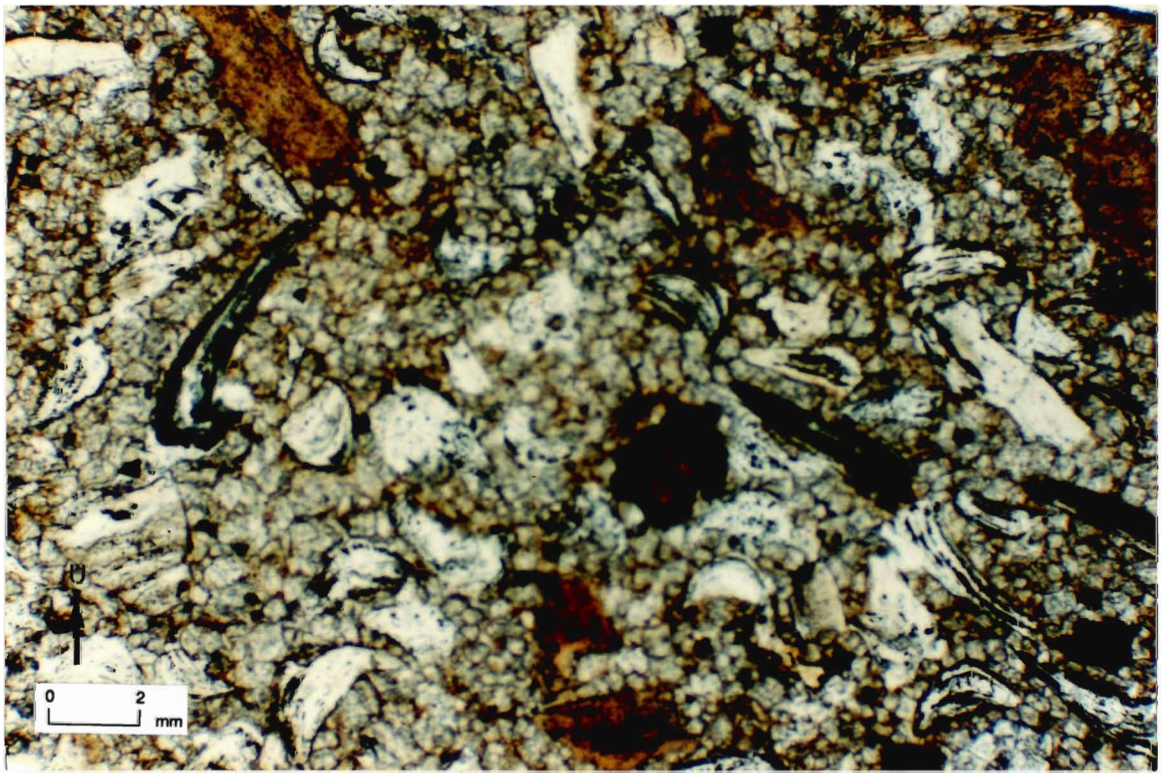
U
0
2
mm

conodonts, Plate 9a), and is also found lining what appears to be pre-existing phosphate nodules (Plate 9b). Presumably the nodules formed during the disconformable event prior to deposition of the shales of the overlying Collingwood Formation shales.

Crystalline pyrite also occurs with saddle dolomite and calcite cements within large vugs. It is also found as a major fracture lining mineral (Plate 10) in the 34160 Romney 5-8-II core. The grain size is variable (0.1-3 mm, average of 1.5 mm).

Anhydrite occurs as a vug filling cement within dolomites. Commonly it is associated with the formation of metalliferous veins and the oxidation of sulfides. Anhydrite can completely occlude the remaining porosity and permeability (Plate 11). Large, elongated laths of anhydrite (2-10 mm) are found in large vugs and fractures where it grew as elongated laths and radially (Plate 12).

Calcite, Sphalerite and Celestite

Late-stage Mississippi-Valley-Type minerals are calcite, sphalerite and celestite. These minerals are found together in vugs and cavities lined with saddle dolomite cement.

Two types of late stage calcite have been observed. Some calcite cement is euhedral with dog-tooth morphology, is of variable crystal size (1-30 mm, with an average crystal size < 10 mm), is ferroan, and generally clear to yellow in colour. This calcite is always associated with saddle dolomite that lines vugs and fractures. In other cases, blocky calcite occurs as late fracture and vug filling cement (Plates 9 and 13). Blocky calcite has variable crystal size (0.5-2 mm), is ferroan, and white to clear in colour.

Sphalerite occurs as euhedral to subhedral botryoidal masses (average grain size of 0.4 mm; Plate 14), characteristically is dark brown with amber terminations, and has a pyrite centre (Plate 15) which places its formation as post-pyrite. Sphalerite is followed by dog-tooth calcite

Plate 10: Photomicrograph of stained thin section under polarized light of dolomite matrix (on left) fractured and filled with pyrite and coarse blocky calcite cement. Pyrite crystals vary in size and are typically sub-euhedral. (CV = centre of vug; U = up direction in core).

Plate 11: Photomicrograph of stained thin section under plane light of a large fracture filled by saddle dolomite and elongated laths of anhydrite cement. These cements completely fill the fracture obliterating porosity and permeability. (U = up direction in core).

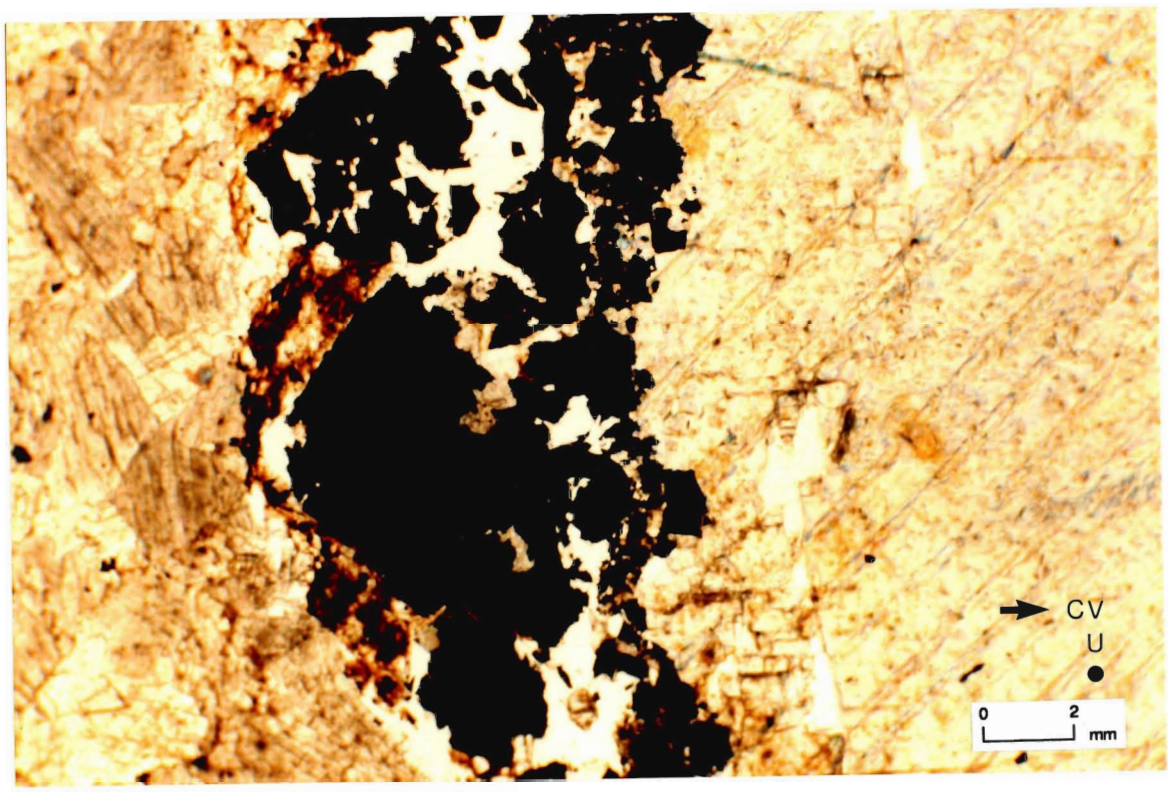
CV
U
0
2
mm

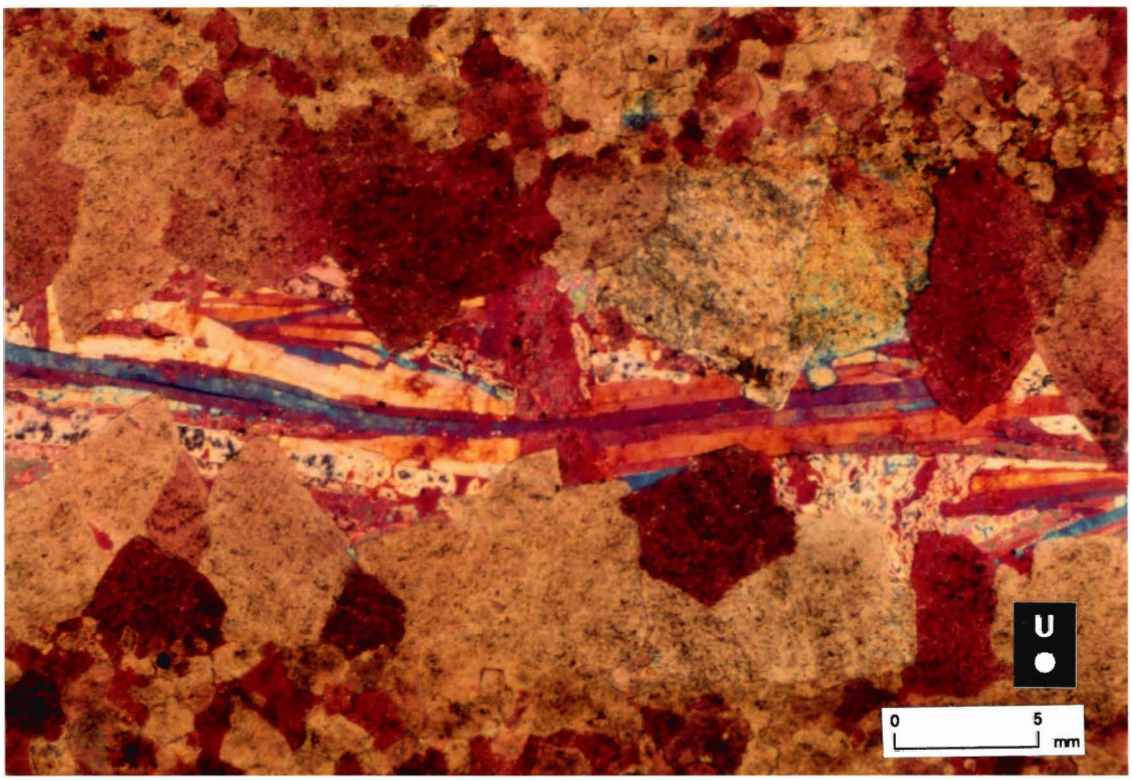
U
0
5
mm

Plate 12: Photomicrograph of stained thin section in plane light shows elongated laths of anhydrite within a large fracture. Pyrite occupies intercrystalline pore space. (U = up direction in core).

Plate 13: Photomicrograph of stained thin section under plane light of pyrite-lined fracture filled with late coarse blocky calcite.
(CV = centre of vug; U = up direction coming out of page).

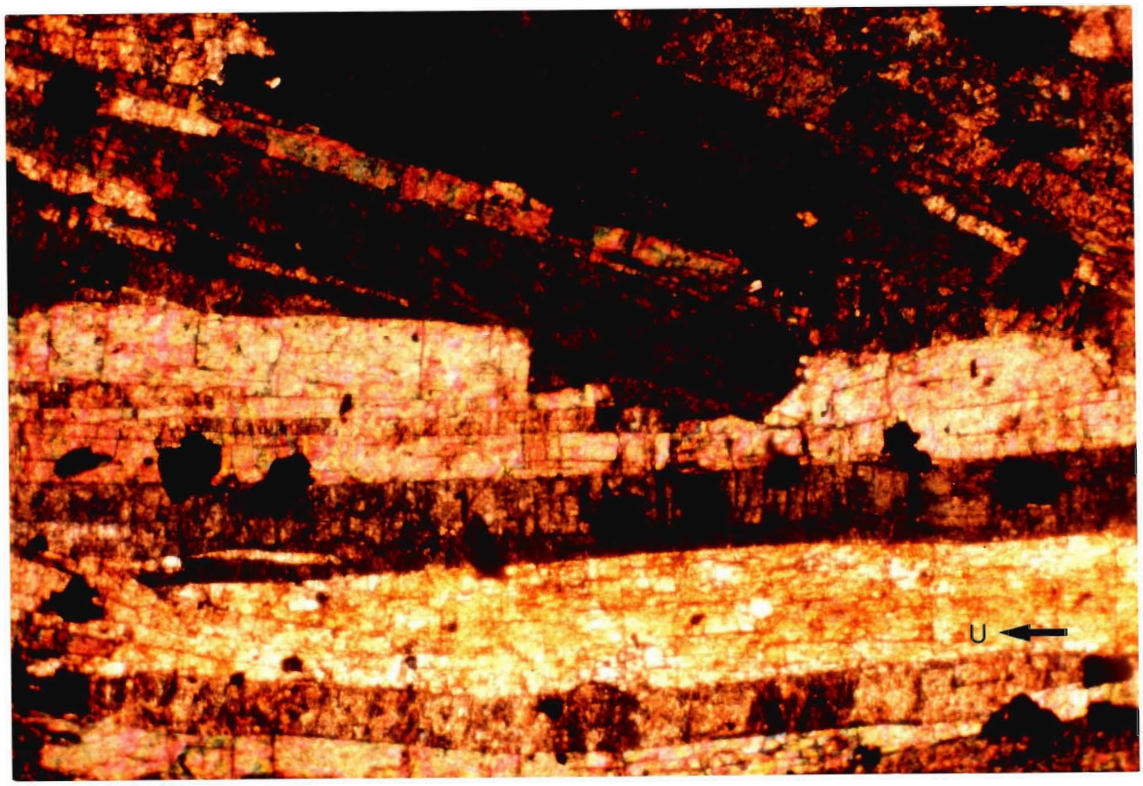
U

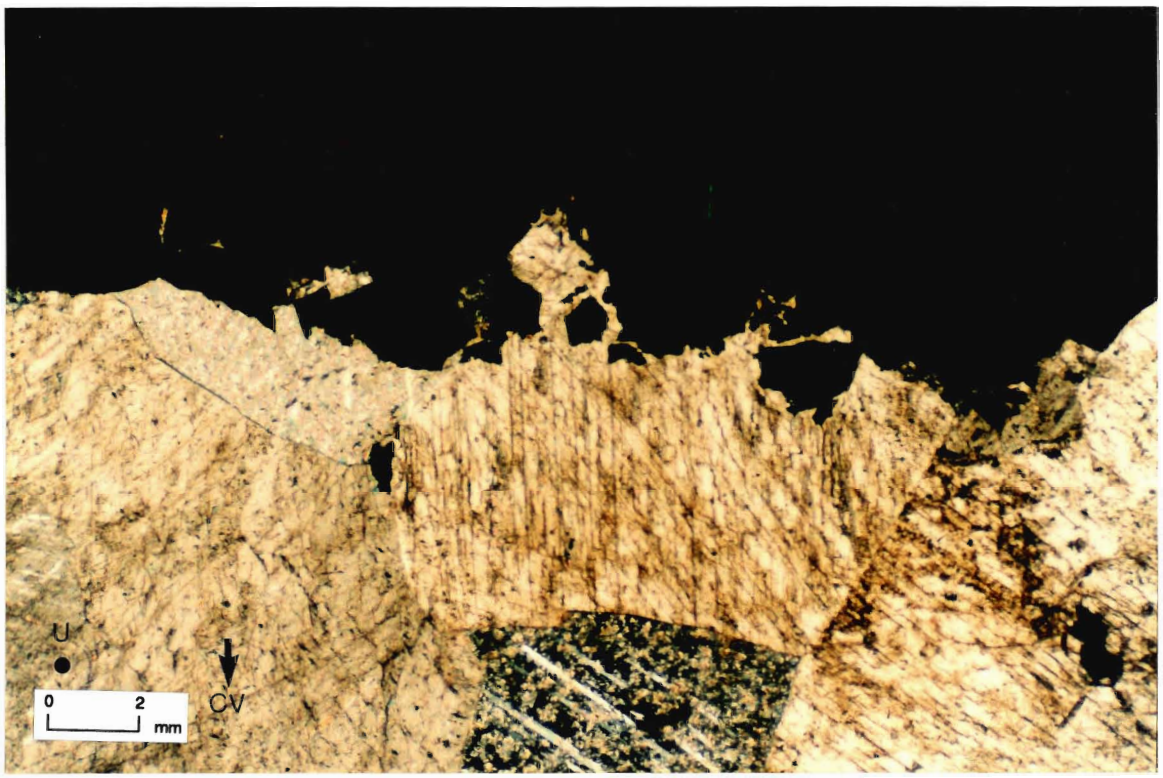
U
CV
0
2
mm

Plate 14: Botryoidal mass of sphalerite within a large vug (>7 cm in dia. x 4 cm in height). Rare botryoidal sphalerite occurs with dog-tooth calcite (white in photo) and pyrite within large cavities that are lined with saddle dolomite cement.

Plate 15: Photograph of the core of botryoidal sphalerite. Sphalerite has a core of pyrite.

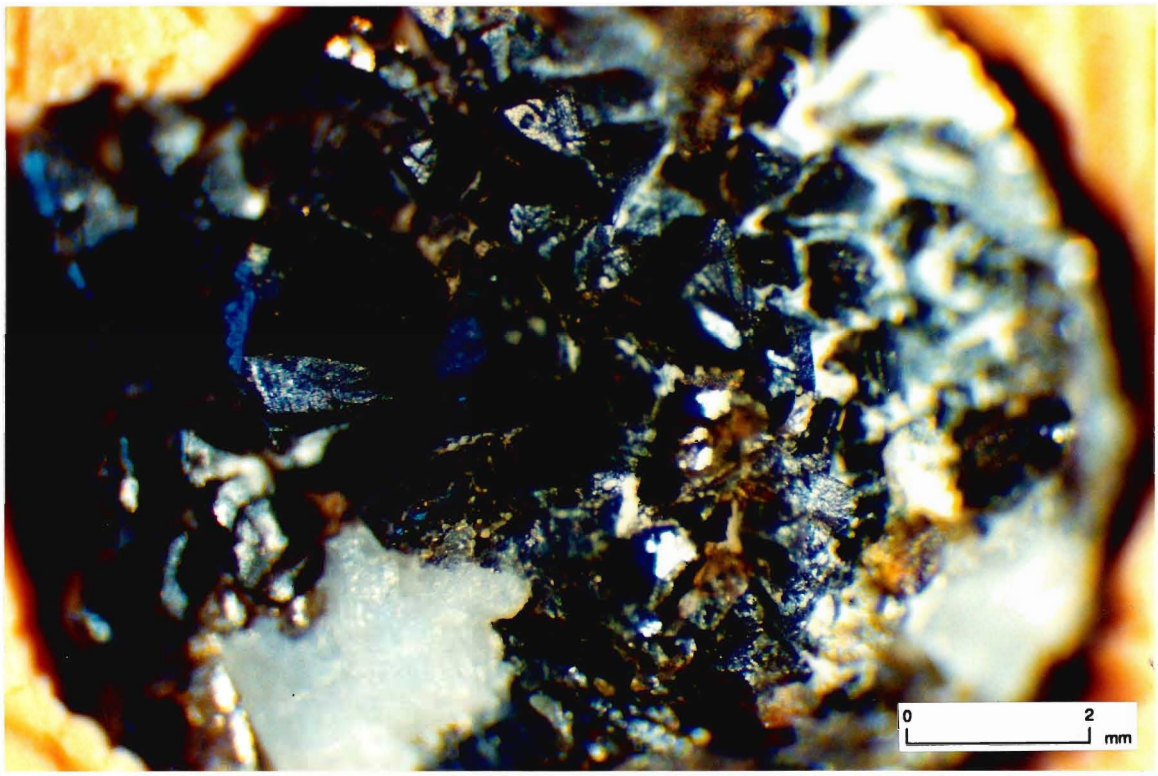
0
2
mm

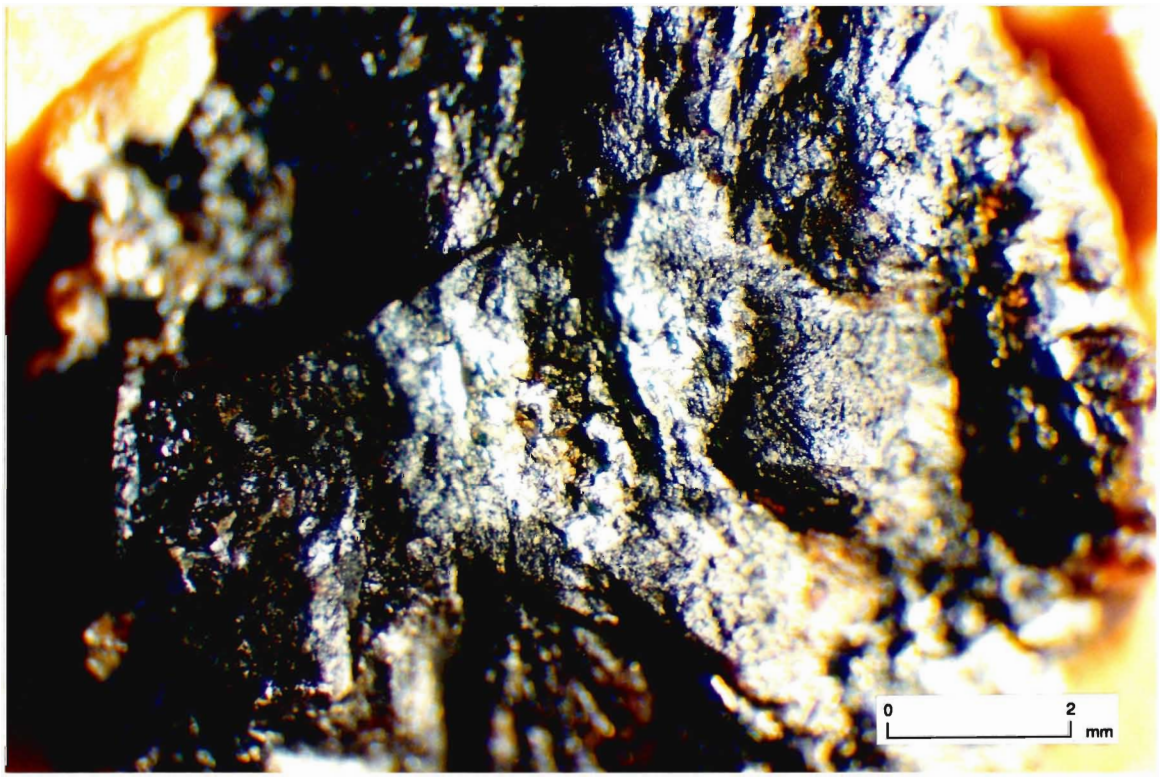
0
2
mm

cement placing its time of formation as post-pyrite formation and pre-dog-tooth calcite precipitation.

Celestite is the last mineral in the paragenetic sequence. It is typically coarse-grained, 5-10 mm, with elongated prisms which have a fine fibrous radiating character (Plate 16), and is white to reddish in colour. It occurs in large vugs (1-2 cm), or is deposited on the saddle dolomite, calcite, pyrite and sphalerite cements.

Porosity and Permeability

Most of the porosity occurs in Idiotopic-E dolomite which dominates the reservoir rock (Plates 3 and 4). The Xenotopic-A and Idiotopic-S dolomite form tightly interlocking crystals which exhibit very little or no porosity. The pore spaces within the Idiotopic-E dolomite are irregular in size and shape and are dependant on crystal size and arrangement. The overall distribution and percentage of porosity is uncertain since Idiotopic-E dolomite occurs with a variety of other dolomites. It may be that it is related to the original sediment type or rock type. Idiotopic-E dolomite commonly occurs within stylolites (highly argillaceous seams) suggesting that it is related to pressure solution and burial processes (Plate 17).

Other forms of porosity include minor occurrences of moldic, pinpoint, large vug (cavity), and fracture types within the Idiotopic-S dolomites and rare intercrystalline porosity within Xenotopic-A dolomites, that may account for less than 5% of the total. However, porosity has been reduced due to later filling by either coarsely crystalline saddle dolomite cement and/or late calcite cement within all the dolomites.

Plate 16: Blocks of fibrous celestite with orthorhombic cleavage terminations. Celestite occurs in large vugs lined with saddle dolomite (> 2 cm in diameter). Minor amounts of celestite occurs on crystal faces of many of the preceding mineralogies within large fractures and cavities.

Plate 17: Photomicrograph of stained thin section under polarized light of Idiotopic-E dolomite. Stylolite seams cross-cut allochems. Abundant bitumen fills both the intercrystalline pore space and the stylolites. (U = up direction in core).

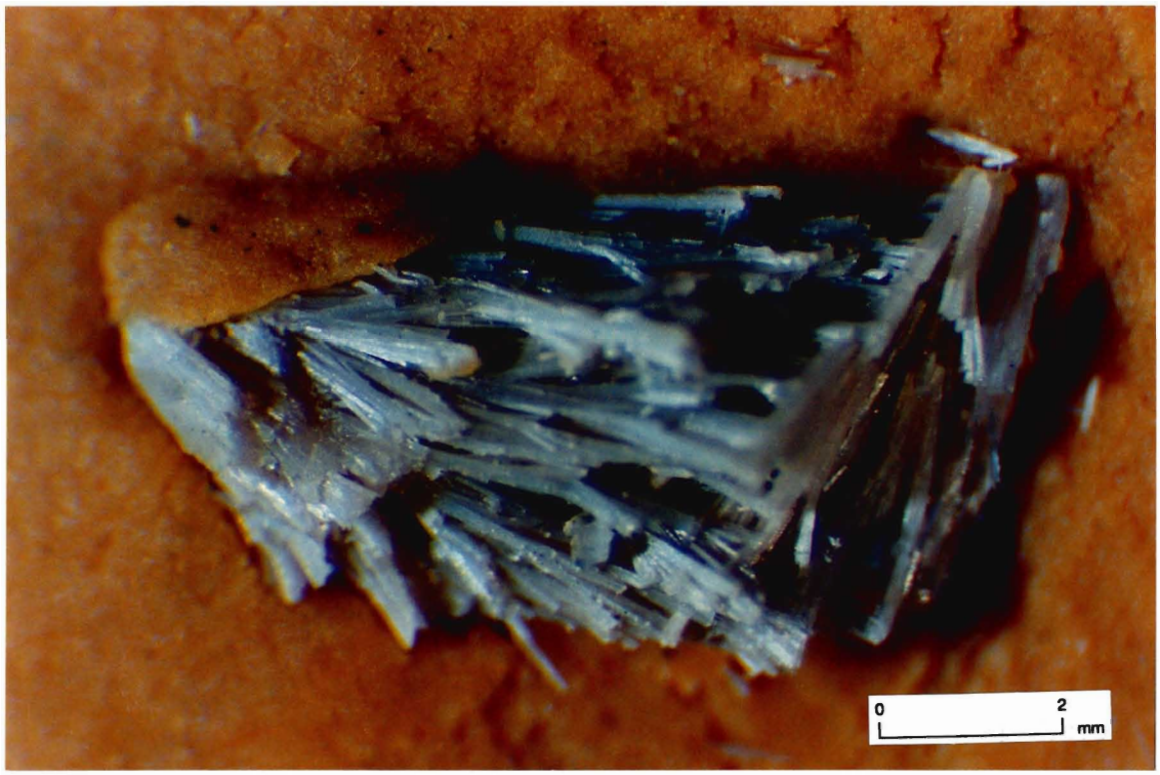
0
2
mm

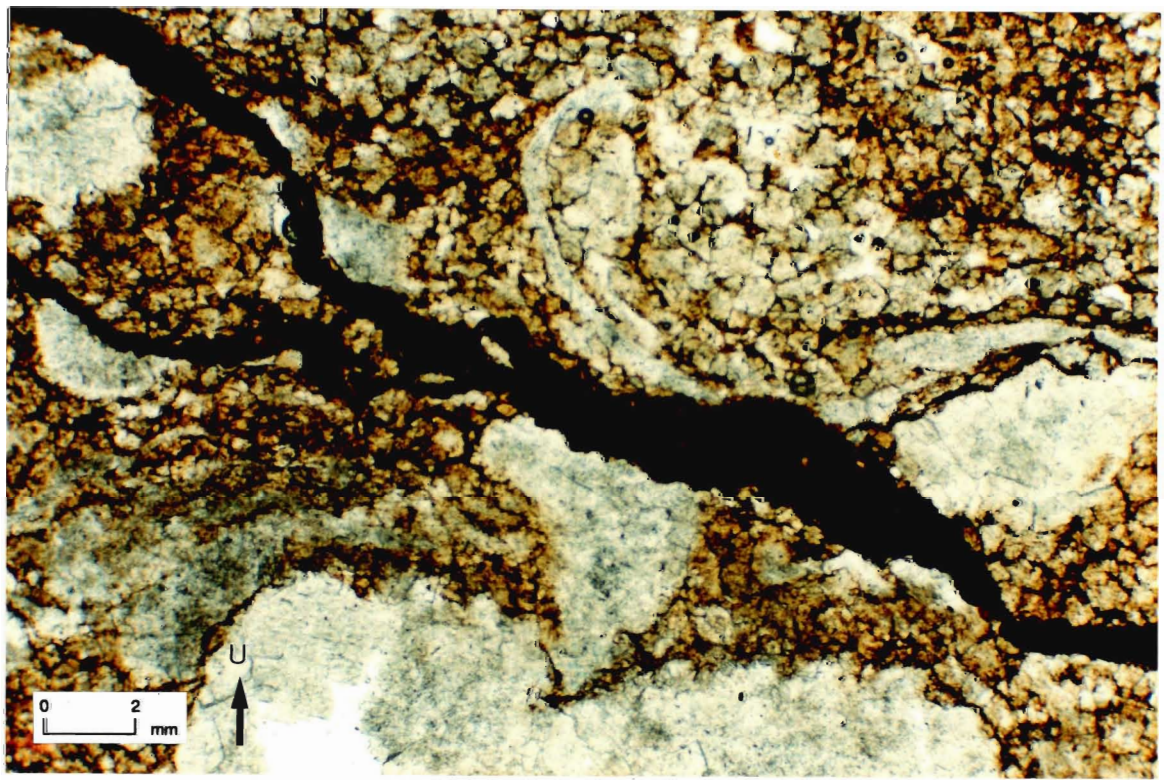
U
0
2
mm

Part 2: Cathodoluminescence

Textures produced from dedolomitization and calcite cements associated with dedolomite are;

1) Coarse-grained, euhedral dolomites (0.2-0.3 mm) are zoned within a finer-grained dolomite groundmass;

2) Coarse-grained, euhedral dolomite crystals (0.3-0.4 mm) are zoned;

3) Dedolomitization textures (physical breakdown with calcite replacement) are luminescent;

4) Calcite cement surrounding dedolomite;

5) Breakdown of saddle dolomite crystals with the replacement by calcite cement (see Plate 7);

6) Multi-zoned, more than two stages of zonation, Idiotopic dolomite crystals (0.3-0.4 mm) adjacent to lesser zoned dolomite crystals (0.2 mm) occur where pore space is present;

7) Local areas of groundmass luminesce dark red;

8) Calcite cement within the thin fracture luminesces yellow, and occurs with Fe-quenched Idiotopic dolomite which luminesces dark red. (Plates 18 a,b).

Textures that aid in determining the relative chemical composition of the fluids involved in the formation of saddle dolomite and calcite cements are:

1) Homogeneous luminescence of coarsely crystalline saddle dolomite and blocky calcite cements that occur within large vugs (Plates 19 a,b). This blocky form of calcite exhibits uniform equant crystal growth.

2) Homogeneous luminescence of saddle dolomite and dog-tooth calcite cements that occur within large fractures and vugs (Plates 20 a,b).

Dolomite rhombs and saddle dolomite crystals next to porous areas of the reservoir rock exhibit up to four stages of zonation, whereas dolomite within the tight matrix only show two stages of zonation. Homogeneous

Plate 18a: Photomicrograph under polarized light of dolomitized crinoid ossicle (light) that has been partially replaced by pyrite. (U = up direction in core).

Plate 18b: Cathodoluminescence photo of Plate 18a. Luminescence reveals the presence of a thin fracture of brightly luminescent calcite which cross cuts the matrix dolomite and the monocrystalline crinoid ossicle. (U = up direction in core).

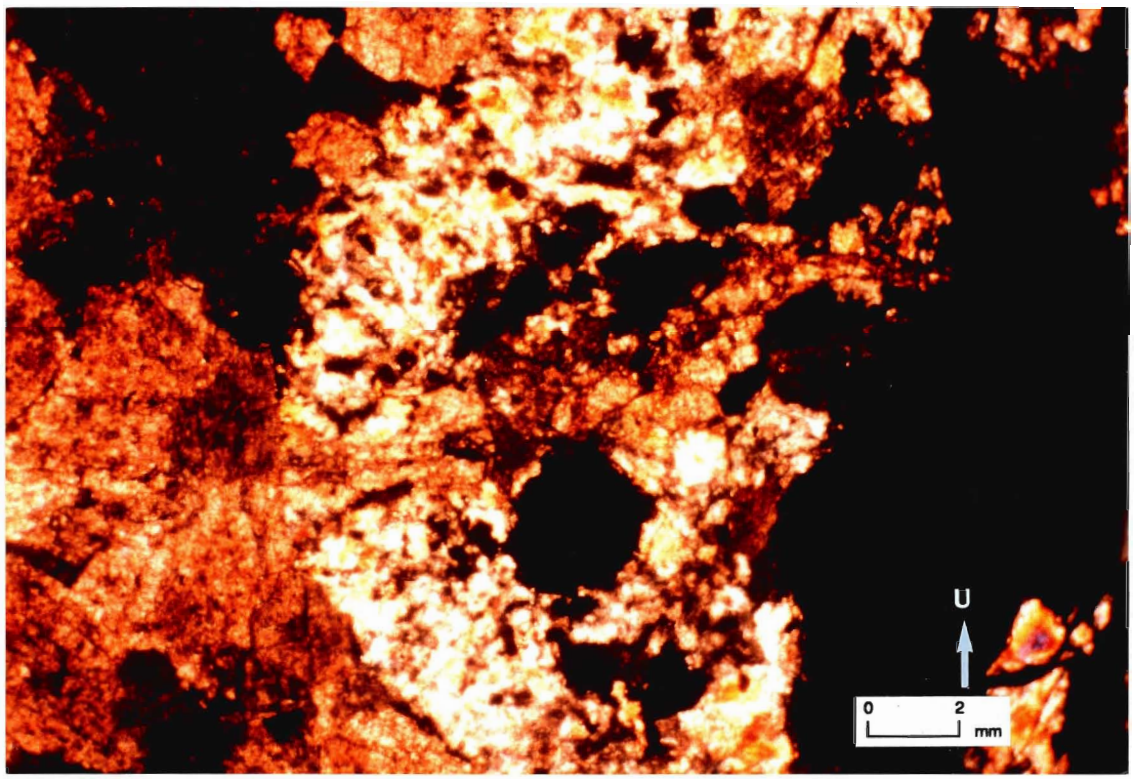
U
0
2
mm

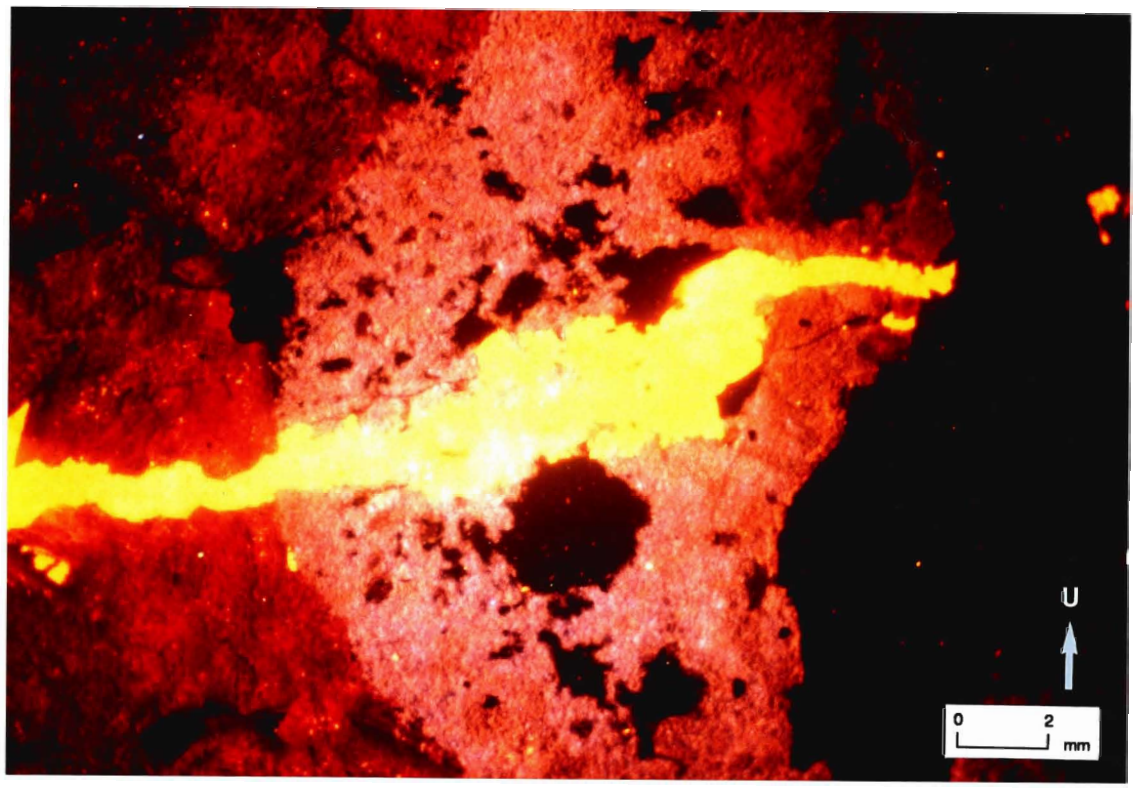
U
0
2
mm

Plate 19a: Photomicrograph under polarized light of a large saddle dolomite crystal within equant, blocky calcite cement. Saddle dolomite has a cloudy inner core with a lighter outer zone. The calcite cement appears homogeneous under polarized light.
(CF = centre of fracture; U = up direction in core).

Plate 19b: Cathodoluminescence photo of Plate 19a. Both cements show relatively homogeneous luminescence. A small saddle dolomite crystal in calcite cement has the same luminescence as the neighboring saddle dolomite crystal. (CF = centre of fracture;
U = up direction in core).

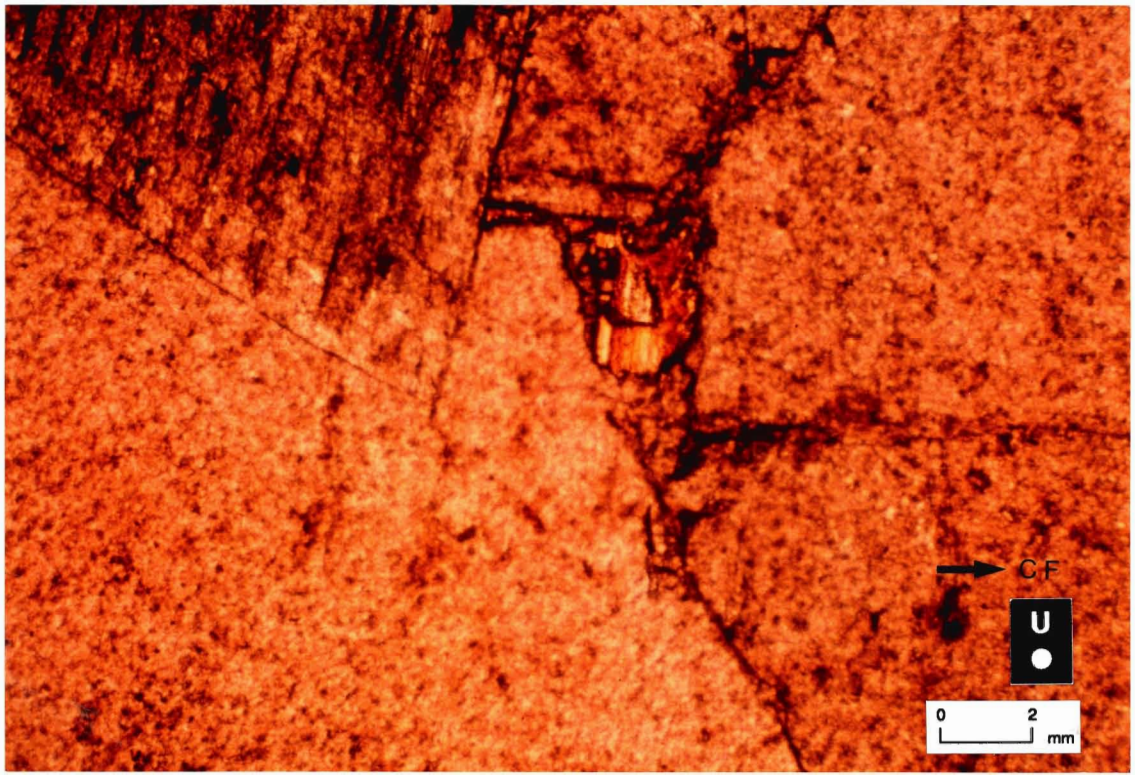
CF
U
0
2
mm

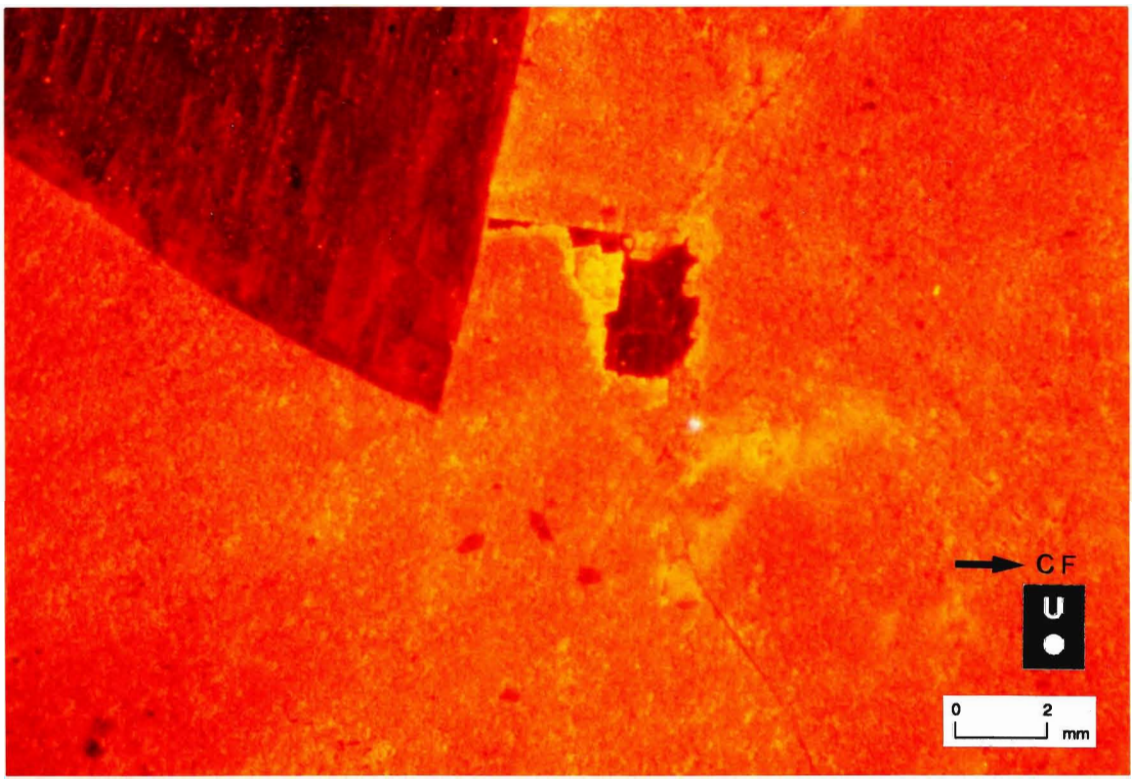
CF
U
0
2
mm

Plate 20a: Photomicrograph under polarized light of late dog-tooth calcite cement growing within large fractures showing typical calcite twinning and relative homogeneous composition.
(CC = centre of crystal; U = up direction in core).

Plate 20b: Cathodoluminescence photo of Plate 20a showing relative homogeneous luminescence. (CC = centre of crystal).

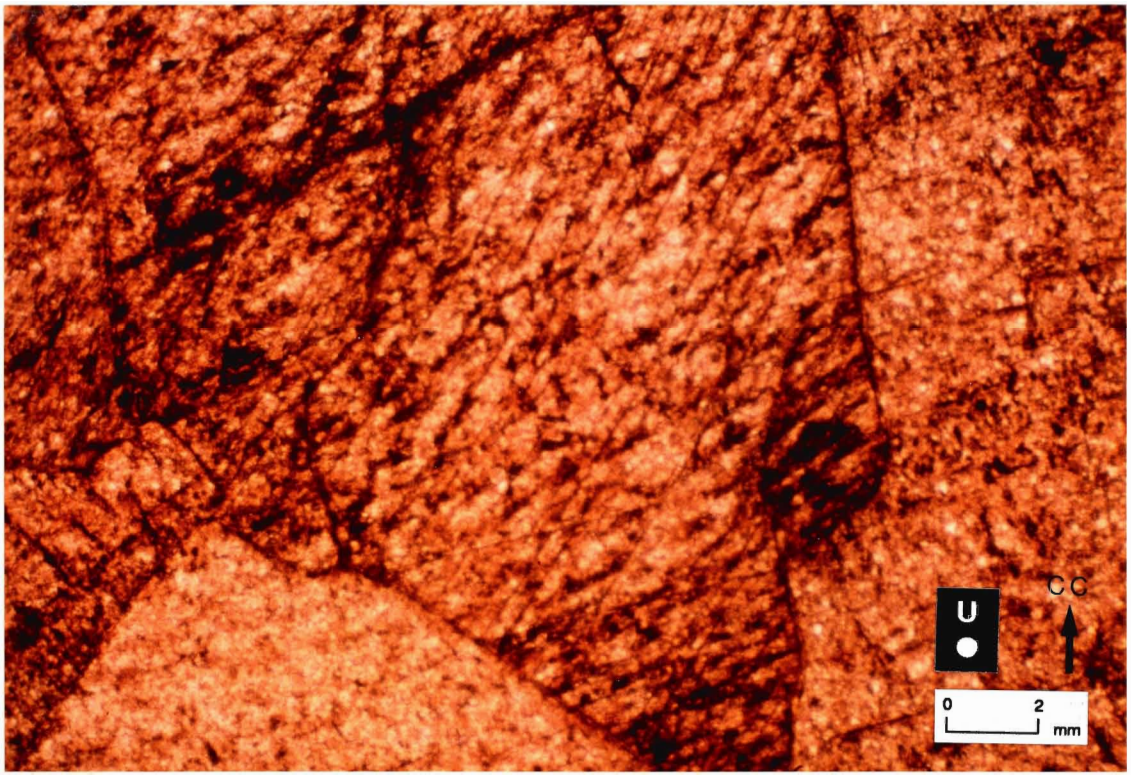
U
CC
0
2
mm

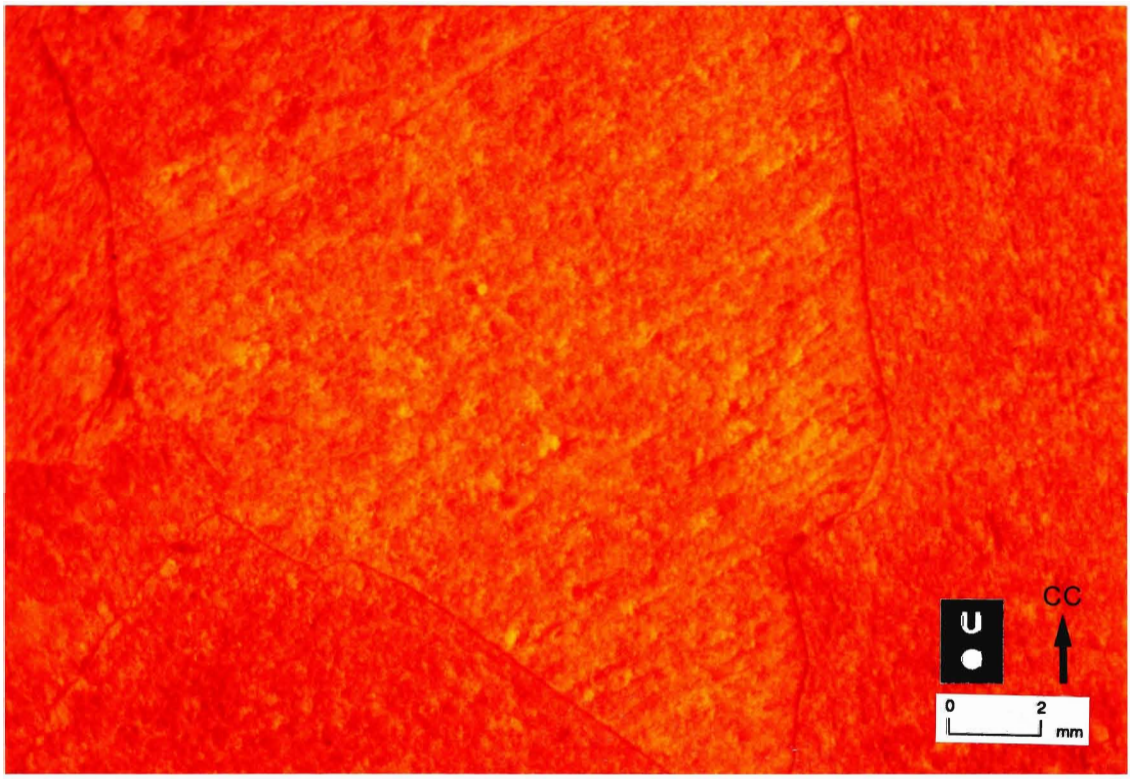
U
CC
0
2
mm

luminescence of saddle dolomite, blocky calcite and dog-tooth calcite cements within large fractures and vugs (Plates 19b and 20b) suggest that they precipitated from fluids with little or no variation in the fluid chemistry throughout their precipitation processes.

Cathodoluminescence illustrates the compositional zoning within calcite cements due to the variability in the Fe and Mn content within subsequent growth layers, and to a lesser extent Mg (Meyers, 1978). Meyers (1978) stated that luminescent zones can be interpreted simply as being Mn-rich, and non-luminescent zones as being Mn-poor. Luminescence is dependant, however, on the Fe/Mn ratio and not the absolute concentrations of either cation. Each zone represents a discrete episode of cementation (Meyers, 1974) or a "time stratigraphic" unit (Meyers, 1978) indicative of compositional variation of Fe and Mn in the diagenetic fluids.

The dolomite crystals examined under cathode luminescence exhibit similar physical features described by Fairchild (1980) as type 2 dolomite. This is a chemically altered dolomite with pronounced crystal faces, often with compromise crystal boundaries, formed during the replacement of a carbonate precursor. This dissolution-reprecipitation process generally takes place along a moving solution film during cementation.

Part 3: Ultraviolet Fluorescence

Fifty thin sections were examined under Ultraviolet fluorescence. Fluorescence of hydrocarbon inclusions are abundant in saddle dolomite cements that line fractures (Plates 21 a,b). Hydrocarbon inclusions also occur in the later stage saddle dolomite and pyrite cements, within fracture-related cements (Plates 22 a,b). Lack of hydrocarbon inclusions in calcite cements may be due to the small size of the inclusions or their complete absence.

Plate 21a: Photomicrograph under polarized light of earliest saddle dolomite within a large fracture. Boundary of dolomite crystal is outlined to establish a reference point.
(CF = centre of fracture; U = up direction in core).

Plate 21b: Photomicrograph under ultraviolet fluorescence showing the boundary of earliest saddle dolomite cement within a fracture. Fluorescence of hydrocarbons (yellow) in fluid inclusions within saddle dolomite cement. (CF = centre of fracture;
U = up direction in core).

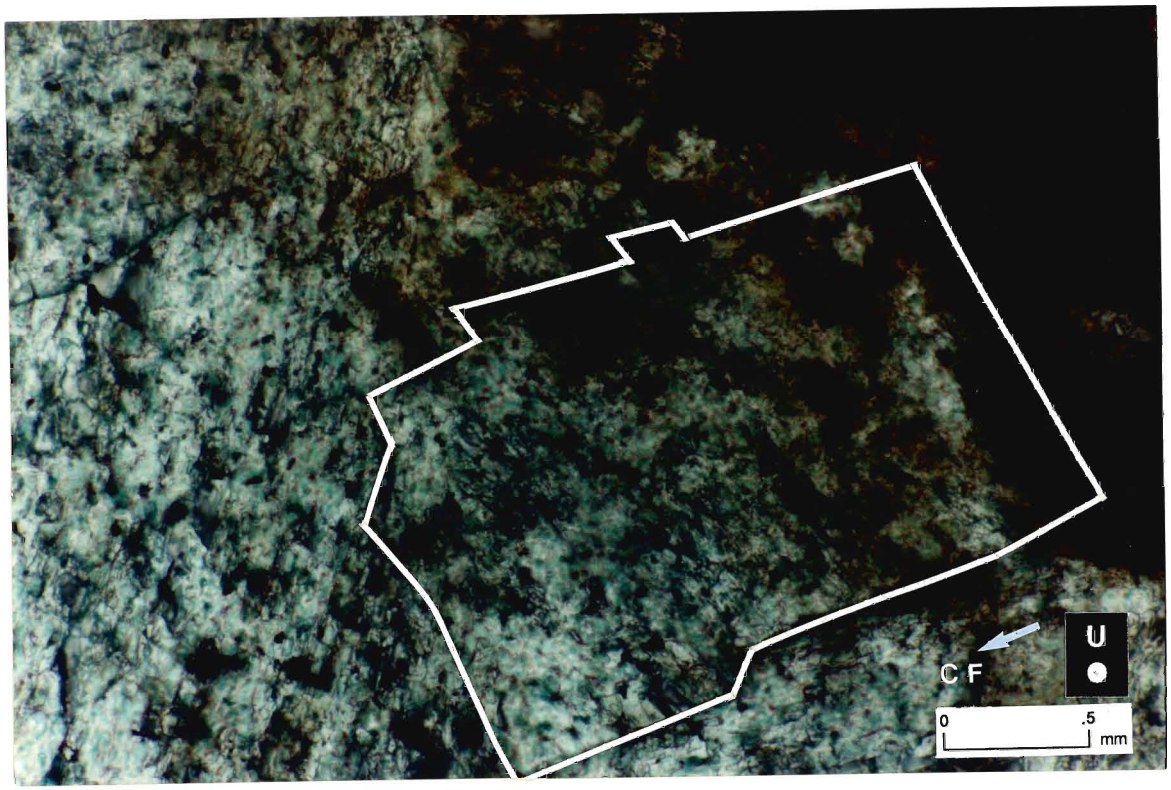
C F
U
0
.5
mm

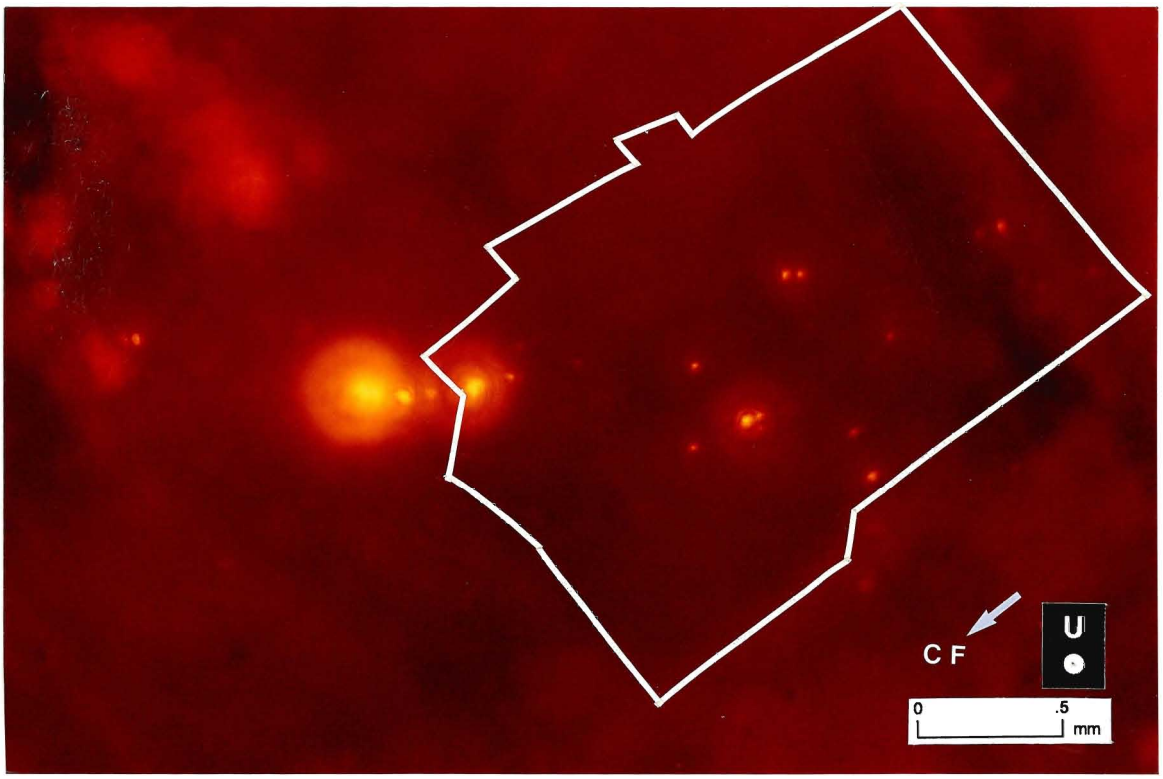
C F
U
0
.5
mm

Plate 22a: Photomicrograph under polarized light of intercrystalline pyrite within a fracture filled with saddle dolomite cement. (CF = centre of fracture; U = up direction in core).

Plate 22b: Photomicrograph under ultraviolet fluorescence shows the fluorescence of hydrocarbons in fluid inclusions within saddle dolomite and pyrite cements. (CF = centre of fracture; U = up direction in core).

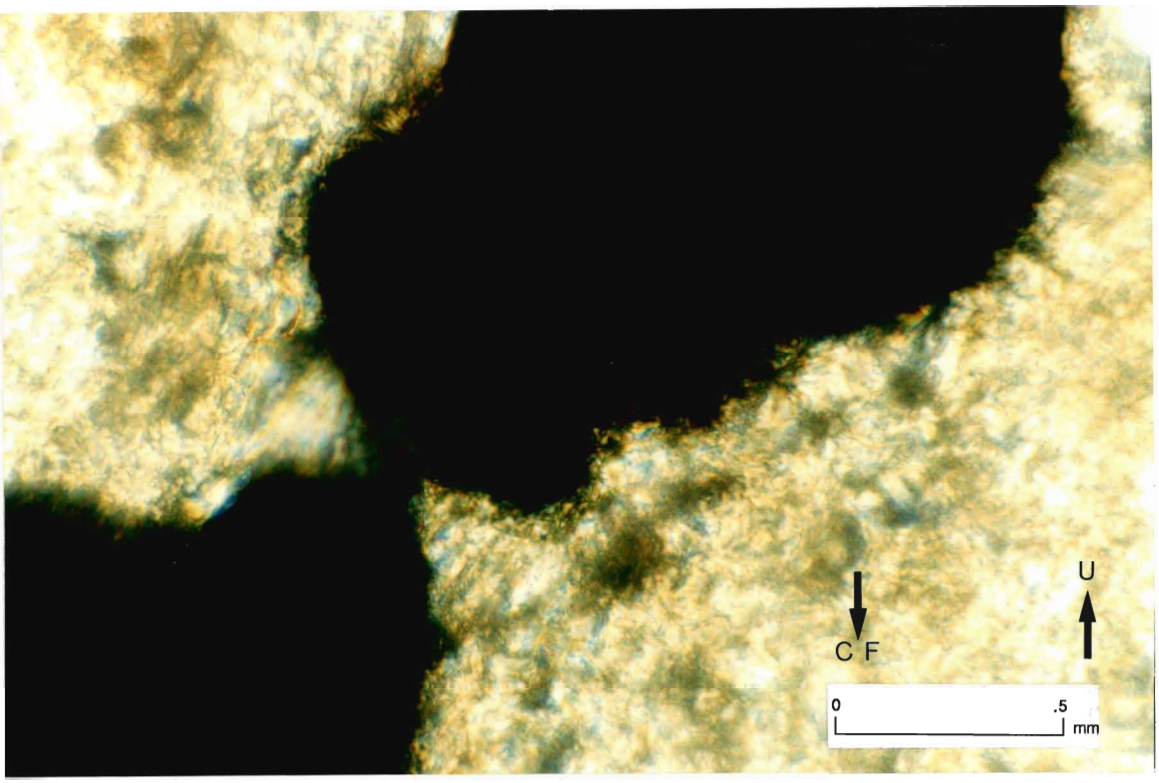
C F
U
0
.5
mm

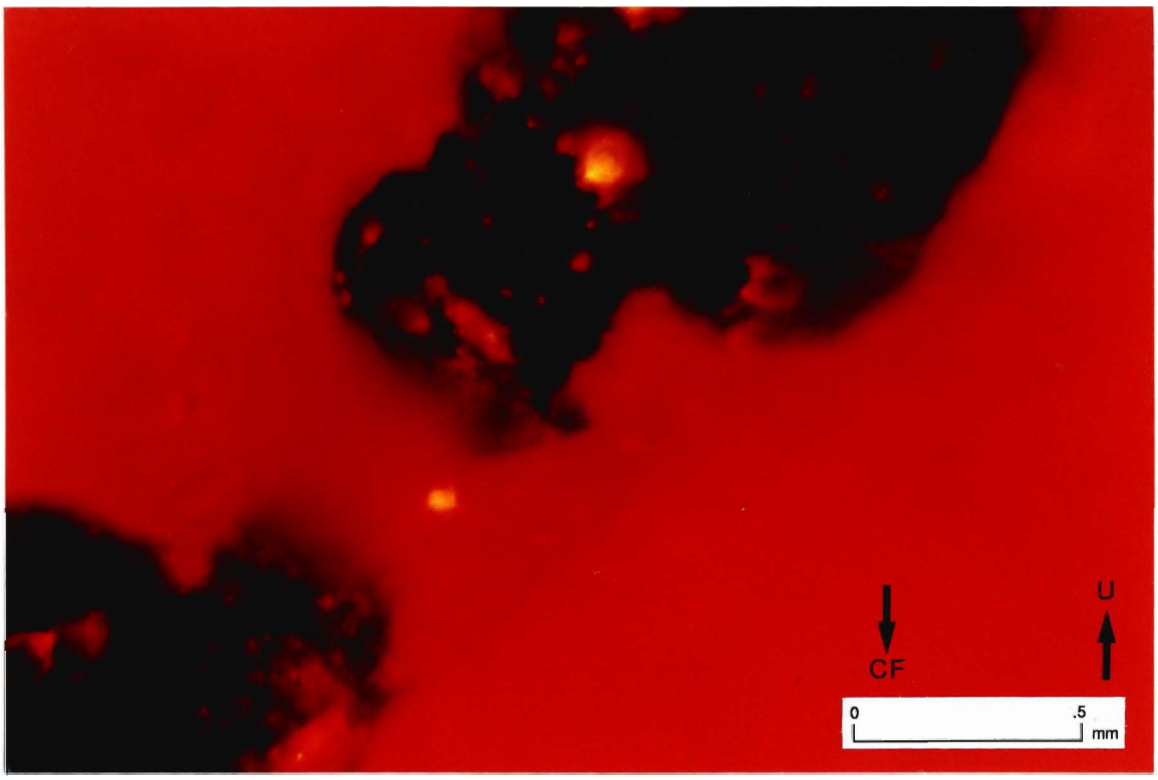
CF
U
0
.5
mm

Geochemical Results and Discussion

Calcium and Magnesium

The limestones from the 33821 Mersea 3-12-I and the 33823 Mersea 1-12-A wells have concentrations of Ca (300,00 to 290,000 ppm Ca), and exhibit corresponding depletions in Mg (36,000 to 24,000 ppm Mg) (Appendix III).

The matrix dolomites from the four wells contain variable concentrations of Ca and Mg (240,000 to 200,000 ppm Ca and 120,000 to 98,000 ppm Mg), whereby their absolute concentrations are due to the variable insoluble residue and high Fe contents (28,000 to 20,000 ppm) (Appendix III). The variations in the Mg and Ca concentrations are a reflection of the variable limestone content within these dolomites, which occurs in both the 33821 Mersea 3-12-I and the 33823 Mersea 1-12-A wells.

Strontium

The Sr concentrations for the limestone varies between 74 - 828 ppm, with an average of 541 ppm (N = 14 samples). The dolomitic limestones have Sr concentrations between 12 - 490 ppm (average 242 ppm, N = 15 samples), and dolomites have much lower Sr concentrations of 22 - 133 ppm (average 70 ppm, N = 323 samples; Appendix III). The progressive depletion is suggested to be due to the effects of the smaller partition coefficient for Sr in dolomite. Dolomites which form in normal sea water have theoretical equilibrium concentrations between 470 to 550 ppm of Sr (Veizer, 1983). Limestones and dolomitic limestones usually have Sr concentrations between 100 - 1000 ppm, whereas the Sr content of late diagenetic dolomites are between 30 - 100 (150) ppm (Veizer and Demovic, 1974; Veizer et al., 1978c), or between 60 to 105 ppm for burial dolomites (Machel and Anderson, 1989). Ancient dolomites with Sr concentrations in excess of 600 ppm are thought to have formed in the

presence of hypersaline solutions (Veizer, 1983). It has been postulated that only under evaporative conditions, accompanied by the precipitation of gypsum, could the $^{m}Sr/^{m}Ca$ ratio of sea water be elevated to values necessary for precipitation of dolomite with Sr values greater than 600 ppm (Veizer, 1983). However, Machel and Anderson (1989) suggested that dolomites formed under evaporitic conditions have Sr concentrations as low as 155 ppm.

Assuming that the dolomite formed in equilibrium with the bulk aquifer pore waters, the diagenetic dolomites of the Trenton Group could not have formed in a normal marine environment. Generally, the older or more mature the dolomite the more depleted it will be with respect to Sr. Land (1980) reported that dolomitization of an limestone leads to an enrichment in Mg and depletions in Sr and Na in the resultant dolomite. With the additional flushing of the pore fluids over long periods of time after burial, the Sr contents of dolomites can be reduced due to dissolution-reprecipitation processes (Sears and Lucia, 1980).

Sodium

The Na concentrations of the limestones varied between 463 - 1000 ppm (average 641 ppm), the dolomitic limestones have elevated Na values between 410 - 2000 ppm (average 718 ppm), and the dolomites have even more enriched Na values between 400 - 2300 ppm (average about 1000 ppm) (Appendix III). The average Na values of the Trenton dolomites are much higher than dolomites forming under normal marine conditions which have Na concentrations between 110 - 160 ppm (Veizer, 1983). Burial dolomites from the Nisku Formation are reported to have Na concentrations between 30 to 370 ppm (Machel and Anderson, 1989). The elevated Na values in Trenton dolomites may be due to NaCl liquid and/or solid inclusions within the various carbonate matrix. Land (1980) attributed the increase in Na concentration in dolomites to the

recrystallization of the rock by dolomitizing fluids that are enriched with respect to Na. The use of Na as a paleosalinity indicator for dolostones is possible if the origin of the Na ion can be determined, and if Na is not derived from fluid inclusions.

Covariant Trace Element Trends
Strontium and Sodium

There is a noticeable increase in Sr concentration (accompanied by a large increase in Na) in the upper three metres within all the wells. The Sr concentrations for the matrix dolomites increase from an average of 60 ppm up to 500 ppm over a 3 m interval just beneath the overlying Collingwood Shale Member of the Lindsay Formation. Corresponding Na concentrations for these dolomites vary between 400 ppm up to 2000 ppm (Appendix III).

The rock samples that reflect the highest enrichments in both the Sr and Na trace elements are generally an argillaceous dolomite that lies just beneath a 2 cm thick seam of pyrite (-765.5 m), that occurs in the 33821 Mersea 3-12-I and the 33823 Mersea 1-12-A wells.

Strontium and Manganese

The covariant trace element trend between Sr and Mn suggests upward migration of the dolomitizing fluids near the top of the Cobourg Formation from the 34160 Romney 5-8-II well (Figure 10). The variation of Sr and Mn trace elements in matrix dolomites versus depth demonstrates an enrichment of Sr but not Mn at the top of the cored interval. This anomaly occurs in all the wells. According to Machel (1988), the qualitative analysis of the Sr and Mn trace element distribution of bulk dolomite samples can be used to identify flow direction of the dolomitizing fluids. The Sr increases in the flow direction of the dolomitizing fluids with a concomitant depletion in Mn. This relationship is

possible for trace elements, such as Sr, with partition coefficients << 1, and assuming that the $^{m}Sr/^{m}Ca$ ratio of the fluid is equal to or lower than the carbonate precursor (Machel, 1988). The trace elements with distribution coefficients greater than 1, such as Mn, should either decrease in the downflow direction, or become sympathetic or antipathetic to the trend for Sr (Machel, 1988). This apparent trace element trend occurs approaching the top of the Cobourg Formation at the 807 to 805 m level (Figure 10). This relationship in the Sr and Mn trace element distribution does not appear to occur elsewhere except at the 822 m level. However, this apparent trend in the Sr and Mn trace element distribution suggests that the dolomitizing fluids moved vertically from depth before moving horizontally along the contact with the impermeable overlying shales.

Limestone Diagenesis: Trace Element Trends

Factor analysis of the compiled data for all limestones and dolomitic limestones (Factor 1, Table IX.1, Appendix IX) demonstrates that the predominant factor controlling trace element variations was dolomitization of the rock. The greatest variations in the trace element chemistry were the substitution of Mg, Fe and Mn for Ca during the dolomitization of the limestones. The trace elements Fe and Mn have distribution coefficients greater than one, therefore they are preferentially incorporated into carbonates during diagenesis under a wide range of reducing conditions (Veizer, 1983; Land, 1985).

In order to evaluate the diagenetic alteration of the limestones, the 1000 Sr/Ca trace element ratio versus the Mg trace element distribution is used to establish the pathway of alteration from the inferred original mineralogy of the carbonate precursor. Progressive enrichment in Mg concentration with subsequent depletion in the 1000 Sr/Ca ratio occurs with dolomitization (Figure 11). This variation is attributed to the dolomitization of the limestones in the presence of formational fluids

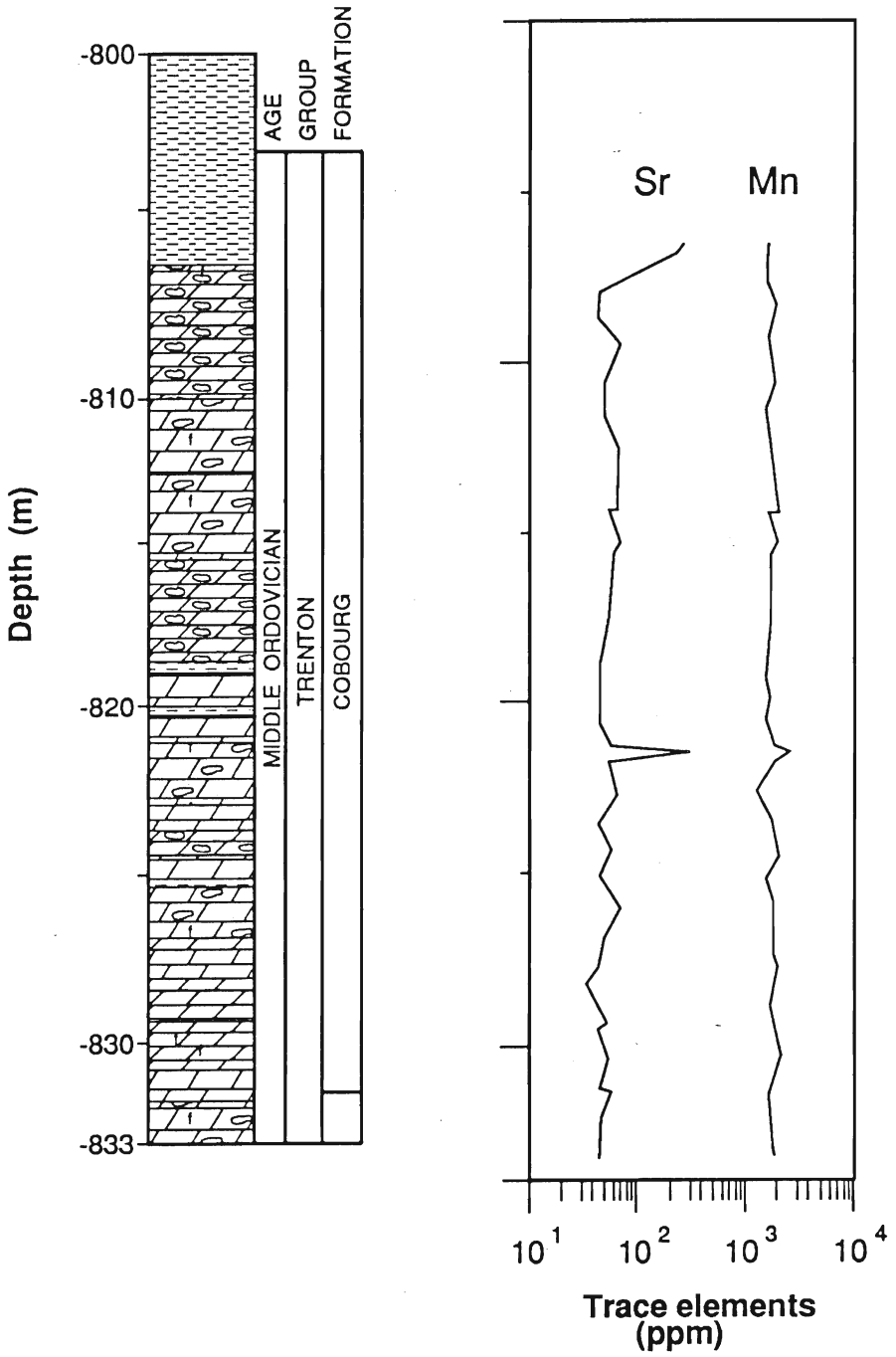

Figure 10: Strontium and Mn distribution of matrix dolomite vs depth within the upper portion of core of the 34160 Romney 5-8-II well.

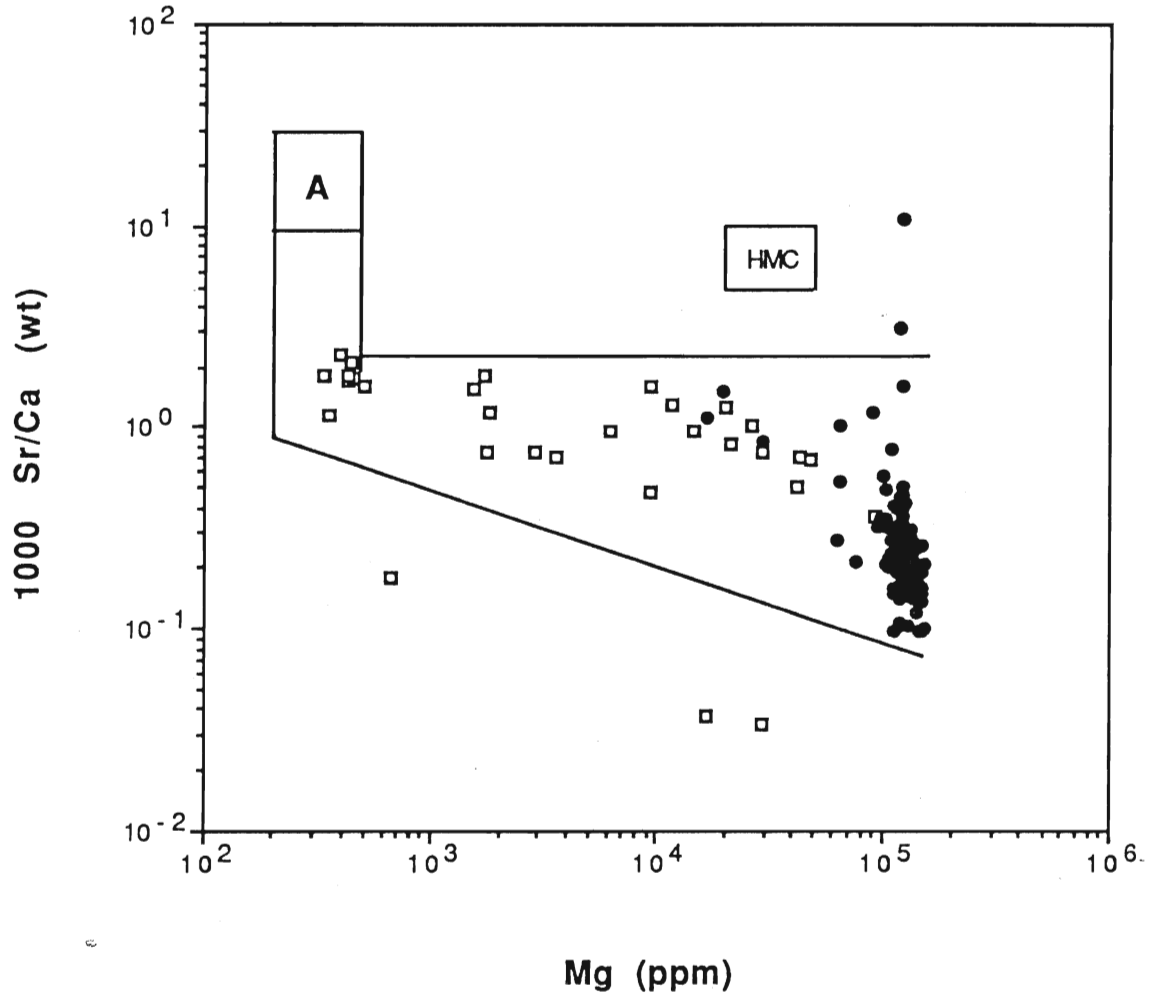

Figure 11: 1000 Sr/Ca ratio vs Mg demonstrates the diagenetic alteration of the limestones and dolomitization of the rock. Fields are outlined which represent the theoretical possible ranges for an inorganic aragonite (A) and that of high magnesium calcite (HMC) in elemental equilibrium with present day sea water (Bathurst, 1975; Milliman, 1974; similar to trends established by Brand and Veizer, 1980). (□) represent the subsurface limestone and dolomitic limestone samples. (●) represent the subsurface dolomite samples.

becoming enriched with respect to Mg and progressively depleted with respect to Sr. This alteration trend of the carbonate precursor is similar to alteration trends considered to represent progressive diagenesis from an originally aragonitic mineralogy (c.f. Brand and Veizer, 1980).

Limestone Diagenesis: Stable Isotope Trends

Isotopes of four brachiopods were analyzed from limestones in the 33821 Mersea 3-12-I and the 33823 Mersea 1-12-A wells along with their limestone matrix counterparts to establish changes during diagenesis. The stable isotopic composition of the most pristine signatures of the LMC and limestones plots with the expected isotopic signature of an Ordovician carbonate (Figure 12). The stable isotopic composition of an Ordovician carbonate was established by extrapolating the stable isotope values inferred from secular variation reconstructions for the Paleozoic (cf. Veizer and Hoefs, 1976; Veizer et al., 1986).

The progressive depletion in the $\partial^{18}O$ from -4 ‰ to -10 ‰, with a minor but positive variation in the $\partial^{13}C$ isotopic composition, between 0 and 1 ‰, suggests that the limestones and LMC mineralogies were altered during burial diagenesis due to rock-water interactions . Similar trends have been established (Milliman, 1974; Brand and Veizer, 1980; Dickson and Coleman, 1980). The depletion in the $\partial^{18}O$ isotopic composition of the limestones and dolomitic limestones suggests that the rocks had been altered in the presence of an isotopically light $\partial^{18}O$ formational fluid that evolved during burial diagenesis.

Further evidence of the evolution of isotopically light and, perhaps, warmer waters responsible for the alteration of the subsurface limestone and LMC minerals is provided by evaluation and comparison with the stable isotopic distribution of outcrop-equivalent Verulam limestones and brachiopods (Figure 13). If the stable isotopic composition, $\partial^{18}O$ from -4 to -6 ‰ and $\partial^{13}C$ from 1 to 2 ‰, from the outcrop brachiopod LMC represents

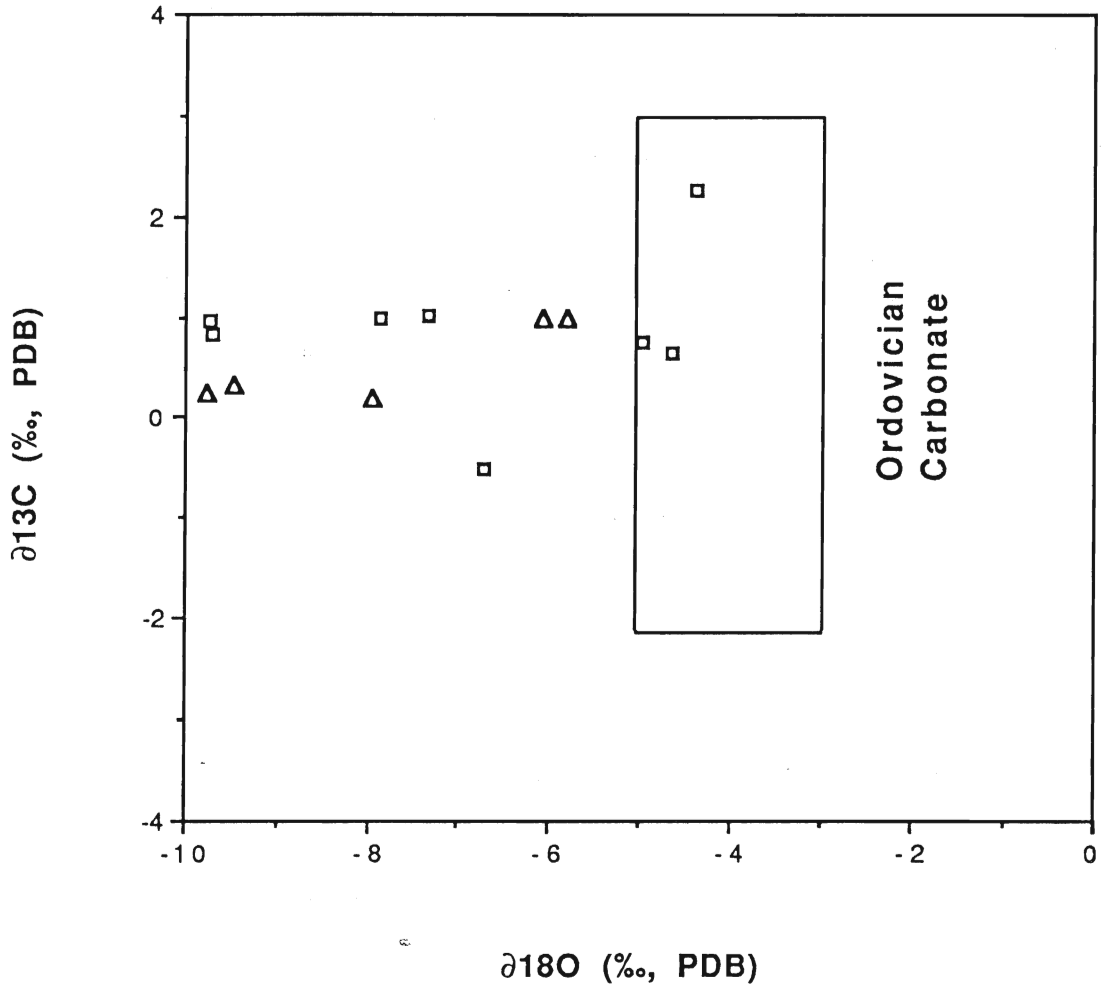

Figure 12: Stable isotopic compositions of the subsurface brachiopod (LMC) samples with their accompanying limestone counterparts. (□) represent subsurface limestone samples, and (Δ) represent the subsurface brachiopod samples. Field representing an Ordovician carbonate was determined by extrapolation of secular variation data from Veizer and Hoefs (1976) and Veizer et al. (1986).

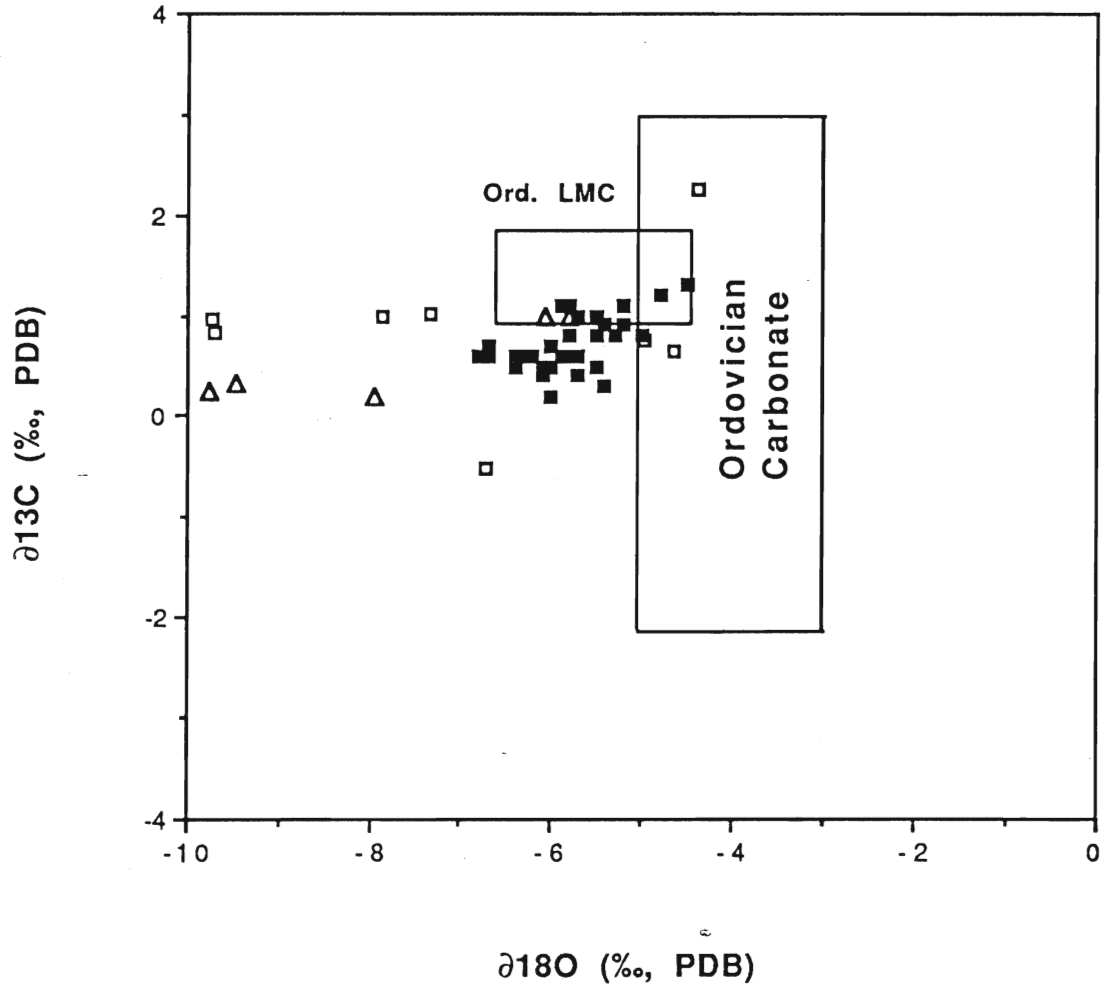

Figure 13: Stable isotopic compositions of the subsurface brachiopods (LMC) (Δ), with their accompanying limestone counterparts (□), and surface equivalent Verulam limestone (■), (Brand and Terasmae, 1986). Smaller rectangle represents the field for the best preserved surface equivalent brachiopod (LMC) samples, data from Bates (1989). Field of a typical Ordovician carbonate was determined by extrapolation of secular variation data from Veizer and Hoefs (1976) and Veizer et al. (1986).

the physicochemical composition of the ambient sea waters which precipitated the limestones, then the depletion in the oxygen isotope composition of the carbonates suggests that alteration proceeded during burial with increasing temperature.

Dolomitization: *Trace Element Trends*

Factor analysis of the trace element distributions for the dolomites from all wells illustrates that the greatest variations were enrichments in Mg, Fe and Mn with a corresponding depletion in Sr (Factor 1, Table IX.2, in Appendix IX). The variation in these trace element distributions is attributed to the variability of the dolomitizing fluids.

The Fe and Mg trace element distribution for the surface equivalent limestones and brachiopods, the subsurface limestones and brachiopods, and the subsurface dolomite samples, demonstrate the progressive diagenesis of the carbonates (Figure 14). The predominant diagenetic trend is the progressive enrichment in both Mg and Fe from the surface limestones to dolomitic limestones and dolomites. Dolomite samples have Fe and Mg trace element chemistry representative of ferroan dolomite, indicating that the dolomites formed from dolomitizing fluids with high Mg and Fe contents. It is postulated that the resultant 'ferroan' dolomite matrix formed in equilibrium with the dolomitizing fluids within a fluid-dominated process, or due to a high water/rock ratio (Brand and Veizer, 1980).

Also evident is the depletion in the Mg and Fe trace element composition of some limestones, which is expressed as an inverted J-shaped trend (Figure 14). This suggests that the undolomitized limestones experienced further diagenetic alteration. This is suggested to be due to progressive rock-fluid interactions with a fluid depleted with respect to Fe and Mg subsequent to the dolomitization process. This would also explain

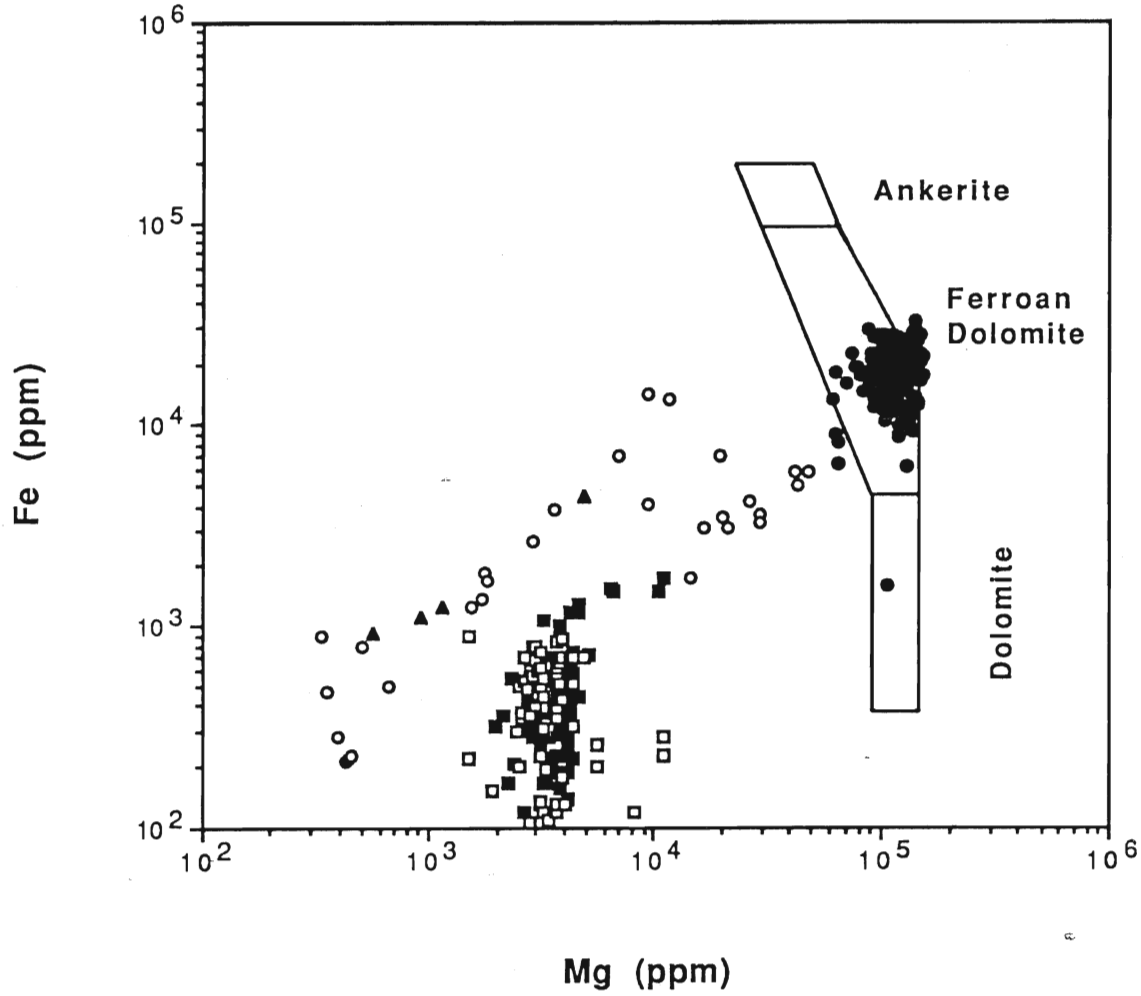

Figure 14: The Fe and Mg trace element distribution for surface limestones (■) (Brand and Terasmae, 1986), surface brachiopods (□) (Bates, 1989), subsurface limestone (o), subsurface brachiopods (▲), and subsurface dolomite (●). The trace element distributions of the carbonates are superimposed with the fields representing ankerite, ferroan dolomite and dolomite (Brand, in press).

the shift in the stable isotope and trace element trends in the subsurface brachiopod LMC components compared to those in outcrop.

Dolomitization: Stable Isotope Trends

The stable isotopic composition of the dolomites (Figure 15) are plotted relative to fields representing burial diagenesis from Figure 13. The $\partial^{18}O$ of the dolomites is more depleted than the limestones altered during burial diagenesis. If the dolomite had formed in equilibrium with the same parent solutions responsible for the precipitation of the limestones, then the $\partial^{18}O$ isotopic composition of the dolomites should be heavier than their limestone counterparts (Degens and Epstein, 1964; Veizer and Hoefs, 1976). However, post-depositional alteration of a limestone can lead to an overall decrease in $\partial^{18}O$ (Brand and Veizer, 1981) due to variations in temperature and the composition of the intervening fluids.

The dolomite samples from the four wells demonstrate considerable variation in $\partial^{18}O$. The depletion in the $\partial^{18}O$ isotopic composition for dolomites from the 33821 well, between -7.5 and -9 ‰, compared to the dolomites from the 34160 well, between -10 and -11.6 ‰, suggest that they are the result of the degree of diagenetic alteration and stabilization, and/or increased temperatures, or both.

The $\partial^{18}O$ mean values for the various dolomite types for all four wells show a systematic variation. The grainstones have the most depleted $\partial^{18}O$ values of -10.37 +/- 0.40 ‰, followed by the wackestones with $\partial^{18}O$ of -10.28 +/- 0.77 , and the mudstones with a mean $\partial^{18}O$ of -9.25 +/- 0.27 ‰. The limestones have also been separated by lithology and demonstrate a similar relationship. The wackestones have a mean $\partial^{18}O$ of -7.14 +/- 2.18 ‰, and the mudstones have a mean $\partial^{18}O$ of -6.89 +/- 0.99 ‰. The small variation in the overall mean $\partial^{18}O$ isotopic compositions between the dolomitized grainstones and wackestones can be attributed to the degree

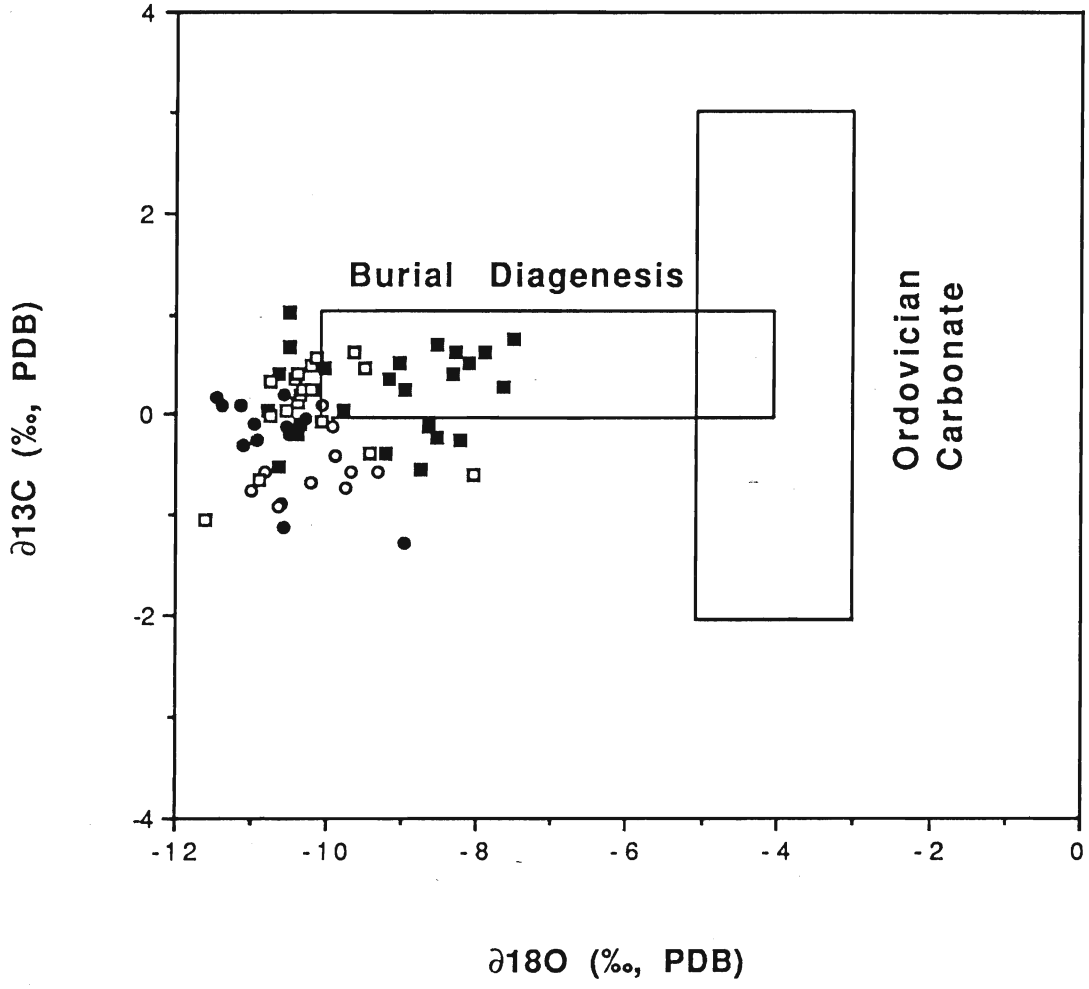

Figure 15: Stable isotopic composition of the dolomites from the 34160 well (●), the 34151 well (o), the 33821 well (■), and the 33823 well (□). Also shown are the stable isotope fields representing burial diagenesis and that of an Ordovician carbonate precipitated in the marine environment. Field representing an Ordovician carbonate was determined by extrapolation of secular variation data from Veizer and Hoefs (1976) and Veizer et al. (1986).

of diagenetic alteration. The systematic difference in the average $\partial^{18}O$ isotopic compositions between the dolomitized and undolomitized grainstones, wackestones, and mudstones, is postulated to be due to precipitation from different diagenetic fluids.

The variability in the $\partial^{13}C$ isotopic composition for the dolomites, when compared to the field representing burial diagenesis of the limestone, can be explained by a number of factors. The shift in $\partial^{13}C$ of 1 ‰ can be accounted for by diagenetic alteration (Brand and Veizer, 1981). The overall shift from positive $\partial^{13}C$ values to slightly negative $\partial^{13}C$ values suggest that the fluids responsible for the isotopic shift may have resulted from precipitation from basin brines at elevated temperatures (Degens and Epstein, 1964; Dickson and Coleman, 1980). Thode et al. (1965) and Bottinga (1968) demonstrated that at higher temperatures isotopic fractionation between carbon dioxide and carbonate is between 1-2 ‰ and is even smaller for bicarbonate-carbonate pairs. Large amounts of bicarbonate can originate from the non-equilibrium dissociation of marine carbonates due to thermal decomposition or dissolution by hydrothermal fluids. Carbonate precipitating in equilibrium with such bicarbonate will have similar isotopic composition of the original marine carbonates (Fritz, 1971). The limestones and dolomites have a relatively consistent range of $\partial^{13}C$ values, with only slightly negative values for the dolomites. This suggests that the fluids responsible for dolomitization could not have been dominated by meteoric fluids.

Saddle Dolomite and Calcite Cements: Trace Element Trends

The saddle dolomite cements contain Ca and Mg concentrations (200,000 to 240,000 ppm Ca, and 98,000 to 120,000 ppm Mg; Appendix III) similar to the enclosing dolomite rock matrix. The calcite cements contain relatively variable concentrations of both Ca and Mg (320,000 to 420,000 ppm Ca, and 200 to 10,000 ppm Mg; Appendix III). The

variability in the saddle dolomite, and particularly in the calcite cements, is attributed to the variable and high Fe contents of both cements.

Factor analysis of the trace element distributions for the saddle dolomites demonstrate the positive correlation for Mg, Fe and Mn (Factor 2, Table IX.3, Appendix IX). This is attributed to the preferential incorporation of these elements into the dolomite lattice. Radke and Mathis (1980) provided evidence that saddle dolomites are generally enriched in Ca, whereas their Mn and Fe concentrations generally reflect association with the host rock or the local conditions during their formation. Depletion in Ca is generally compensated by enrichments in Mg, Fe and Mn.

Factor 3 shows a strong positive correlation between Ca and Zn. The apparent enrichment in Ca is attributed to the physical adsorption of calcium on the saddle dolomite crystal (Radke and Mathis, 1980). It is the large Ca cation that initiates lattice distortion. This in turn is responsible for the crystal symmetry (Radke and Mathis, 1980). The apparent enrichment in Zn is probably attributed to the presence of the metal during formation of saddle dolomite cement. A number of base-metals, such as Pb-Zn-Cu, are concentrated within hydrocarbons. Since the hydrocarbons were present during saddle dolomite formation (seen under ultraviolet fluorescence), this may account for the relative enrichment in Zn for the saddle dolomite cements.

Another positive correlation exists between the insoluble residue (IR) and the Ni and V trace element distribution (Factor 1). An increase in IR was correlated to enrichments in both Ni and V trace elements. This correlation is postulated to be related to the hydrocarbons, present under ultraviolet fluorescence of the saddle dolomite cement, within the IR. This would provide an enriched source for both these elements into the late diagenetic carbonate phase.

Factor analysis of the trace element distributions within the calcite cements show increases in Mg and Fe with a corresponding depletion in Ca (Factor 1, Table IX.4, in Appendix IX). This is attributed to the enrichment of these elements in the interstitial pore fluids which became undersaturated with respect to dolomite. This documents the evolution of the pore fluid chemistry during subsequent precipitation of calcite cement. Ferroan calcite cements in other carbonate complexes are commonly interpreted as burial cements (Scholle and Halley, 1985).

The saddle dolomite cements have characteristically high Fe and Mg concentrations (Figure 16) similar to their enclosing dolomite matrix (see Figure 14). The similarity in the Mg and Fe contents of the saddle dolomite cements to the enclosing dolomite matrix suggests that they precipitated as the result of rock-fluid interactions with the dolomite matrix and the evolving pore fluids. It is postulated that the final chemical composition of the ferroan saddle dolomite cement is due to the equilibration of the warm basinal fluids with the dolomite matrix.

However, the Fe and Mg trace element compositions for the calcite cements, along with textural evidence, demonstrate that they precipitated from pore fluids that post date the dolomitization and saddle dolomite formation. The consistent depletion in both the Fe and Mg trace element composition of the calcite cements suggests that they precipitated in the presence of a fluid that became more depleted with respect to these elements throughout the precipitation process. The presence of the Mg- and Fe-rich calcite supports the formation of a mixed-water setting (Holail et al., 1988).

The Fe and Mn trace element distribution of all the diagenetic carbonates is shown in Figure 17. The cluster of four limestone samples, at the bottom left portion of the diagram, represent the Fe and Mn concentrations of the least altered limestones from the 33821 Mersea 3-12-I well. The progressive enrichment in the Fe and Mn concentrations

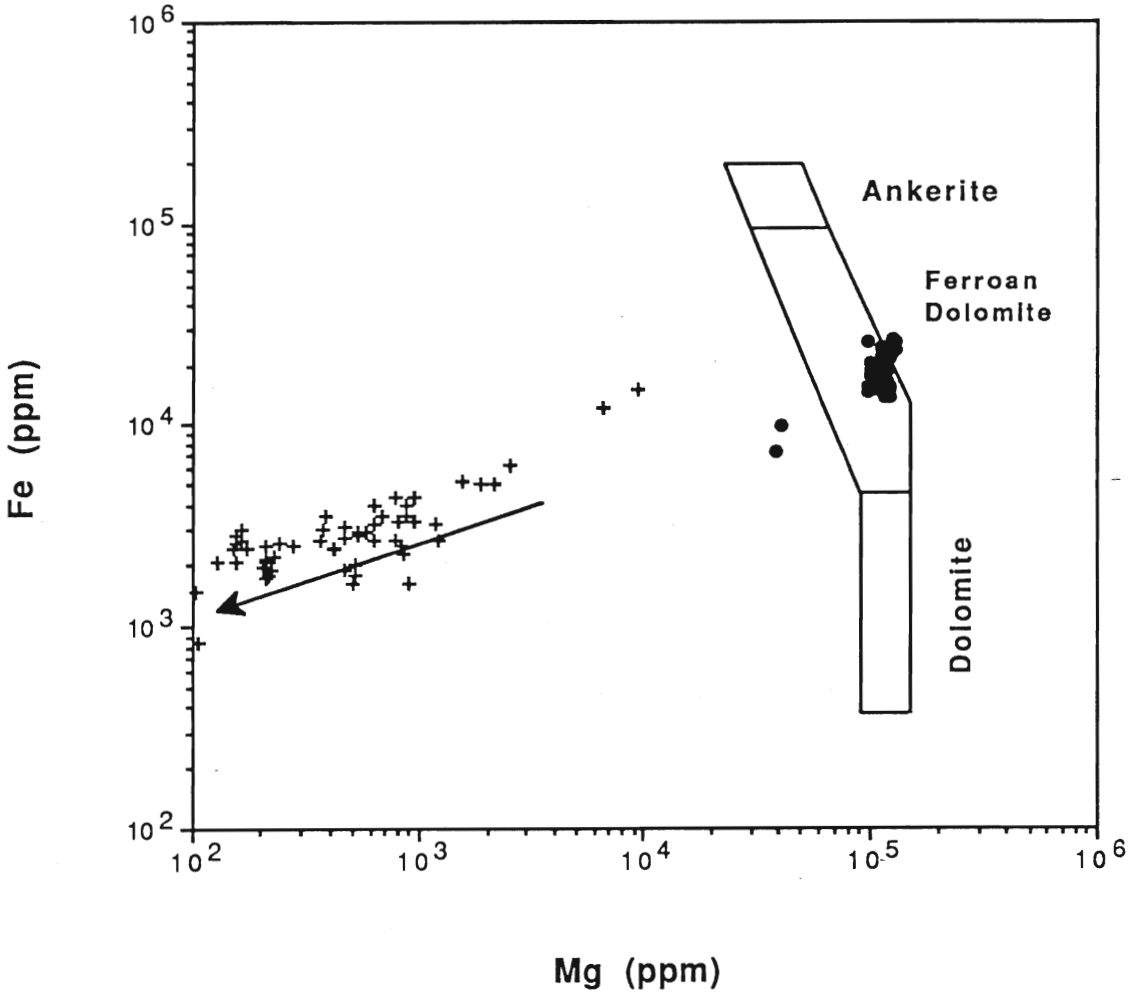

Figure 16: The Fe and Mg distribution for saddle dolomite cements (•), and calcite cements (+), from all four wells. The trace element distributions are superimposed with the fields representing ankerite, ferroan dolomite, and dolomite (Brand, in press).

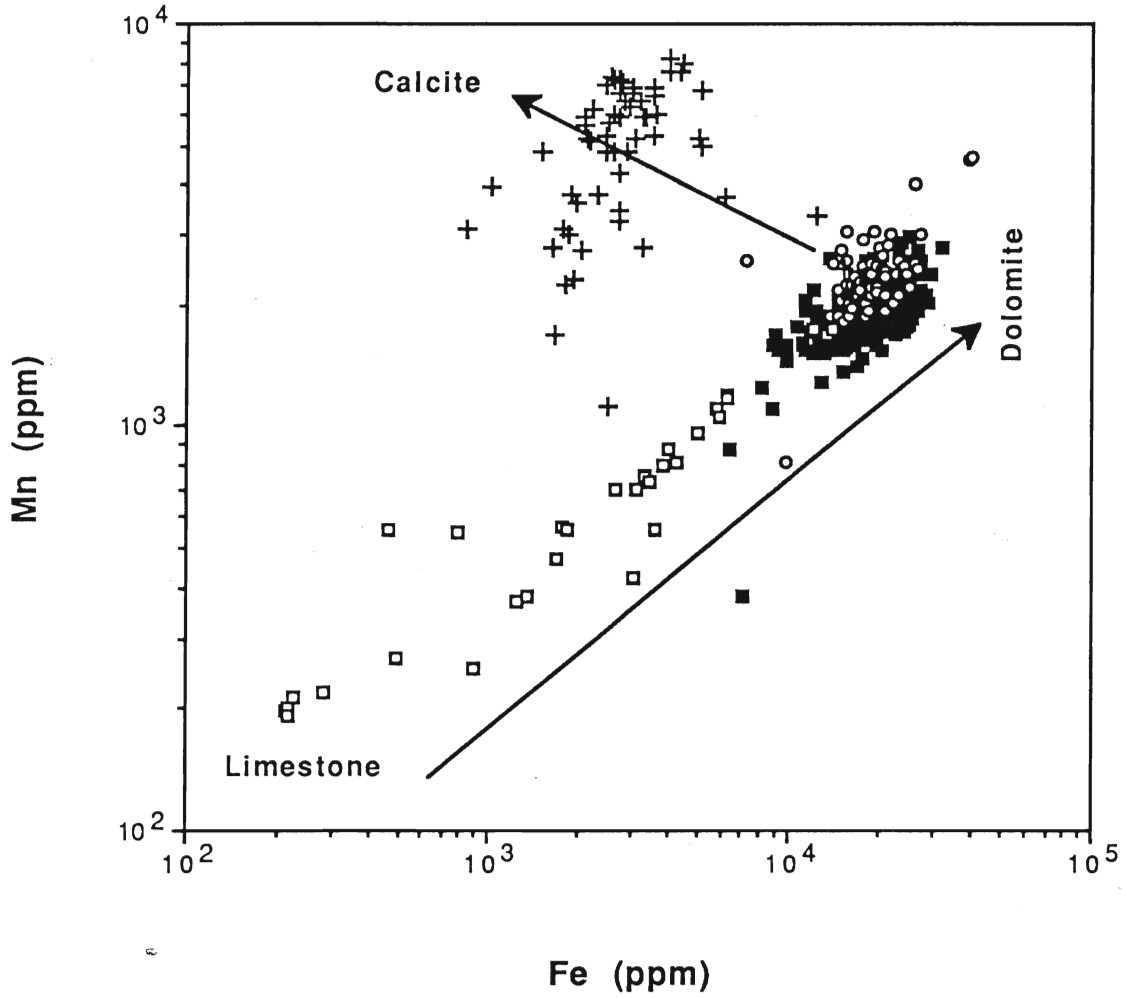

Figure 17: The redox-controlled Fe and Mn distribution for saddle dolomite cements (o), calcite cements (+), dolomite matrix (■), and limestone matrix (□), from all four wells.

reflects the variable degree of alteration of the limestones due to both burial diagenesis and dolomitization. However, during dolomitization and the formation of saddle dolomite the Fe and Mn contents did not change significantly, suggesting that the fluids were more uniform with respect to both Fe and Mn during dolomitization. This chemical trend also suggests that the formation of saddle dolomite cement occurred under similar conditions that prevailed during dolomitization of the carbonate precursor. In contrast, the late calcite cements were enriched with respect to Mn and depleted in Fe. This can be explained by precipitation during, either; (1) the evolution of a pore fluid representing a mixture of the dolomitizing fluids and a more oxidizing meteoric fluid depleted with respect to both Fe and Mn, or (2) the evolution of 'hydrothermal fluids' within a closed system. Trace element distributions of Mg, Fe, and Mn, suggest that the precipitation mechanism for the calcite cements was dominated by an evolving pore fluid chemistry rather than interactions with the adjacent saddle dolomites (Figures 16 and 17).

The distribution and incorporation of Fe and Mn appears to reflect the redox conditions during the formation of diagenetic carbonates (Brand and Veizer, 1980a; Veizer, 1983; Land, 1985). The preferential incorporation of both Fe and Mn into the diagenetic carbonate phase during diagenesis is due to the similarity in the ionic size of the trace elements with respect to Ca, and is also a function of the distribution coefficients being greater than one (Veizer, 1983; Land, 1985).

Saddle Dolomite and Calcite Cements: Stable Isotope Trends

Saddle dolomite cements had $\partial^{18}O$ values between -9.0 and -10.5 ‰, (average of -9.7 ‰), and $\partial^{13}C$ values between 0.8 and -1.3 ‰, (average of -0.01 ‰). The blocky calcite cements had $\partial^{18}O$ values between -10.8 and -12.2 ‰, (average of -11.5 ‰) and $\partial^{13}C$ values between -0.3 and -1.2 ‰, (average of -0.7 ‰). The dog-tooth calcite cements had $\partial^{18}O$ values

between -7.6 and -9.6 ‰, (average of -8.2 ‰), and $\partial^{13}C$ values between 0.6 and -2.9 ‰, (average of -1.0 ‰). The stable isotopic compositions of the saddle dolomite cements and later blocky and dog-tooth calcite cements are compared to the stable isotope fields for burial diagenesis and dolomitization (Figure 18).

The $\partial^{18}O$ and $\partial^{13}C$ isotopic compositions of the saddle dolomite cements are similar to the enclosing dolomite rock matrix (Figure 18), with average $\partial^{18}O$ values of -9.7 ‰ for both matrix and cement. This also precludes the formation of the saddle dolomite cement being related to C derived from maturation of organic matter, which would have resulted in very negative $\partial^{13}C$ values. This is postulated because the dominant carbon source within a dolomite-water system is the host rock. This evidence, in conjunction with the Mg, Mn and Fe trace element chemistry, demonstrates that the saddle dolomites formed due to extensive rock-fluid interactions with the diagenetic pore fluids and the host dolomite rock matrix. Cathode luminescence photomicrographs of the saddle dolomite cements demonstrated that the fluids responsible for the precipitation of the saddle dolomite cements were of constant chemical composition throughout the precipitation process (Plate 19b). Thus the fluid chemistry must have been in chemical equilibrium with the host rock dolomite and was of homogeneous chemical composition representative of those fluids responsible for the hydrothermal dolomitization of the rocks.

The stable isotopic composition of the late-diagenetic calcite cements exhibit two distinct stable isotopic populations. The first sequence of calcite cements, predominantly blocky calcite cements, were precipitated with $\partial^{18}O$ and $\partial^{13}C$ isotopic compositions similar to that of the dolomite rock matrix and saddle dolomite cements, $\partial^{18}O$ between -10.5 to -12.0 ‰ (Figure 18). The minor depletion in $\partial^{18}O$ of the few calcite cements relative to the saddle dolomite reflects the increasing temperature of

formation and/or the progressive depletion in $\partial^{18}O$ of the evolving hydrothermal brine.

The second population of calcite cements, predominantly of dog-tooth morphology, possess $\partial^{18}O$ isotopic compositions between -7.6 and -9.6 ‰, which are enriched with respect to the enclosing saddle dolomite cements. The apparent enrichment in the ^{18}O isotopic compositions of the calcite cements can be attributed to either the mixture of the hydrothermal pore fluids with another type of fluid enriched with respect to $\partial^{18}O$, and/or a decrease in the temperature during the formation of the calcite cements. A third possibility is the direct precipitation from a pore fluid that had undergone rock-water interactions with the carbonate precursor, which could have provided an enriched source in ^{18}O. Since the fluid pathways responsible for the precipitation of the diagenetic carbonate cements do not intersect the limestone sequences that escaped dolomitization, the heavier $\partial^{18}O$ signatures are probably due to either a decrease in temperature, the introduction of an isotopically heavier meteoric fluid, or both.

These dog-tooth calcite cements also exhibit an evolutionary depletion in the $\partial^{13}C$ isotopic composition (Figure 18). This trend in the $\partial^{13}C$ stable isotopic composition of the calcites can be attributed to the influence of either; a) the mixing of the pore fluids with an evolving meteoric fluid, b) the decomposition of organic matter during the formation of the calcite cements, or c) the progressive addition of lighter carbon from the interaction with the carbonate precursor (Allan and Matthews, 1982).

The second hypothesis can be eliminated because the decomposition of organic matter due to either thermochemical or bacterial sulphate reduction would result in much lighter $\partial^{13}C$ values, between -5 to -18 ‰ PDB (cf. Machel, 1987; Jensenius et al., 1988). The possibility of the introduction of isotopically lighter $\partial^{13}C$ from rock-water interaction of the

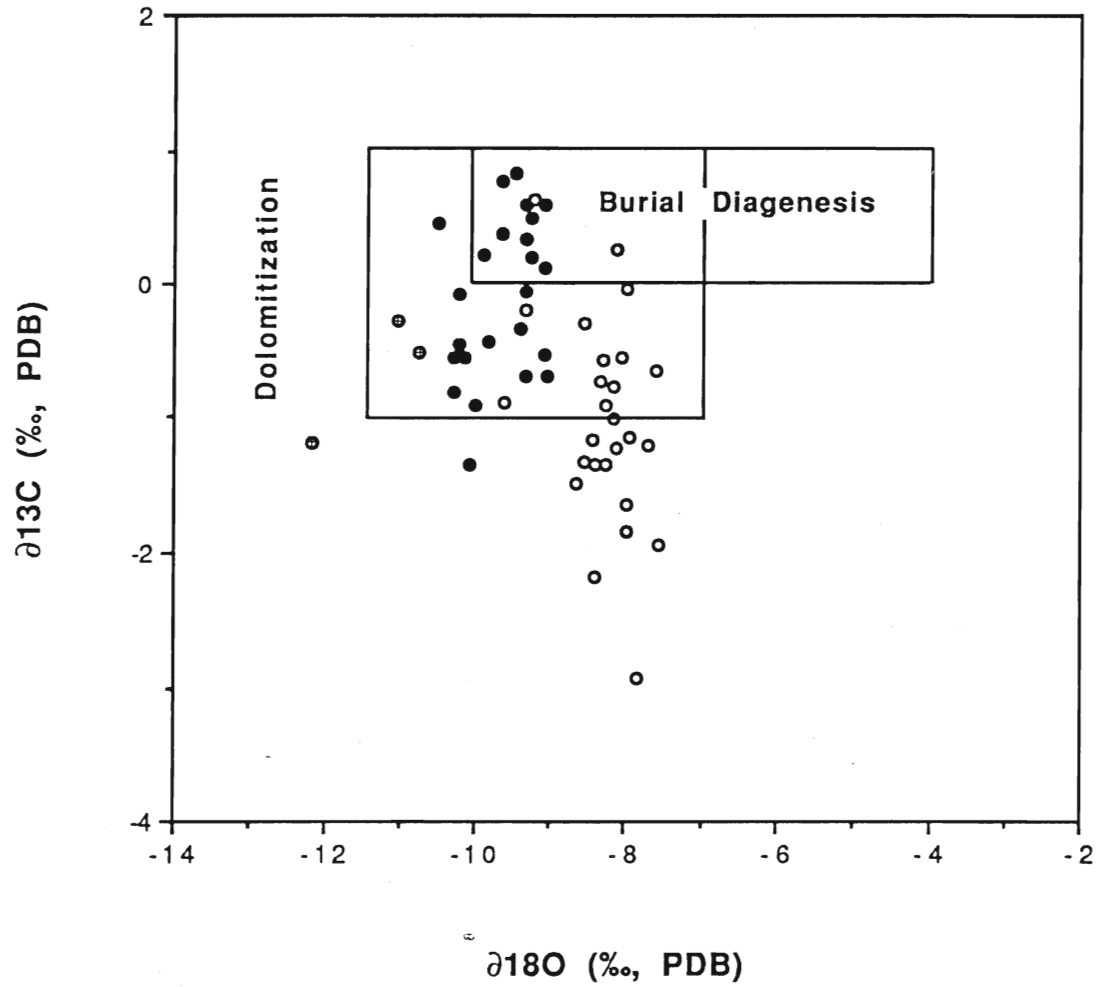

Figure 18: The stable isotopic compositions of saddle dolomite cements (●), and late blocky calcite cements (⊕), late dog-tooth calcite cements (o) superimposed with the stable isotopic composition for burial diagenesis and dolomitization, this study.

pore fluids with the carbonate precursor is not preferred because the fracture-related conduits for the fluids appear to be confined to the dolomitized rock.

However, many studies from a variety of ages have shown the depletion in both the $\partial^{13}C$ and $\partial^{18}O$ in carbonates as formed in a meteoric environment (Allan and Matthews, 1977; 1982; Moldovanyi and Lohmann, 1984; Meyers and Lohmann, 1985; Hurley and Lohmann, 1989). Due to the relatively small carbon reservoir in groundwaters compared to the oxygen reservoir, carbon will equilibrate very rapidly with the host-rock carbon (Hurley and Lohmann, 1989). The rate of oxygen equilibration with the host rock is much slower by the time the rock-water interactions have affected the $\partial^{18}O$ isotopic composition of the carbonate mineralogy, and the $\partial^{13}C$ will have already become invariant. Therefore, with the constant introduction and evolution of isotopically lighter water with respect to $\partial^{13}C$, the final chemistry of the precipitating carbonate cements should reflect the evolution of the mixing of the fluids. Secondly, the cements effectively decreased the existing permeability and porosity within the rock units.

The isotopic model derived for burial cements, presented in Hurley and Lohmann (1989), demonstrates that temperature, although a main controlling factor in the variation of oxygen isotopic compositions, does not affect the final carbon isotopic composition of burial cements but may exhibit slightly depleted values if the burial cements are derived from an autochthonous pore fluid. However, changes in the pore fluid chemistry with burial and time due to basin dewatering involving waters at higher temperatures (Cathles and Smith, 1983), the oxidation of hydrocarbons (Donovan, 1974), or the decarboxylation of organic matter (Irwin et al., 1977), may also contribute to decreased carbon isotope ratios in burial cements.

The depletion in $\partial^{13}C$ by 1 to 2 ‰ in the dog-tooth calcite, compared to the blocky calcite cement, is postulated to be due to the introduction and evolution of isotopically lighter waters with respect to $\partial^{13}C$. A distinctive "upside down-J shape" trend is observed in the $\partial^{18}O$ and $\partial^{13}C$ compositions for most of the dog-tooth calcite cements when compared to the oxygen and carbon isotope compositions of the saddle dolomite cements (Figure 18). The latest dog-tooth calcite cements show small variations in $\partial^{18}O$ compositions with variable $\partial^{13}C$ compositions. The resultant stable isotope compositions of these calcite cements is proposed to have formed during water-dominated, dissolution-precipitation reactions in the presence of $\partial^{13}C$ depleted fluids derived from the influx of soil-gas CO_2.

These Mg- and Fe-enriched dog-tooth calcites possess depleted values with respect to $\partial^{13}C$, and demonstrate a minor enrichment in $\partial^{18}O$, about 2 ‰ compared to the saddle dolomite cements. This may reflect a decrease in the temperature of formation. The presence of a secondary fluid provided stable isotopic signatures observed for the calcites which are characteristically similar to meteorically precipitated carbonates. The presence of a meteoric fluid must have been responsible for the calcite precipitation process. However, cathodoluminescence analysis of the dog-tooth calcite (Plate 20b) cements did not show differences in luminescence compared to blocky calcite cements (Plate 19b).

Dolomites formed during burial, as described by Mattes and Mountjoy (1980), Taylor and Sibley (1986), and Qing and Mountjoy (1989), have textural and chemical characteristics similar to those of the Trenton dolomites.

Evidence for Dolomitization and Cement formation during burial at elevated temperatures

Evidence for the dolomitization during late burial of the sediments at increased temperatures includes the pervasive occurrence of coarsely crystalline dolomite and the presence of minor finely crystalline idiotopic forms within the argillaceous and/or organic stylolitic accumulation seams which essentially post-date the dolomitization process. Zenger (1983) demonstrated that the pervasive occurrence of coarsely crystalline dolomite is indicative of dolomitization during burial, and suggests dolomitization during higher temperatures. Xenotopic dolomite, which predominates the matrix associated with extensive fracturing, has been postulated to form above the 'critical roughening temperature', > 50 °C to < 100 °C (proposed by Gregg and Sibley, 1984), however Shukla (1986) has recently proposed the temperature of formation for the Xenotopic texture at temperatures > 35 °C.

The carbon isotopic composition of all the dolomites plot with only minor variability, whereas the oxygen isotopic composition of the dolomites plot with more depleted values (Figure 15) suggestive of late burial diagenesis (Fritz, 1971; Zenger, 1983; Mattes and Mountjoy, 1980). The matrix dolomites exhibit a narrow range in $\partial^{13}C$ (between 1.0 and -1.0 ‰) and a wide range of $\partial^{18}O$ values from -7.5 to -11.6 ‰ (average of -9.7 ‰). The 4 ‰ shift in $\partial^{18}O$ can be interpreted as a 20°C change in temperature during precipitation, assuming a shift of 2 ‰ correlates to a 10°C variation in the temperature of formation (Friedman and O'Neil, 1977). The oxygen isotopic values for the Trenton limestones averaged about -7.0 ‰, which is similar to late diagenetic dolomite cements in the Illinois basin (mean $\partial^{18}O$ of -6.24 ‰; Choquette, 1971), and the intermediate-scale, hydrothermally alterated Carboniferous Leadville Limestone of Colorado (mean $\partial^{18}O$ of -6.76 ‰; Engel et al., 1958).

The trace element contents (Sr, Na, Fe, and Mn) of the Trenton dolomites also indicate the effects of late diagenesis. This is supported by low concentrations of Sr (average of 70 ppm) compared to normal marine dolomites formed in normal sea water which should have theoretical equilibrium concentrations of 470 to 550 ppm Sr (Veizer, 1983) and reported concentrations of 128 to 155 ppm (Machel and Anderson, 1989). The dolomitization of the carbonate precursor has been characterized by low $\partial^{18}O$ values due to sequential phase formations (Matthews and Katz, 1977). Dolomite is expected to precipitate in isotopic equilibrium with the bulk solution, via a dissolution-reprecipitation process (Matthews and Katz, 1977).

Estimating the temperatures of diagenetic pore fluids using $\partial^{18}O$

The sampled limestones studied are suggested to represent alteration from an originally aragonitic carbonate precursor (see Figure 11). The dolomites represent, in part, the diagenetic alteration of the limestones. The saddle dolomites and later calcite cements represent direct precipitates from the diagenetically evolved pore fluids. The approximate temperature of formation or precipitation can be calculated using the $\partial^{18}O$ of the constituents within a multi-component system if the $\partial^{18}O$ isotopic composition of the ambient water present during its formation can be estimated.

Temperatures were calculated for the saddle dolomite and calcite cements as outlined in Table 1. The equation used in the temperature calculations for dolomite came from Katz and Matthews (1977). The equation used in the temperature calculation for calcite came from Epstein et al. (1953). It is evident from the high temperatures of formation (Table 1), the coarse crystallinity of the dolomites, and the occurrence of idiotopic dolomite within stylolitic seams that dolomitization occurred under conditions of increasing temperature and burial.

Table 1: Oxygen Isotope Temperature Reconstruction Table

Carbonate Mineralogy	Measured Oxygen Isotopic Composition (PDB)	Estimated Oxygen Isotopic Composition of Ambient Water (SMOW)		Salinity Values (ppt)	Estimated Temperature of Alteration/Precipitation (°C)	
LMC	-5.80 to -6.10	-4.00 (1)		35.5 to 40	25 to 32	
Limestone Matrix	-6.00 to -8.00	-4.00 (1)		40 to 50	30 to 50	
Dolomite Matrix	-9.00 to -11.60	-4.00 (1)		40 to 50	60 to 76	
Saddle Dolomite Cement	-9.00 to -10.00	-4.00 (1)	-2.4 (5)	40 to 50	60 to 66	69 to 76 (6)
Calcite Cement Stage I	-9.00 to -11.30	-6.00 to -4.00 (2)	-2.4 (5)	50	55 to 85	77 to 94 (6)
Calcite Cement Stage II	-8.15 to -8.40	-10.0 to -7.0 (2)	-2.4 (5)	47 (3)	25 to 40 (4)	66 to 67 (6)

Equations used in paleotemperature calculations: Katz and Matthews (1977) for dolomite, and Epstein et al. (1953) for calcite

1. Estimate of the stable isotopic composition of Ambient Sea Water (Popp et al., 1986a)
2. Estimate of the stable isotopic composition of Meteoric Waters (after approx. 238 Ma)
3. The average salinity of all 18 brines analyzed used as first approximation of salinity during formation of calcite cement
4. Temperature range corresponds with present day bore hole temperatures (approx. 30 °C), and estimated geothermal gradient (approx. 19.1 °C/km)
5. Mean stable isotopic composition of Formation Waters analyzed
6. Estimated temperature of alteration/precipitation using the mean oxygen isotopic composition of Formation Waters

If the mean oxygen isotopic composition of the present day formation waters (-2.4 ‰ SMOW) is used in place of the evolving stable isotopic compositions for the diagenetic waters, the estimated temperatures of precipitation for the carbonates increases slightly (Table 1). Using these values assumes that the chemistry of the present day brines has not changed significantly since the precipitation of the saddle dolomite cement. The estimate for the temperature of formation for the saddle dolomite cements (between 69 to 76°C) would be reasonable and closer in agreement with Ordovician saddle dolomites in the Albion-Scipio trend, around 80°C, determined from fluid inclusion analyses by Shaw (1975). The saddle dolomite cements analyzed from the Albion-Scipio reservoir have undergone a similar paragenetic history (cf. Ells, 1969; Shaw, 1975) and occurred at depths of about 1200 m, similar to the cements found within the Ordovician reservoirs of southwestern Ontario (about 800-1000 m).

Using a value of -2.4 ‰ (SMOW) would increase the estimate for the temperature of formation for the later calcite cements, and would preclude the presence of meteoric waters during their formation. This assumes that the chemistry of the brines did not change over time. This is not an acceptable hypothesis since the trace element and stable isotopic trends for the late stage cements demonstrate a change in fluid chemistry during their formation.

Geochemistry of Formation Waters

Trace Element Trends

Mean molar concentrations of the trace elements (Mg, Na, Sr, Fe, Mn) with Ca of the formation waters (brines) from all eighteen wells are presented with average present day estimates for meteoric and sea water (data taken from Veizer, 1983, pp. 3-13, 3-26), as well as the calculated molar concentrations for the liquid responsible for limestone diagenesis

(Figure 19). The theoretical diagenetic waters responsible for limestone diagenesis were determined by; (1) computing the mean molar concentrations of the trace elements with respect to Ca in the solid phase for the limestones (data from trace element analysis, Appendix III); (2) by using the accepted partition coefficients for the trace elements of the appropriate calcium carbonate phase (c.f. Veizer, 1983; in Appendix III); and (3) derive the elemental molar concentrations within the diagenetic liquid phase by using the partitioning equation (in Appendix III); and (4) assuming equilibration with the bulk aquifer pore waters.

The present day formation waters do not represent a simple mixture of meteoric and sea waters. A chemical signature representing a mixture of these two types of waters is expected if diagenetic equilibration between these waters occurred during early diagenesis (Figure 19). In general, meteoric waters would have been expected to have been present during early diagenesis of relatively shallow buried carbonates. The presence of hardgrounds is well documented in the surface exposures of the Trenton Group carbonates of southeastern Ontario (Brett and Brookfield, 1984). A number of non-deposition periods exist between the fining-upward cycles (Brookfield and Brett, 1988), however, there is still no evidence for a true unconformity within the Ordovician carbonates, particularly along the contact with the overlying shale sequences. In the core of the wells observed there is no evidence of subaerial exposure throughout the Trenton and Black River carbonates. The introduction of meteoric fluids during early limestone diagenesis could then be attributed to the proximity of the study area to the Finlay Arch, which would represent a suitable recharge area during lithification and early burial.

The Sr and Na molar concentrations verify that the dominant components of the diagenetic waters are enriched relative to present day sea water. This is possibly due to the recrystallization of the sediments from an increasingly Na-rich diagenetic fluid that evolved during burial of

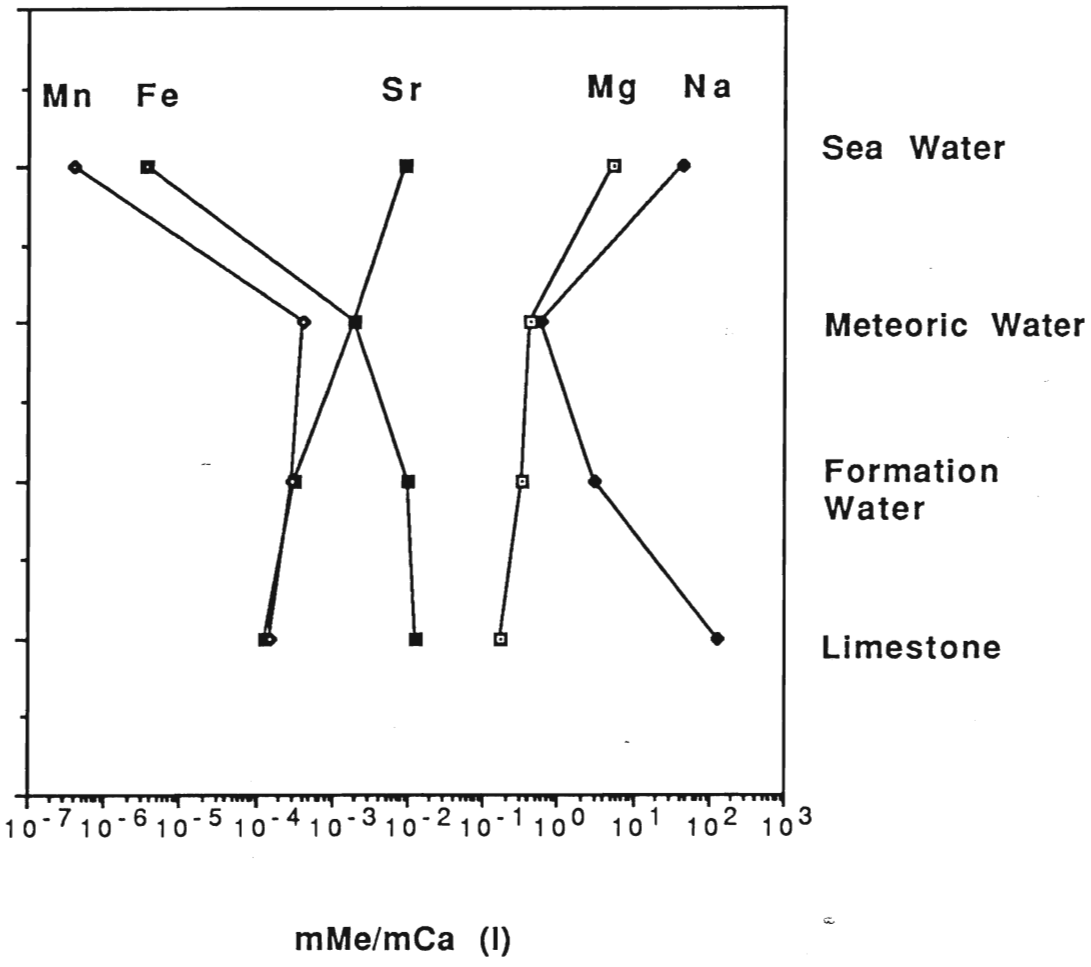

Figure 19: Mean $^{m}Me/^{m}Ca$ for natural waters (average present day sea water and assumed meteoric waters; from Veizer, 1983), brine samples (formation waters) from the study area, and the theoretical diagenetic waters calculated from the limestones. Reproduced after Veizer (1983) and Majid and Veizer (1986).

the sediments. The chemical signature exhibited by the diagenetic waters is suggested to be due to rock-water interactions during the evolution of the original formational waters during burial.

It is also important to note that the mean $^{m}Mg/^{m}Ca$ of the brines illustrate that they could not effectively dolomitize the rocks because of their low Mg/Ca ratios, calculated between 1:4 to 1:6. However, Mattes and Mountjoy (1980) have suggested that with deep burial and increased temperature, dolomitization can proceed at lower Mg/Ca ratios. However, due to the relatively high ionic strength of these brines, indicated by the high Na concentrations (Appendix V), it would require a high Mg/Ca ratio to effectively dolomitize the rocks since the presence of Na is suggested to inhibit dolomitization (Folk and Land, 1975; Friedman, 1980).

The mean $^{m}Me/^{m}Ca$ have been calculated for the assumed diagenetic fluids responsible for dolomitization of the limestones (Figure 20). The procedure and assumptions used in calculating these fluids is similar to the calculated fluids representing limestone diagenesis.

The fluid representing the progressive dolomitization of the limestones were deduced by separating the dolomitic limestones from the coarsely recrystallized limestones. The dolomitic limestones altered in the presence of the dolomitizing fluids reflect $^{m}Mg/^{m}Ca$ ratios between 0.5 and 0.99, and the coarsely recrystallized limestones altered by the evolution of the pore fluids during burial diagenesis reflect $^{m}Mg/^{m}Ca$ ratios between 0 and 0.49. (Figure 20). The theoretical liquid during dolomitization is not represented as a mixture of sea water and the assumed meteoric waters (Figure 20). The theoretical fluid responsible for dolomitization is expected to have a chemical composition representing a mixture of sea water and meteoric waters if dolomitization occurred in the early diagenetic environment. Therefore it would be important to establish constraints on the type and evolution of the pore fluids responsible for the dolomitization process.

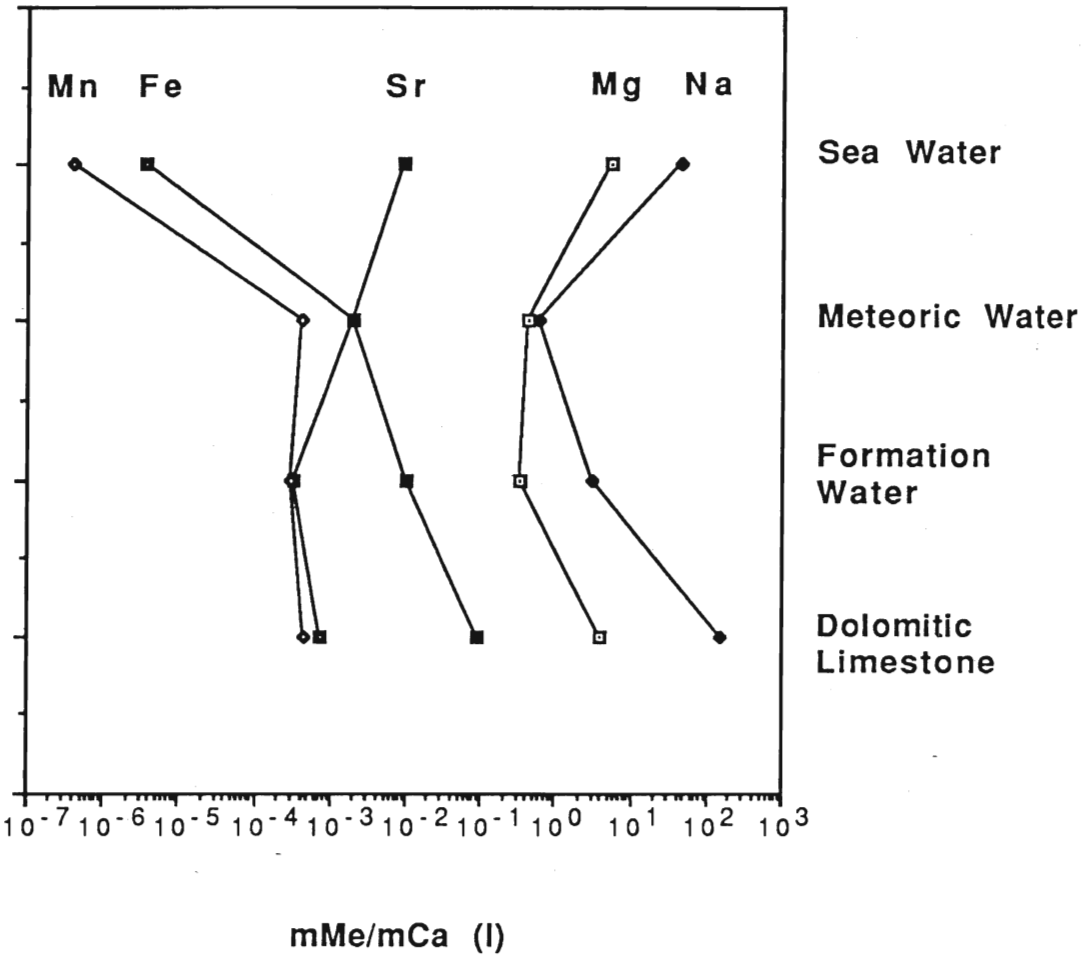

Figure 20: Mean $^{m}Me/^{m}Ca$ for natural waters (average present day sea water and assumed meteoric waters; from Veizer, 1983), brine samples (formation waters) from the study area, and the theoretical diagenetic waters calculated from the dolomitic limestones. Reproduced after Veizer (1983) and Majid and Veizer (1986).

In order to establish the chemical composition and type of the fluids responsible for the diagenetic alteration and precipitation of the various diagenetic carbonate components, the mean $^{m}Sr/^{m}Ca$ ratio was determined for each of the theoretical liquid phases. The mean $^{m}Sr/^{m}Ca$ ratio was used because the trace element strontium is representative of the diagenetic environment. This is attributed to the solubility, origin, distribution of the element, and also because the repartitioning of Sr into solution generally results in the increase of $^{m}Sr/^{m}Ca$ in the downflow direction (Veizer, 1983). Veizer (1983) demonstrated that this is possible for Na>Mg>UO2>Sr>Ba with trace element repartitioning being proportional to the deviation of the distribution coefficient from unity, the magnitude in difference in the $^{m}Me/^{m}Ca$ between sea water and the diagenetic water, and the solute index or water/rock ratio of the diagenetic system. The resulting chemical composition of the carbonate cements precipitated from diagenetic (meteoric) waters may be related to the chemical composition and temporal variations of the bulk aquifer pore water (Veizer, 1983).

The calcite cements and saddle dolomite cements have similar 1000 Sr/Ca ratios (Figure 21), however the calcite cements are more enriched in Mn. This suggests that they precipitated from different diagenetic fluids, probably due to the introduction of a secondary pore fluid.

To determine the chemical composition of the diagenetic fluids responsible for the alteration and precipitation processes, the $^{m}Sr/^{m}Ca$ ratio for the theoretical liquid phases for all the diagenetic carbonate will aid in determining the chemistry of the diagenetic fluids.

Figure 22 plots the mean $^{m}Sr/^{m}Ca$ ratio of the theoretical pore fluids responsible for; (1) limestone diagenesis; (2) initial dolomitization of the limestones; (3) dolomitization; (4) precipitation of saddle dolomite cements; and (5) precipitation of calcite cements. The upper and lower estimation of the partition coefficient for a high temperature form of dolomite is presented (Saddle Dolomite A, $k = 0.025$; Saddle Dolomite B, $k = 0.05$).

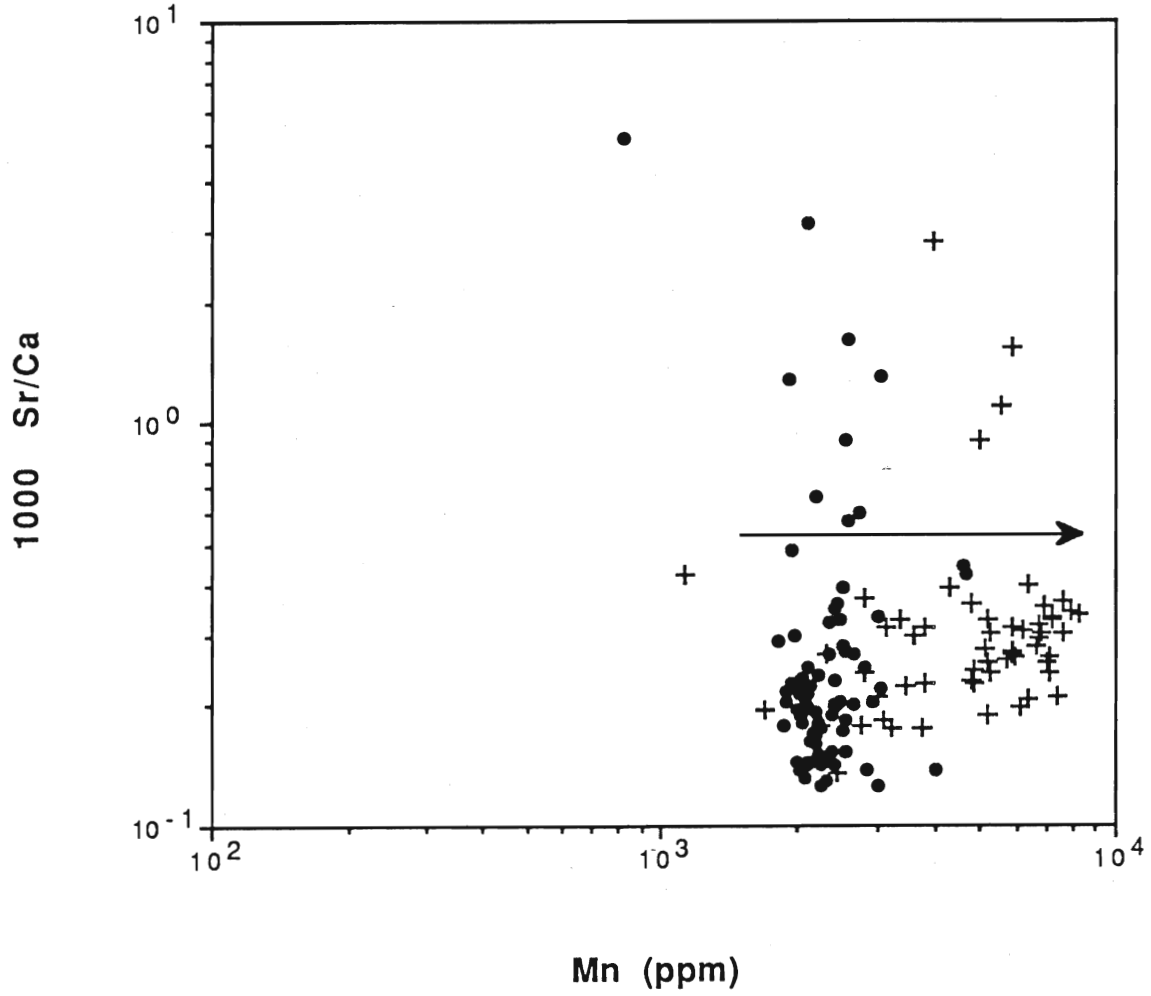

Figure 21: The 1000 Sr/Ca vs Mn distribution of the saddle dolomite cements (o), and all the late calcite cements (+).

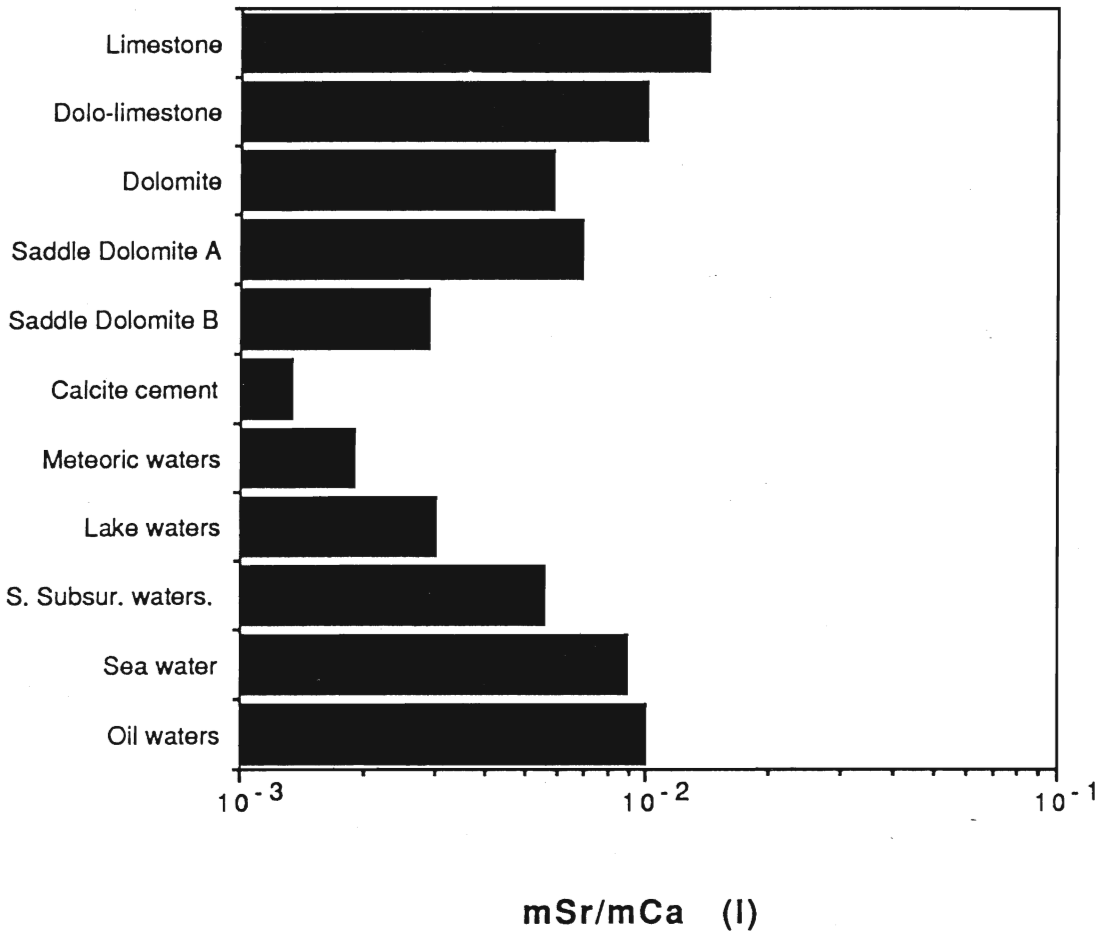

Figure 22: The $^{m}Sr/^{m}Ca$ ratios for theoretical diagenetic fluids responsible for the alteration of limestones (burial diagenesis), dolomitic limestones, dolomite, saddle dolomite, and calcite cements with a number of known natural waters (data from Veizer (1983) and Majid and Veizer (1986)).

These theoretical diagenetic fluids are superimposed with some known $^{m}Sr/^{m}Ca$ ratios from a variety of natural waters in order to constrain the types of fluids that may have contributed to the diagenetic re-equilibration of the final carbonate products (data taken from Majid and Veizer, 1986).

The limestones used to calculate the chemistry of the diagenetic pore waters were dominantly mudstones, whose original mineralogy has been postulated to represent the altered product of a dominantly aragonitic (A) carbonate precursor (see Figure 11). The interbedded wackestones and grainstones consist of disarticulated crinoidal material, whose original mineralogy is assumed to be high-magnesium calcite (HMC). This did not pose a problem since the distribution coefficient for Sr during the diagenetic re-equilibration of both A and HMC to dLMC is 0.050 (see Veizer, 1983, Table 3-1, p. 3-6).

The liquids responsible for the limestone diagenesis have a mean $^{m}Sr/^{m}Ca$ ratio that may represent the evolution of original formational waters during early burial. The enrichment in the $^{m}Sr/^{m}Ca$ ratio determined for these waters is postulated to represent the (depositional) pore waters becoming progressively enriched in the downflow direction during burial diagenesis.

The dolomitization of the rock proceeded with the re-equilibration of the pore waters with a fluid representing a chemical composition similar to that of present day sea water. The resultant pore waters responsible for the dolomitization of the rock became dominated by the subsurface component, whose chemical composition is unknown, but reflects a chemical composition between present day sea water and a shallow subsurface water.

The precipitation of the saddle dolomite cements took place after considerable evolution of the diagenetic pore fluids, but also demonstrates a re-equilibration of the diagenetic water with the earlier dolomites. This

has been demonstrated by the compositional similarity in the trace element chemistry and the stable isotopes of the saddle dolomite cements when compared to the host dolomite matrix (Figs. 14, 15, 16, and 18). Therefore it is suggested that the formation of saddle dolomite was due to a fluid-dominated diagenetic process (Brand and Veizer, 1980; 1981).

The dog-tooth calcite cements $^{m}Sr/^{m}Ca$ ratio, compared to assumed meteoric waters in Figure 21, suggests that they were derived from a meteoric type of fluid. The carbon isotopic trend for the dog-tooth calcite cements (Figure 18) support the interpretation that meteoric waters were involved in their formation.

It is postulated that the predominant fracture systems, "Tulip structures" as described by Versical (1990), which extend from the basement to the surface, could have allowed for the accumulation of meteoric waters down to these rather shallow burial depths, ~ 800 m. The introduction and mixing of meteoric waters is suggested to have taken place during the unloading and cooling of the basin.

Formation Waters: Stable Isotope Trends

The stable isotopic composition of the formation waters relative to standard mean ocean water (SMOW), the global meteoric water line (GMWL), and the trends representing the stable isotopic composition of Michigan Basin and Illinois Basin brines (from Clayton et al., 1966) are illustrated in Figure 23. The variability in the stable isotopic composition of the Trenton brines suggest evolution of different pore waters. McNutt et al., (1987) noted that the southern Ontario brines plotted closer to the GMWL than the Michigan brines. The distribution of the stable isotopic compositions of the present day brines from southwestern Ontario suggest that some of the brines may represent a mixture of deeper sedimentary brines from the Michigan Basin with a meteoric fluid.

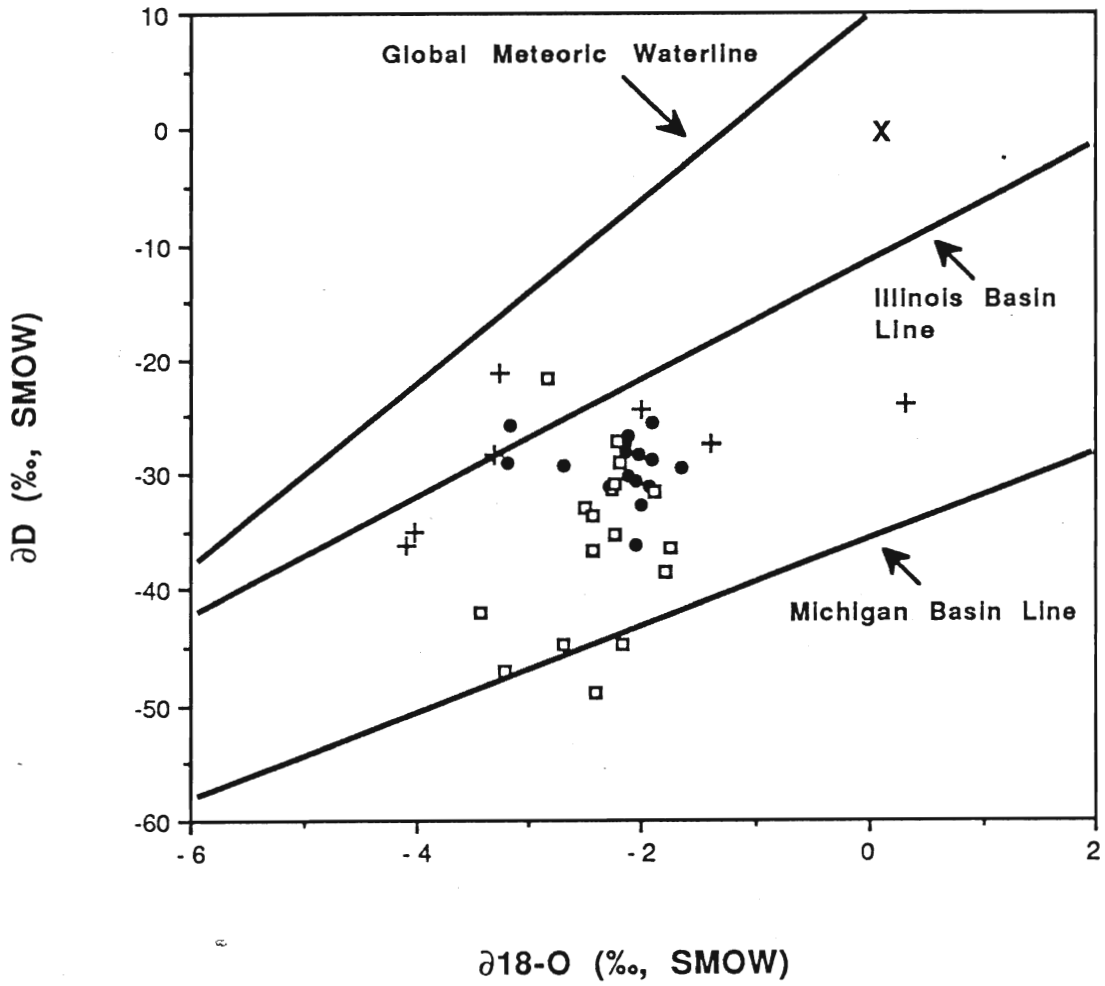

Figure 23: Stable isotopic trend for the formation waters (brines) of the Ordovician Trenton Group reservoirs, southwestern Ontario, of this study, (□); McNutt et al., (1987) Trenton brines, (●), and McNutt et al., (1987) Cambrian brines, (+). GMWL represents the Global Meteoric Water Line, the Illinois and Michigan Basin lines (from Clayton et al., 1966).

The stable isotopic composition of the formation waters show an overall enrichment with respect to $\partial^{18}O$. Knauth and Beeunas (1986) suggested that the most common source for ^{18}O enriched waters are connate brines, waters resulting from gypsum dehydration, the evaporation of meteoric waters, waters from salt, and mixtures of all the above. McNutt et al., (1987) suggested that the formation waters may represent a mixing of an evolved Appalachian Basin brine with an evolved Michigan Basin brine since the present day water chemistries plot similar to brines found in Cambrian units from Ohio, originally documented by Breen et al., (1985).

A number of Trenton Group and Cambrian brines from southwestern Ontario also show a similar isotopic composition with the Illinois Basin brines. This may suggest similar evolution in the respective brine chemistries for the two basins. It seems possible that the complex stable isotope signatures of the southern Ontario brines may be the result of mixing of formational waters (originally responsible for the hydrothermal alteration of the rock), a deeper sedimentary brine, and meteoric waters during the later stages of basin development.

Thermal Maturation Analysis: Results and Discussion

Estimates of conodont colour alteration indices (CAI; Tables 2-5) were based on comparative analysis with prepared type-Ordovician conodonts from various diagenetic environments (prepared by Anita Harris). The thermal maturation of the rocks from the four wells varies vertically. If the thermal maturation of these strata were simply due to burial, the resultant CAI values of the conodonts should be more homogeneous. However, Trenton Group rocks exhibit variable maturation probably due to the introduction of hot fluids along fracture systems.

The CAI of the most pristine conodonts found within the preserved limestone section of the 33821 Mersea 3-12-I well were used as a standard to calculate the ancient geothermal gradient. The remaining conodont CAI's were used to establish limits on thermal maturation and temperature of alteration of the other diagenetic rocks.

The conodonts from limestones in the 33821 Mersea 3-12-I well have consistent CAI values between 1.5 to 2.0. This corresponds to a 'host' temperature of < 50°C, as estimated by temperature of alteration studies by Epstein et al. (1977). The CAI values of the conodonts from the pay-zone dolomites are 2-2.5, which correspond to temperatures of alteration of 45 - 78°C (Figure 24). The conodonts examined from highly fractured rocks lined with saddle dolomite (hydrothermal) have CAI's between 3-3.5, which corresponds to temperatures of alteration of 78 - 150°C (Figure 24). This suggests that these rocks were probably affected by fluids at elevated temperatures, which played a role in their diagenesis. There are a number of reasons which suggest that the conodont CAI's are not the result of an elevated and uniform ancient geothermal gradient; (1) The conodonts from limestones have CAI's of 1.5-2, whereas the conodonts from dolomites which overly these limestones have CAI's between 2-2.5 (Tables 2-5), and (2) the conodonts with CAI's of 3-3.5 are associated with

Table 2: Conodont Colour Alteration results from rocks of the 33821 Mersea 3-12-I well

Conodont Sample (m)	CAI	Temp. (°C)	Colour	Fixed Carbon Range (%)
769.9 - 770.0 Dolomite	2	60 - 140	lt. brown	55 - 70
779.78 - 779.85 Hydrothermal Dolomite	3 - 3.5	110 - 240	brown/black	70 - 80
781.05 - 781.15 Dolomite		No Conodonts		
786.85 - 787.0 Pay Zone Dolomite	2 - 2.5	60 - 150	brown/black	55 - 70
787.0 - 787.10 Pay Zone Dolomite	2 - 2.5	60 - 150	brown/black	55 - 70
788.30 - 788.40 Dolomite	1.5 - 2	50 - 140	lt. brown	55 - 70
797.95 - 798.05 Dolo-limestone	1.5	50 - 90	lt. brown - amber	55 - 70
800.00 - 800.13 Limestone	1 - 1.5	50 - 90	lt. brown - amber	< 60
809.60 - 809.70 Limestone	1 - 1.5	50 - 90	lt. brown - amber	< 60
860.49 - 860.58 Limestone		No Conodonts		
868.15 - 868.30 Dolomite		No Conodonts		
872.49 - 872.58 Dolomite	2	60 - 140	lt. brown	55 - 70
947.88 - 947.95 Dolomite	2	60 - 140	lt. brown	55 - 70
941.14 - 941.23 955.65 - 955.77	Saddle Dolomite, Glauconite, FeO		No Conodonts	

Table 3: Conodont Colour Alteration results from rocks of the 33823 Mersea 1-12-A well.

Conodont Sample (m)	CAI	Temp. (°C)	Colour	Fixed Carbon Range (%)
770.75 - 770.85 Dolomite	2	60 - 140	lt. brown	55 - 70
778.75 - 778.85 Hydrothermal Dolomite	3 - 3.5	110 - 240	brown/black	70 - 80
785.80 - 785.90 Dolo-limestone	1 - 1.5	50 - 90	lt. brown - amber	< 60
798.50 - 798.60 Limestone	1 - 1.5	50 - 90	lt. brown - amber	< 60
799.50 - 799.60 Dolo-limestone	1 - 1.5	50 - 90	lt. brown - amber	< 60
800.70 - 800.77 Dolo-limestone	1.5 - 2	50 - 140	lt. brown	55 - 70
805.00 - 805.10 Dolomite	2	60 - 140	lt. brown	55 - 70

Table 4: Conodont Colour Alteration results from rocks of the 34151 Mersea 7-18-VIII well.

Conodont Sample (m)	CAI	Temp. (°C)	Colour	Fixed Carbon Range (%)
801.26 - 801.35 Dolomite	2.5 - 3	110 - 200	brown/black	70 - 80
812.04 - 812.15 Dolomite	2	60 - 140	lt. brown	55 - 70
820.22 - 820.28 Dolomite	1.5 - 2	50 - 140	lt. brown	55 - 70
825.96 - 826.06 Dolomite	1.5 - 2	50 - 140	lt. brown	55 - 70
833.11 - 833.19 Dolomite	2	60 - 140	lt. brown	55 - 70

Table 5: Conodont Colour Alteration results from rocks of the 34160 Romney 5-8-II well

Conodont Sample (m)	CAI	Temp. (°C)	Colour	Fixed Carbon Range (%)
809.33 - 809.40 Pay Zone Dolomite	2 - 2.5	60 - 150	brown/black	55 - 70
818.95 - 819.05 Pay Zone Dolomite	2.5	110 - 200	brown/black	55 - 70
819.84 - 819.96 Hydrothermal Dolomite	2.5 - 3	110 - 200	brown/black	70 - 80
822.61 - 822.70 Dolomite	1.5	50 - 90	lt. brown - amber	55 - 70
825.96 - 826.03 Porous Dolomite	2	60 - 140	lt. brown	55 - 70
827.14 - 827.25 Pay Zone Dolomite	2	60 - 140	lt. brown	55 - 70
828.07 - 828.15 Porous Dolomite	2	60 - 140	lt. brown	55 - 70
832.39 - 832.49 Dolomite	2	60 - 140	lt. brown	55 - 70
839.58 - 839.66 Hydrothermal Dolomite	3	110 - 240	brown/black	70 - 80
845.05 - 845.09 Dolomite	2.5 - 3	110 - 200	brown/black	70 - 80
847.85 - 847.92 Dolomite	2	60 - 140	lt. brown	55 - 70
857.25 - 857.32 Dolomite	2	60 - 140	lt. brown	55 - 70
859.72 - 859.80 Dolomite	1.5	50 - 90	lt. brown - amber	< 60
865.11 - 865.28 Dolomite	2	60 - 140	lt. brown	55 - 70

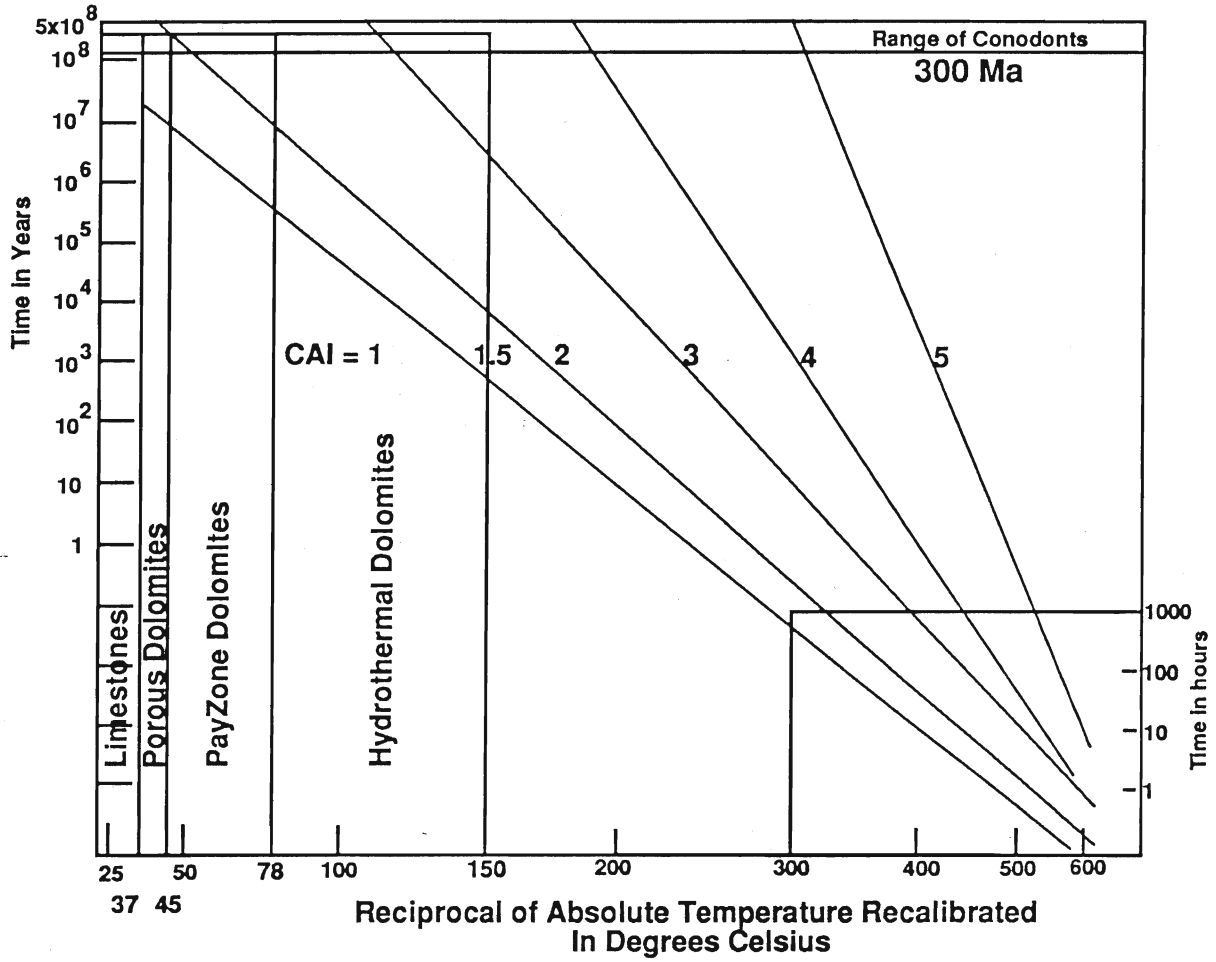

Figure 24: Modified Ahrrenius plot of the conodont colour alteration data (modified from Epstein et al., 1977 experimental results). Maximum duration of burial based on CAI ranges for the conodonts found within the various rock types (300 Ma). This is extrapolated to the x-axis to derive minimum and maximum temperatures of alteration.

hydrothermal mineralization, including Xenotopic-A and saddle dolomite, which are high temperature forms of dolomite (> 60°C). Pay-zone dolomites either consist of, or are associated with zoned Idiotopic-E dolomite (< 50°C).

Re-construction of the Ancient Geothermal Gradient

Reconstruction of the original geothermal gradient is possible by utilizing the most pristine conodonts with respect to the reconstruction of the burial history of the Michigan Basin within southwestern Ontario. To evaluate the ancient geothermal gradient, one must exclude the conodonts from local zones that indicate higher paleotemperatures. This also requires an estimation of the surface temperature during deposition of the Middle Ordovician carbonates, as well as an estimation of the alteration temperature responsible for the CAI values of the more pristine conodonts. Alteration temperature for the conodonts can be determined by extrapolation from the Arrhenius plot (cf. Epstein et al., 1977), if the duration of maximum burial for the sediments can be estimated.

A surface temperature of 25°C is assumed during the deposition and subsequent burial of the Middle Ordovician carbonates. This has been approximated by using the paleocontinental reconstructions by Zeigler et al., (1977) and Morel and Irving (1978). The reconstruction places southwestern Ontario about 10° - 15° south of the equator during the Ordovician, which would provide a mean annual surface temperature of 25 °C, based on present day equivalents.

Estimate of the duration of maximum burial can be done by evaluating the structural and depositional history of the Michigan Basin with reference to the Paleozoic rocks of southwestern Ontario. Poole et al., (1970) argued for a latest possible time of unloading of these rocks by Late Mississippian or Early Pennsylvanian since continental conditions were established by this time. Crough (1981) argued that the Ontario-New

England region was uplifted and eroded during Early Triassic-Late Jurassic time (225 Ma), which would correspond to durations of burial of about 160-215 Ma for the Middle Ordovician rocks. However, a review of the subsidence history of the Michigan Basin determined that basin subsidence was greatest between 425 to 350 Ma, and subsidence discontinued at approximately 300 Ma (c.f. Jerome, 1988; Fig. 8).

A shale compaction study by Vugrinovich (1988) provided substantial physical evidence that a post-Desmoinesian, pre-Kimmeridgian (286 +/- 12 Ma), depositional episode left no more than 850 m of additional sediment in the central Lower Peninsula, and no more than 200 m in the southern and northern Lower Peninsulas of the Michigan Basin.

If the estimate of 300 Ma for the maximum burial time (cf. Jerome, 1988) for the Michigan Basin is accepted, this sets the minimum and maximum temperature of alteration of the conodonts with a CAI of 1.5 - 2.0 between 37°C and 45°C (Figure 24). Employing these minimum and maximum temperature of alteration between 37°C and 45°C for the most pristine conodonts found in this study, and burial depths between 800 to 1000 m (incorporating the lowest estimate of additional overburden of 200 m from Vugrinovich, (1988)), a geothermal gradient can be approximated between 17 to 25 °C/km. The resultant estimation for the geothermal gradient is supported in theory by geothermal reconstructions for the Paleozoic and Mesozoic time periods for southern Ontario, whereby the assumed geothermal gradients are estimated between 20 - 30°C/km (Legall et al., 1981). Hogarth and Sibley (1985) established that the northern and central portions of the basin were affected by a uniform geothermal gradient of approximately 23°C/km, based on conodont colour alteration evaluation. A present day basin-wide geothermal gradient of 19.2°C/km has been estimated based on the compilation of bottomhole pressure surveys, drillstem tests, wireline logging, and subsurface temperature tests (Vugrinovich, 1988). Therefore

the present estimate for the geothermal gradient within the southeastern portion of the Michigan Basin is also in agreement with previous findings.

Paleogeothermal gradient reconstructions for the northern, central and southern extents of the Michigan Basin have been attempted using the Lopatin method (c.f. Cercone, 1984a, b). However, the results of the modeling by using the thermal alteration indices of spores and amorphous organic matter from shales of Precambrian to Mississippian age has consistently overestimated the thermal maturities of the southern Lower Peninsula. Cercone (1984 a,b) believed that deeper burial was responsible for the observed high temperature of alteration indices of the organic matter. Her evaluation resulted in reconstructed paleogeothermal gradients of 35°C to 45°C, rather than proposing elevated temperature gradients for the southern Lower Peninsula. Hogarth and Sibley (1985) postulated that an additional burial depth of 600 - 700 m, or an elevated paleogeothermal gradient of 31 °C/km was required to explain the observed color alteration indices of conodonts from Middle Ordovician Trenton limestones in the southern Lower Peninsula. These authors used mean annual temperatures of 20°C, instead of the 25°C estimate used in this study, for computing of the ancient geothermal gradients.

Legall et al. (1981), using colour alteration of conodonts and acritarchs from rocks within the subsurface, provided evidence of elevated burial temperatures in the range of 60 - 90°C for the lower part of the Middle Ordovician sequences in southwestern Ontario. They concluded that the sedimentary sequences within southwestern Ontario, from the top of the Paleozoic section down to the middle Ordovician, had undergone only minimum burial based on consistently low CAI values of 1.5. Legall et al. (1981) characterized two regimes of thermal maturation within southwestern Ontario. The first extends from the top of the Paleozoic succession to the mid-Ordovician Trenton Group strata representing an organically immature to marginally mature zone. The second thermal

alteration regime extends from the mid-Ordovician strata to the base of the Paleozoic succession which represents the organically mature zone. These data infer only limited petroleum-generating potential from rocks down to the level of the Middle Ordovician Trenton Group according to Powell et al. (1984).

Fluid inclusions from late diagenetic fracture-filling calcite found within the reefs in the northern Lower Peninsula (Cercone, 1984b) indicated temperatures of formation of 80°C and 120°C, with a average temperature of 90°C. These samples were taken from depths of 1800 - 1900 m where the present day subsurface temperature is 45°C. Late diagenetic, saddle dolomite was found within the Devonian Dundee Limestone within the southern Peninsula (Prouty, 1983). As postulated by Radke and Mathis (1980), the formation of saddle dolomite does not occur below about 60°C and in most cases forms above 100°C. However, the best evidence for proposed higher temperatures within these rocks is the presence of oil in the Michigan Basin. Oil generation does not occur below 60°C to 80°C, and recent studies suggest that oil found within the Devonian Traverse Group (Rullkotter et al., 1986), the Silurian Niagaran Reef trend (Gardner and Bray, 1984; Rullkotter et al., 1986), and the Middle Ordovician Trenton and Black River group limestones (Reed et al., 1986; Rullkotter et al., 1986) either originated as in situ oil deposits or migrated from adjacent source rocks which immediately overlie their reservoir rocks.

Thermal Maturation and Lopatin Basin Modeling

Since the southern and southeastern portions of the Michigan Basin have been evaluated to be over mature for its sedimentary thickness and assumed maximum depth of burial, it is obvious that the reconstruction of a geothermal gradient and burial history curve for these areas of the basin should not be based on the 'apparent' CAI of the conodonts alone.

Thermal maturation indices have been compiled by many authors (c.f. Epstein et al., 1977; Waples, 1980; Hogarth and Sibley, 1985). Due to the low CAI values for the conodonts from the core in this study, CAI of 1.5 for the conodonts from the best preserved limestones, correlation of the CAI estimates to the time temperature index (TTI) may provide a more accurate estimate of the thermal maturity of these rocks. Hogarth and Sibley (1985) successfully utilized the correlation of the CAI of conodonts to the TTI equivalent of the host rocks in their evaluation of conodonts as useful thermal maturation indicators. They proposed that a CAI of 1.5 would correspond to a TTI of at least 20-40, and a CAI of 2 correlates to a TTI of 40-160. They further established that a minimum geothermal gradient of 31°C/km must have existed to give a CAI of 1.5 for the southern portion of the Michigan Basin, based on the sedimentary history and assumed maximum depth of burial.

Correlating the TTI index with the observed maturity of the conodonts for those rocks which have been established to represent the pay zone dolomites, in this study, may provide a useful estimate of the thermal maturation and hydrocarbon generating potential of these rocks. According to the correlation chart (c.f. Hogarth and Sibley, 1985; Figure 1, Table 1), a CAI of 2 - 2.5 correlates to a minimum TTI of 20 - 40, which also corresponds to the top of the oil generation window (TTI of 15). In order to estimate the hydrocarbon generating potential of the rocks, the Lopatin Basin Modeling technique was run by reconstructing the sedimentologic history for the units within the study area (using the lowest estimate of additional overburden of 200 m), and employing geothermal gradients until the theoretical maturation of the rocks (TTI = 15) was observed (see Appendix X for sedimentological and maturation summary). This provided a minimum hypothetical 'paleogeothermal gradient', or temperature gradient, of 45°C/km.

The observed thermal maturation for the pay zone dolomites can be estimated by extrapolating the minimum (45°C) and maximum (78°C) temperature of alteration from the 'observed' CAI of the conodonts (CAI of 2 - 2.5). The resultant 'paleogeothermal gradient' is estimated between 20 and 50°C/km, employing a mean annual surface temperature of 25°C. Since many of the conodonts from these pay zone dolomites correspond to the higher estimate of the CAI determination, the upper estimate of the 'paleogeothermal gradient' is favoured.

Oxygen isotope analysis of the saddle dolomites and calcite cements from this study suggested temperatures of formation between 60 - 85°C, which would require the presence of paleotemperature gradients between 35 and 60°C/km during their formation (using a mean annual surface temperature of 25°C). However, the formation of these diagenetic cements have been determined to be the product of autochthonous fluids during the hydrothermal alteration of the carbonates, rather than normal thermal and kinetic effects that could have taken place with during progressive deep burial.

Therefore, the determination of the theoretical (45°C/km) and observed estimate of the 'paleogeothermal gradient' (between 20 and 60°C/km), provides an estimated 'paleogeothermal gradient' of 45°C/km. This was used in the final generation of the burial history curve using the Lopatin Basin Modeling technique (Figure 25). The 'paleogeothermal gradient' is implied to be the result of a localized temperature gradient that existed during the thermal maturation of the Middle Ordovician rocks within southwestern Ontario. The origin and duration of the elevated temperature gradient can not be verified at present.

From Figure 25, it can be postulated that the process of hydrocarbon maturation and generation was possible in the lower part of the Middle Ordovician carbonates soon after 300 Ma, if the present evaluation of the thermal maturation of these rocks is acceptable.

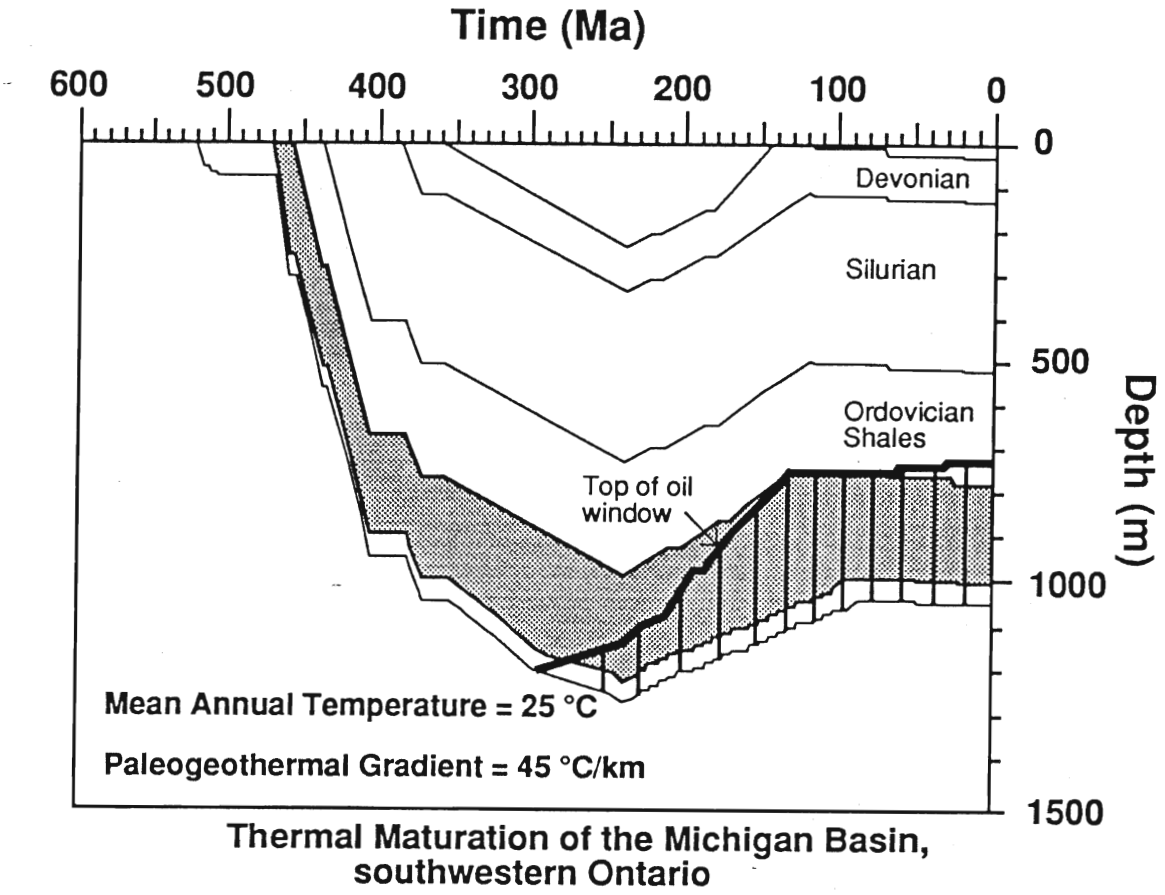

Figure 25: Burial history curve for the stratigraphic sequences within southwestern Ontario. Calculated paleogeothermal gradient of 45 °C/km used in the final approximation of the thermal maturation history of the organic bearing lithologies. Mean annual temperature of 25 °C; onset of oil generation at a Time Temperature Index (TTI) = 15.

Evaluation of Hydrocarbon Potential: Results and Discussion

An evaluation of the distribution of the organic carbon and reduced pyritic sulphur contents of the Trenton and Black River groups provide an estimate of the regional organic carbon preservation potential for the various carbonate facies within the basin. This was done by separating cored wells with respect to their geographic location as well as the stratigraphic group (Trenton vs Black River group) from which the samples were taken.

The total organic carbon and reduced sulphur concentrations for the Black River sediments from the Rowe Ram #7 Dover 3-12-VE well (located northeast of the study area within the Chatham Sag synclinal structure) are shown in Figure 26. The distribution of the these elements suggests that they have been deposited in a deep water, euxinic, sedimentary environment. The evaluation of Black River sediments within the subsurface from the Dover well (Appendix I) suggests that the 'deep' water sediments probably contributed little to the preservation of organic carbon (< 0.5 % TOC).

The organic carbon and reduced sulphur concentrations of the various Trenton Group carbonate lithologies found within the 34428 Romney 6-206-I and the 34160 Romney 5-8-II wells, in the northeastern part of the study area, is presented in Figure 27. The carbonate lithologies of the Trenton Group in Romney township contain organic carbon and reduced sulphur concentrations suggestive of a normal marine depositional environment. However, a number of samples contain elemental concentrations representing a deeper water, and euxinic environment. The organic carbon preservation potential for these rocks is reflected by slightly higher concentrations of organic carbon (from 0.5 to 1.2 % TOC).

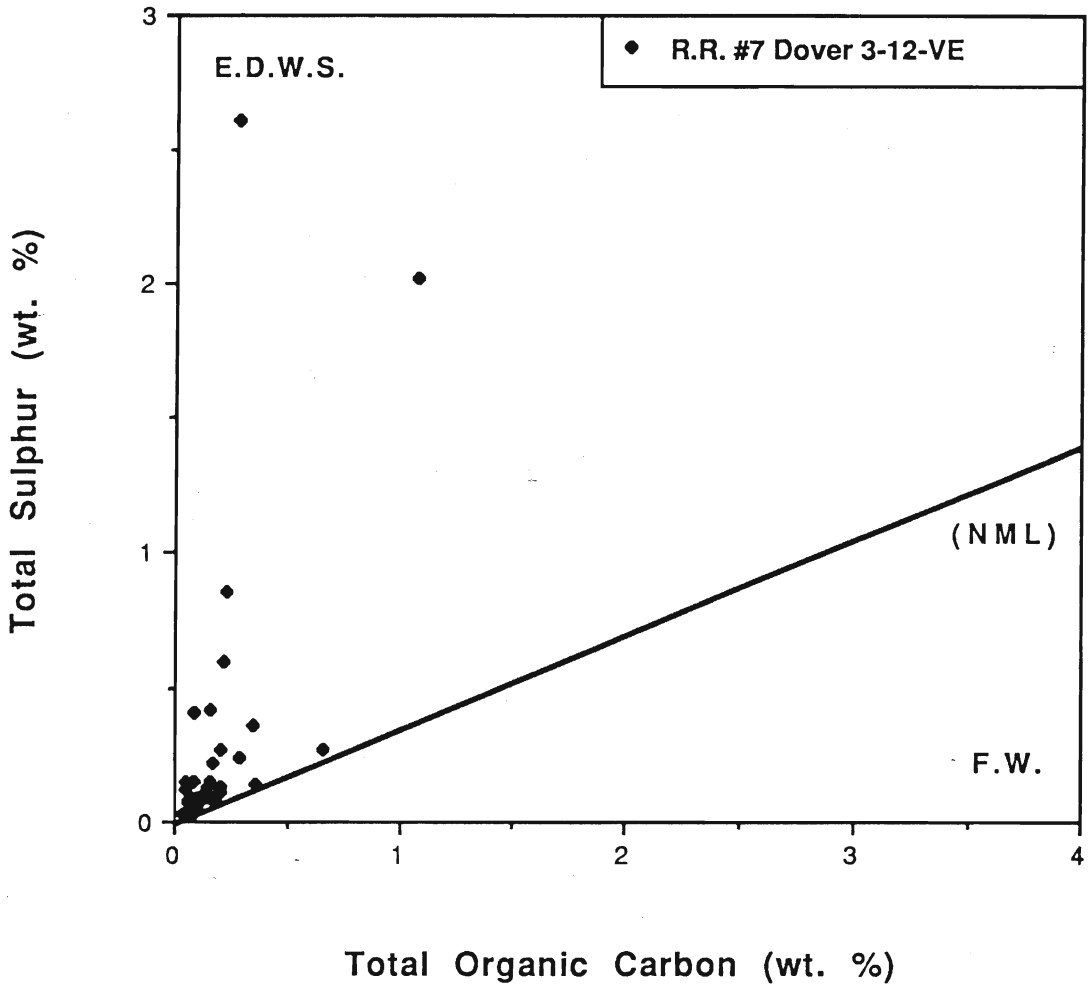

Figure 26: Total organic carbon and reduced pyritic sulphur contents for the Black Riveran Group sediments found within the Rowe Ram #7 Dover 3-12-VE well, Dover Township. NML represents the normal marine line as established by Berner and Raiswell (1983); EDWS = portion on the diagram where euxinic deep water sediments occur; FW = portion of the diagram where fresh water sediments occur (Berner and Raiswell, 1983; Raiswell and Berner, 1985).

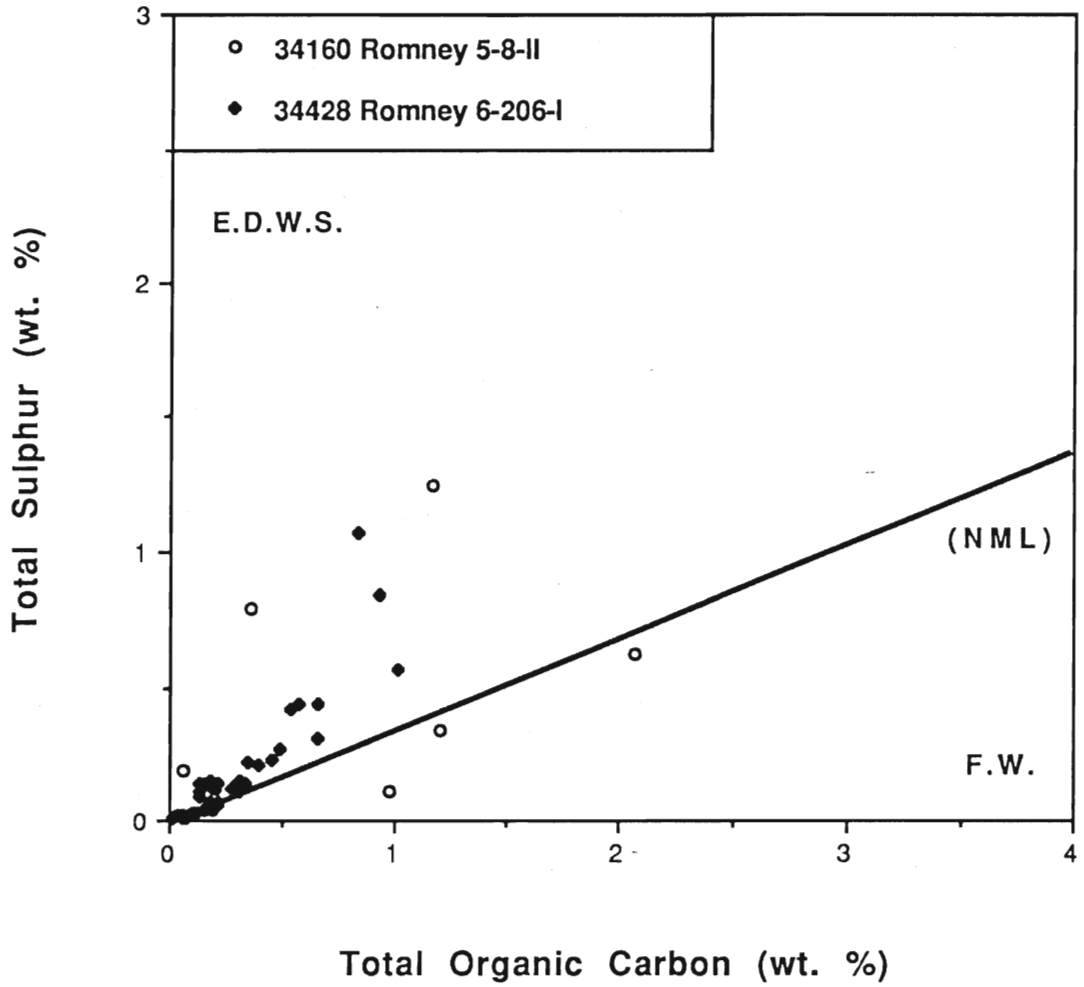

Figure 27: Total organic carbon and reduced pyritic sulphur contents for the Trenton Group sediments of the 34428 Romney 6-206-I and the 34160 Romney 5-8-II wells, Romney township. NML represents the normal marine line as established by Berner and Raiswell (1983); EDWS = portion on the diagram where euxinic deep water sediments occur; FW = portion of the diagram where fresh water sediments occur (Berner and Raiswell, 1983; Raiswell and Berner, 1985).

Organic carbon and reduced sulphur analysis on core samples from three wells within Mersea township is presented in Figure 28. Two of these wells are located within the Hillman oil field, the 33821 Mersea 3-12-I and the 33823 Mersea 1-12-A wells. The 34151 Mersea 5-8-II well is from the northwest portion of the Goldsmith-Wheatly oil field. All three wells represent Cobourg and Sherman Fall formations, Trenton Group, except for a few samples in the 33821 Mersea 3-12-I well from the underlying Black River Group.

The organic carbon and reduced sulphur elemental concentrations of the Trenton carbonates within Mersea township suggest a normal-marine depositional environment (Figure 28). Two samples from the Black River Group contain low organic carbon and high reduced sulphur contents (characteristic of deeper water, and euxinic environments; Figure 28).

Overall, the highest preservation of marine-derived organic carbon occurs in Trenton Group sediments in Mersea township. Lower preservation of organic carbon occurs in Trenton and Black group in Dover and Romney townships. In general, the lithofacies of the Trenton Group are dominated by beds characterized by coarse-grained grainstones, at the base, which grade into finer-grained grainstones and wackestones overlain by thick argillaceous calcisiltite sheets and capped with finely-laminated and nodular mudstones. Some of these beds are enriched with organic carbon. In the paleoenvironmental setting postulated by Brookfield and Brett (1988), this lithofacies represents rapid deposition of carbonate debris by storm-generated currents (Aigner, 1985). This mechanism of deposition is conducive to the preservation of organic carbon, especially if the grainstones were immediately blanketed with several centimetres of finely-laminated mud.

To test the hypothesis that the amounts of organic carbon in the various carbonate lithologies may be sufficient to generate hydrocarbons, requires a more detailed examination of the distribution of these elements

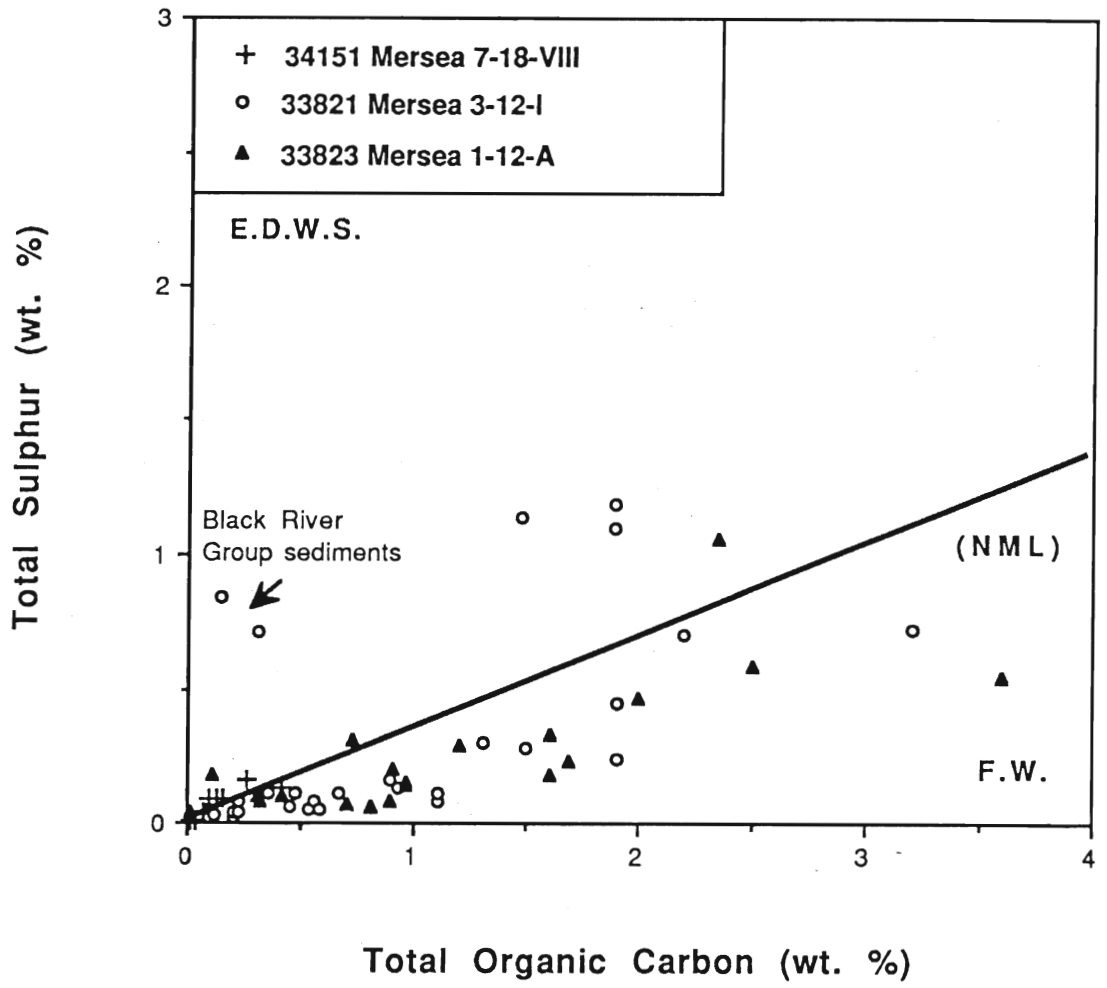

Figure 28: Total organic carbon and reduced pyritic sulphur contents for the Trenton Group sediments of Mersea township. Two of these wells are located within the Hillman oil field, the 33821 Mersea 3-12-I and the 33823 Mersea 1-12-A wells. The 34151 Mersea 7-18-VIII well came from the northwest Goldsmith-Wheatly field. NML represents the normal marine line as established by Berner and Raiswell (1983); EDWS = portion on the diagram where euxinic deep water sediments occur; FW = portion of the diagram where fresh water sediments occur (Berner and Raiswell, 1983; Raiswell and Berner, 1985).

with respect to the diagenetic properties of the various lithologies and their observed hydrocarbon saturation.

The logarithmic distribution of the organic carbon to reduced sulphur ratio, and the calculated hydrocarbon saturation are plotted relative to depth (Figures 29-32). Only cored wells with significant hydrocarbon producing zones are presented. The present surface is used as a datum.

The relative increase in the carbon/sulphur ratio appears to mimic the trend of increased oil to water saturation. Large increases and decreases in the oil saturation of the rocks, particularily the pay zones, show correlation with increased organic carbon/reduced sulphur ratios.

These measurements represent modified organic carbon and reduced sulphur contents of the rocks resulting from chemical processes during burial. The original C/S ratios were probably lower. Raiswell and Berner (1986) documented that C/S ratios in sediments older than Devonian were probably lower than the ratios that occurred after diagenesis of the sediments since there was no vascular plant-derived organic matter prior to the Devonian. Regardless, this does not reduce the significance of the relatively high organic carbon content of these carbonates. High C/S ratios which correlate to increased oil saturation suggests that these carbonates, which presently act as hydrocarbon reservoirs, also may have possessed the potential to generate hydrocarbons.

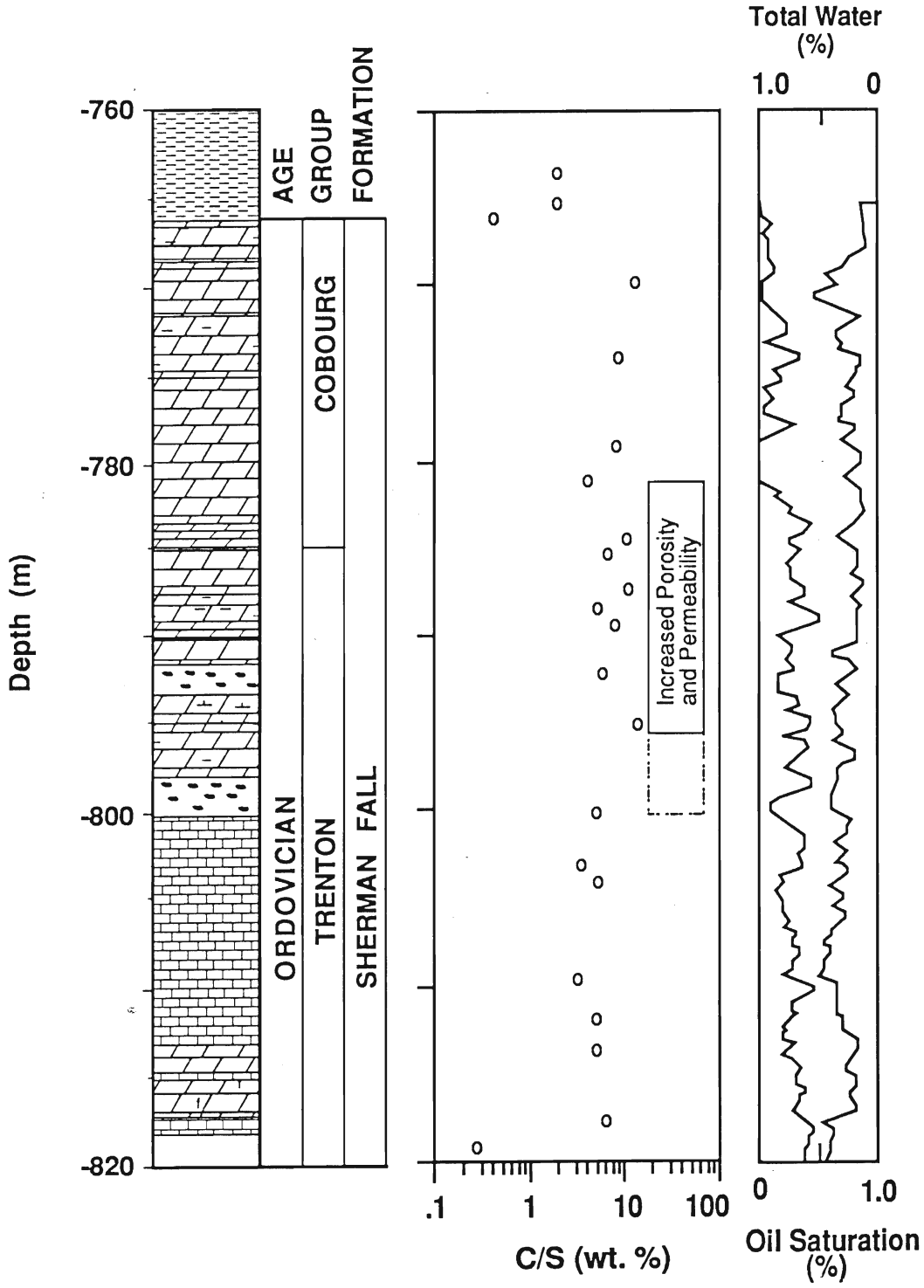

Figure 29: Stratigraphic log, C/S ratio, and hydrocarbon saturation data for rocks of the hydrocarbon producing zones for the 33821 Mersea 3-12-I well. Oil saturation on the left, and water saturation on the right.

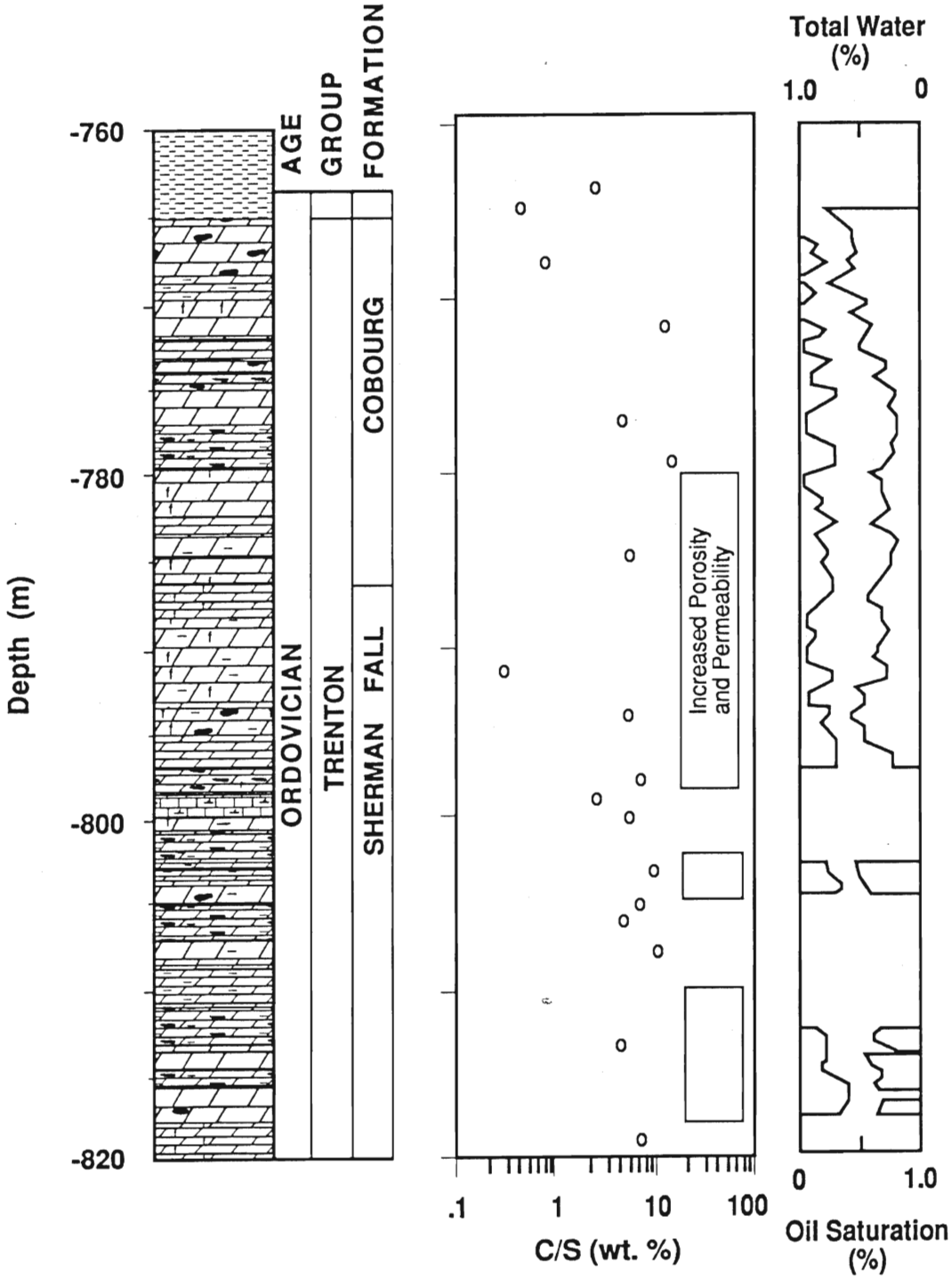

Figure 30: Stratigraphic log, C/S ratio, and hydrocarbon saturation data for rocks of the hydrocarbon producing zones for the 33823 Mersea 1-12-A well. Oil saturation on the left, and water saturation on the right.

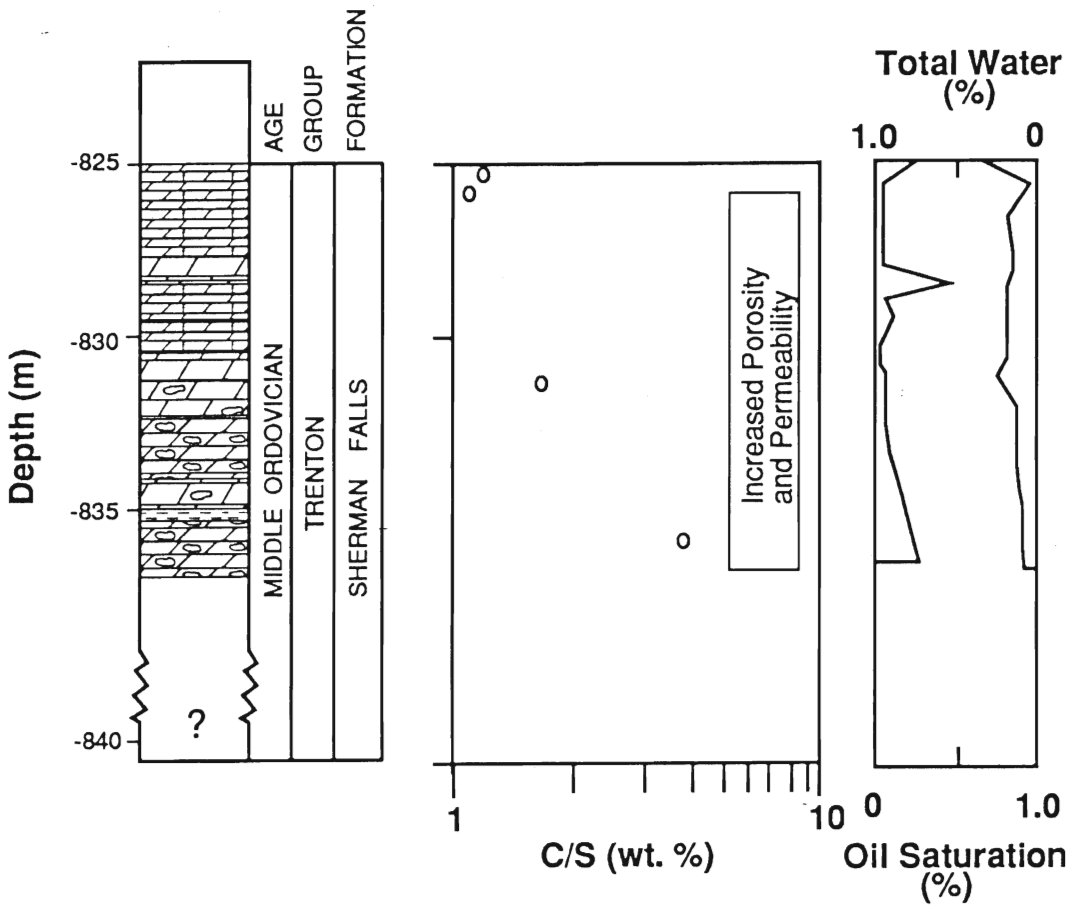

Figure 31: Stratigraphic log, C/S ratio, and hydrocarbon saturation data for rocks of the hydrocarbon producing zones for the 34151 Mersea 7-18-VIII well. Oil saturation on the left, and water saturation on the right.

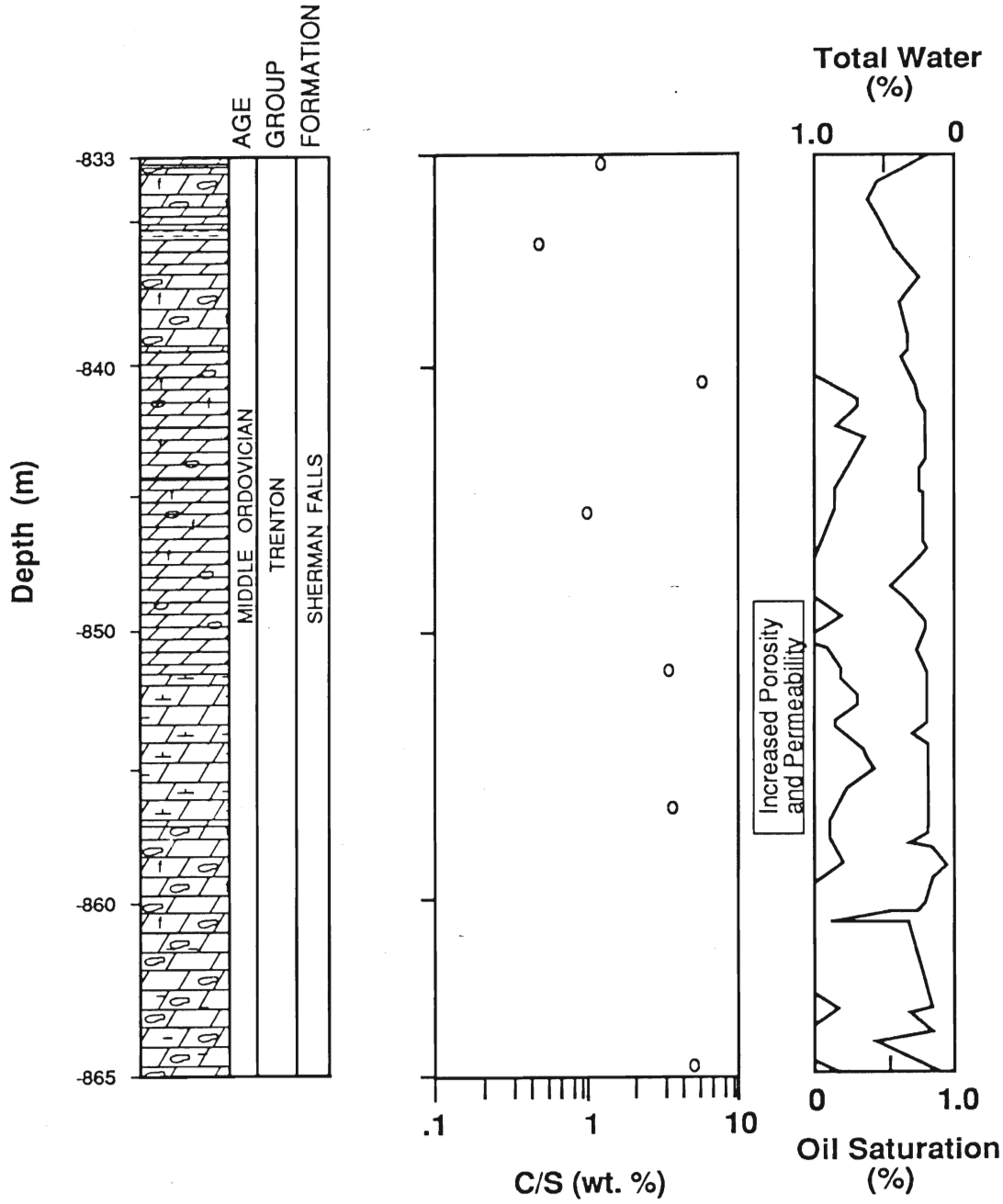

Figure 32: Stratigraphic log, C/S ratio, and hydrocarbon saturation data for rocks of the hydrocarbon producing zones for the 34160 Romney 5-8-II well. Oil saturation on the left, and water saturation on the right.

Hydrocarbon Geochemistry: Results and Discussion

Ni and V contents and their vertical variations in rock matrix samples are illustrated in Figures 33-36. Shale beds and the overlying Collingwood Formation shales contain the highest concentrations of Ni and V in the 33821 and 33823 wells.

Figure 37 is a representation of the mean and standard deviation for the Ni and V contents of the various diagenetic carbonate mineralogies associated with the hydrocarbon reservoirs. Dolomites are apparently depleted in vanadium and enriched with Ni relative to the limestone precursor (Figure 37). The saddle dolomite and ferroan calcite cements are marked by apparent enrichments in V and depletions in Ni relative to matrix dolomites. These trends in Ni and V distribution are very subtle and suggest that there was a minor re-distribution of these trace elements during the formation of the saddle dolomite and calcite cements. The cementation processes effectively reduced the pore space of the conduits in which the hydrocarbons and accompanying waters were emplaced, and probably participated in the confining of the hydrocarbons. On this basis, Ni and V concentrations in the oils may be useful in determining the migration pathways of hydrocarbons.

The Hillman-Klymer oil field presents a good opportunity to test this hypothesis on a local scale. The orientation of the oil field (NW-SE) has been defined by structural features over the reservoir. This allowed for selecting ten oil samples from the NW - SE transect through the oil field (Figure 38).

The Ni and V distribution of the ten oil samples along the NW-SE transect from the Hillman-Klymer oil field is presented in Figure 39. The V distribution decreases in a NW direction, but forms two distinct apparent depletion trends from the SE to the NW. The apparent trace element break has been correlated to increased hydrocarbon accumulation

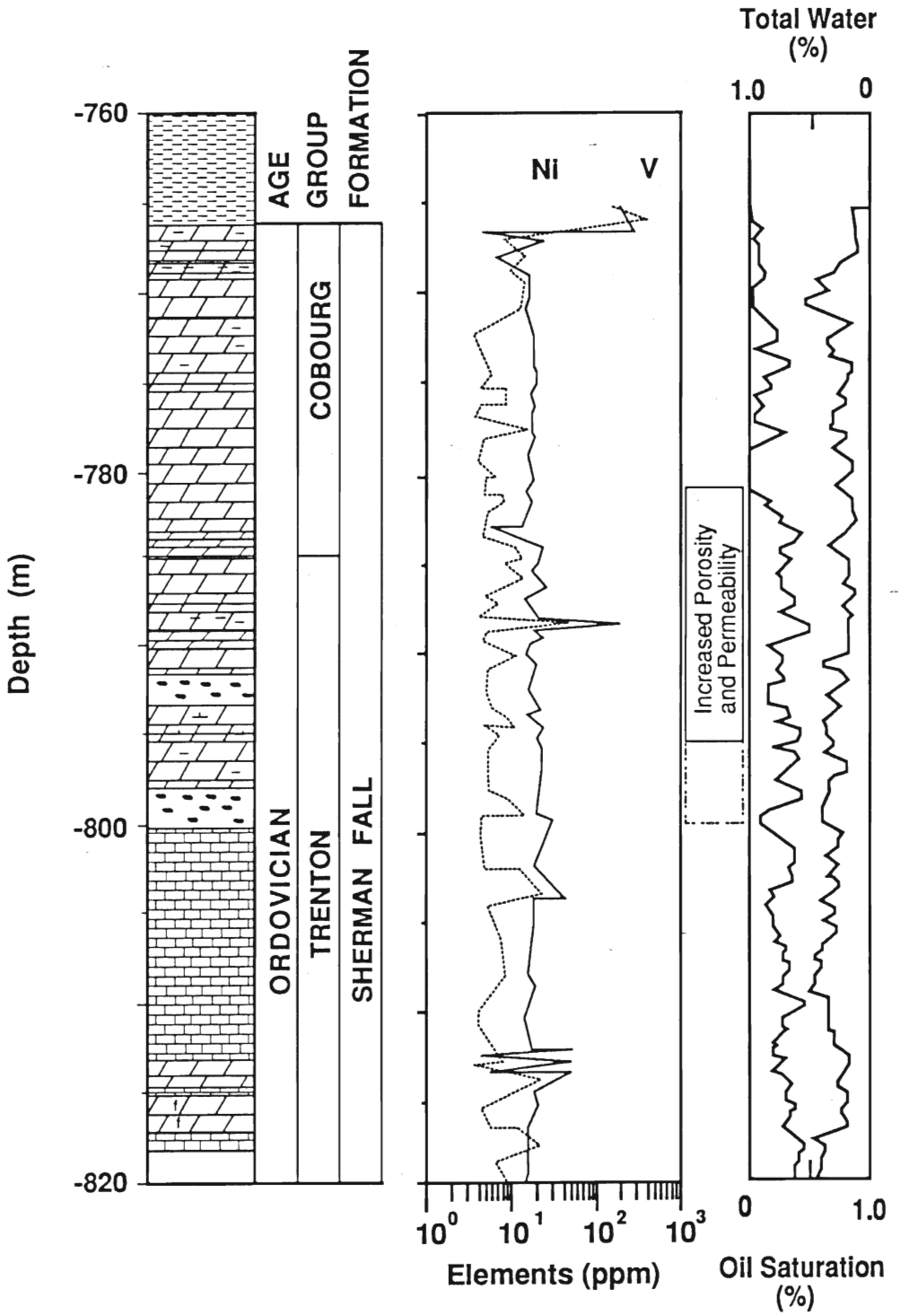

Figure 33: The Ni and V distribution of the matrix dolomite and limestone samples of the 33821 Mersea 3-12-I well. This is plotted with the stratigraphic log and the hydrocarbon saturation of the various rock lithologies.

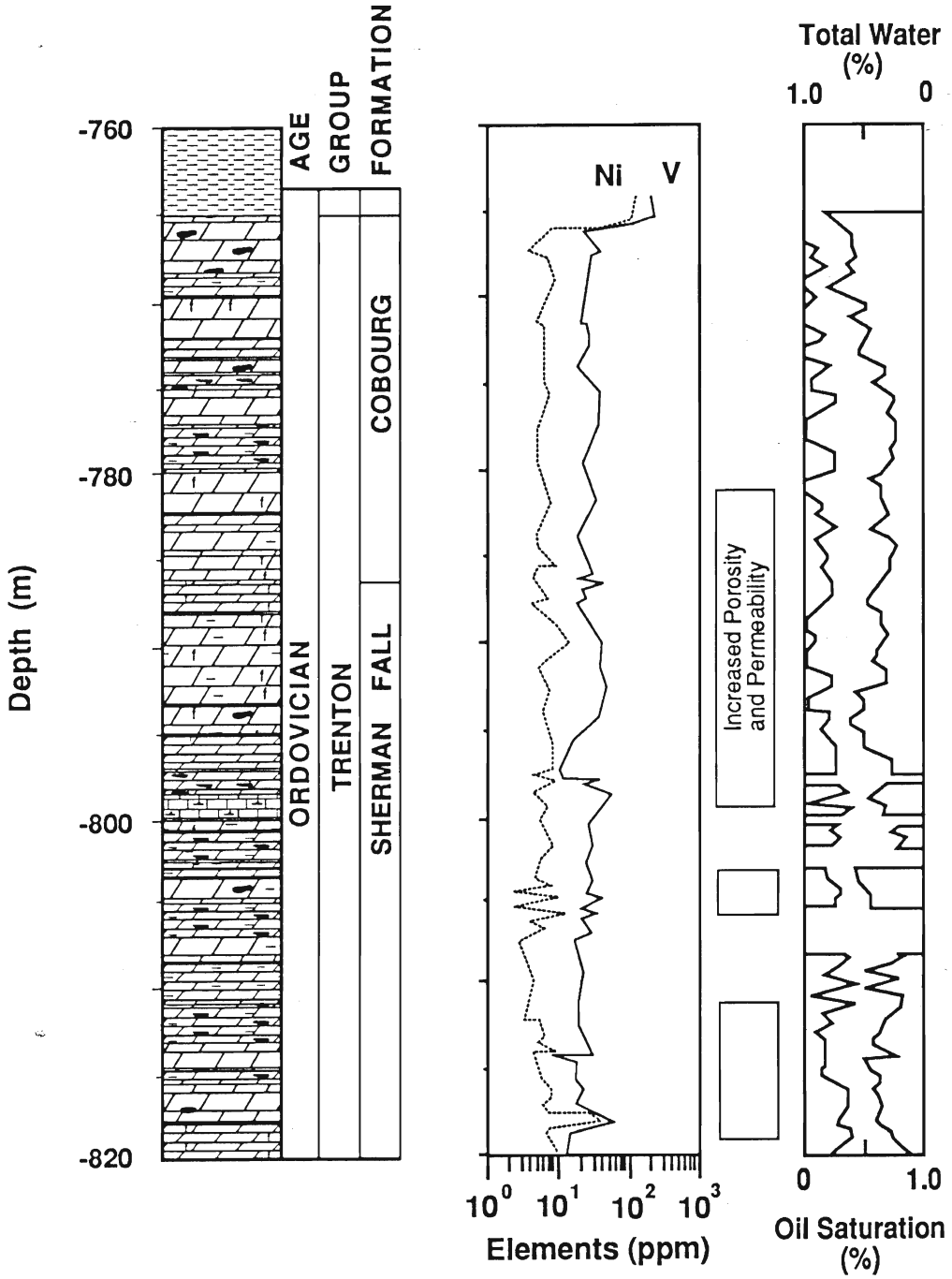

Figure 34: The Ni and V distribution of the matrix dolomite and limestone samples of the 33823 Mersea 1-12-A well. This is plotted with the stratigraphic log and the hydrocarbon saturation of the various rock lithologies.

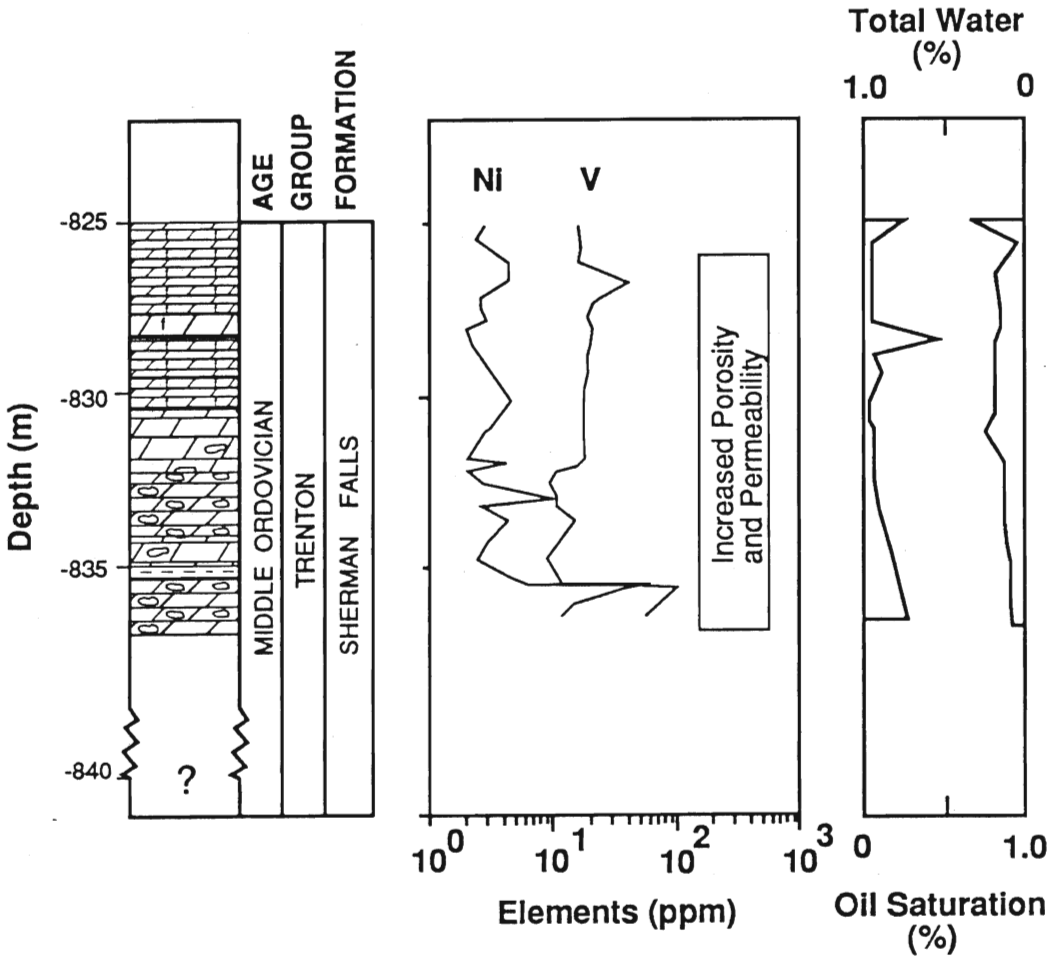

Figure 35: The Ni and V distribution of the matrix dolomite samples of the 34151 Mersea 7-18-VIII well. This is plotted with the stratigraphic log and the hydrocarbon saturation of the various rock lithologies.

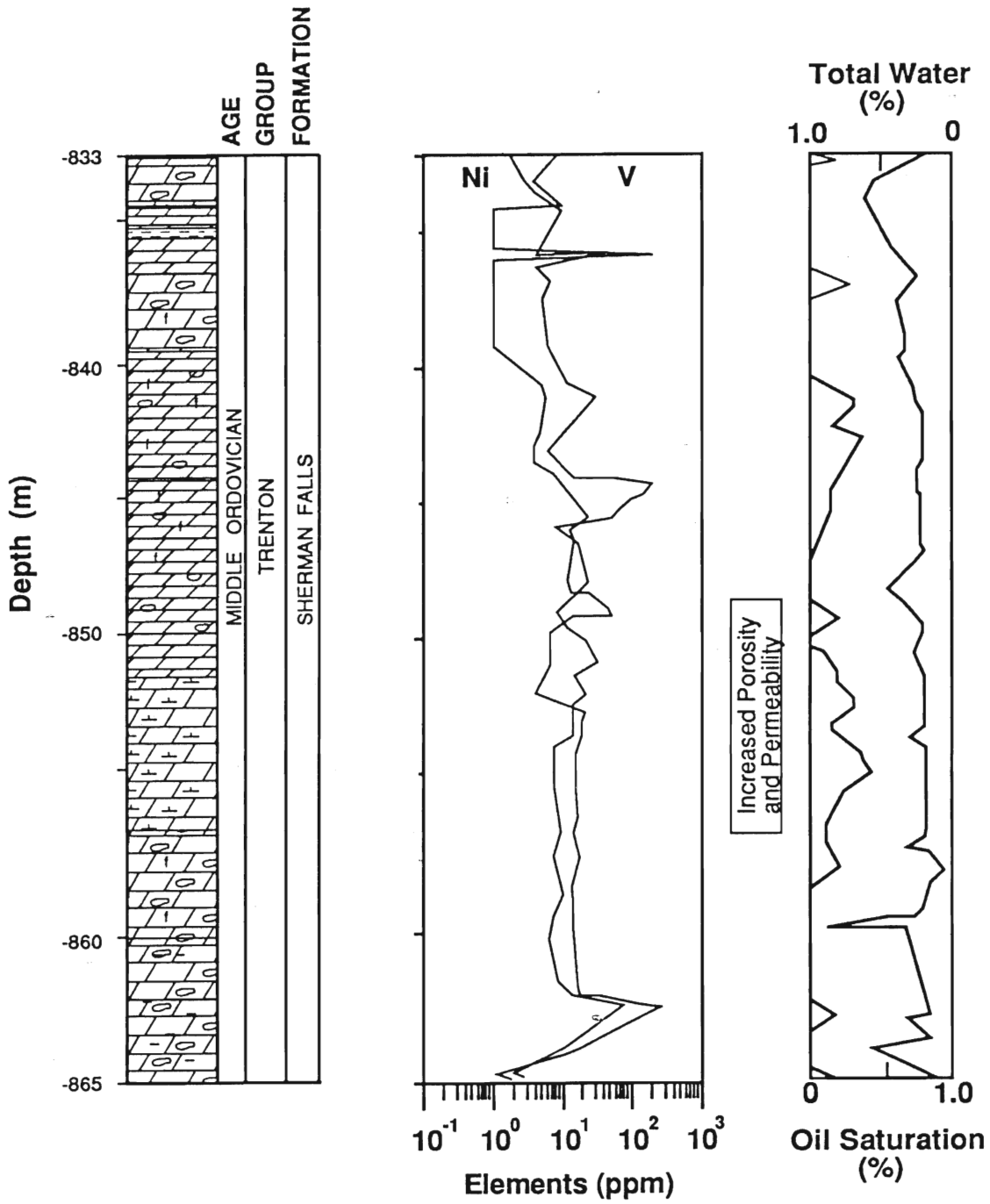

Figure 36: The Ni and V distribution of the matrix dolomite samples of the 34160 Romney 5-8-II well. This is plotted with the stratigraphic log and hydrocarbon saturation of the various rock lithologies.

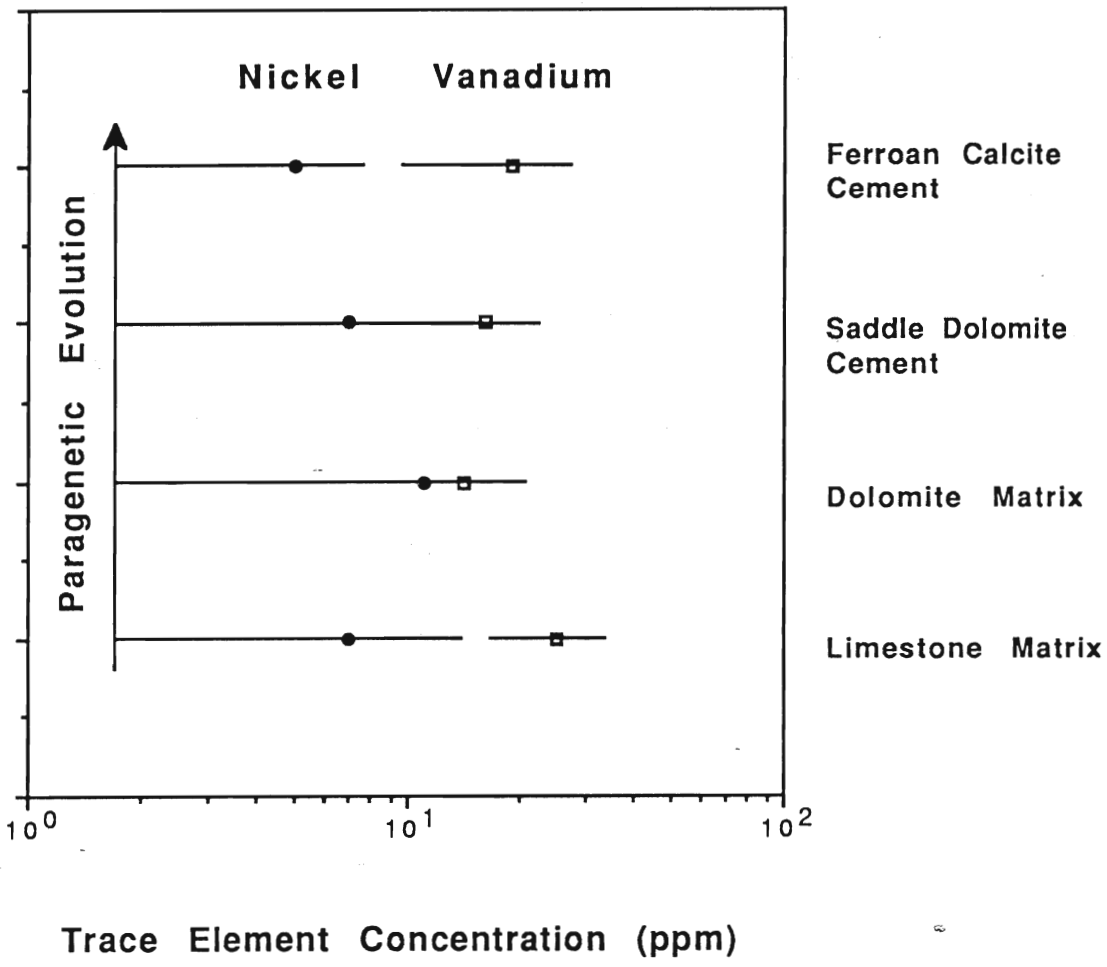

Figure 37: Mean Ni and V distribution for the diagenetic carbonate mineralogies. Data has been plotted with a log normal distribution to enhance the diagenetic trend between carbonate species. Standard deviation for the total number of samples is also presented to express the variance of the very trace, trace element distribution within the carbonate mineralogies.

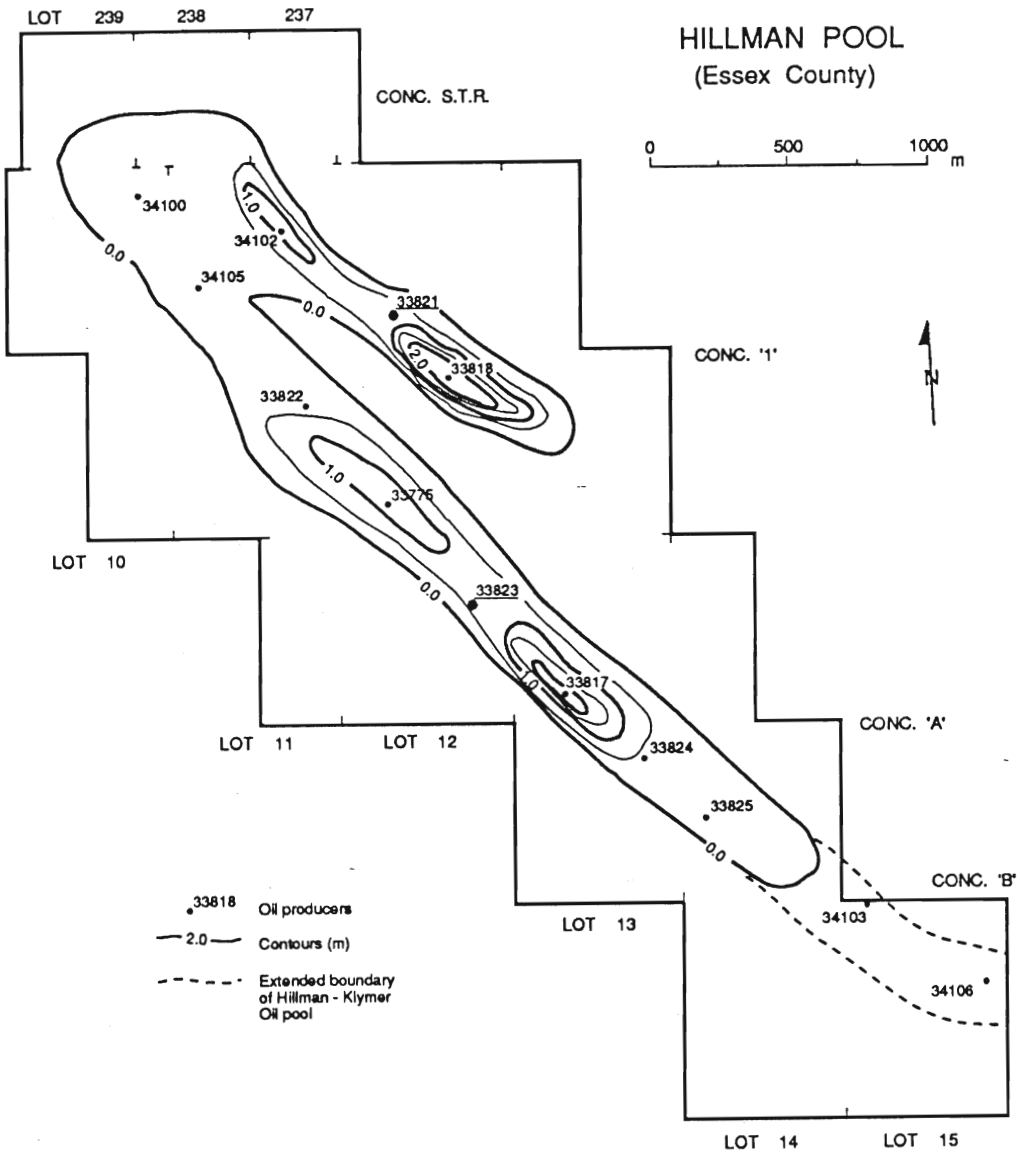

Figure 38: Hydrocarbon isopach map for the Hillman oil pool, Mersea township, Essex County. Location of oil wells are delineated along the NW-SE transect with repect to hydrocarbon accumulation thickness and their respective producing zones.

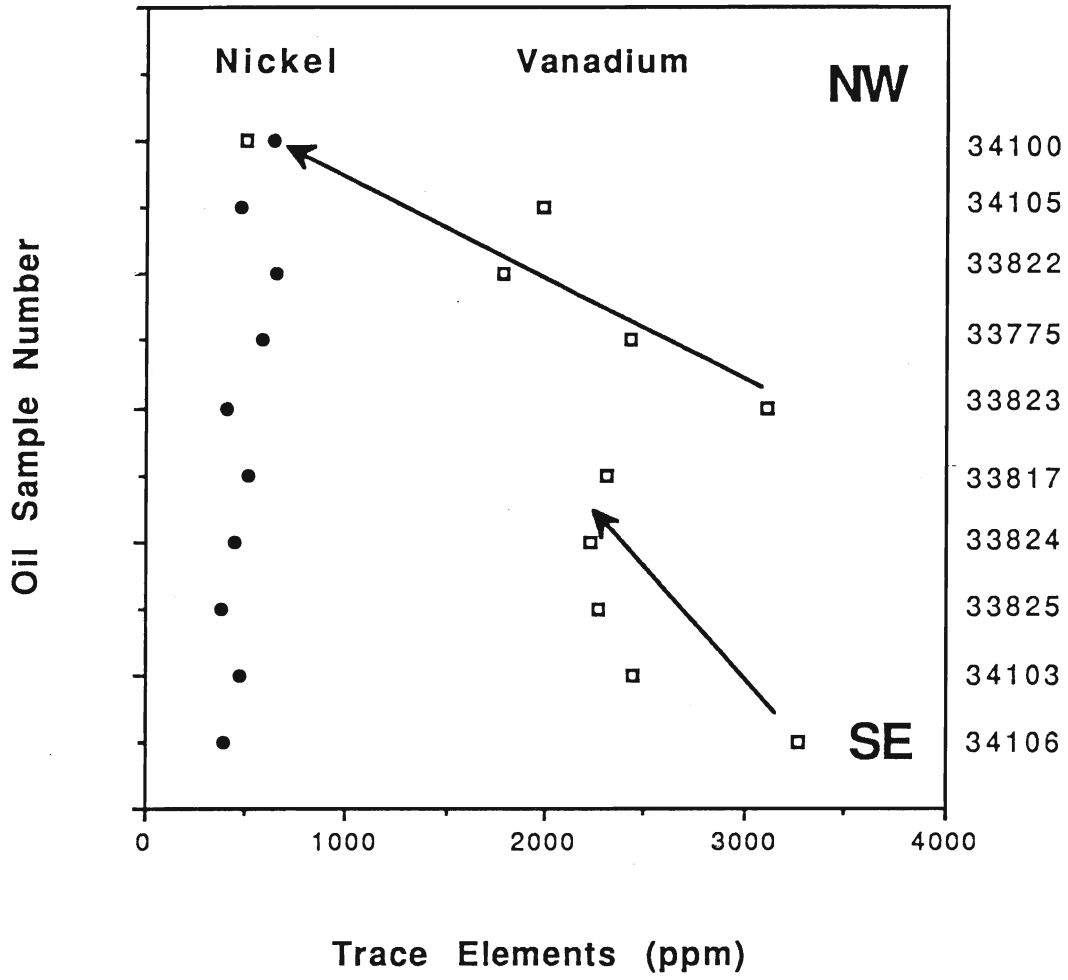

Figure 39: Mean Ni and V distribution for ten selected hydrocarbon samples which form a NW - SE transect within the Hillman oil pool, Mersea township, Essex County. Lines drawn through the V distribution are used to demonstrate apparent depletion trends towards the NW. The up-dip direction is towards the NW towards the Findlay Arch.

within the pay zones for well samples 33817, 33823, and 33776 (Figure 38). If Ni and V behave in accordance with rock-water-oil interactions during their migration through the rocks, the apparent depletion in the V distribution in the NW direction within the Hillman-Klymer trend may be interpreted as a migration direction. Although this argument is not substantiated on the basis of theoretical considerations (due to lack of chemical data on the distribution coefficients for Ni and V) the regional distribution of Ni and V in hydrocarbon samples was evaluated.

Figure 40 is a representation of the mean Ni and V distributions, along with their standard deviation, for all of the oil samples analyzed within the study area. A total of 13 oil samples from the Hillman-Klymer trend were used to evaluate the southwestern most extent of the study area, 3 oil samples from the Goldsmith-Wheatly trend representing the northeastern most portion, and 2 samples from the Renwick trend which fall between the two end members. There is an apparent depletion in the overall V content in the oil samples in a NE direction but only minor variation in the Ni trace element distribution across the proposed transect. From a purely qualitative point of view, the depletion in the V again corresponds with the structural and stratigraphic dip of the rocks in the up direction towards the Findlay Arch. Bonham (1956) and Mast et al. (1973) suggested that decreasing concentrations of vanadium and nickel in oils decrease basinward with increasing depth. Mast et al. (1973) further suggested that decreasing V concentrations correspond with the paleostructural features of the basin. The apparent depletion in the V concentrations in the oils was suggested to correlate with oils migrating great distances from their original source or to different loci of origin (Bonham, 1956). He further suggested that during migration the metallo-organic components may have been removed by selective absorption on clays, or other rock constituents.

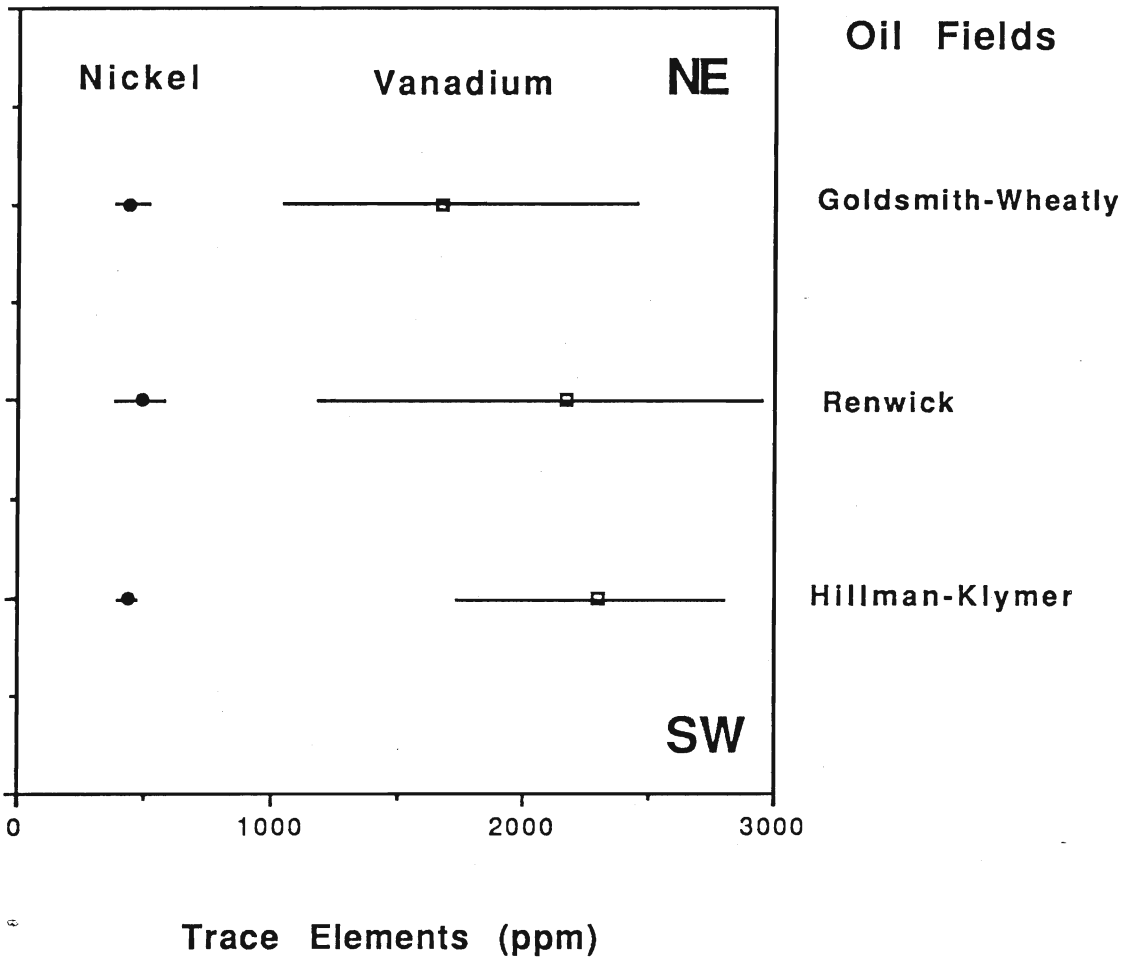

Figure 40: Mean Ni and V distribution for all hydrocarbon samples collected within the Hillman oil pool, Mersea township, Essex County, N = 13; the Renwick oil pool, Romney township, Kent County, N = 2; and the Goldsmith-Wheatly oil pool, located in Mersea and Romney townships, Essex and Kent Counties, N = 3.

In summary, the interpretations with respect to the apparent depletion of V in hydrocarbons needs to be examined in more detail. It is suggested that this should be done with respect to hydrocarbon isopach data for individual oil fields, and put into perspective with the parameters which control the physical characteristics of reservoir. There also appears to be little correlation of the relative concentrations of both Ni and V with the residual oil saturation in the carbonate matrix. It is necessary to develop theoretical considerations on the distribution of Ni and V into dolomite and calcite before attempting to model their distribution in the fluids. To estimate the validity of using Ni and V concentrations as possible indicators of hydrocarbon migration would require a more detailed analysis of permeability, porosity, percent dolomite, and grain density of the various lithologies from producing zones.

Dolomitization Model and Reservoir Development

Early Burial History

In constructing a dolomitization model for a thick sequence of carbonates, which is overlain by a relatively thick sequence of marine shales and sediments, the question of subaerial or submarine exposure has major implications for the model of dolomitization and reservoir development. There is evidence of no subaerial exposure for Trenton Group carbonates (Wilman and Kolata, 1978; Fara and Keith, 1984), with the possible exception of sediments in the Albion-Scipio area of southern Michigan; as suggested from a sharp contact between the Utica Shale and Cobourg formations, and the development of cavernous (vuggy) porosity which crosscuts the stratigraphic dip of the strata (Rooney, 1966).

Lack of a subaerial exposure implies that meteoric fluids had little to do with early burial diagenesis or with early dolomitization of the limestones. The trace element chemistry and their stable isotopic compositions of the carbonates demonstrate that meteoric fluids were not present until the latest stages of calcite precipitation which postdates hydrothermal dolomitization and mineralization events.

Dolomitization Model

The reservoirs within southwestern Ontario are postulated to have developed during dolomitization from fluids migrating upwards into faults and fracture systems (Figure 41). The formational waters had the ability to dissolve limestone. The fluids acquired heat, metals and other solutes required to deposit the sulphides in the carbonates as they emerged from the deeper parts of the basin. This would have been possible when the compactional and/or hydrodynamically driven brine carried the metals as chloride and organometallic-complexes and precipitated them when they encountered H_2S; produced from sulphate-reducing bacteria in the presence of hydrocarbons (Spirakis and Heyl, 1988). Present day

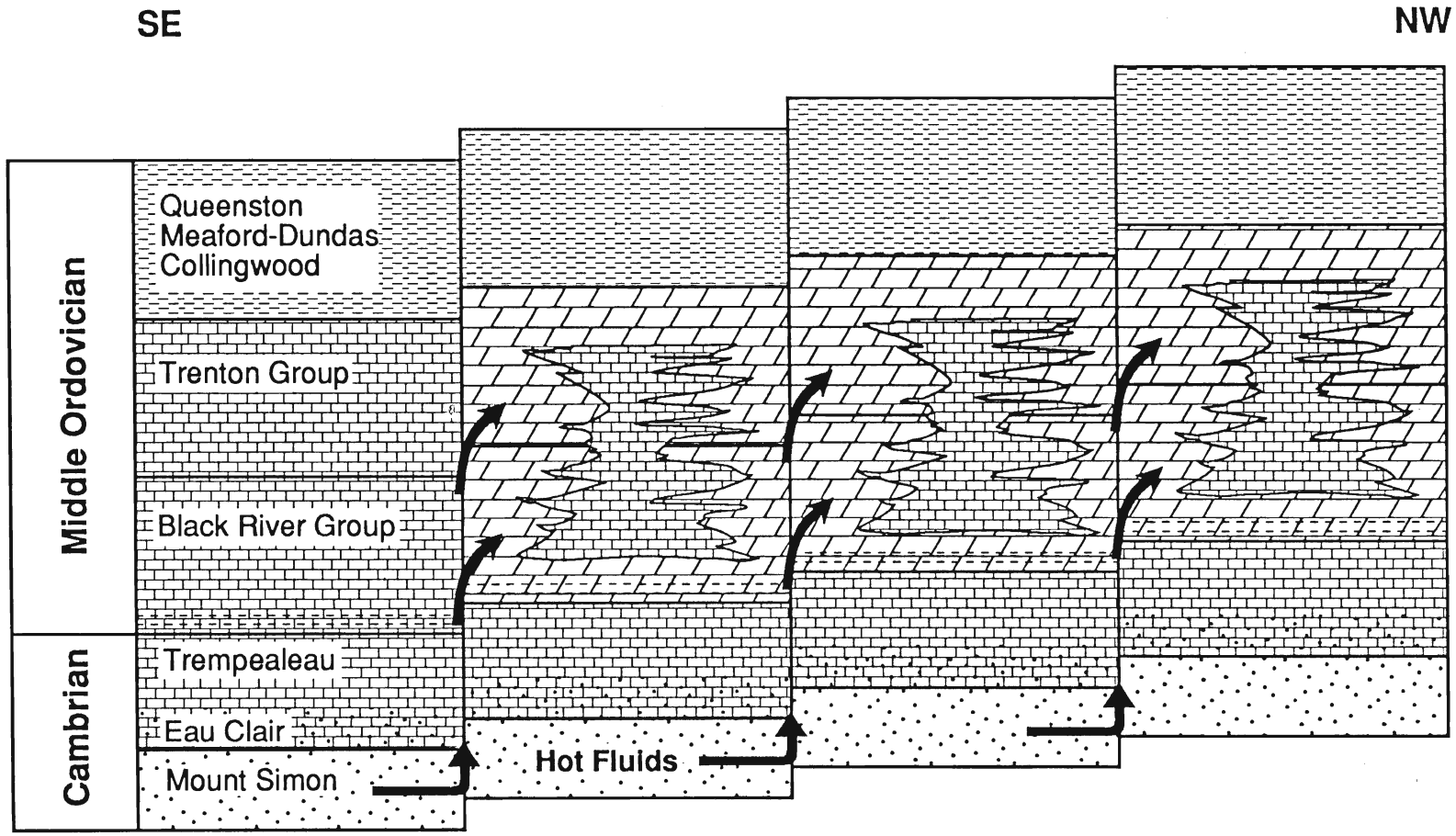

Figure 41: Conceptual model for the dolomitization of the rocks within southwestern Ontario. Only the distribution pattern for the dolomite of the middle Ordovician carbonates is presented based on the limited knowledge of the underlying units. Inferred paleodip and structural interpretations are conceptual.

precipitation of galena and sphalerite occurs within the dolomites of the Eramosa, Goat Island, and Gasport members of the Middle Silurian Lockport Formation along the northern margin of the Niagara Peninsula between Niagara Falls and Hamilton (cf. Haynes and Mostaghel, 1982). The mechanics of the process are simple. The upward migration of the reducing brine meets an oxygenated barrier, the original formational waters would represent a oxygenated reservoir compared to the reduced brine, whereby the oxidation process releases hydrogen ions and lowers the activity constants of the complexed trace elements (Fe, Pb, Zn, Cu, etc.) which results in the precipitation of the sulphide phases (Phelps, 1978).

Evidence for Mississippi Valley-type processes in the Michigan Basin

From this study, the presence of various hydrothermally produced minerals which formed at relatively shallow burial depths (saddle dolomite, anhydrite, silica, pyrite, sphalerite, calcite, and celestite), are similar to Mississippi Valley-type deposits. This requires that the fluids responsible for their emplacement were not typical formational fluids which had undergone progressively elevated temperatures during burial. An autochthonous source for the fluids is preferred and it is interpreted that these fluids migrated upward from underlying Cambrian clastics along major faults and associated fractures.

Shaw (1975) observed 2-phase fluid inclusions within the Albion-Scipio saddle dolomite cements and concluded that hydrocarbons were present during their formation. Ultraviolet fluorescence of the fracture-filling (pore-occluding) cements, in this study, verified the presence of hydrocarbons during the precipitation of the saddle dolomites. Fluid inclusion analysis of the saddle dolomites from the fracture-related processes in the Albion-Scipio field yielded temperatures around 80°C (Shaw, 1975; Taylor and Sibley, 1986). Budai and Wilson (1986) identified many MVT accessory minerals in association with saddle dolomite cements

and related their presence to a hydrothermal process. They suggested that the lower Paleozoic and Precambrian basement rocks acted as sources for the trace metals deposited in the Trenton-Black River carbonates during the early Paleozoic.

Other distinctive features of reservoirs within the Michigan Basin, which are similar to MVT mineral deposits, include synclinal sag structures, solution breccias, secondary porosity, and high-temperature carbonates. The hydrocarbons may have played a role in the reduction of sulphate in the pore water to sulphide (Beales and Hardy, 1980) seen by the persistent sulphide mineralization throughout the paragenetic sequence in this study.

Phelps (1978) suggested that the fault-controlled Pb-Zn occurrence along the Clearville, Electric, and Dover faults in Essex and Kent Counties, was the result of a Mississippi Valley-type deposit due to upward migration of hot brines along these faults. Cooling and dilution of the brines resulted in the deposition of metal sulphides in the overlying rocks (Phelps, 1978).

Summary of Results

Evolution of Stable Isotopes in Diagenetic Waters

Stable isotope analyses of the limestones, dolomites, saddle dolomite and late calcite cements have demonstrated that the Trenton Group carbonates have been altered by a number of diagenetic processes. These processes have been summarized into the following stages (Figure 42):

Stage I represents burial diagenesis. Stable isotope analysis of Trenton brachiopods (LMC) and limestones suggest that burial diagenesis was the only 'early' diagenetic process. This is suggested from depletion in their $\partial^{18}O$ compositions from -5 to -10 ‰.

Stage II represents dolomitization of the limestone. Stable isotopic compositions of the dolomites, $\partial^{18}O$ between -7.5 and -11.6 ‰ (average of

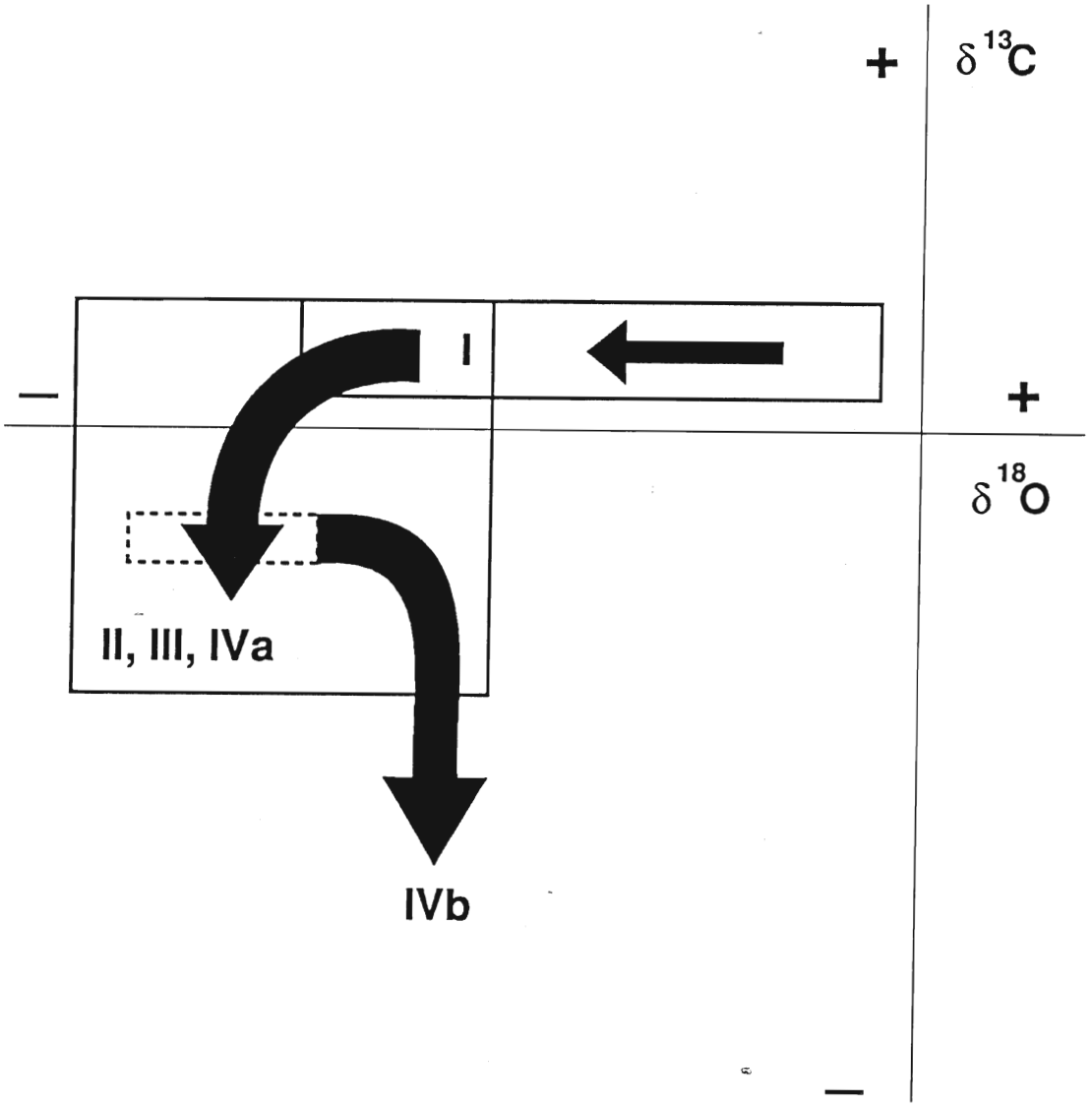

Figure 42: Inferred evolution of stable isotopes in diagenetic fluids. Stage I = burial diagenesis; Stage II = dolomitization; Stage III = precipitation of saddle dolomite cement; Stage IVa = precipitation of late (ferroan) blocky calcite cement; and Stage IVb = precipitation of late (ferroan) dog-tooth calcite cement.

-9.7 ‰) and $\partial^{13}C$ between 1.0 and -1.0 ‰ (average of 0 ‰), suggests that dolomitization was the result of hot basinal fluids which had migrated from depth.

Stage III represents the precipitation of saddle dolomite cements. Stable isotopic compositions, $\partial^{18}O$ between -9.0 and -10.5 ‰ (average of -9.7 ‰) and $\partial^{13}C$ between 1.0 and -1.2 ‰ (average of -0.1 ‰), suggests that hot basinal fluids were also responsible for the precipitation of saddle dolomite within the fault and fracture systems.

Stage IVa represents the precipitation of late blocky calcite cement. Stable isotopic compositions, $\partial^{18}O$ between -10.8 and -12.2 ‰ (average of -11.5 ‰) and $\partial^{13}C$ between -0.3 and -1.2 ‰ (average of -0.7 ‰), suggests that the precipitation of late blocky calcite cements represents the latest fracture filling event by hot basinal fluids.

Stage IVb represents the precipitation of late dog-tooth calcite cement. Stable isotopic compositions, $\partial^{18}O$ between -7.6 and -9.6 ‰ (average of -8.2 ‰) and $\partial^{13}C$ between 0.4 and -2.9 ‰ (average of -1.0 ‰), which forms the apparent 'upside-down J-shaped curve', suggests the introduction of meteoric fluids into the fracture systems. The presence and predominance of dog-tooth calcite cement post-dates all of the other Mississippi Valley-type minerals.

Paragenetic History

The paragenetic history of all the diagenetic processes is summarized in Figure 43 and is based on petrographic textural relationships and their relationship to hydrocarbon generation.

The paragenetic sequence relative to the burial history curve is presented in Figure 44 which includes the interpreted temperatures for each diagenetic stage during basin development.

Stage I represents burial diagenesis. Temperatures of alteration during burial diagenesis ranged from 30 to 50°C, based on $\partial^{18}O$

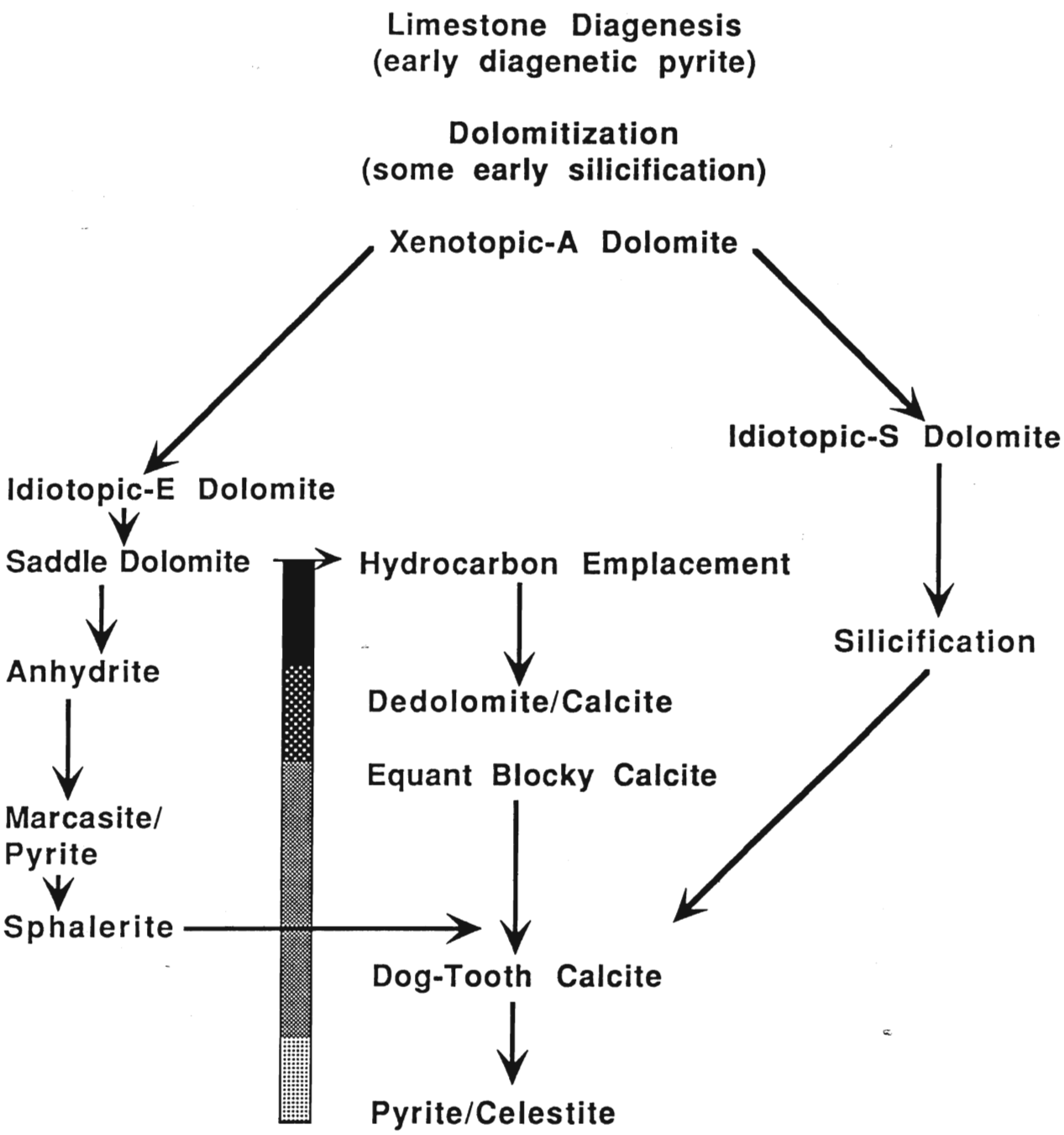

Figure 43: Paragenetic history of various stages of diagenesis of Trenton Group carbonates and their relationship to the introduction/generation of hydrocarbons. The vertical bar represents observed hydrocarbons; (dark = 100 % of the time, stippled = 25 % of the time.)

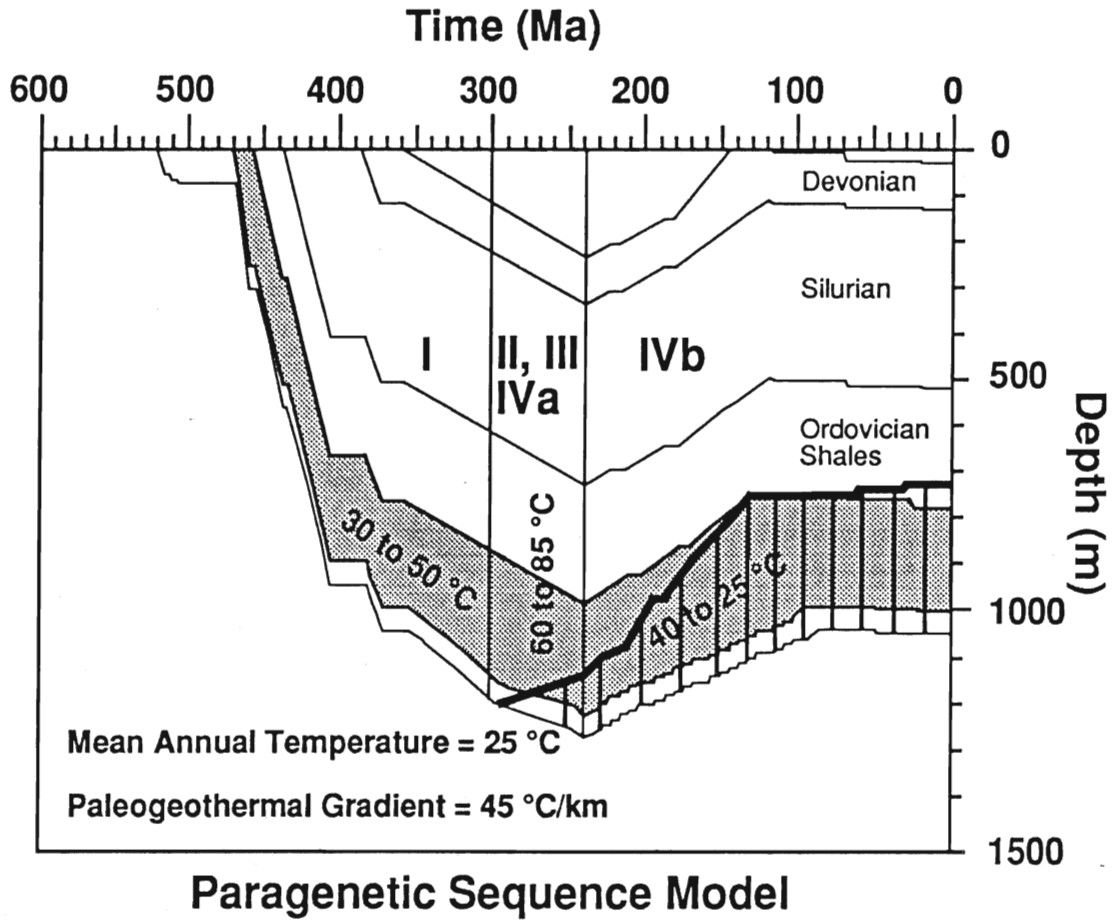

Figure 44: Paragenetic sequence model illustrating progressive basin development, timing and duration of diagenetic processes, and the onset of oil generation /introduction into lower Paleozoic rocks, southwestern Ontario.

temperature calculations. Evaluation of the conodont colour alteration indices suggest a geothermal gradient during burial diagenesis between 17 and 25°C/km. Burial diagenesis is suggested to have taken place before the maximum subsidence of the basin, estimated around 300 Ma.

Diagenetic Stages II, III, and IVa, represent dolomitization, saddle dolomite precipitation, and precipitation of blocky calcite cement, respectively. Hydrothermal processes, similar to Mississippi Valley-types, are suggested to have occurred at paleotemperatures between 60 and 85°C, based on $\partial^{18}O$ temperature calculations. Hydrothermal alteration probably occurred some time between maximum subsidence of the basin (estimated around 300 Ma) and up to the unloading and cooling of the basin (estimated around 238 Ma).

Diagenetic Stage III corresponds to the earliest time at which oil may have been generated. Hydrocarbons were introduced during the precipitation of saddle dolomite, the earliest fracture filling stage.

Diagenetic Stage IVb represents the precipitation of late dog-tooth calcite cement. It is suggested that they precipitated during the introduction of meteoric waters corresponding with the unloading and cooling of the basin (which is estimated after 238 Ma). Paleotemperatures during the precipitation of dog-tooth calcite cements were probably between 60 to 25°C, based on $\partial^{18}O$ temperature calculations. The majority of the dog-tooth calcite cements, which make up the 'upside-down J-shaped curve' (Figure 42), probably precipitated at paleotemperatures between 40 to 25°C, based on $\partial^{18}O$ temperature calculations.

Conclusions

The rock matrix and cements from cores from four oil wells within southwestern Ontario were examined.

1) Geochemical analyses of brachiopods and limestones suggest that diagenetic alteration resulted from rock-fluid interactions in the presence of mixed waters during increasing burial. Burial diagenesis is suggested to have occurred at paleotemperatures between 30 to 50°C (based on $\partial^{18}O$ temperature calculations) before the maximum subsidence of the Michigan Basin (estimated around 300 Ma).

2) Dolomitization of the carbonate precursor took place within a fluid-dominated environment. $\partial^{18}O$ compositions between -7.5 and -11.6 ‰ (average of -9.7 ‰) and $\partial^{13}C$ compositions between 1.0 and -1.0 ‰ (average of 0 ‰) suggest dolomitization occurred in the presence of hot basinal fluids which migrated from depth along faults and fractures. Temperature calculations from $\partial^{18}O$ data suggest that dolomitization took place at paleotemperatures between 60 - 75°C. However, the occurrence of saddle dolomite and conodont colour alteration indices evaluated from the fractured dolomites (Xenotopic-A with saddle dolomite) suggest that temperatures may have exceeded 100°C. Further evidence of MVT type processes is the presence of saddle dolomite, anhydrite, pyrite, sphalerite, calcite and celestite occluding pore space within variable-sized vugs and fractures. This is suggested to have occurred some time between maximum subsidence of the basin (estimated around 300 Ma) and up to the unloading and cooling of the basin (estimated around 238 Ma).

3) Saddle dolomite precipitation proceeded due to rock-fluid interactions in the presence of hydrothermal fluids. $\partial^{18}O$ compositions between -9.0 and -10.5 ‰ (average of -9.7 ‰) and $\partial^{13}C$ compositions between 1.0 and -1.2 ‰ (average of -0.1 ‰) suggest their precipitation during the hydrothermal process at paleotemperatures between 60 - 70°C

(based on $\partial^{18}O$ temperature calculations). The precipitation process and fluids were homogeneous as demonstrated by the homogeneous luminescence of the saddle dolomite cements. Ultraviolet fluorescence suggests that hydrocarbons were present during the earliest formation of saddle dolomite.

4) Blocky calcite cements were precipitated in a fluid-dominated environment. $\partial^{18}O$ compositions of the late blocky calcite cements, between -10.8 and -12.2 ‰, and $\partial^{13}C$ compositions between -0.3 and -1.2 ‰, suggest that they precipitated at the end of the hydrothermal process. They are suggested to have precipitated at paleotemperatures between 85 and 55°C, based on $\partial^{18}O$ temperature calculations.

5) Dog-tooth calcite cements were precipitated in a fluid-dominated environment. $\partial^{18}O$ compositions of the late dog-tooth calcite cements, between -7.6 to -9.6 ‰, and $\partial^{13}C$ compositions between 0.4 to -2.9 ‰, suggest that they precipitated in the presence of meteoric waters. These calcite cements are suggested to have precipitated at paleotemperatures between 60 and 25°C, based on $\partial^{18}O$ temperature calculations. This is suggested to have taken place some time after the unloading and cooling of the basin, estimated around 238 Ma.

6) Hydrocarbon generation within the Trenton Group carbonates was possible after 300 Ma, as suggested by Lopatin burial modelling of the reconstructed Paleozoic sequence within southwestern Ontario. The Trenton Group carbonates appear to represent good source rocks, with TOC's from 1 to 3.5 %. The generation of hydrocarbons is suggested to have been possible due to localized thermal maturation under the influence of hot Mississippi Valley-type fluids.

7) An apparent depletion in vanadium concentrations in hydrocarbon samples from the Hillman oilfield, trends northwest towards the Findlay Arch. An apparent depletion in vanadium concentrations in hydrocarbon samples from the Hillman-Klymer oil field, the Renwick oilfield, to the

Goldsmith-Wheatly oil field, trends northeast towards the Findlay Arch. The apparent depletion in vanadium concentrations in hydrocarbon samples parallel the structural and stratigraphic integrity of the Michigan Basin within southwestern Ontario. The vanadium trends suggest its use as a tracer of hydrocarbon migration.

REFERENCES

Ahr, W.M., 1973. The carbonate ramp: an alternative to the shelf model: Gulf Coast Association Geological Societies Transactions, **23**, p. 221-225.

Aigner, T., 1985. Storm depositional systems: Dynamic stratigraphy in modern and ancient shallow marine sequences: Lecture Notes in Earth Sciences, **3**, Springer-Verlag, Berlin, 174p.

Allan, J.R., and Matthews, R.K., 1977. Carbon and Oxygen isotopes as diagenetic and stratigraphic tools: surface and subsurface data, Barbados, West Indies. Geology, **5**, p. 16-20.

_____, 1982. Isotopic signatures associated with early meteoric diagenesis. Sedimentology, **29**, p. 797-817.

Amoruso, J.J., 1957. A structural study of the Northville oil field, Washtenaw and Oakland Counties. M.A. Thesis, University of Michigan, Ann Arbor, 25 p.

Anderson, G.M., and Macqueen, R.W., 1982. Ore Deposit Models-6. Mississippi Valley-Type Lead-Zinc Deposits. Geoscience Canada, **9**, no. 2, p. 108-117.

Ardrey, J.J., 1957. A structural study of the Northwille Oil Field, Washtenaw, and Oakland counties: M.A. Thesis, University of Michigan, Ann Arbor, 25p.

Arthur, M. A., Anderson, T. F., Kaplan, I. R., Veizer, J., and Land, L. S., 1983. Stable Isotopes in Sedimentary Geology. SEPM Short Course No. **10**, Dallas, Texas, p. 3-1 - 3-31.

Baker, E.W., and Louda, J.W., 1986. Porphyrins in the geological record. In Biological Markers in the Sedimentary Record, ed., R.B. Johns, p. 125-225. Elsevier, New York.

Baker, P.A., and Kastner, M., 1981. Constraints on the formation of sedimentary dolomite. Science, **213**, p. 214-216.

Barwise, A.J.G., 1987. Mechanism involved in altering Deoxophylloerythroetioporphyrin-Etioporphyrin ratios in sediments and oils. In Metal Complexes in Fossil Fuels: Characterization and Processing, eds., R.H. Filby and J.F. Branthaver. A.C.S. Symposium Series 344, p. 100-109.

_____, and Park, P.J.D., 1983. Petroporphyrin fingerprinting as a geochemical marker. In Advances in Organic Geochemistry 1981, eds., M. Bjoroy et al., p. 668-674.

Bates, N., 1989. Biogeochemistry of Paleozoic brachiopods from New York State and Ontario. Unpublished M.Sc. Thesis, Brock University, 257p.

Bathurst, R.G.C., 1975. Carbonate sediments and their diagenesis: Elsevier, Amsterdam, 658 p.

Bausch, W., and Hoefs, J., 1972. Die Isotopenzusammensetzung von Dolomiten und Kalken aus suddeutschen. Malm. Contrib. Mineral. Petrol., **37**, p. 121-130.

Beales, F.W. 1971. Cementation by white sparry dolomite. In Bricker, O. P. (ed.), Carbonate cements. John Hopkins University Press, p. 330-338.

_____, 1975. Precipitation mechanisms for Mississippi Valley-Type Ore Deposits. Econ. Geology, **70**, p. 943-948.

_____, and Hardy, 1980. Criteria for the recognition of diverse dolomite types with an emphasis on host rocks for Mississippi Valley-type ore deposits, in Zenger, D.H., Dunham, J.B., and Ethington, R.L., (eds.), Concepts and Models of Dolomitization, SEPM Special Publication 28, p. 197-213.

Becker, R.H., and Clayton, R.N., 1972. Carbon isotopic evidence for the origin of a banded iron formation in Western Australia. Geochim. Cosmochim. Acta, **36**, p. 577-595.

Berner, R.A., and Raiswell, R., 1983. Burial of organic carbon and pyrite sulphur in sediments over Phanerozoic time: a new theory. Geochim. Cosmochim. Acta, **47**, p. 855-862.

Blumer, M., 1965. Organic pigments: their long term fate. Science, **149**, p. 722-726.

_____, 1973. Chemical fossils: trends in organic geochemistry, in Swain, T., (ed.), Chemistry in Evolution and Systematics, London, Butterworths, p. 591-609.

Bonham, L.C., 1956. Geochemical investigation of crude oils. Amer. Assoc. Petrol. Geologists, Bull., **40**, p. 897-908.

Bonnet, R., Burke, P.J., and Czechowski, F., 1987. Metalloporphyrins in lignite, coal, and calcite, in Filby, R.H., and Branthaver, F., (eds.), Metal complexes in Fossil Fuels: Characterization and Processing, ACS Symposium Series 344, p. 177-185.

Bottinga, Y., 1968. Calculated fractionation factors for carbon and hydrogen isotope exchange in the system calcite-carbon dioxide-graphite-methane-hydrogen-water vapour. Geochim. Cosmochim. Acta,**15**, no. 1, p. 49-64.

Boreham, C.J., Fookes, C.J.R., Popp, B.N., and Hayes, J.M., 1989. Origins of etioporphyrins in sediments: Evidence from stable carbon isotopes. Geochem. Cosmochem. Acta, **53**, p. 2451-2455.

Bownocker, J.A., 1903. The occurrence and exploitation of petroleum and natural gas in Ohio: Geological Survey of Ohio, 4th series, Bulletin 1, 325 p.

Brand, U., 1982. The oxygen and carbon isotope composition of Carboniferous fossil components: sea water effects. Sedimentology, **29**, p. 139-147.

Brand, U., (in press). Chemical Diagenesis and Dolomitization of Paleozoic High-Mg Calcite Crinoids.

_____, and Terasmae, J., 1986. Source rock geochemistry of Pleistocene tills of southern Ontario. OGS Open File Report 56, 56-16, 136 p.

_____, and Veizer, J., 1980. Chemical diagenesis of a multicomponent carbonate system - 1: trace elements. Journal of Sedimentary Petrology, **50**, p. 1219-1236.

_____, and Veizer, J., 1981. Chemical diagenesis of a multicomponent carbonate system-2: Stable isotopes. J. Sed. Petrol., **51**, p. 987-997.

_____, and Veizer, J. 1983. Origin of coated grains: trace element constraints, in Peryt, T. (ed.), Coated Grains: Springer-Verlag, Berlin, Heidelberg, New York, Tokyo.

Braun, M., and Friedman, G.M., 1970. Dedolomitization fabrics in peels; a possible clue to unconformity surfaces. Jour. Sed. Petrology, **40**, p. 417-418.

Brett, C.E., and Brookfield, M.E., 1984. Morphology, faunas and genesis of Ordovician hardgrounds from southern Ontario, Canada: Palaeogeography, Palaeoclimatology, Palaeoecology, **46**, p. 233-290.

Brigham, R. J. 1971. Structural geology of southwestern Ontario and southeastern Michigan. Ontario Department of Mines and Northern Affaires Petroleum Resources Section, Paper **71-2**, 110p.

Budai, J.M., Lohmann, K. C. and Owen, R. M. 1984. Burial dedolomite in the Mississippian Madison Limestone, Wyoming and Utah thrust belt. Journal of Sedimentary Petrology, **42**, p. 276-288.

_____, and Wilson, J.L., 1986. Depositional patterns and diagenetic history of Trenton-Black River Formations in Michigan Basin (abs.). Amer. Assoc. Petrol. Geologists, Bull., **70**, p. 1063.

Burgess, R.J., 1960. Eastern Canada has a new exploratory target...oil in Trenton synclines. Oil and Gas Journal, **58**, No. 33, p. 124-131.

Burns, S.J., and Baker, P.A., 1985. A geochemical study of dolomite in the Monterey Formation, California. Jour. Sed. Petrol., **57**, No. 1, p. 128-139.

Calvert, W.L., 1964. Sub-Trenton rocks from Fayette County, Ohio to Brant County, Ontario. Report of Inv. No. 52, Ohio Geol. Survey.

Carpenter, A. B. 1980. The chemistry of dolomite formation 1: The stability of dolomite. In Zenger, D. H., Dunham, J. B. and Ethington, R. L. (eds). Concepts and Models of Dolomitization: Society of Economic Paleontologists and Mineralogists, Spec. Pub. **28**, p. 111-122.

Carroll, D., 1958. Role of clay minerals in the transportation of iron. Geochim. Cosmochim. Acta, **14**, p. 21-26.

Carter, T.R., and Campbell, G.R., 1989. Oil and Gas Developments in Eastern Canada in 1988. Amer. Assoc. Petrol. Geologists, **73**, p. 45-56.

Cathles, L.M., and Smith, A.T., 1983. Thermal constraints of the formation of Mississippi Valley-type lead-zinc deposits and their implications for episodic basin dewatering and deposit genesis. Econ. Geol., **78**, p. 983-1002.

Cercone, K.R., 1984a. Thermal history of the Michigan Basin. Amer. Assoc. Petrol. Geologists, Bull., **68**, p. 130-136.

_____., 1984b. Diagenesis of Niagaran (Middle Silurian) pinnacle reefs, northwest Michigan (carbonate, stable isotopes, thermal modeling). Ph.D. thesis, Ann Arbor, University of Michigan, 382 p.

Chase, C.G., and Gilmer, T.H., 1973. Precambrian plate tectonics: The mid-continent gravity high. Earth and Planetary Science Letters, **21**, p. 70-78.

Chafetz, H. S. 1972. Surface diagenesis of limestone. Journal of Sedimentary Petrology, **42**, p. 325-329.

Chicarelli, M.I, Kaur, S. and Maxwell, J.R., 1987. Sedimentary porphyrins: Unexpected structures, occurence, and possible origins. In Metal Complexes in Fossil Fuels: Characterization and Processing, eds., R.H. Filby and J.F. Branthaver. A.C.S. Symposium Series 344, p. 40-67.

Choquette, P.W., 1968. Marine diagenesis of shallow marine lime mud sediments; insights from $d^{18}O$ and $d^{13}C$ data. Science, **161**, p. 1130-1132.

_____, 1971. Late ferroan dolomite cement, Mississippian carbonates, Illinois Basin, U.S.A. in Bricker, O.P. ed., Carbonate Cements, Baltimore, Johns Hopkins Press, p. 339-346.

_____, and Steinen, R. P. 1980. Mississippian non-supratidal dolomite, Ste. Genevieve Limestone, Illinois Basin: Evidence for Mixed-Water Dolomitization. In Zenger, D. H., and Dunham, J. B. and Ethington, R. L. (eds). Concepts and Models of Dolomitization: SEPM, Spec. Pub. **28**, p. 163-196.

Churcher, P.L., 1985. Geology and Geochemistry of the Collingwood member, Lindsay Formation, southern Ontario. M.A. Thesis, University of Waterloo, Ontario, 46 p.

Clarke, D.L., et al., 1981, Miscellanea, Conodonta: Treatise on Invertebrate Paleontology, Part W, Supplement 2, 202 p.

Claypool, R.N., and Kaplan, I.R., 1974. The origin and distribution of methane in marine sediments, in I.R. Kaplan (ed.), Natural Gases in Marine Sediments. Plenum, N.Y., p. 99-139.

Clayton, R.N., and Degens, E.T., 1959. Use of C isotope analyses for differentiating fresh-water and marine sediments. Amer. Assoc. Petrol. Geology. Bull., **43**, p. 890-897.

_____, Friedman, I., Graf, D.L., Mayeda, T.K., Meents, W.F., and Shimp, N.F., 1966. The origin of saline formation waters. 1. Isotope composition. J. Geophys. Res., **71**, p. 3869-3882.

_____, Jones, B.F., and Brenner, R.A., 1968. Isotope studies of dolomite formation under sedimentary conditions. Geochim. Cosmochim. Acta, **32**, p. 415-432.

Cohee, G.V., 1945. Lower Ordovician and Cambrian rocks in the Michigan Basin, Michigan and Adjoining Areas. U.S. Geological Survey Oil and Gas Inv. (Prelim.) Chart No. 9.

_____, 1947. Cambrian and Ordovician rocks in Recent wells in southeastern Michigan. Bull. A.A.P.G., **32**, p. 293-307.

_____, 1948. Cambrian and Ordovician rocks in Michigan Basin and Adjoining Areas. Bull. A.A.P.G., **32**, p. 1417-1448.

Cole, G.A., Drozd, R.J., Sedivy, R.A., and Halpem, H.I., 1987. Organic geochemistry and oil-source correlations, Paleozoic of Ohio. Amer. Assoc. Petrol. Geologists, Bull., **71**, p. 788-809.

Collinson, C., 1963, Collection and preparation of conodonts through mass production techniques: Illinois State Geological Survey, Circular 343, 16 p.

Compston, W., 1960. The carbon isotopic composition of certain marine invertibrates and coals from the Australian Permian. Geochim. Cosmochim. Acta, **18**, p. 1-22.

Cooper, P., 1978. Paleoenvironments and Paleocommunities in the Ordovician-Silurian sequence of Manitoulin Island, in J.T. Sanford and R.E. Mosher, eds., Geology of the Manitoulin Area: Michigan Basin Geological Society Special Papers 3, p. 47-61.

Corwin, A.H., 1960. Petroporphyrins. Proc. 5th World Petroleum Congress, New York, Paper V-10, p. 119-129.

Craig, H., 1953. The geochemistry of the stable isotopes of carbon. Geochim. Cosmochim. Acta, **3**, p. 53-92.

Crough, S.T., 1981, Mesozoic hotspot epeirogeny in eastern North America. Geology, **9**, p. 2-6.

Curtis, 1967. Diagenetic iron minerals in some British Carboniferous sediments. Geochim. Cosmochim. Acta., **31**, p. 2109-2123.

Dana, J. D., 1837. A system of mineralogy. Durrie and Peck and Herrick and Noyes, New Haven, 452 p.

Dansgaard, W., 1964. Stable isotopes in precipitation. Tellus, **16**, p. 436-468.

Degens, E.T., and Epstein, S., 1962. Relationship between O^{18}/O^{16} ratios in coexisting carbonates, cherts and diatomites. Amer. Assoc. Petrol. Geol. Bull., **46**, p. 534-542.

_____, and Epstein., S, 1964. Oxygen and carbon isotope ratios in coexisting calcites and dolomites from recent and ancient sediments. Geochim. Cosmochim. Acta, **28**, 23-44.

deGroot, K., 1967. Experimental dedolomitization. Jour, Sed. Petrology, **37**, p. 1216-1220.

DeRito, R.F., Cozzarelli, FA., and Hodge, D.S., 1983, Mechanisms of subsidence of ancient cratonic rift basins. Tectonophysics, **94**, p. 141-168.

Dickson, J.A., and Coleman, M.L., 1980. Changes in carbon and oxygen isotope composition during limestone diagenesis. Sedimentology, **27**, p. 107-118.

Donovan, T.J., 1974. Petroleum microseepage at Cement, Oklahoma: evidence and mechanism. Amer. Assoc. Petroleum Geologists Bull., **58**, p. 429-446.

Dunham, J. B. and Olson, E. R. 1980. Shallow subsurface dolomitization of subtidally deposited sediments in the Hanson Creek formation (Ordovician-Silurian) of Central Nevada. In Zenger, D. H., Dunham, J. B. and Ethington, R. L. (eds). Concepts and Models of Dolomitization: Society of Economic Paleontologists and Mineralogists, Spec. Pub. **28**, p.139-162.

Ells, G., 1962. Structures associated with the Albion-Scipio Oil Field trend: Michigan Geol. Survey Pub., 86 p.

_____, 1967. Correlation of Cambro-Ordovician rocks in Michigan. Michigan Basin Geol. Soc. Annual Field Excursion Guidebook, p. 42-57.

_____, 1969. Architecture of the Michigan Basin. Michigan Basin Geol. Soc. Annual Field Excursion Guidebook, p. 60-88.

Engel, A.E.G., Clayton, R.N., and Epstein, S., 1958. Variations in isotopic composition of oxygen and carbon in Leadville limestone (Mississippian, Colorado) and its hydrothermal and metamorphic phases. Journal of Geology, **66**, p. 374-393.

Epstein, S., Graf, D.L., and Degens, E.T., 1964. Oxygen isotope studies on the origin of dolomites. In: Isotopic and Cosmic Chemistry, (eds. H. Craig, S.L. Miller and G.J. Wasserburg), p. 169-180. North Holland.

Epstein, A.G., Epstein, J.B., and Harris, L.D., 1977, Conodont colour alteration- an index of organic metamorphism: United States Geological Survey, Professional Paper 995, 27 p.

Evamy, B.D., 1967. Dedolomitization and the development of rhombohedral pores in limestones. Jour. Sed. Petrology, **37**, p. 1204-1215.

Fara, D.R., and Keith, B.D., 1984. Depositional facies and diagenetic history of Trenton limestone in northern Indiana (Abst), Amer. Assoc. Petrol. Geologists, Bull., **68**, p. 1919.

Fairchild, I. J. 1983. Stages in a Precambrian dolomitization, Scotland: cementing versus replacement texture. Sedimentology, **27**, p. 631-650.

Filby, R.H., and Van Berkel, G.J., 1987. Geochemistry of metal complexes in petroleum, source rocks and coals; An overview In Metal Complexes in Fossil Fuels: Characterization and Processing, eds., R.H. Filby and J.F. Branthaver. A.C.S. Symposium Series 344, p. 2-39.

Fisher, J.H., 1969. Early Paleozoic History of the Michigan Basin. Michigan Basin Geol. Soc. Annual Field Excursion Guidebook, p. 89-93.

_____, 1983. Tectonic evolution of the Michigan Basin. Geol. Soc. America Abs., w/prgms, **15**, p. 573.

Folk, R. L., and Asserto, R. 1974. Gaint aragonite rays and baroque white dolomite in tepee-fillings, Triassic of Lombardy, Italy. Abstract, American Association of Petroleum Geologists, Abstracts with Program, Annual Meeting, San Antonio, p. 34-35.

_____, and Land, LS., 1975. Mg/Ca ratio and salinity: two controls over crystallization of dolomite. Amer. Assoc. Petrol. Geol. Bull., **59**, p. 60-68.

Friedman, G. M., 1980. Dolomite is an evaporite mineral: Evidence from the rock record and from Sea-Marginal ponds of the Red Sea. In Zenger, D. M. Dunham, J. B. and Ethington, R. L. (eds). Concepts and Models of Dolomitization: Society of Economic Paleontologists and Mineralogists, Spec. Pub. **28**, p. 69-80.

_____, and Radke, B. M. 1979. Evidence for sabkha overprint and conditions of intermittent emergence in Cambrian-Ordovician carbonates of northeastern North America and Queensland, Australia. Northeastern Geology, **1**, p. 18-42.

_____, and Sanders, J.E., 1967. Origin and occurrence of dolostones: in Chilingar, G.V., Bissel, H.J., abd Fairbridge, R.W., (eds.), Carbonate rocks, origin, occurrence, and classification. Amsterdam, Elsevier Pub. Co., 471 p.

Friedman, I., and O'Neil, J.R., 1977. Compilation of stable isotope fractionation factors of geochemical interest, in Fleischer, M., ed., Data of Geochemistry (6th ed.), U.S. Geol. Survey Prof. Paper 440-KK.

Fritz, P., 1971. Geochemical characteristics of dolomites and the ^{18}O content of Middle Devonian oceans. Earth Planet. Sci. Lett., **11**, p. 277-282.

_____, and Smith, D., 1970. The isotopic composition of secondary dolomites. Geochim. Cosmochim. Acta, **34**, p. 1161-1173.

Fyfe, W. S., Kerrich, S. R., Hicock, S. R. and Colloza, F. C. 1987. Lithoprobe: Faults and Fluids. Geoscience Canada, **14**, no. 2, p. 75-81.

Gaines, A. M. 1980. Dolomitization Kinetics: Recent experimental studies. In Zenger, D. M., Dunham, J. B. and Ethington, R. L. (eds.), Concepts and Models of Dolomitization: Society of Economic Paleontologists and Mineralogists, Spec. Pub. **28**, p. 81-86.

Gale, N.H., Beckinsale, R.D., and Wedge, A.J., 1979. A Rb-Sr whole rock isochron for the Stockdale Rhyolite of the English Lake District and a revised mid-Paleozoic time-scale. Jour. Geol. Society London, **136**, p. 235-242.

Gardner, W.C., and Bray, E.E., 1984. Oils and source rocks of Niagaran reefs (Silurian) in the Michigan Basin. Amer. Assoc. Petrol. Geologists, Studies in Geology 18, p. 33-44.

Gehman, H.M., 1962. Organic matter in limestones. Geochim. Cosmochim. Acta, **26**, p. 885-894.

Given, R.K., and Lohmann, K.C., 1985. Carbon and oxygen isotopic composition of Permian marine cements. Jour. Sed. Petrology, **55**, p. 430-439.

Goldberg, M., 1967. Supratidal dolomitization and dedolomitization in Jurassic rocks of Hamakhtesh Haqatan, Isreal. Jour. Sed. Petrology, **37**, p. 760-773.

_____, and Bogoch, R. 1978. Dolomitization and hydrothermal mineralization in the Brur calcarenite (Jurassic), southern coastal plain, Israel. Israel Journal of Earth Sciences, **27**, p. 36-41.

Gregg, J. M., 1983. On the formation and occurrence of saddle dolomite-discussion. Journal of Sedimentary Petrology, **53**, p. 1025-1026.

_____, 1985. Regional epigenetic dolomitization in the Bonneterre dolomite (Cambrian), southeastern Missouri. Geology, **13**, p. 503-506.

_____, and Sibley, D. F. 1984. Epigenetic dolomitization and the origin of xenotopic dolomite texture. Journal of Sedimentary Petrology, **54**, p. 908-931.

Hanshaw, B.B., Back, W., and Deike., 1971. A geochemical hypothesis for dolomitization by groundwater. Econ. Geol., **66**, p. 710-724.

Hardie, L.A., 1987. Dolomitization: A critical view of some current views. Jour. Sed. Petrology, **57**, p. 166-183.

Harland, W.B., Cox, A.V., Llewellyn, P.G., Pickton, C.A.G., Smith, A.G., and Walters, R., 1982. A geological time scale. Cambridge University Press, published in Cambridge, London, New York, New Rochelle, Melbourne, Sidney, p. 12-26.

Haxby, WF., Turcotte, D.L., and Bird, J.M., 1976, Thermal and mechanical evolution of the Michigan basin. Tectonophysics, **36,** p. 57-75.

Haynes, S.J., and Mostaghel, M.A., 1982. Present-day precipitation of Lead and Zinc from groundwaters. Mineralium Deposita, Springer-Verlag, **17**, p. 213-228.

Haywick, D. W. and James, N. P. 1984. Dolomites and dolomitization of the Lower Ordovician St. George Group of western Newfoundland. Geologic Survey of Canada, Paper **84-1A**, p. 531-536.

Hitchon, B. and Friedman, I., 1969. Geochemistry and origin of formation waters in Western Canada Sedimentary Basin. Geochim. Cosmochim. Acta, **33**, p. 1321-1349.

Hogarth, C.G., and Sibley, D.F., 1985. Thermal history of the Michigan Basin: evidence from conodont colour alteration indices: in Cercone, K.R., and J.M. Budai (eds.), Ordovician and Silurian rocks of the Michigan Basin and its margins, Michigan Basin Geological Society, Lansing, Michigan, Special Paper 4, p. 45-57.

Holail, H., Lohmann, K.C., and Sanderson, I., 1988. Dolomitization and dedolomitization of upper Cretaceous carbonates: Bahariya Oasis, Egypt, in Sedimentology and Geochemistry of Dolostones, SEPM Sp. Pub. No. **43**, p. 191-207.

Hsu, K.J., 1967. Chemistry of dolomite formation, in Chilingar, G.V., Bissel, H.J., and Fairbridge, R.W., eds., Carbonate Rocks: Development in Sedimentology 9B. Elsevier, New York, p. 169-191.

Hunt, J.M., 1967. The origin of petroleum in carbonate rocks, in G.V. Chilingar, H.J. Bissel, and R.W. Fairbridge, eds., Carbonate rocks, New York, Elsevier, p. 249-251.

_____, 1979. Petroleum geochemistry and geology. San Francisco, W.H. Freeman, 617 p.

Hurley, N.F., and Lohmann, K.C., 1989. Diagenesis of Devonian reefal carbonates in the Oscar Range, Canning Basin, western Australia. Jour. Sed. Petrology, **59**, p. 127-146.

Irwin, H., 1980. Early diagenetic precipitation and pore fluid migration in the Kimmeridge clay of Dorset, England. Sedimentology, **27**, p. 577-591.

_____, Curtis, C., and Coleman, M.L., 1977. Isotopic evidence for source of diagenetic carbonates formed during burial of organic-rich sediments. Nature, **269**, p. 209-213.

Jacobsen, S.R., Hatch, J.R., Teerman, S.C., and Askin, R.A., 1988. Middle Ordovician organic matter assemblages and their effect on Ordovician-derived oils. Amer. Assoc. Petrol. Geologists, Bull., **72**, p. 1090-1100.

Jarvis, G.T., and McKenzie, D.P., 1980, Sedimentary basin formation with finite extension rates. Earth and Planetary Science Letters, **48**, p. 42-52.

Jensenius, J., Buchardt, B., Jorgensen, N.O., and Pederson, S., 1988. Carbon and oxygen isotopic studies of the chalk reservoir in the Skjold oilfield, Danish North Sea: Implications for diagenesis. Chemical Geology, **73**, p. 97-107.

Jerome, D.M., 1988. The subsidence of the Michigan and Williston basins: Critical review and computer model based on stratigraphic and geophysical data. Unpublished B.Sc. (Hons) thesis. Brock University Geological Library, 69 p.

Joyner, W.B., 1967, Basalt-ecologite transition as a cause for subsidence and uplift. Journal of Geophysical Research, **72**, p. 4977-4998.

Katz, A., and Matthews, A., 1977. The dolomitization of $CaCO_3$: an experimental study at 252-295 ^{o}C. Geochim. Cosmochim. Acta, **41**, p. 297-308.

Keith, B.D., 1985. Facies, diagenesis and the upper contact of the Trenton limestone of northern Indiana. In: R. Cercone and J.M. Budai (eds) Ordovician and Silurian Rocks of the Michigan Basin, Michigan Basin Geol. Soc. Symp., Spec. Paper **4**, p. 15-32.

_____, 1988a. Regional facies of the Upper Ordovician series of Eastern North America, in B.D.Keith, ed., The Trenton Group (Upper Ordovician Series) of Eastern North America: AAPG Studies in Geology #29, p. 1-16.

_____, 1988b. Reservoirs resulting from facies-independent dolomitization: Case histories from the Trenton and Black River carbonate rocks of the Great Lakes area. Carbonates and Evaporates, **1**, p. 74-82.

Keith, M.L., and Weber, J.N., 1964. Carbon and Oxygen isotopic composition of selected limestones and fossils. Geochim. Cosmochim. Acta, **28**, p. 1787-1816.

Kenney, T. 1986. The determination of heavy metals in environment samples through the use of Direct Current Plasma Optical Emission Spectroscopy. Unpublished B.Sc. (Hons), Brock University Chemistry Dept. p. 81.

Kinsman, D.J.J., 1969. Interpretation of Sr^{2+} concentrations in carbonate minerals and rocks. Jour. Sed. Petrology, **39**, p. 486-508.

Knauth, L.P., and Epstein, S., 1976. Hydrogen and Oxygen isotope ratios in nodular and bedded cherts: Geochim. Cosmochim. Acta, **40**, p. 1095-1108.

Kobluk, D.R., and Brookfield, M.E., 1982. Lower Paleozoic carbonate rocks and paleoenvironments in southern Ontario: IAS, Eleventh International Congress on Sedimentology, Excursion Guidebook 12A, 62 p.

Land, L.S., 1973. Contemporaneous dolomitization of Middle Pleistocene reefs by meteoric water, north Jamaica. Bull. Marine Sci., **23**, p. 64-92.

_____, 1980. The isotope and trace element chemistry of dolomite: The state of the art, in Zenger, D. H., Dunham, J. B. and Ethington, R. L., (eds). Concepts and Models of Dolomitization: Society of Economic Paleontologists and Mineralogists, Spec. Pub. **28**, p. 87-110.

_____, 1983. The application of stable isotopes to studies of the origin of dolomite and to problems of diagenesis of clastic sediments, in Stable Isotopes in Sedimentary Geology. SEPM Short Course No. 10, p. 4-1 - 4-22.

_____, 1985. The origin of massive dolomite. Jour. Geological Education, **33**, p. 112-125.

_____, and Hoops, G.K., 1973. Sodium in carbonate sediments and rocks: A possible index to salinity of diagenetic solutions. Jour. Sed. Petrology, **43**, p. 614-617.

Landes, K.K., 1970. Petroleum geology of the United States. Wiley-Interscience, New York, 571 p.

Lawrence, J.R., Gieskes, J.M., and Brecker, W.S., 1975. Oxygen isotope and cation composition of DSDP pore waters and the alteration of Layer II basalts. Earth Planet. Sci. Lett., **27**, p. 1-10.

Lee, I.L., Friedman, G.M., 1987. Deep-burial dolomitization in the Ordovician Ellenburger Group carbonates, west Texas and southeastern New Mexico. J. Sed. Petrol., **57**, p. 544-557.

Legall, F. D., Barnes, C. R. and Macqueen, R. W. 1981. Thermal maturation, burial history and hotspot development, Paleozoic strata of southern Ontario-Quebec, from conodont and arcitarch colour alteration studies. Bulletin of Canadian Petroleum Geology, **78**, p. 1-25.

Lewan, M.D., and Maynard, J.B., 1982. Factors controlling enrichment of vanadium and nickel in the bitumen of organic sedimentary rocks. Geochim. Cosmochim. Acta, **46**, p. 2547-2560.

Liberty, B.A., 1969. Paleozoic Geology of the Lake Simcoe Area, Ontario: Geological Survey of Canada, Memoir 355, 201p.

_____, and Bolton, T.E., 1971. Paleozoic Geology of the Bruce Peninsula Area, Ontario: Geological Survey of Canada, Memoir 360, 163 p.

Lindholm, R. C. and Finkelman, R. W. 1972. Calcite staining: semi-quantitative determination of ferrous iron. Journal of Sedimentary Petrology, **42**, p. 239-242.

Lizotte, M., 1962. Structural and lithological controls on oil and gas producing zones in Trenton limestones. M.A. Thesis, University of Michigan, Ann Arbor.

Lockett, J.R., 1947. Development of structures on basin areas of northeastern United States. Bull. A.A.P.G., **31**, p. 429-446.

Logan, B.W., and Semenuik, V., 1976. Dynamic metamorphism: processes and products in Devonian carbonate rocks Canning Basin, Western Australia. Geol. Soc. Australia, Special Paper 6, 138 p.

Lohmann, K.C., 1983. Unravelling the diagenetic history of carbonate reservoirs: integration of petrographic and geochemical techniques, in A Short Course: New ideas and methods for exploration of carbonate reservoirs. Dallas Geol. Soc., p. V1-41.

_____, and Walker, J.C.G., 1984. Secular variation in $\partial^{13}C$ and $\partial^{18}O$ composition of Phanerozoic oceans. Geol. Soc. Amer. Abstr. w. Prog., **16**, p. 578.

Longman, M. W. and Mench, P. A. 1978. Diagenesis of Cretaceous limestones in the Edwards aquifer system of south-central Texas: a scanning electron microscope study. Sedimentary Geology, **21**, p. 241-276.

Louda, J.W., and Baker, E.W., 1981. Geochemistry of tetrapyrole, carotenoid and perylene in sediments from the San Miguel Gap (site 467) and Baja California borderland (site 471), Deep Sea Drilling Project, Leg 63. Init. Repts. DSDP **63**, p. 785-818.

Lowenstam, H.A., 1961. Mineralogy, 18O/16O ratios, and strontium and magnesium contents of recent and fossil brachiopods and their bearing on the history of the oceans. Jour. Geol. **69**, p. 241-260.

Ludvigsen, R., 1978. Towards an Ordovician trilobite biostratigraphy of southern Ontario, in J.T. Sanford and R.E. Mosher, eds., Geology of the Manitoulin Area: Michigan Basin Geological Survey Special Papers 3, p. 101-106.

Machel, H.G., 1987. Saddle dolomite as a by-product of chemical compaction and thermochemical sulfate reduction. Geology, **15**, p. 936-940.

_____, 1988. Fluid flow direction during dolomite formation as deduced from trace-element trends, in V. Shukla and P.A. Baker, (eds.), Sedimentology and Geochemistry of Dolostones, Society of Economic Paleontologists and Mineralogists Spec. Pub. No. 43, p. 117-125.

_____, and Anderson, G.M., 1989. Pervasive subsurface dolomitization of the Nisku Formation, central Alberta. Jour. Sed. Petrology, **59**, p. 891-911.

_____, and Mountjoy, E.W., 1986. Chemistry and environments of dolomitization-A reappraisal. Earth Science Reviews, **23**, p. 175-137.

_____, and Mountjoy, E.W., 1987b. Chemistry and environments of dolomitization-A reappraisal (reply): Earth Science Reviews, **24**, p. 213-215.

MacKenzie, A.S., Quirke, J.M.E., and Maxwell, J.R., 1980. Molecular parameters of maturation in the Toarcian Shales, Paris Basin, France-II. Evolution of metalloporphyrins. In Advances in Organic Geochemistry 1979, eds., J.R. Maxwell and A.G. Douglas, p. 239-248.

McKenzie, J. A., Hsu, K. J. and Schneider, J. F. 1980. Movement of subsurface waters under the Sabhka, Abu Dhabi, UAE, and its relation to evaporite dolomite genesis. In Zenger, D. H., Dunham, J. B. and Ethington, R. L. (eds). Concepts and Models of Dolomitization: Society of Economic Paleontologists and Mineralogists, Spec. Pub. **28**, p. 11-30.

Magaritz, M. and Kafri, U. 1981. Stable isotope and Sr^{2+}/Ca^{2+} evidence of diagenetic dedolomitization in a schizohaline environment: Cenomanian of northern Israel. Sedimentary Geology, **28**, p. 29-41.

Majid, A. H. and Veizer, J. 1986. Deposition and chemical diagenesis of Tertiary carbonates, Oil Field, Iraq. American Association of Petroleum Geologists Bulletin, **70**, no. 7, p. 898-913.

Mast, R.F., Ruch, R.R., and Meents, W.F., 1973. Vanadium in Devonian, Silurian, and Ordovician Crude Oils of Illinois. Illinois State Geological Survey, Circular 483, 14 p.

Mathews, A., and Katz, A., 1977. Oxygen isotope fractionation during the dolomitization of calcium carbonate. Geochim. Cosmochim. Acta, **41**, p. 1431-1438.

Mattavelli, L., Chilingarian, G. V. and Storer, D. 1969. Petrography and diagenesis of the Taormina Formation, Gela Oil Field, Sicily (Italy). Sedimentary Geology, **3**, p. 50-86.

Mattes, B. W., and Mountjoy, E. W. 1980. Burial dolomitization of the Upper Devonian Miette Buildup, Jasper National Park, Alberta. In Zenger, D.H., Dunham, J. B. and Ethington, R. L. (eds). Concepts and Models of Dolomitization: Society of Economic Paleontologists and Mineralogists, Spec. Pub. **28**, p. 259-297.

Mazzullo, S. J. 1981. Facies and burial diagenesis of a carbonate reservoir: Chapman Deep (Atoka) Field, Delaware Basin, Texas. American Association of Petroleum Geologists Bulletin, **65**, p. 850-865.

McCrossan, R.G., 1973, The future petroleum provinces of Canada-their geology and potential. The Canadian Society of Petroleum Geologists.

McIntire, W.L., 1963. Trace element partition coefficients - a review of theory and application to Geology: Geochim. Cosmochim. Acta, **27**, p. 1209 - 1264.

McNutt, R.H., Frape, S.K., and Dollar, P., 1987. A strontium, oxygen and hydrogen isotopic compositions of brines, Michigan and Appalachian Basins, Ontario and Michigan. Applied Geochemistry, **2**, p. 495-505

Meyers, W. J., 1974. Carbonate cement stratigraphy of the Lake Valley Formation (Mississippian) Sacramento Mountains, New Mexico. Journal of Sedimentary Petrology, v. **44**, p. 837- 861.

_____, 1978. Carbonate cements: Their regional distribution and interaction in Mississippian limestones of southwestern New Mexico Sedimentology, **25**, p. 371-400.

_____, and Lohmann, K.C., 1985. Isotope geochemistry of regionally extensive calcite cement zones and marine components in Mississippian limestones, New Mexico. In: N. Schneidermann and P.M., Harris (eds) Carbonate Cements. Soc. Econ. Paleon. Mineral. Spec. Pub. No. **36**, p. 223-240.

Milankovich, T. 1984. Dolomitization and luminescence stratigraphy of the Irondequoit Formation, Ontario and New York. Unpublished B.Sc. (Hons) Thesis, Brock University Geology Dept., 88p.

Milliman, J.D., 1974. Marine carbonates: Springer, Berlin, 375 p.

Moldovanyi, E.P., and Lohmann, K.C., 1984. Isotopic and petrographic record of phreatic diagenesis: Lower Cretaceous Sligo and Cupido Formations. Jour. Sed. Petrol., **54**, p. 972-985.

Morel, P., and Irving, E., 1978, Tentative paleocontinental map for the Early Phanerozoic and Proterozoic. Journal of Geology, **86**, p. 535-561.

Moore, C.H., 1971. Psuedospar dedolomite cements of evaporite solution collapse breccias, in Bricker, O.P., (ed.), Carbonate cements. Baltimore and London, The John Hopkins Univ. Press, 365 p.

_____, and Druckman, Y. 1981. Burial diagenesis and porosity evolution, Upper Jurassic Smackover, Arkansas and Louisiana. American Association of Petroleum Geologists, **65**, p. 597-628.

Morrow, D. W., 1982. Diagenesis 1. Dolomite-Part 1: The chemistry of dolomitization and dolomite precipitation. Geoscience Canada, **9**, no. 1, p. 5-13.

_____, 1982. Diagenesis 2. Dolomite -Part 2: Dolomitization models and ancient dolostones. Geoscience Canada, **9**, no. 2, p. 96-107.

Muir, M., Lock, D. and Borch, C. von der. 1980. The Coorong Model for Pene-contemporaneous dolomite formation in the Middle Proterozoic McArthur Group, Northern Territory, Australia. In Zenger, D. H., Dunham, J. B. and Ethington, R. L. (eds.). Concepts and Models of Dolomitization: Society of Economic Paleontologists and Mineralogists, Spec. Pub. **28**, p. 51-68.

Northrop, D.A., and Clayton, R.N., 1966. Oxygen isotopic fractionation in system dolomite. J. Geology., **74**, p. 174-196.

Odin, Gilles, S., Renard, M., and Grazzini, Colette, Vergnaud, 1982. Geochemical events as a means of correlation: in Numerical dating in stratigraphy (Odin, Gilles, Serge, editor) John Wiley and Sons, Chichester, U.K., 37-71. IGCP Project No. 133.

O'Neil, J.R., and Epstein, S., 1966. Oxygen isotopic composition of the system dolomite-calcite-carbon dioxide. Science, **152**, p. 198-201.

O'Shea, K.J., Miles, M.C., Fritz, P., Frape, S.K., and Lawson, D.E., 1988. Oxygen-18 and carbon-13 in the carbonates of the Salina formation of southwestern Ontario. Can. Jour. Earth Sci., **25**, p. 182-194.

Perry, E.C., 1967. The oxygen isotope chemistry of ancient cherts. Earth Planet. Sci. Lett., **3**, p. 62-66.

_____, and Tan, F.C., 1972. Significance of oxygen and carbon isotope variations in Early Precambrian cherts and carbonate rocks of southern Africa. Bull. Geol. Soc. Amer., **83**, p. 647-664.

Perry, E.A. Jr., Gieskes, J.M., and Lawrence, J.R., 1976. Mg, Ca and O^{18}/O^{16} exchange in the sediment-pore water system. Hole 149, DSDP, Geochim. Cosmochim Acta, **40**, p. 413-423.

Petzoukha, Y., 1988. A new mechano-chemical approach to hydrocarbon generation. Special Publication SP5, Moscow, USSR, p. 251-262.

Phelps, R.K., 1978. A fault-controlled Pb-Zn occurrence in Essex and Kent Counties Ontario. Unpublished M.Sc. Thesis, University of Windsor, 137 p.

Phillips, A.R., Colquhoun, S.A., and Putnam, P.E., 1989. B.A. Liberty Memorial Core Workshop--Cores of the Trenton-Black River. Ontario Petroleum Institute Annual Meeting, London, Ontario, 1989.

Pingitore, N.R., Jr., 1976. Vadose and Phreatic diagenesis: processes, products and their recognition in corals. Jour. Sed. Petrology, **46**, p. 985-1006.

Pirtle, G.W., 1932. Michigan structural basin and its relationship to surrounding areas. Bull. A.A.P.G., **16**, p. 145-152.

Poole, W.H., Sanford, B.V., Williams, H., and Kelley, D.G., 1970, Geology of southeastern Canada, In: Douglas, R.J.W., (ed), Geology and Economic Minerals of Canada. Geological Survey of Canada, Economic Geology Report 1, p. 228-304.

Popp, B.N., Anderson, T.F., and Sandberg, P.A., 1986a. Brachiopods as indicators of original isotopic compositions in some Paleozoic limestones. Geol. Soc. Amer. Bull., **97**, p. 1262-1269.

_____, Anderson, T.F., and Sandberg, P.A., 1986b. Textural, elemental and isotopic variations among constituents in middle Devonian limestones, North America. Jour. Sed. Petrology, **56**, p. 715-727.

_____, Podosek, F.A., Brannon, J.C., Anderson, T.F., and Pier, J., 1986c. 87Sr/86Sr ratios in Permo-Carboniferous sea water from analyses of well-preserved brachiopod shells. Geochim. Cosmochim. Acta, **50**, p. 1321-1328.

Powell, T. G., Macqueen, R. W., Barker, J. F. and Bree, D. G. 1984. Geochemical character and origin of Ontario oils. Bulletin of Canadian Petroleum Geology, **32**, no. 3, p. 289-312.

Premovic, P. I., Pavlovic, N. S. and Pavlovic, N. Z. 1986. Vanadium in ancient sedimentary rocks of marine origin. Geochemica et Cosmochimica Acta, **50**, no. 9, p. 1923-1931.

Prouty, C.E., 1970. Michigan Basin-Paleozoic evolutionary development. Geol. Soc. America Abs., **2**, pt. 7, p. 657-658.

_____, 1976. Michigan Basin-A wrenching deformation model? Geol. Soc. America Abs., **8**, pt. 4, p. 505.

_____, 1980. Petroleum exploration and wrenching model, Michigan Basin (abs.), Amer. Assoc. Petrol. Geol. Bull., **64**, p. 768.

_____, 1983. The tectonic development of the Michigan Basin infrastructures. In Kimmel, R.E. (ed.) Tectonics, Structure, and Karst in Northern Lower Michigan. Michigan Basin Geology Society Handbook, 1983 Field Conference, p. 36-91.

_____, 1984. The tectonic development of the Michigan Basin intrastructures: in Michigan Basin Geol. Soc. Annual Fieldtrip Guidebook, p. 36-81.

Qing, H., and Mountjoy, E.W., 1989. Multistage dolomitization in Rainbow Buildups, Middle Devonian Keg River Formation, Alberta, Canada. Jour. Sed. Petrol., **59**, p. 114-126.

Quinlan, G.M., and Beaumont, C., 1984, Appalachian thrusting, lithospheric flexure, and the Paleozoic stratigraphy of the eastern interior of North America. The Canadian Journal of Earth Science, **21**, p. 973-995.

Radke, B.M., 1978. Carbonate sedimentation in tidal and epeiric environments and diagenetic overprints: the Ninmaroo Formation (Upper Cambrian-Lower Ordovician), Central Australia. Unpublished Ph. D. Thesis, Troy, N.Y., Renesselaer Polytechnic Institute, 254p.

_____, and Mathis, R. L. 1980. On the formation and occurrence of saddle dolomite. Journal of Sedimentary Petrology, **50**, p. 1149-1168.

Raiswell, R., and Berner, R.A., 1985. Pyrite formation in euxinic and semi-euxinic sediments. Amer. Jour. Science, **285**, p. 710-724.

_____, 1987. Organic carbon losses during burial and thermal maturation of normal marine shales. Geology, **15**, p. 853-856.

Reed, J.D., Ilich, H.A., and Horsfield, B., 1986. Biochemical evolutionary significance of Ordovician oils and their sources. Organic Geochemistry, **10**, p. 347-358.

Rejebian, R.A., Harris, A.G., and Huebner, S.S., 1987, Conodont colour and textural alteration: an index to regional metamorphism, contact metamorphism, and hydrothermal alteration. Geological Society of America Bulletin, **99**, pp. 471-479.

Rooney, L.F., 1966. Evidence of unconformity at top of Trenton limestone in Indiana and adjacent states: Amer. Assoc. Petrol. Geol. Bull., **50**, p. 533-546.

Rullkotter, J., Meyers, P.A., Schaeffer, R.G., and Dunham, K.W., 1986. Oil generation in the Michigan Basin: a biochemical marker and carbon isotope approach. Organic Geochemistry, **10**, p. 359-375.

Russel, D.J., and Telford, P.G., 1983. Revisions to the stratigraphy of the Upper Ordovician Collingwood beds of Ontario - a potential oil shale. Can. Jour. Earth Science, **20**, p. 1780-1790.

Sanford, B.V., 1961. Subsurface stratigraphy of Ordovician rocks in southwestern Ontario. Geological Survey of Canada, Paper **60-26**, 54 p.

_____, Thompson, F.J., and McFall, G.H., 1984. Phanerozoic and recent tectonic movements in the Canadian Shield and their significance to the Nuclear Fuel Waste Management Program. In: Workshop on Translational Processes; Proceedings, AECL Report 7822, p. 73-96.

_____, 1985. Plate tectonics-A possible controlling mechanism in the development of hydrocarbon traps in southwestern Ontario. Bull. Can. Petrol. Geology, **33**, no.1, p. 52-71.

Scholle, P.A., and Arthur, M.A., 1980. Carbon isotope fluctuations in Cretaceous pelagic limestones: Potential stratigraphic and exploration tool. Bull. Amer. Assoc. Petrol. Geologists, **64**, p. 67-87.

_____, and Halley, R.B., 1985. Burial diagenesis: out of sight, out of mind! Soc. Econ. Paleontologists Mineralogists Spec. Pub. 36, p. 309-334.

Sears, S. O. and Lucia, F. J. 1980. Dolomitization of Northern Michigan Niagara Reefs by Brine Refluxion and Freshwater/Seawater Mixing. In Zenger, D. H., Dunham, J. B. and Ethington, R. L. (eds). Concepts and Models of Dolomitization: Society of Economic Paleontologists and Mineralogists, Spec. Pub. **28**, 215-236.

Shaw, B., 1975. Geology of the Albion-Scipio trend, southern Michigan. Unpub. M.Sc. Thesis, Univ. of Michigan, 63 p.

Shukla, V., 1986. Sedimentology and geochemistry of a regional dolostone: Correlation of trace elements and dolomite fabric and texture. Society of Economic Paleontologists and Mineralogists Midyear Meeting, Golden, Colorado, Abstrats, v. II, p. 82.

_____, 1988. Sedimentology and geochemistry of a regional dolostone: Correlation of trace elements and dolomite fabric. Society of Economic Paleontologists and Mineralogists Spec. Pub. No. 43, p. 145-157.

_____, and Friedman, G. M. 1983. Dolomitization and diagenesis in a shallowing-upward sequence: The Lockport formation (Middle Silurian), New York State. Journal of Sedimentary Petrology, v. **53**, no. 3, p. 703-717.

Shearman, D. J., Khouri, J. and Taha, S. 1961. On the replacement of dolomite by calcite in some Mesozoic limestones from the French Jura. Proceedings of Geological Association, **1**, p. 1-12.

Sibley, D.F., and Gregg, J.M., 1987. Classification of dolomite rock textures. Jour. Sed. Petrology, **57**, p. 967-975.

Slack, P. B. 1981. Paleotectonics and hydrocarbon accumulation, Powder River Basin, Wyoming. American Association of Petroleum Geologists, **65**, p. 730-743.

Sleep, N.H., 1982. Platform basins, Annual Review Of Earth and Planetary Science Letters, **8**, p. 17-34.

Spirakis, C.S., and Heyl, A.V., 1988. Possible effects of thermal degradation of organic mater on carbonate paragenesis and fluorite precipitation in Mississippi Valley-type deposits. Geology, **16**, p. 1117-1120.

Sundararaman, P., Biggs, W.R., Reynolds, J.G., and Fetzer, J.C., 1988. Vanadylporphyrins, indicators of kerogen breakdown and generation of petroleum. Geochem. Cosmochem. Acta, **52**, p. 2337-2341.

Surdam, R.C., and Crossey, L.J., 1985. Mechanisms of organic/inorganic interactions in sandstone/shale sequences, in Relationship of organic matter and mineral diagenesis. SEPM Short Course 17, p. 177-272.

Sweet, W.C., and Bergstrom, S.M., 1976. Conodont biostratigraphy of the Middle and Upper Ordovician of the United States mid-continent, in M.G. Bassett, ed., The Ordovician System-proceedings of a Paleontological Association symposium. University of Wales and National Museum of Wales, Cardiff, p. 121-151.

Taylor, T.R., and Sibley, D.F., 1986. Petrographic and geochemical of dolomite types and the origin of ferroan dolomite in the Trenton Formation, Ordovician, Michigan Basin, U.S.A.. Sedimentology, **33**, p. 61-86.

Thode, H.G., Shima, M., Rees, C.E., and Krishnamurty, K.V., 1965. Carbon-13 isotope effects in systems containing carbon dioxide, bicarbonate, carbonate and metal ions. Canadian Journal of Chemistry, **43**, p. 582-595.

Tissot, B.P., and Welte, D.H., 1978. Petroleum formation and occurrence: A new approach to oil and gas exploration. Springer-Verlag, Berlin, Heidelberg, New York. 538 p.

Treibs, A., 1936. Chlorphyll and hemin derivatives in organic materials. Angew. Chem. **49**, p. 682-686.

Veizer, J., 1977. Diagenesis of Pre-Quaternary carbonates as indicated by tracer studies. Journal of Sedimentary Petrology, **47**, p. 565-581.

_____, 1983. Chemical diagenesis of carbonates: Theory and application of trace element techniques, in Arthur, M.A., Anderson, T.F., Kaplan, I.R., Veizer, J., and Land, L.S., eds., Stable isotopes in sedimentary geology, SEPM Short Course No. **10.**, p. 3-1 - 3-100.

_____, 1985. Geochemistry of brachiopods: oxygen and carbon isotope records of Paleozoic oceans (abs). Geol. Soc. America Abstracts with Programs, **17**, p. 740.

_____, and Compston, W., 1974. 87Sr/86Sr compositions of sea water during the Phanerozoic. Geochim. Cosmochim. Acta, **38**, p. 1461-1484.

_____, and Demovic, R. 1974. Strontium as a tool in facies analysis. Journal of Sedimentary Petrology, **44**, p. 93-115.

_____, and Hoefs, J., 1976. The nature of O^{18}/O^{16} and C^{13}/C^{12} secular trends in sedimentary carbonate rocks. Geochem. Cosmochim. Acta, **40**, p. 1387-1395.

_____, Holser, W.T., and Wilgus, C.K., 1980. Correlation of C^{13}/C^{12} and $^{34}S/^{32}S$ secular variations. Geochim. Cosmochim. Acta, **44**, p. 579-587.

_____, Fritz, P., and Jones, B., 1986. Geochemistry of brachiopods: oxygen and carbon isotopic records of Paleozoic oceans. Geochim. Cosmochim. Acta, **50**, p. 1679-1696.

_____., Lemieux, J., Jones, B., Gibling, M.R., and Savelle, J., 1978. Paleosalinity and dolomitization of a Lower Paleozoic carbonate sequence, Somerset and Prince of Wales Islands, Arctic Canada: Canadian Jour. Earth Sci., **15**, p. 1448-1461.

Versical, R.T., 1990. Tulip structures in Michigan? A new look at the Origin and Structural Styles of some Michigan Basin Oil and Gas Fields. Abstract, 1990 Amer. Assoc. Petroleum Geologists Eastern Section Meeting, Abstracts w. Program.

von Marlot, A., 1847. Sur l'origine de la dolomite. Acad. Sci. (Paris) Comptes rendus, **26**, p. 311-315.

Vugrinovich, R., 1988. Shale compaction in the Michigan Basin: Estimates of former burial depth and implications for paleothermal gradients. Canadian Petroleum Geology, Bull., **36**, p. 1-8.

Wagner, P.D., and Matthews, R.K., 1982. Porosity preservation in the upper Smackover (Jurassic) carbonate grainstone, Walker Creek field, Arkansas: response of paleophreatic lenses to burial processes. Jour. Sed. Petrology, **52**, p. 3-18.

Wallace, H., 1981, Keweenawan geology of the Lake Superior Basin, In: Basins of Canada, F.H.A. Campbell (ed). Geological Survey of Canada, Paper **81-10**, 379-397.

Walker, J.C.G., 1986. Global cycles of carbon , sulphur, and oxygen. Marine Geology, **70**., p. 159-174.

Wanless, H.R., 1979. Limestone response to stress: Pressure solution and dolomitization. Jour. Sed. Petrology, **49**, p. 437-462.

Waples, D.W., 1980. Time and temperature in petroleum formation: application of Lopatin's method to petroleum exploration. Amer. Assoc. Petrol. Geologists, Bull., **64**, p. 916-926.

Weber, J.N., 1964a. Carbon isotope ratios in dolostones: some implications concerning the genesis of secondary and "primary" dolostones. Geochim. Cosmochim. Acta, **28**, p. 1257-1265.

_____, 1967. Possible changes in the isotopic composition of the oceanic and atmosphere carbon reservoir over geologic time. Geochim. Cosmochim. Acta, **31**, p. 2343-2351.

Welte, D. H. and Yukler, M. A. 1981. Petroleum origin and accumulation in basin evolution--A quantitative model. Amer. Assoc. Petrol. Geologists Bull., **65**, p. 1387-1386.

Wilman, H.B., and Kolata, D.R., 1978. The Platteville and Galena groups in northern Illinois. Illinois state Geol. Survey Cir. 502, 75p.

Winder, C. G. and Sanford, B. V. 1972. Stratigraphy and paleontology of the Paleozoic rocks of southern Ontario. 24th International Geological Congress, Montreal, Guidebook, Excursion A45-C45, 74p.

Wold, R.J., Paull, R.A., Wolosin, C.A., and Freidel, R.J., 1981, Geology of central Lake Michigan. Amer. Assoc. of Petrol. Geologists, **65**, p. 1621-1631.

Zenger, D.H., 1983. Burial dolomitization in the Lost Burro Formation (Devonian) east-central California and the significance of late diagenetic dolomitization. Geology, **11**, p. 519-522.

Zhu, T., and Brown, L.D., 1986, Consortium for continental reflection profiling Michigan surveys: reprocessing and results. Journal of Geophysical Research, **91**, B11, 11 477- 11 495.

Ziegler, A.M., Hansen, K.S., Johnson, M.E., Kelly, M.A., Scotese, C.R., and Van Der Voo, R., 1977, Silurian continental distributions, paleogeography, climatology, and biogeography. Tectonophysics, **40**, p. 13-51.

Appendix 1: Lithofacies Descriptions

The following facies descriptions were compiled by examining 16 cores from southwestern Ontario and 7 cores from southern and eastern Michigan, all from the Michigan Basin. All logged cores have been labeled with respect to location, depth from surface, and mode of preservation (dolomite, black, vs limestone, white). Lithologic identification is provided by the following: SH = shale, M = mudstone, W = wackestone, and G = grainstone; packstones are in most cases too difficult to differentiate in core. The described facies numbers appear to the right on the accompanying logs from the four cored wells within the study area.

Lithofacies 1: Massive Crinoidal Limestone

This facies has only been described in outcrop (c.f. Kobluk and Brookfield, 1982). Generally thick (0.5 - 5 m) units of crinoid-rich, skeletal packstone and wackestone with some rare grainstone beds. These units often show low angle and medium scale cross stratification (Kobluk and Brookfield, 1982). These units have not been found or described in Trenton-Black River core.

Lithofacies 2: Massive Shelly Packstone to Grainstones

Thick (1-3 m) units of massive grainstones with sharp bases often crinoidal with intraclasts. These units often thicken due to vertical and lateral amalgamation of wedges. The litho-boundaries are always stylotized, with development of stylo-bedding caused by extensive pressure solution processes. In many cases the residual clay minerals concentrate to form thin argillaceous seams that resemble minor clay partings. There are many occurences of grainstone beds within both the Trenton and Black River similar to this facies. The fragmental limestones of the Sherman Fall Formation are amalgamated grainstone beds and are

recognized in a number of cored wells (Consumers' et al. Mersea 3-12-I, B.A. #19 Malden 4-67-VI, Consumers' et al. 34160 Romney 5-8-II etc.,)

Lithofacies 3: Skeletal-Pelletal Wackestones, Packstones, Grainstones

Light buff skeletal-peletal packstones and grainstones are interbedded with a much darker wackestone. Micritized shell fragments (crinoids, brachiopods and bryozoans), grains and pellets are condensed with articulated shells and crinoid ossicles. The beds exhibit a sharp base, are poorly graded and are of variable thicknesses throughout.

These beds are restricted to the Sherman Fall Formation of the Trenton, and can be seen in many cored wells (same wells listed in facies 2).

Lithofacies 4: Crinoidal Mudstones and Wackestones

Dark brown bioturbated mudstones with crinoidal and brachiopod dominated wackestones. Lithofacies 4 has been subdivided into 3 subfacies:

Lithofacies 4A: Graded Skeletal Wackestones

Wackestone beds are generally 1-30 cm thick and fine upwards from an erosional lag of shell and crinoidal debris, at the base, to parallel laminations and are sometimes capped with wave ripples in the siltstone cap. The tops are often colonized by crinoids forming a firmground, or by brachiopods forming a shellground, and rarely are capped by boring organisms indicating a hardgound surface; generally interpreted as event bedding planes (Brett and Brookfield, 1984). Note that hardground surfaces have been recognized more commonly in the surface outcrop by Brett and Brookfield (1984).

Lithofacies 4B: Thinly Bedded Limestone

Beds are 1-40 cm thick argillaceous calcisiltite beds which alternate with centimetre thick marlstone (argillaceous calcilutite). These beds have characteristically sharp bases and bioturbated tops.

Lithofacies 4C: Mudstones and Nodular Mudstones

This facies is predominantly muddy, dark brown to black in colour and intensely bioturbated. These beds are generally interbedded with facies 4B and take on a nodular fabric resulting from extensive pressure solution. Thin clay seams envelope the micrite nodules and in some cases preserve the original sedimentary structure and bioturbation.

The three type 4 facies are found interbedded and form the most dominant lithology type of both the Trenton and Black River sequence. Portions of the Cobourg, the "Sherman Fall Argillaceous", and Kirkfield formations are dominated by this facies of the Trenton Group, while the Coboconk and especially the Gull River formations of the Black River Group is dominated by these facies.

Lithofacies 5: Interbedded Mudstones and Grainstones

Fine-grained mudstones are interbedded with the occassional fine-grained grainstone. The base of the grainstone beds are generally sharp with gradation into more muddy facies towards the top. However, stylo-bedding has been recognized in places and seems to represent a form of "diagenetic bedding" which may be obscuring the event bedding plane boundaries between the two lithotypes.

This facies has been recognized in the eastern and southeastern Michigan cores. The facies is predominantly found in association with the facies 4A-C as an occasional interbed.

Legend of symbols and lithologic descriptions used in the compilation of facies described in the subsurface

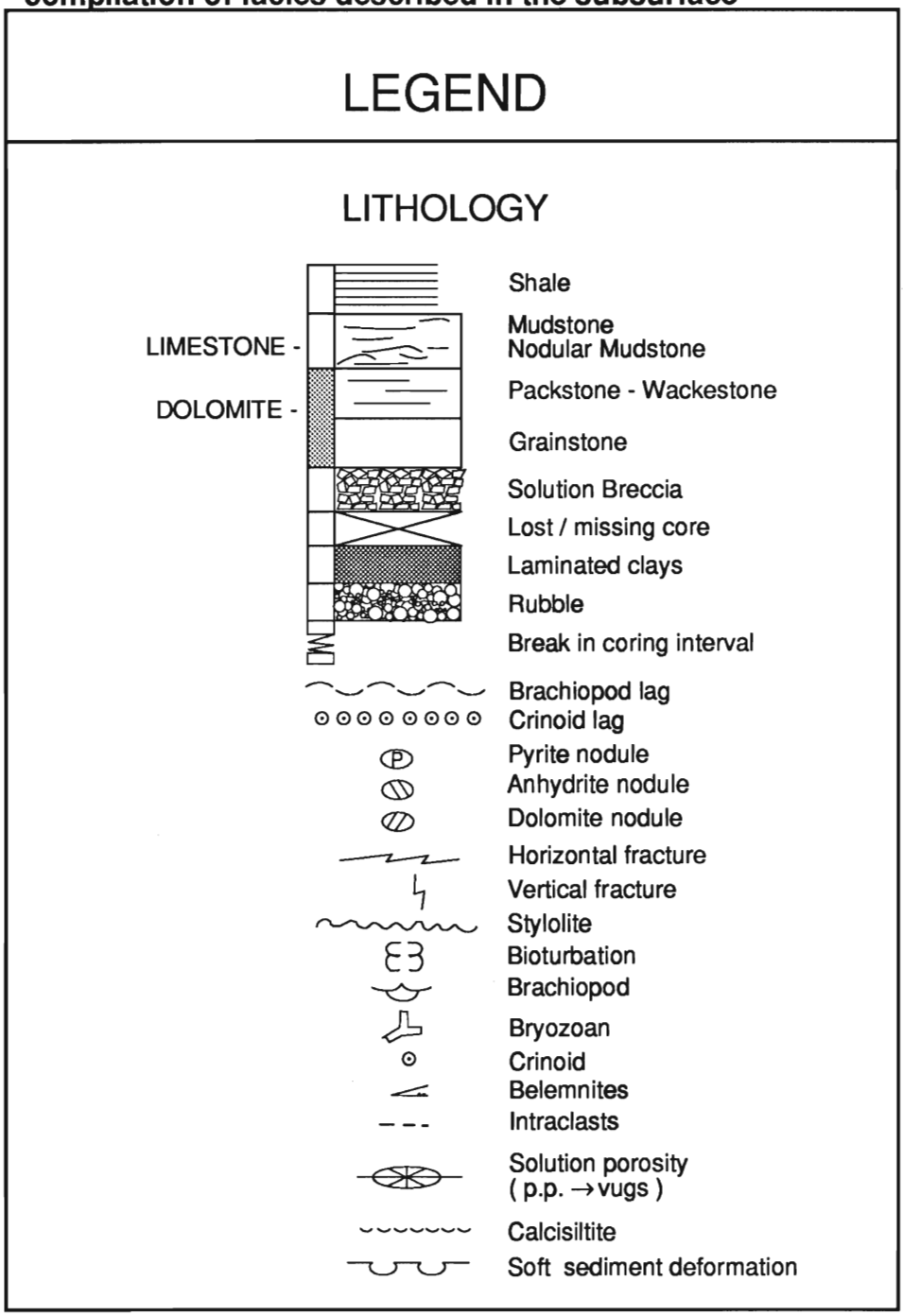

CONSUMERS' ET AL 33821 MERSEA 3-12-I

Core #1 764.0 - 782.0m (recorded 18.0m)
Core #2 782.0 - 800.0m (recorded 18.0m)
Core #3 800.0 - 818.0m (recorded 18.0m)
Core #4 860.0 - 878.0m (recorded 17.7m)
Core #5 940.0 - 958.0m (recorded 17.9m)

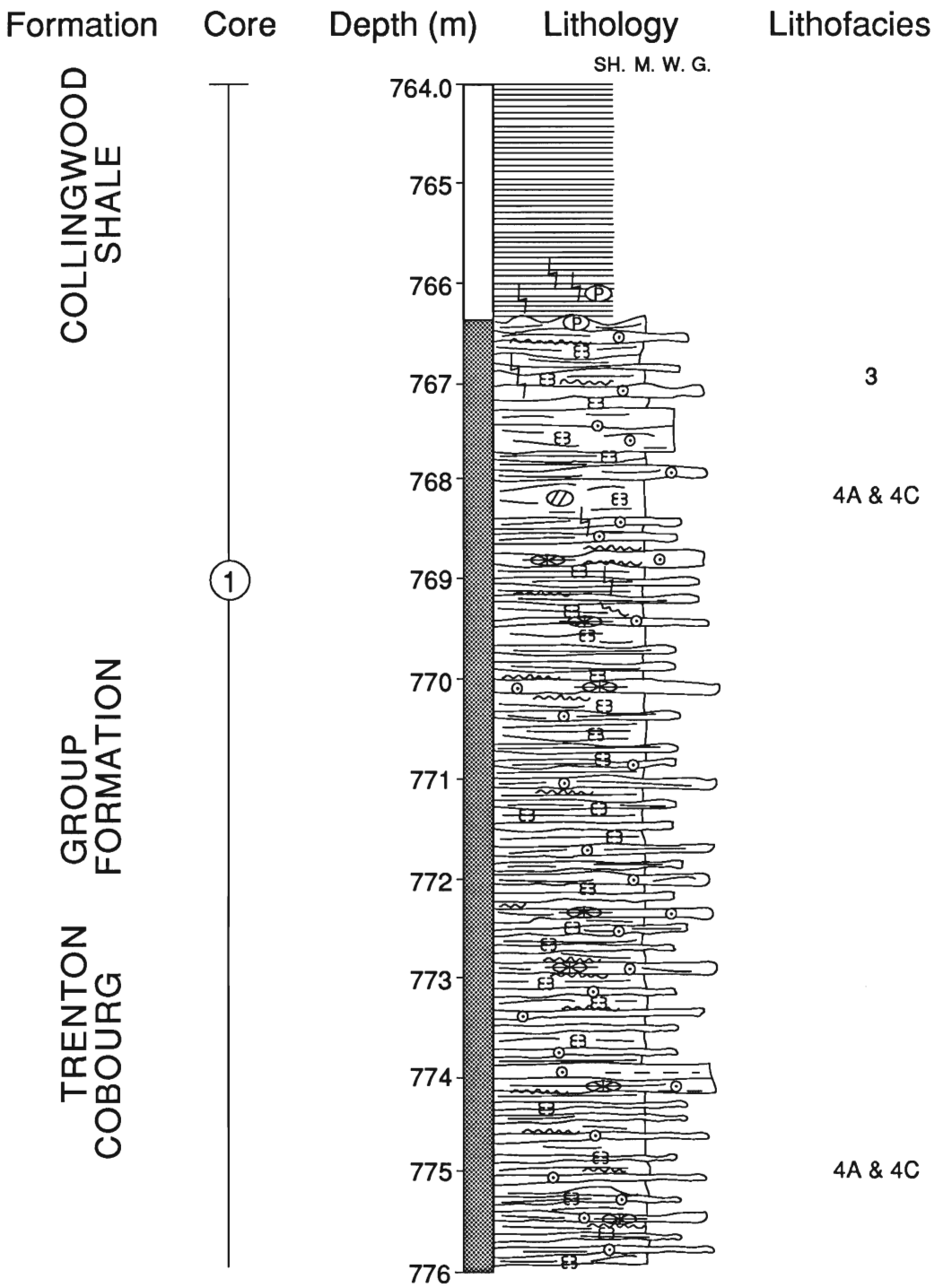

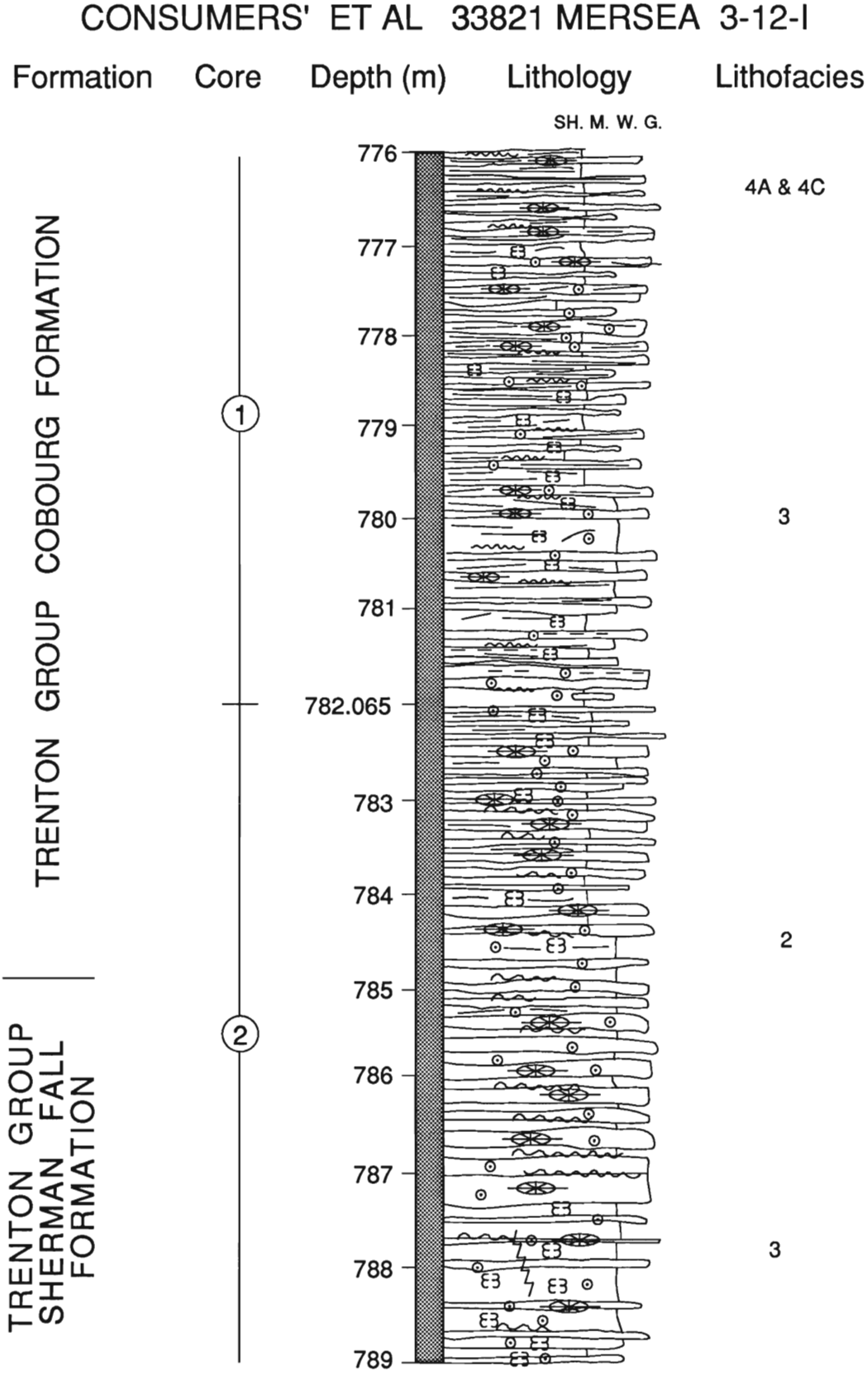
CONSUMERS' ET AL 33821 MERSEA 3-12-I
Formation
Core
Depth (m)
Lithology
Lithofacies
SH. M. W. G.
TRENTON GROUP COBOURG FORMATION
TRENTON GROUP SHERMAN FALL FORMATION
776
777
778
779
780
781
782.065
783
784
785
786
787
788
789
1
2
4A & 4C
3
2
3

CONSUMERS' ET AL 33821 MERSEA 3-12-1

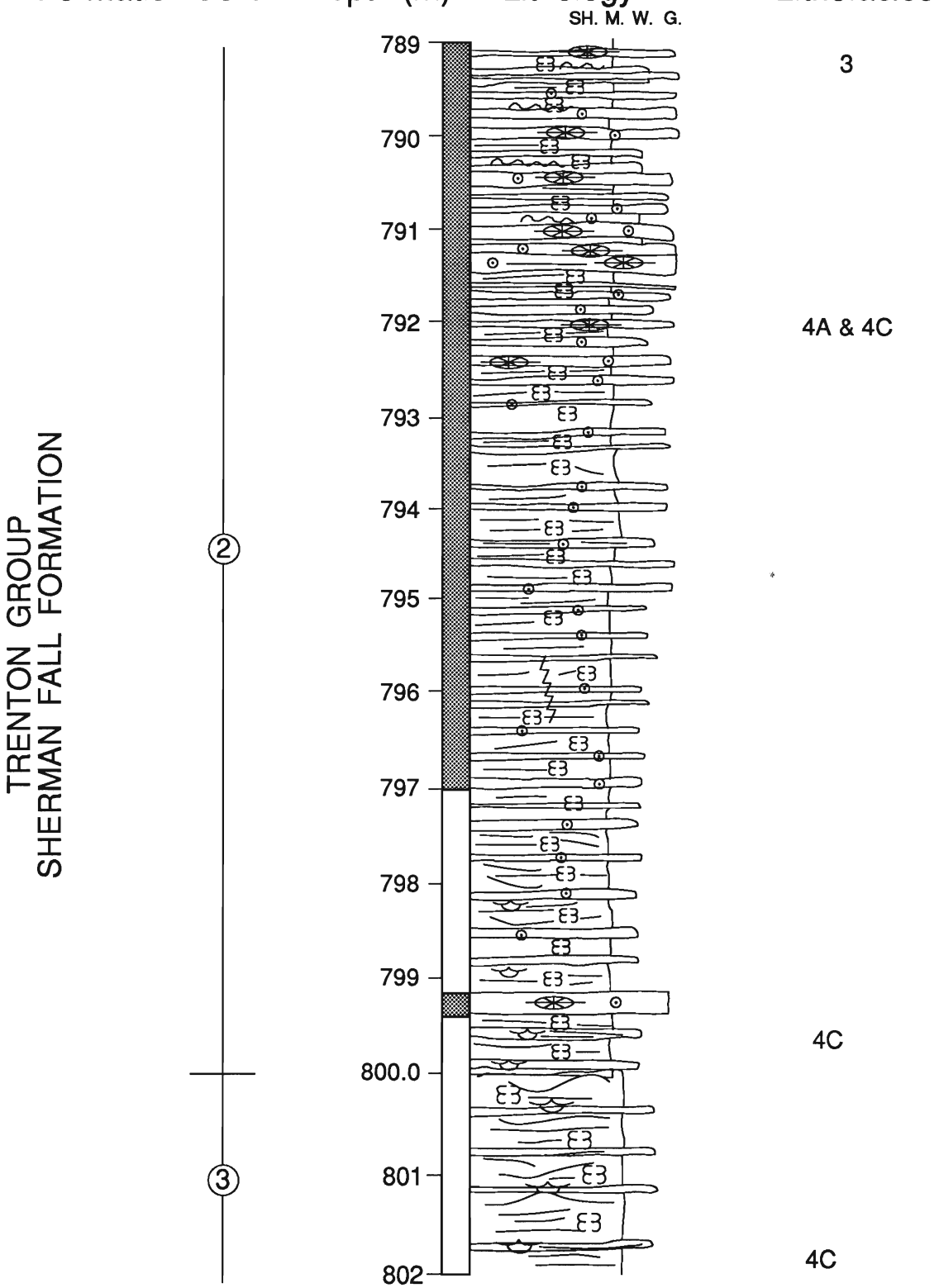

CONSUMERS' ET AL 33821 MERSEA 3-12-1

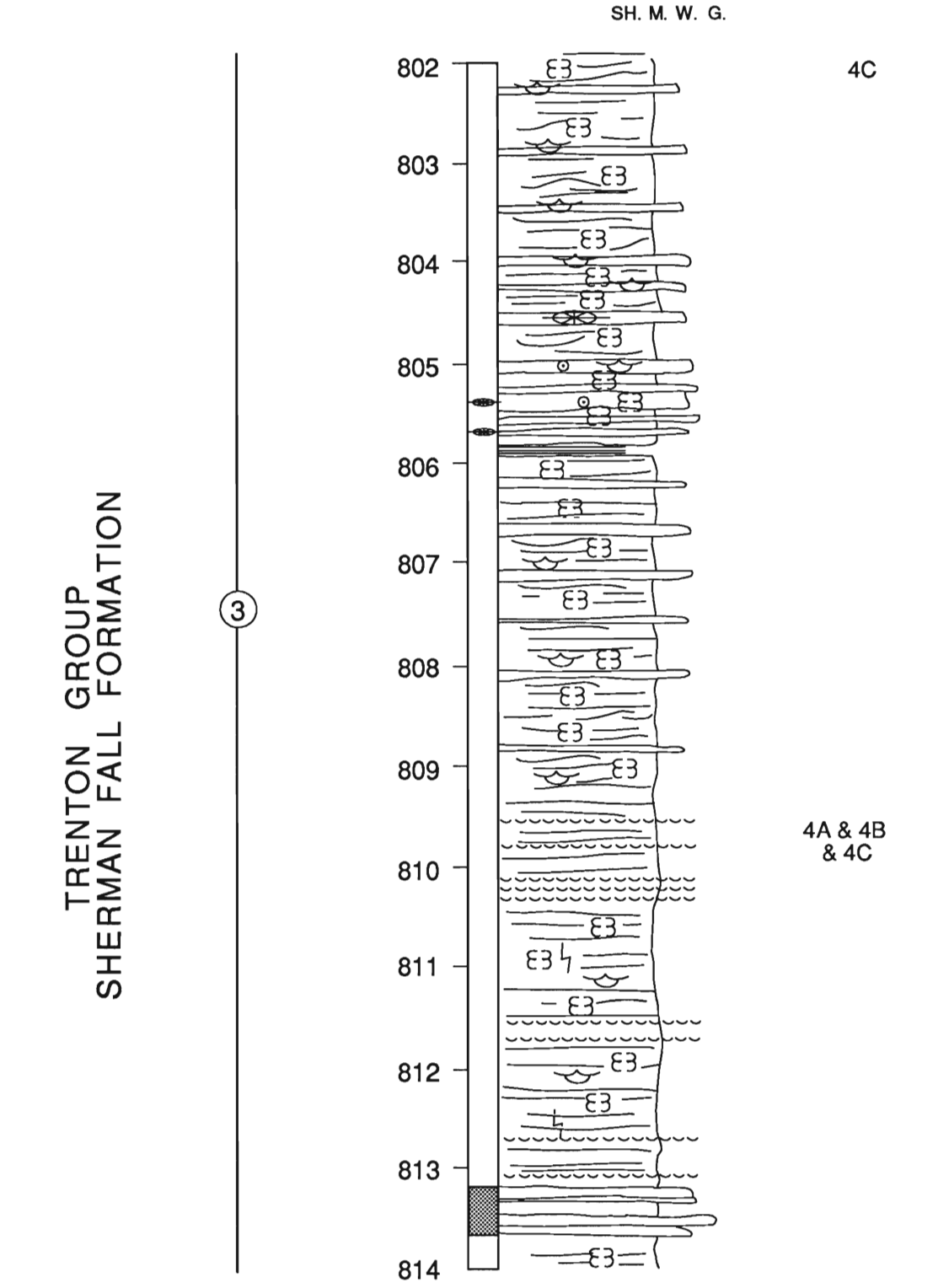

CONSUMERS' ET AL 33821 MERSEA 3-12-1

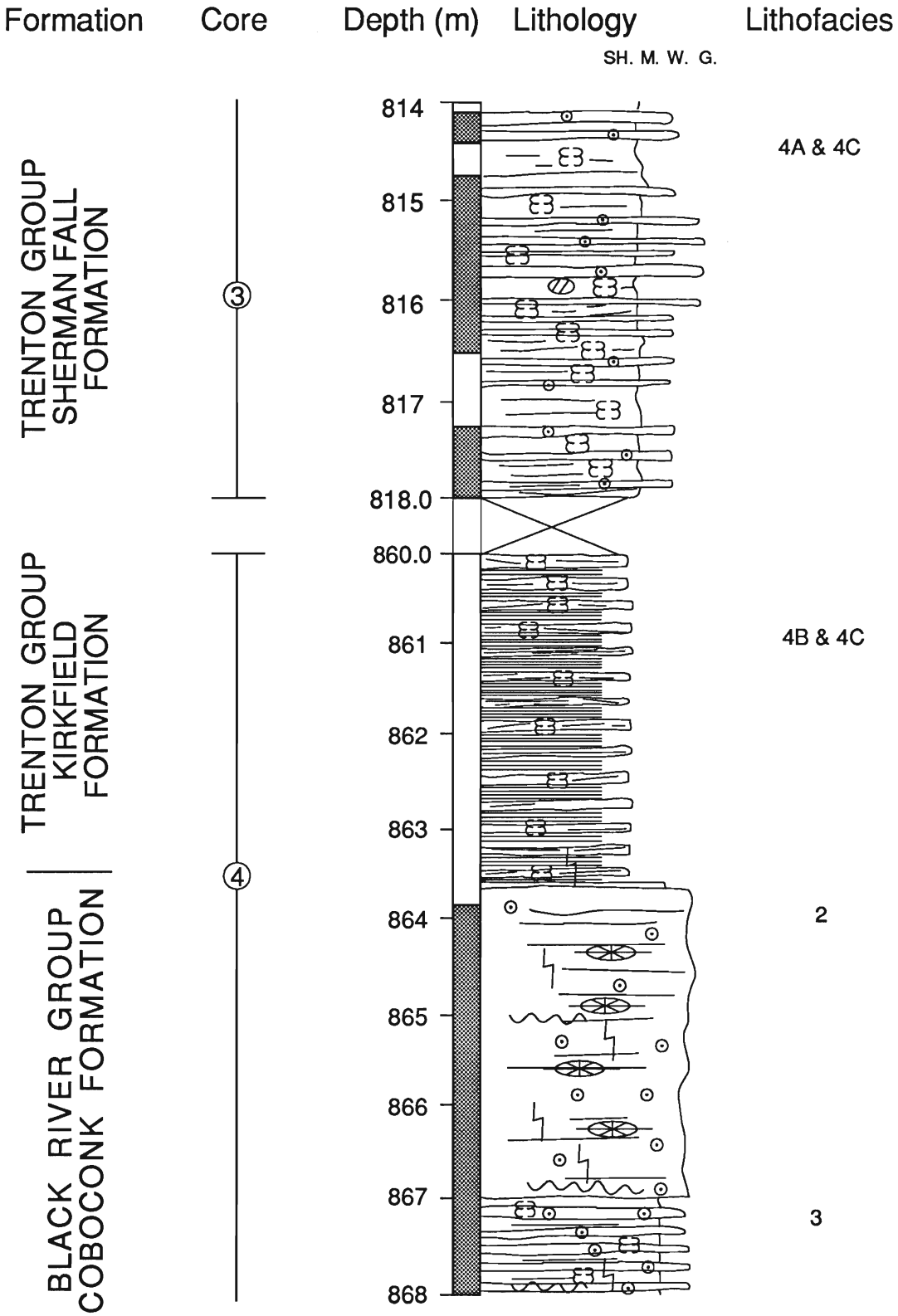

CONSUMERS' ET AL 33821 MERSEA 3-12-1

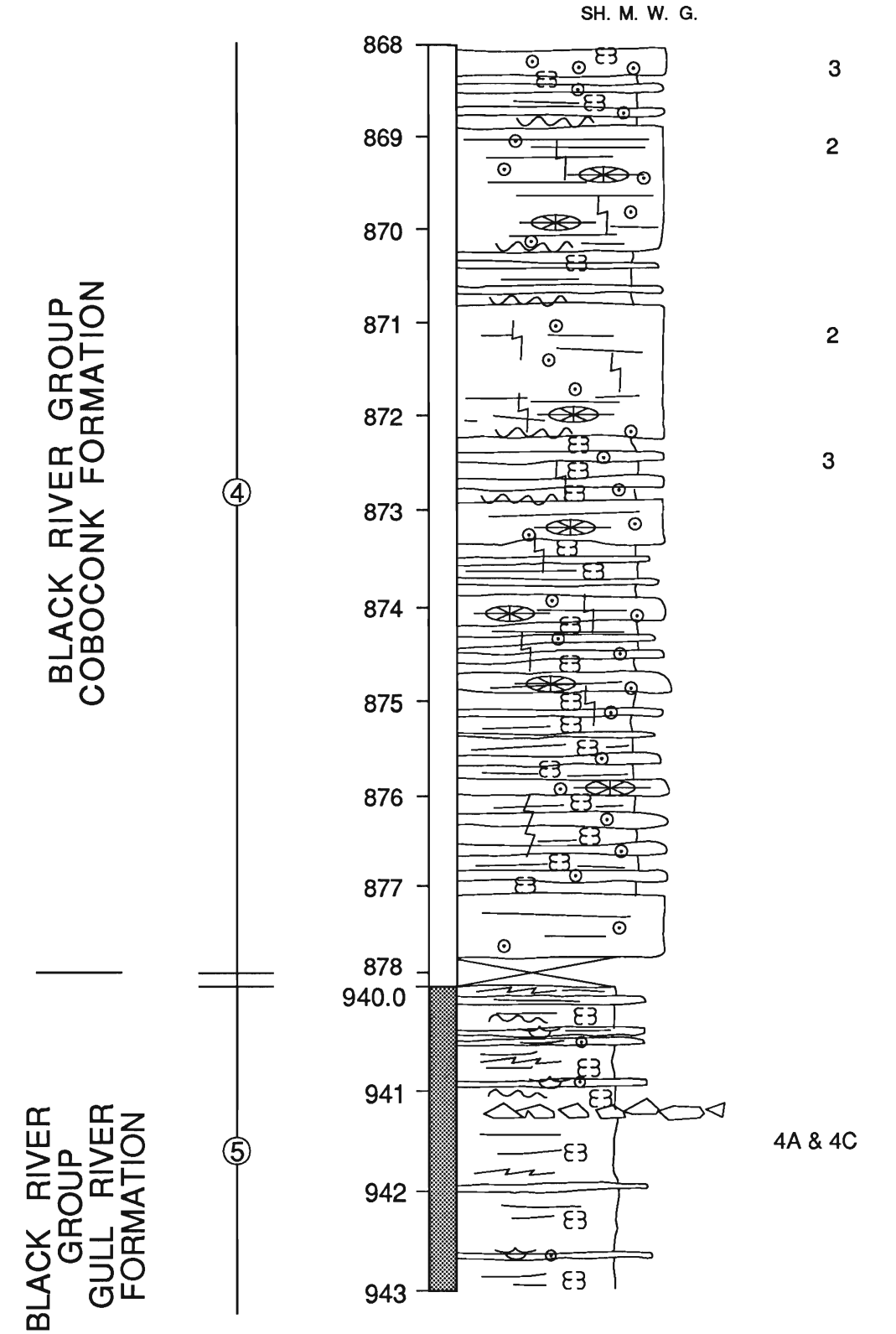

CONSUMERS' ET AL 33821 MERSEA 3-12-1

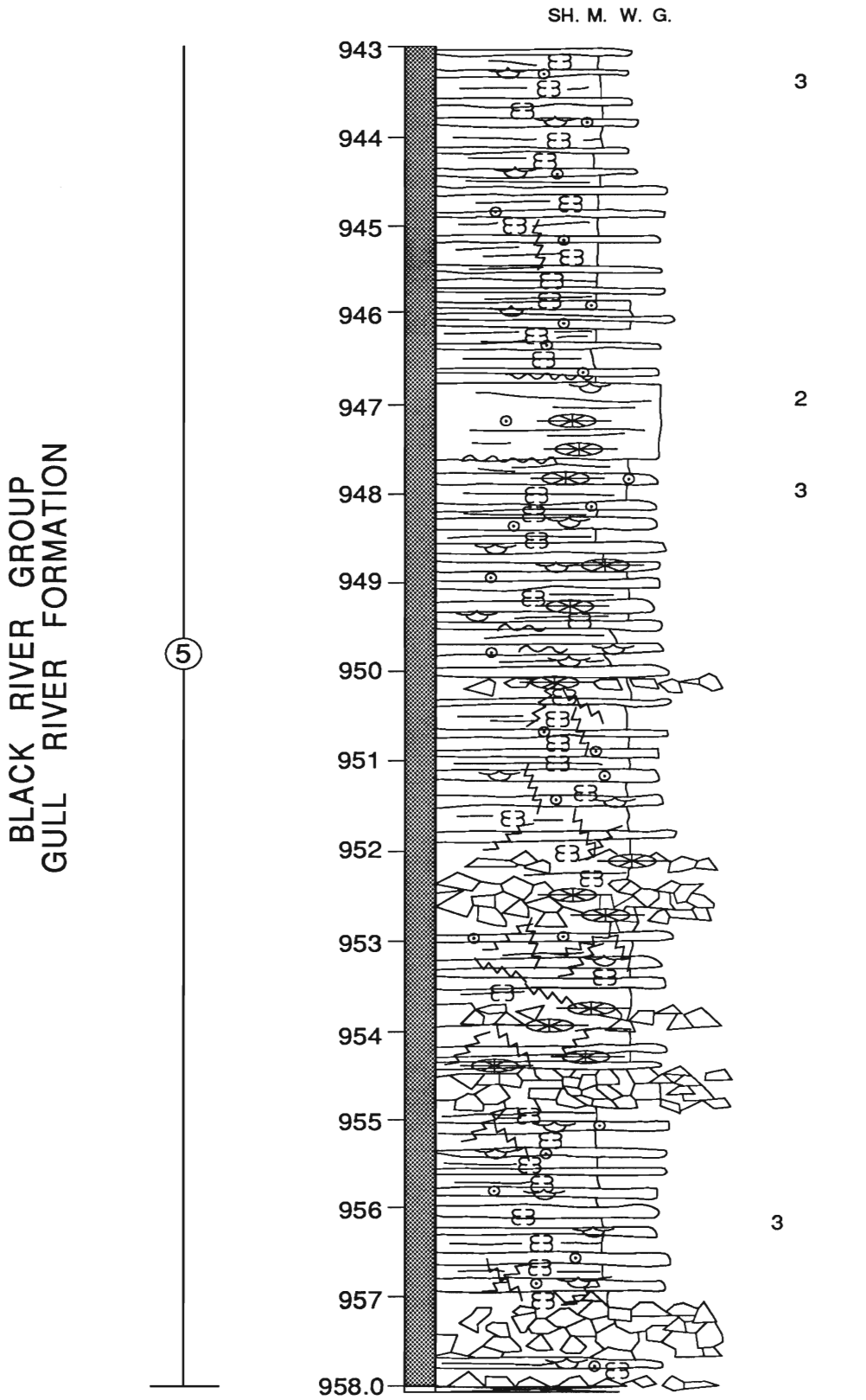

CONSUMERS' AT AL 33823 MERSEA 1-12-A

Core #1 764.0 - 782.4m (recorded 18.4m)
Core #2 782.4 - 800.0m (recorded 18.0m)
Core #3 800.0 - 818.8m (recorded 18.8m)
Core #4 818.8 - 822.0m (recorded 3.2m)
Core #5 822.0 - 823.9m (recorded 1.9m)

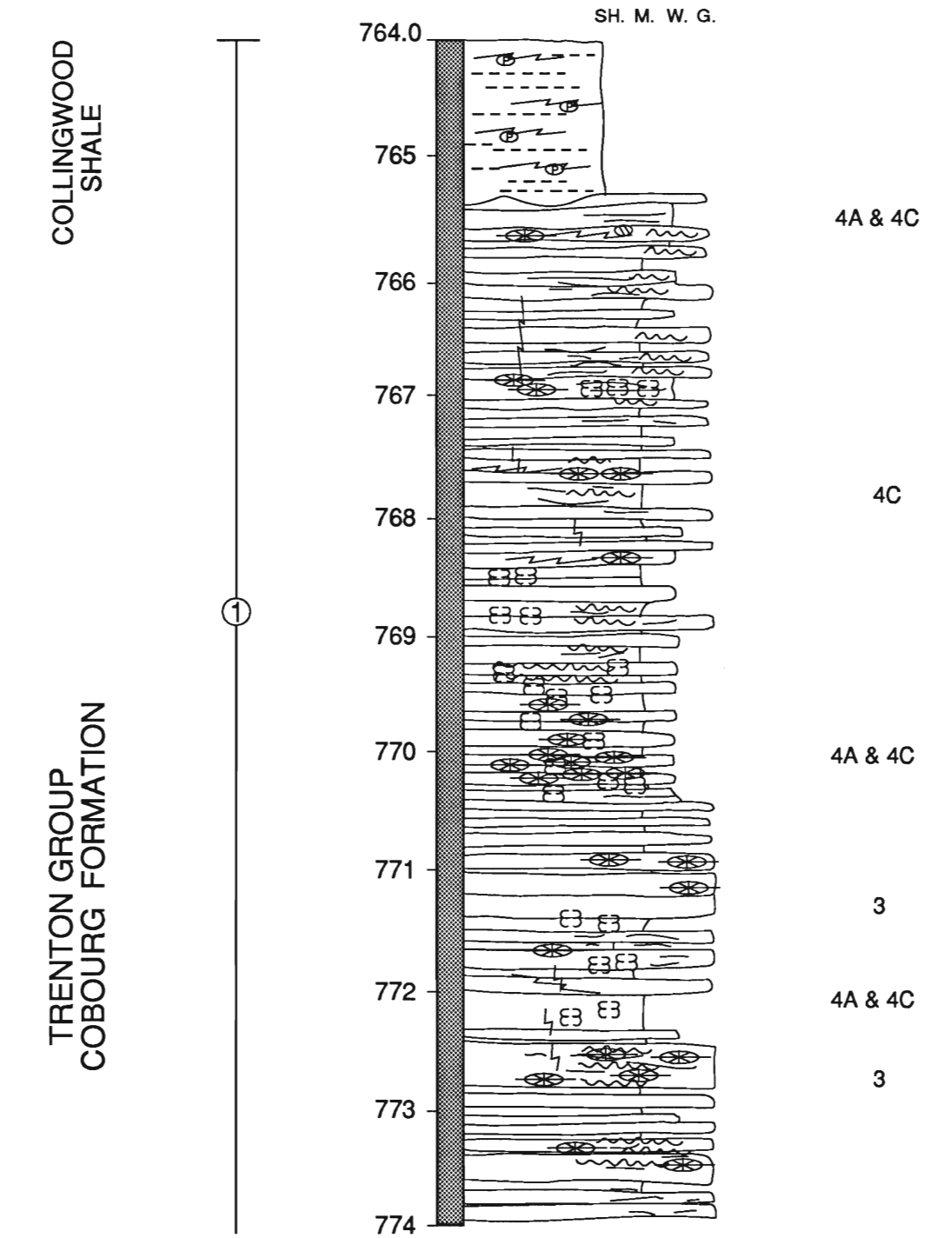

CONSUMERS' AT AL 33823 MERSEA 1-12-A

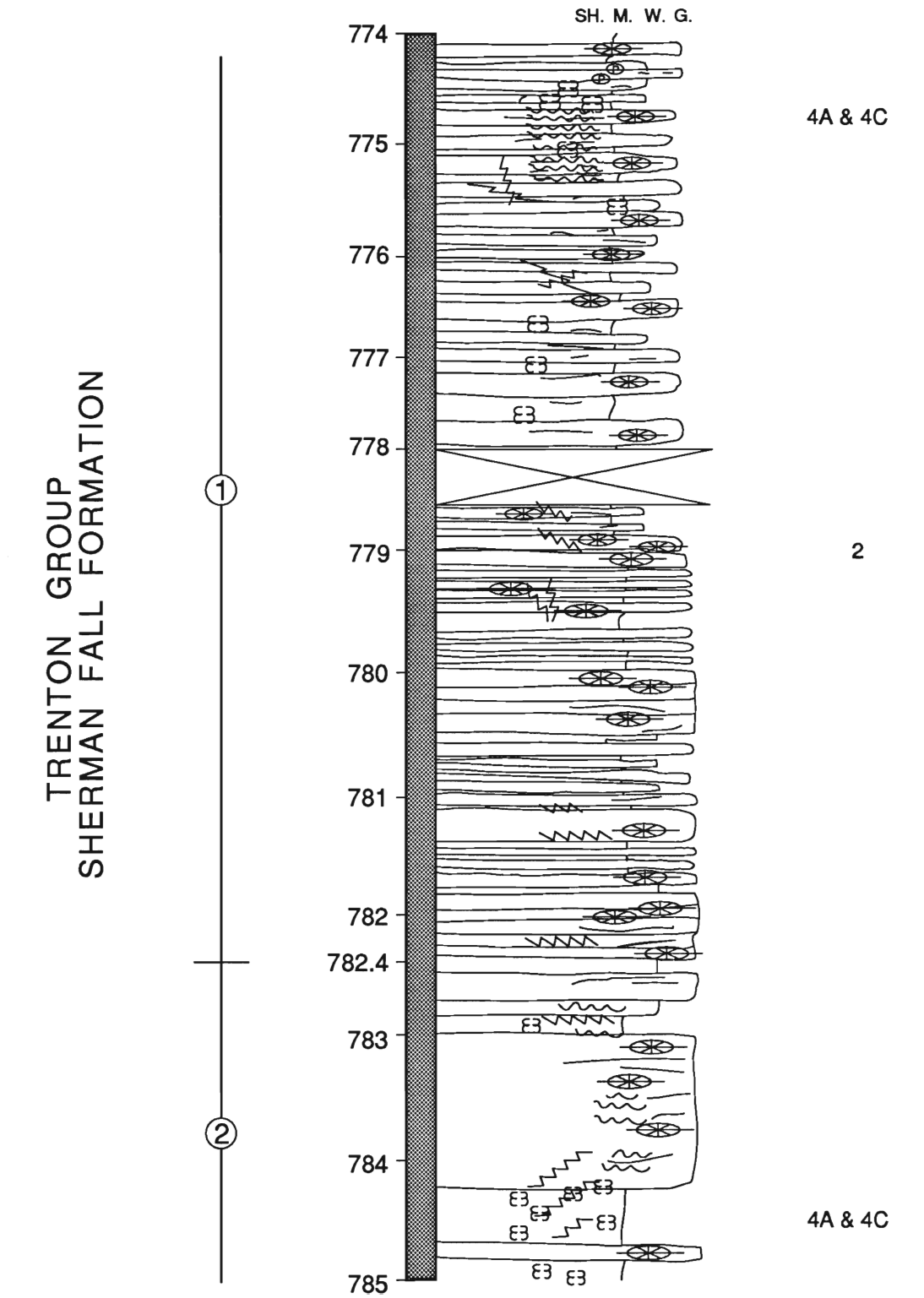

CONSUMERS' ET AL 33823 MERSEA 1-12-A

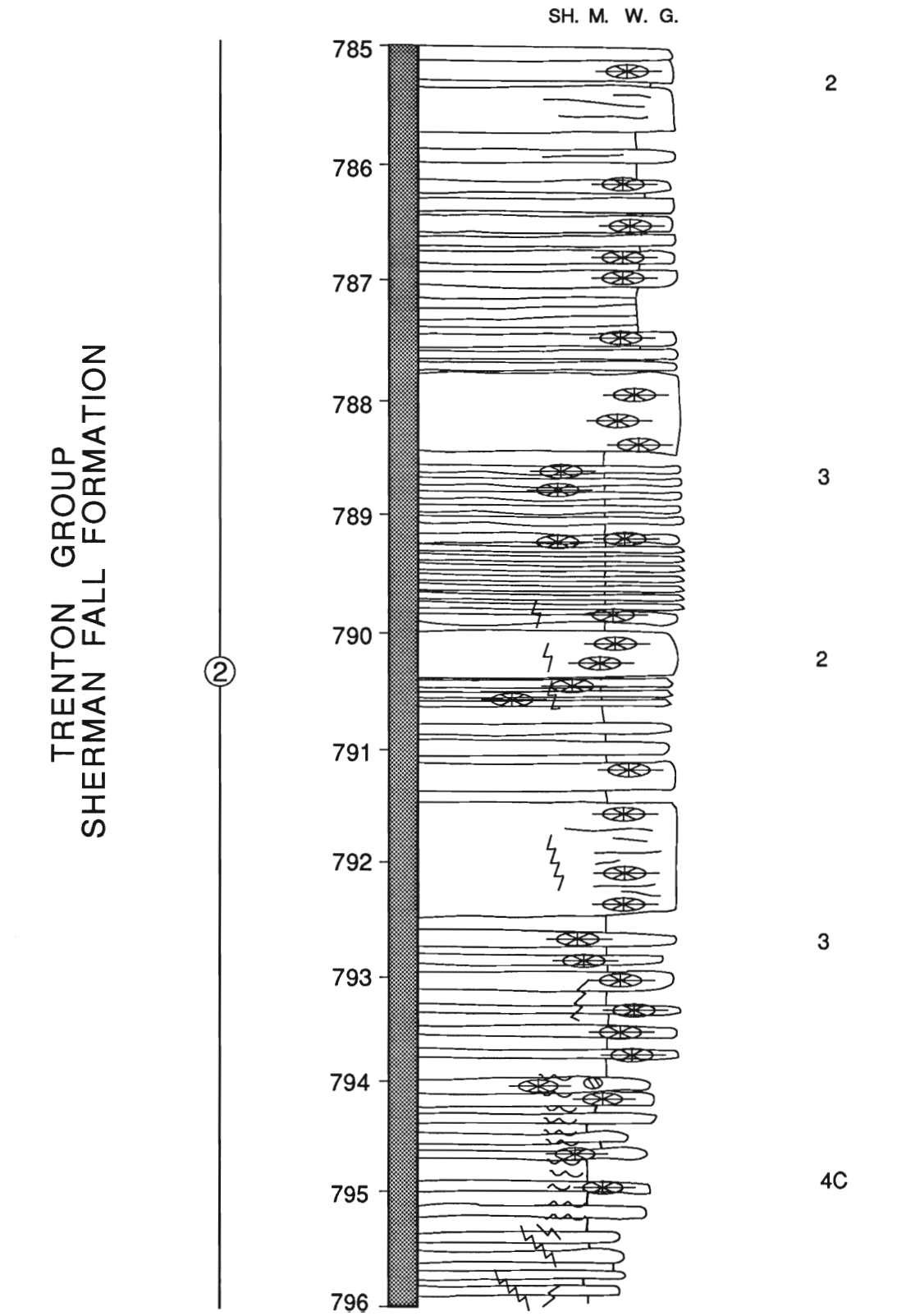

CONSUMERS' ET AL 33823 MERSEA 1-12-A

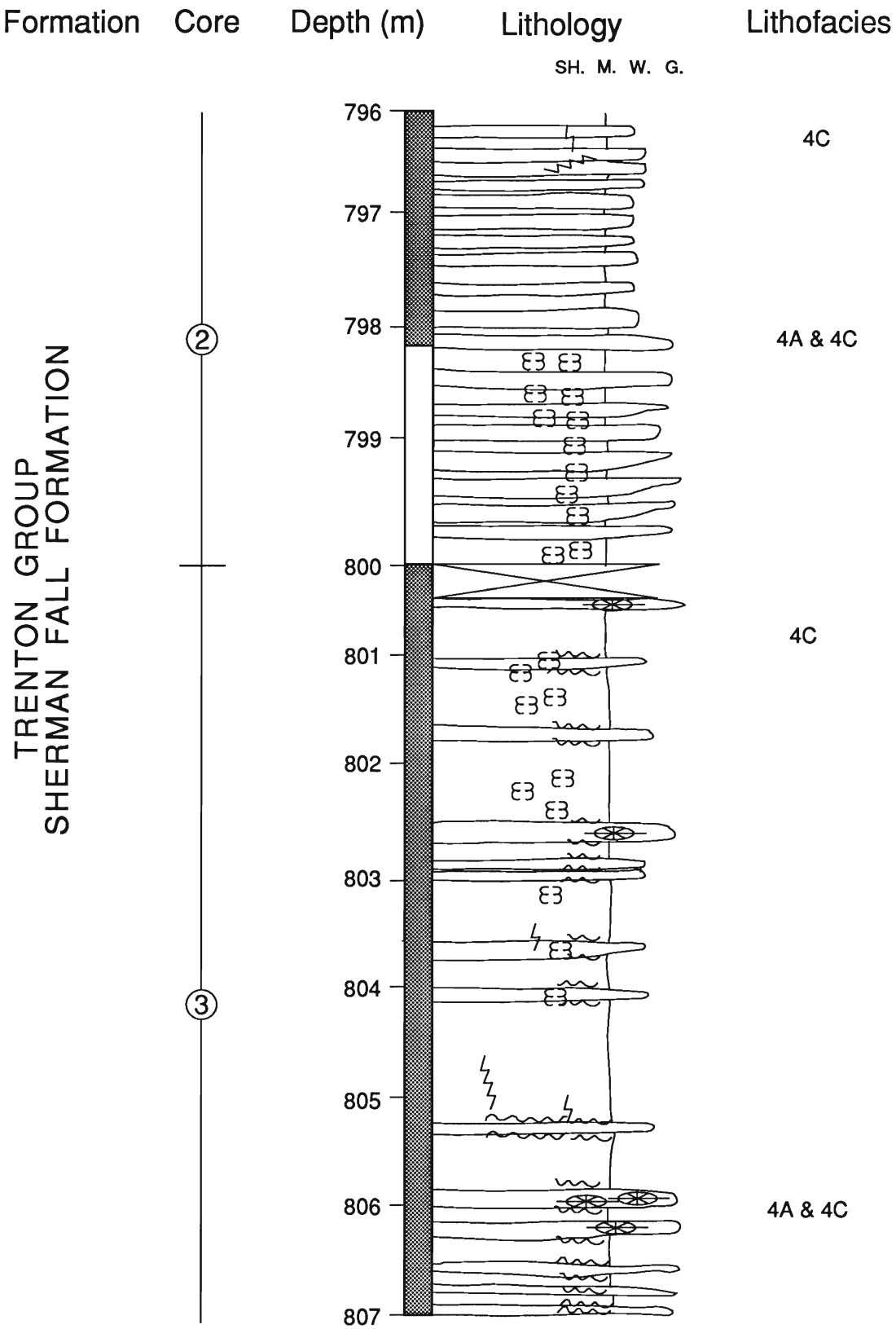

CONSUMERS' ET AL 33823 MERSEA 1-12-A

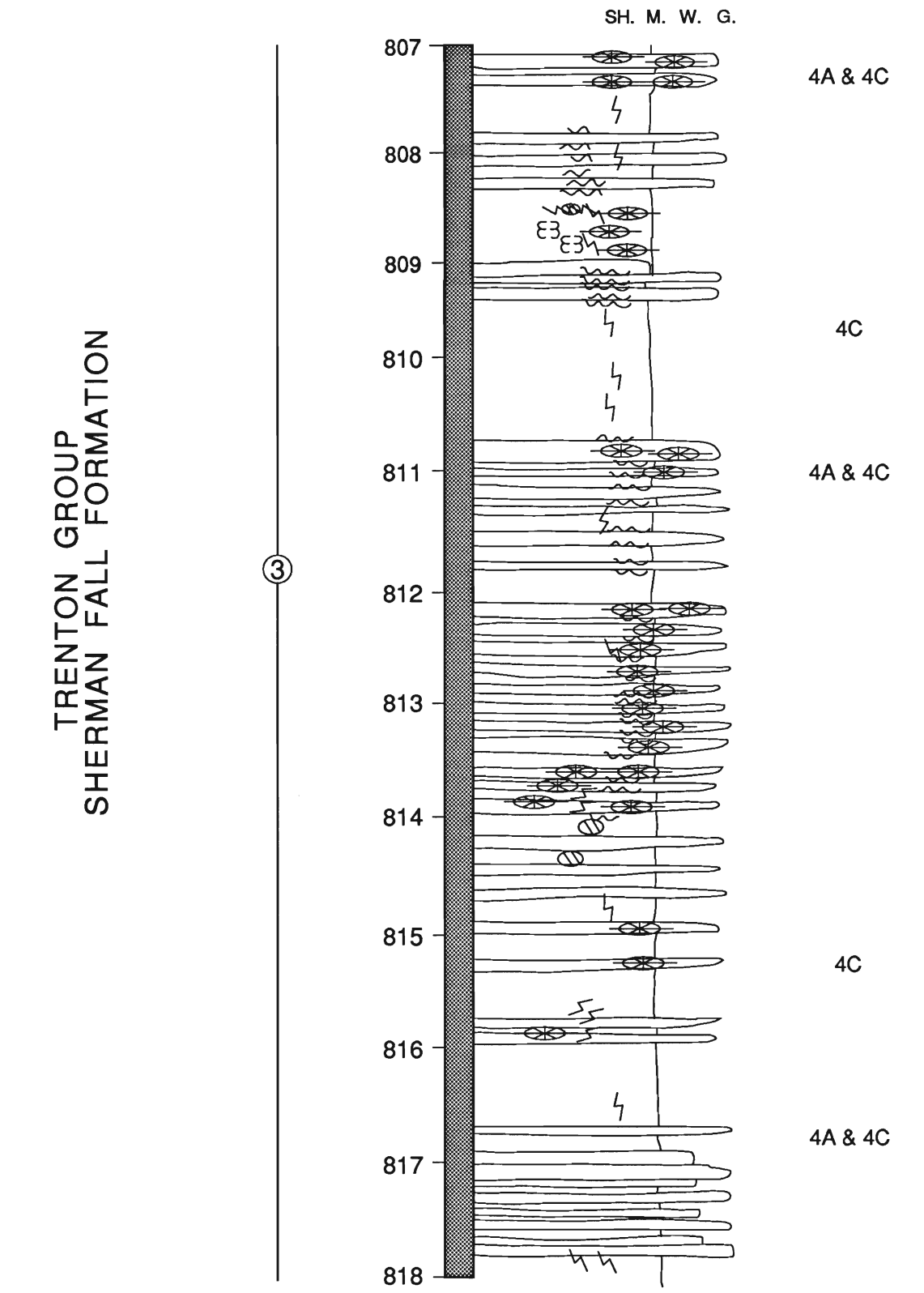

CONSUMERS' ET AL 33823 MERSEA 1-12-A

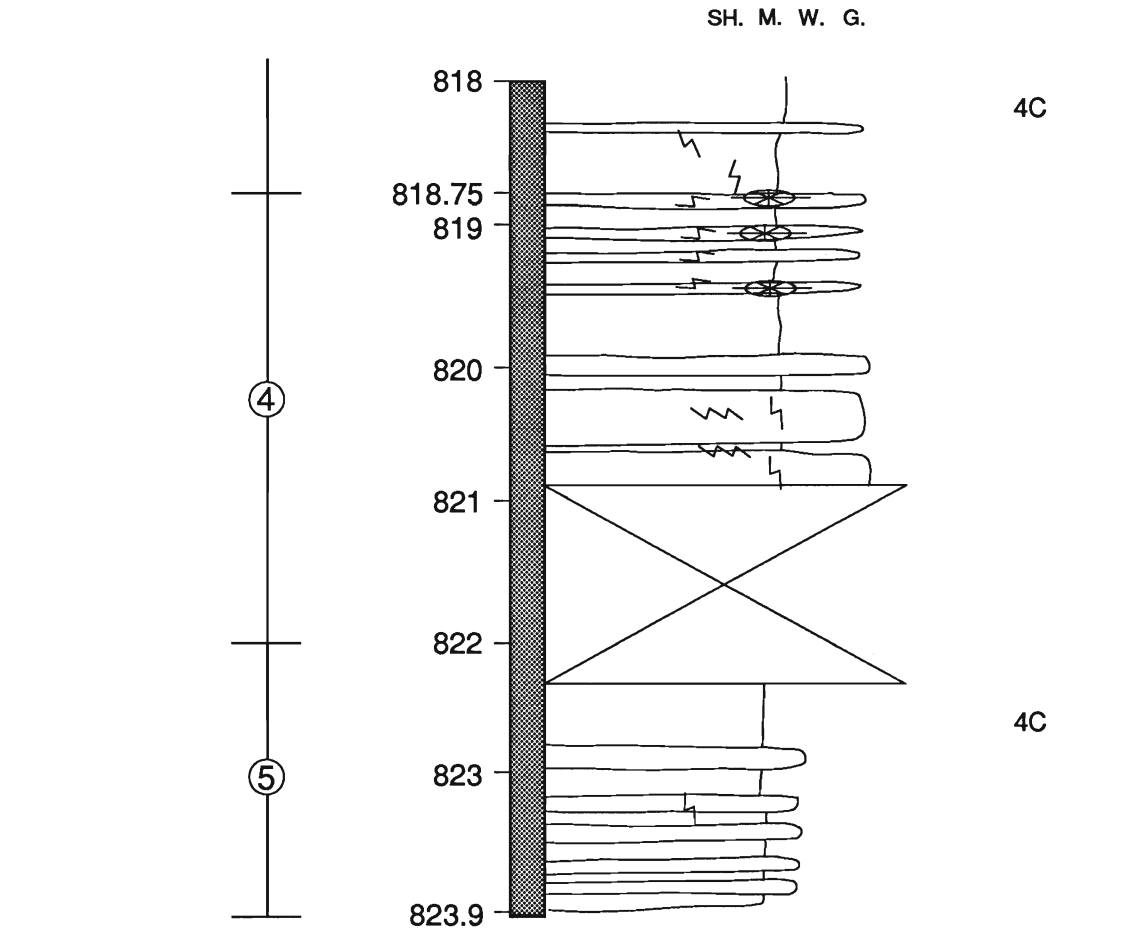

CONSUMERS' ET AL 34151 MERSEA 5-18-VIII

Core #1 797.5 - 808.5m (recorded 11m)
Core #2 808.5 - 822.9m (recorded 14.4m)
Core #3 822.9 - 836.9m (recorded 14m)

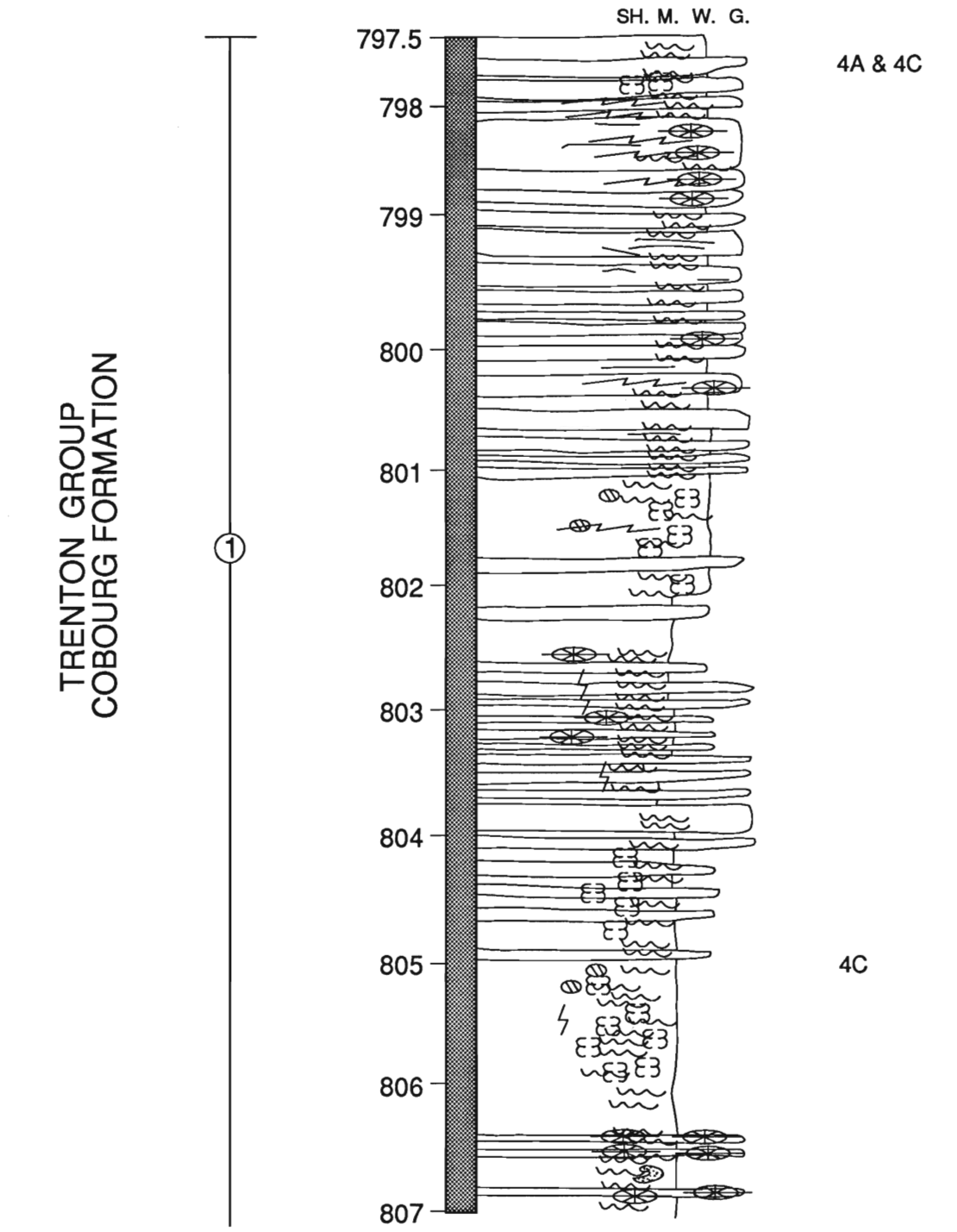

CONSUMERS' ET AL 34151 MERSEA 5-18-VIII

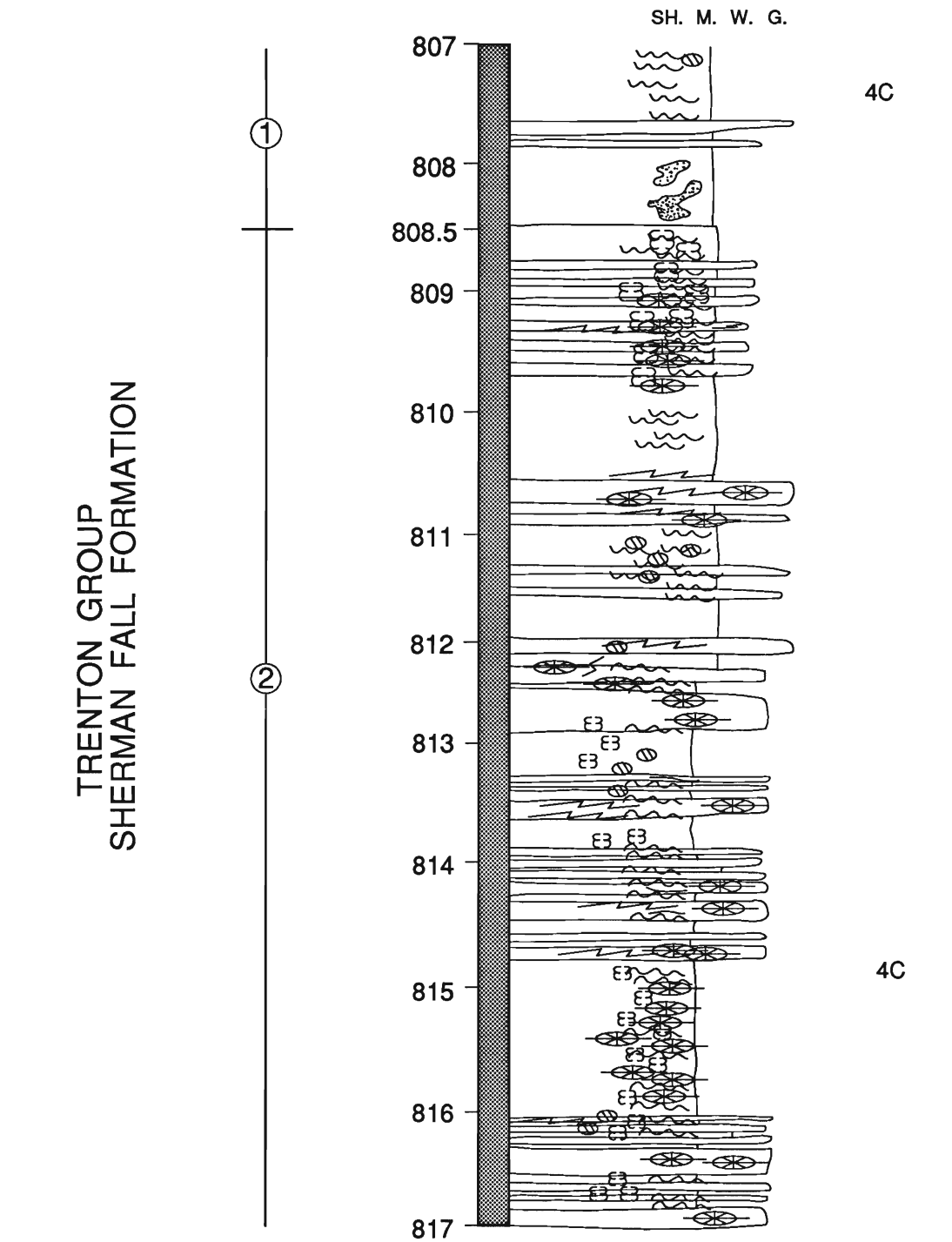

CONSUMERS' ET AL 34151 MERSEA 5-18-VIII

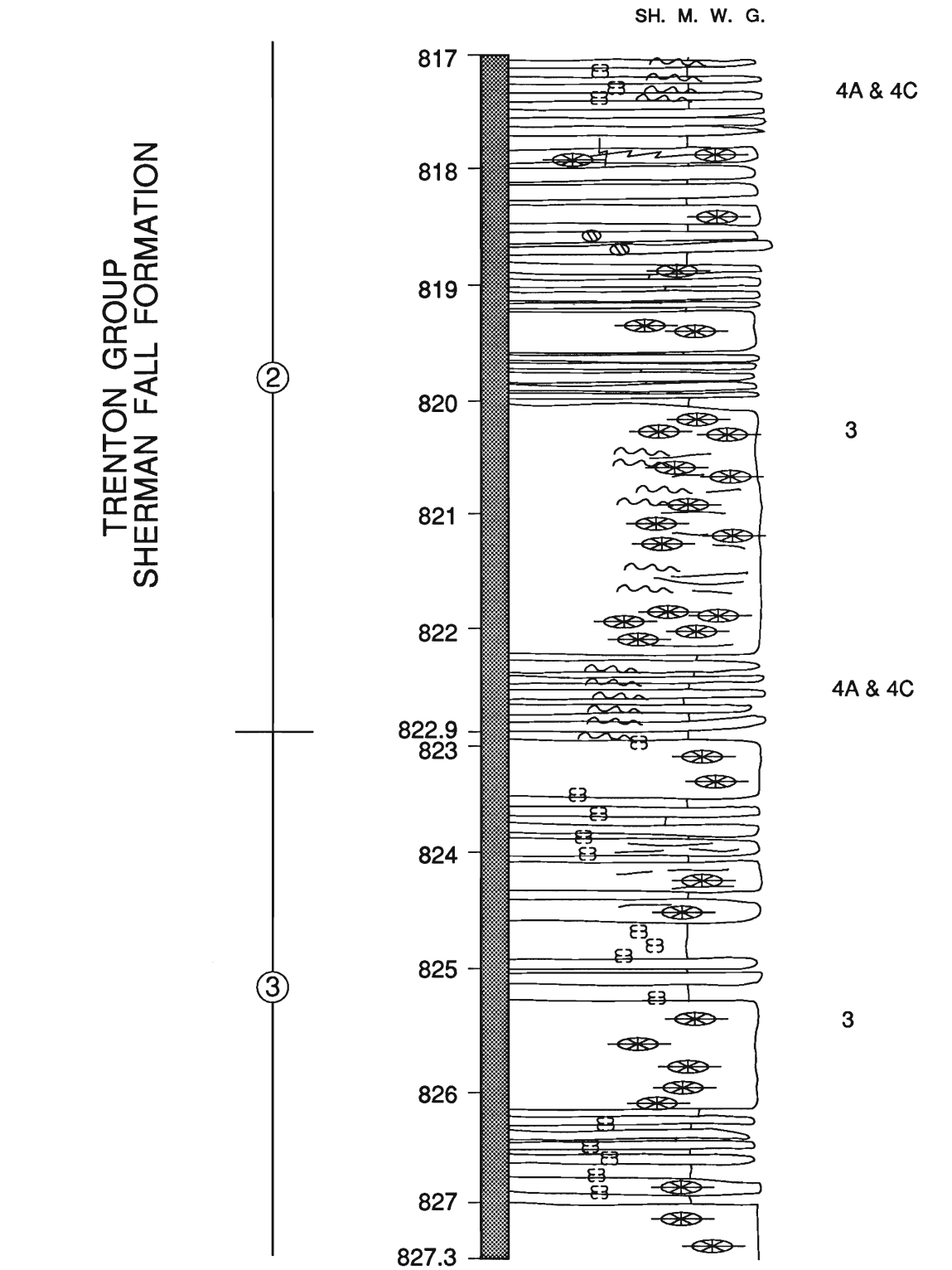

CONSUMERS' ET AL 34151 MERSEA 5-18-VIII

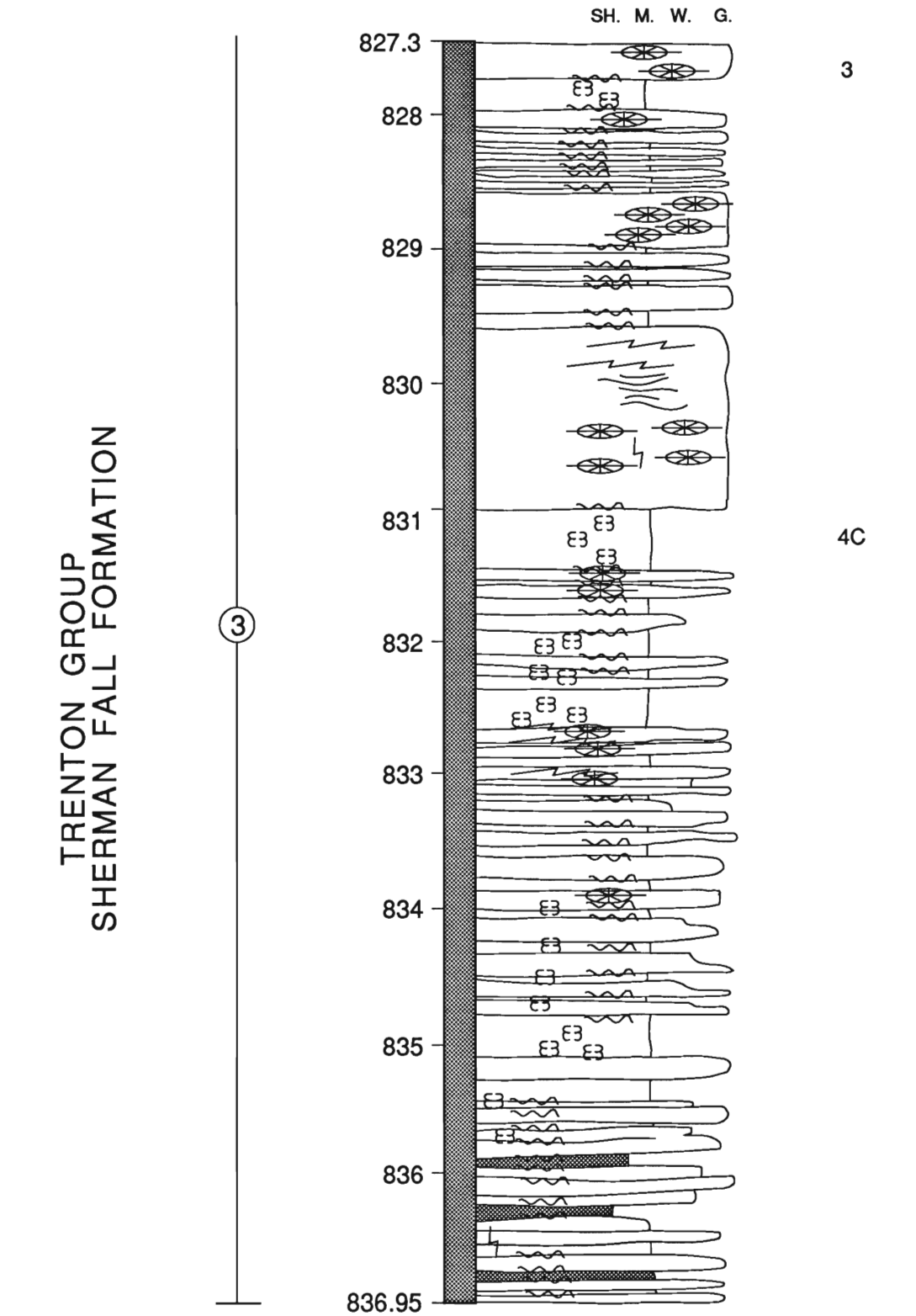

CONSUMERS' ET AL 34160 ROMNEY 5-8-11

Core #1 806.5 - 821.8m (recorded 15.3m)
Core #2 821.8 - 837.1m (recorded 15.3m)
Core #3 837.1 - 852.4m (recorded 15.3m)
Core #4 852.4 - 867.7m (recorded 15.3m)

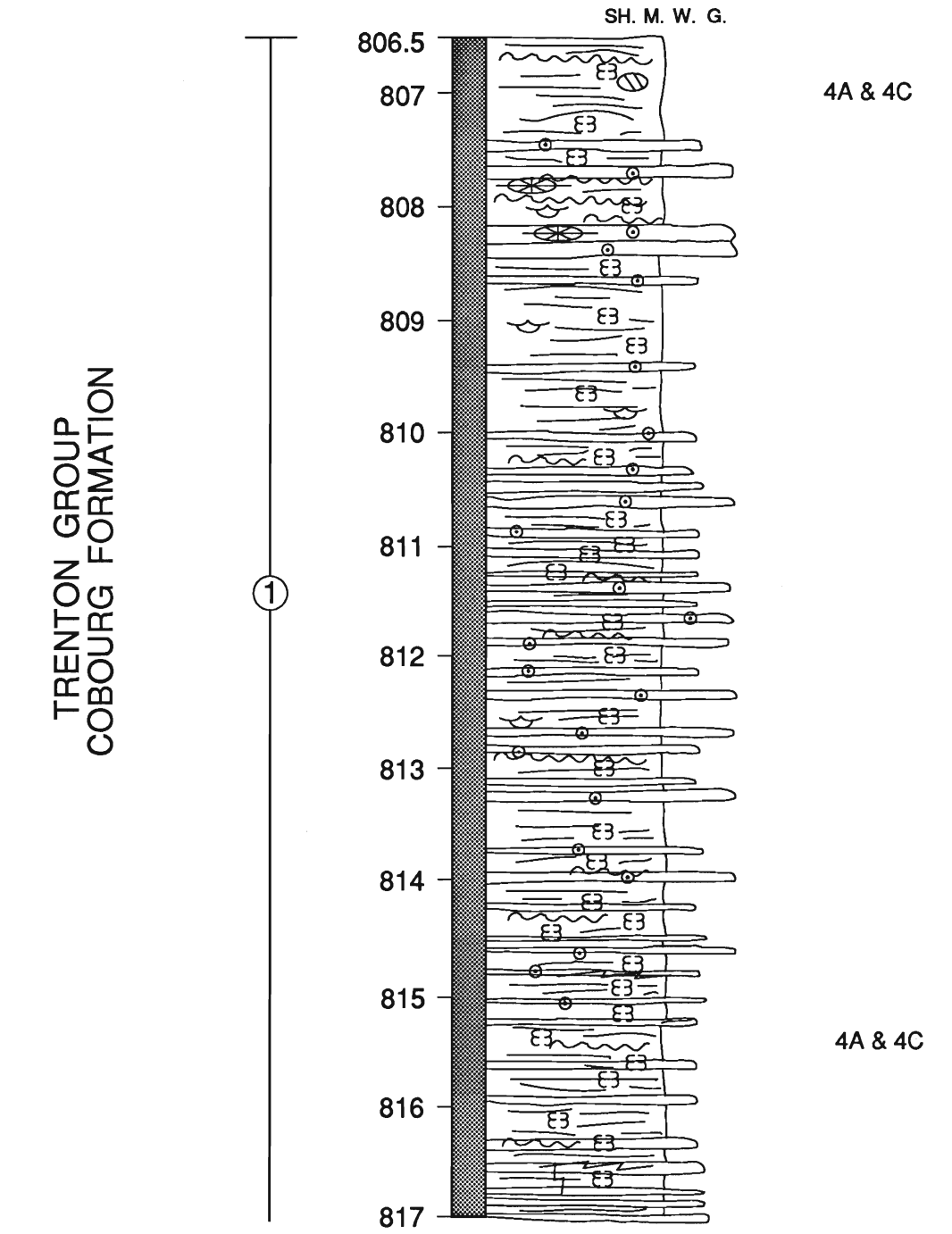

CONSUMERS' ET AL 34160 ROMNEY 5-8-11

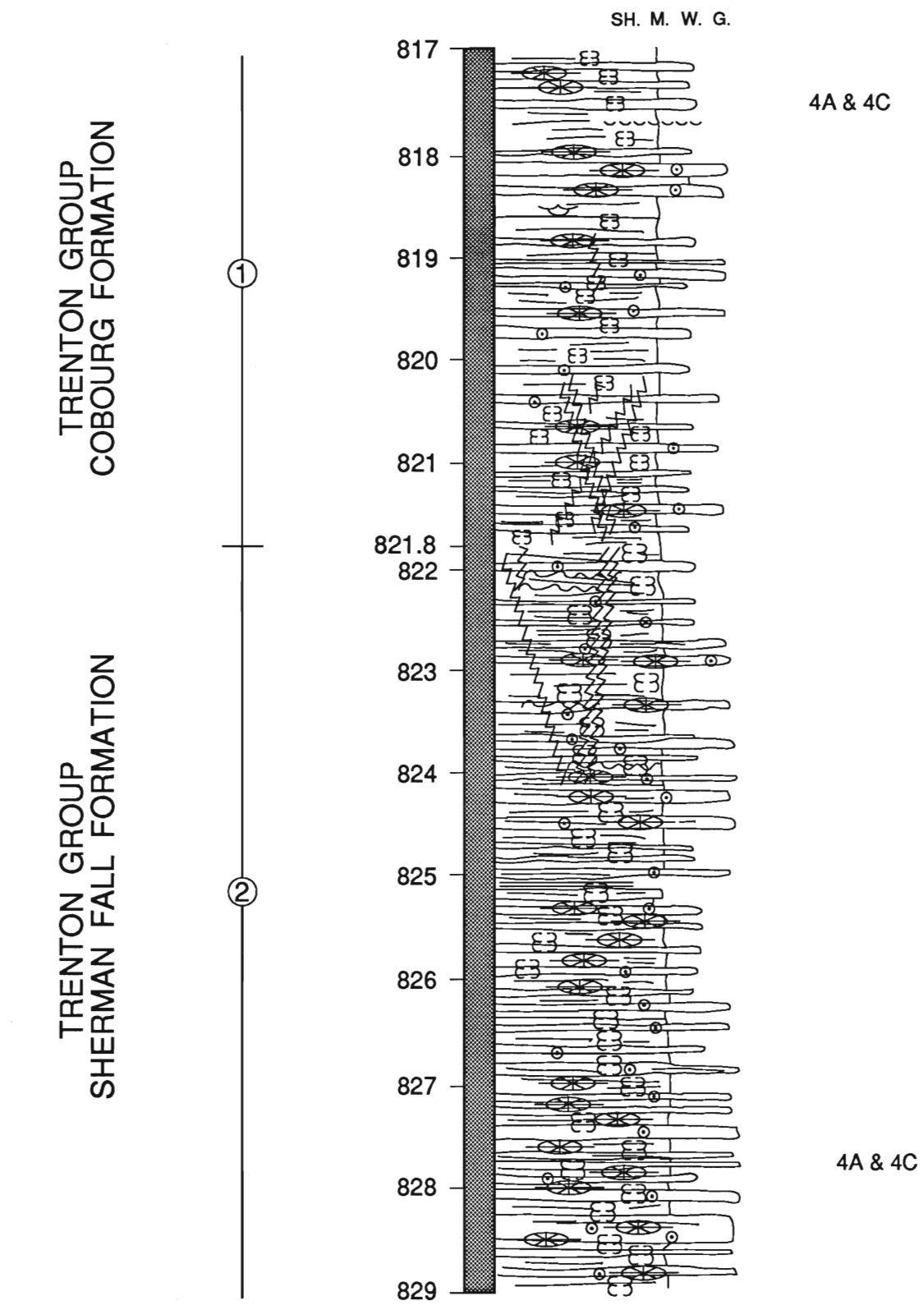

CONSUMERS' ET AL 34160 ROMNEY 5-8-11

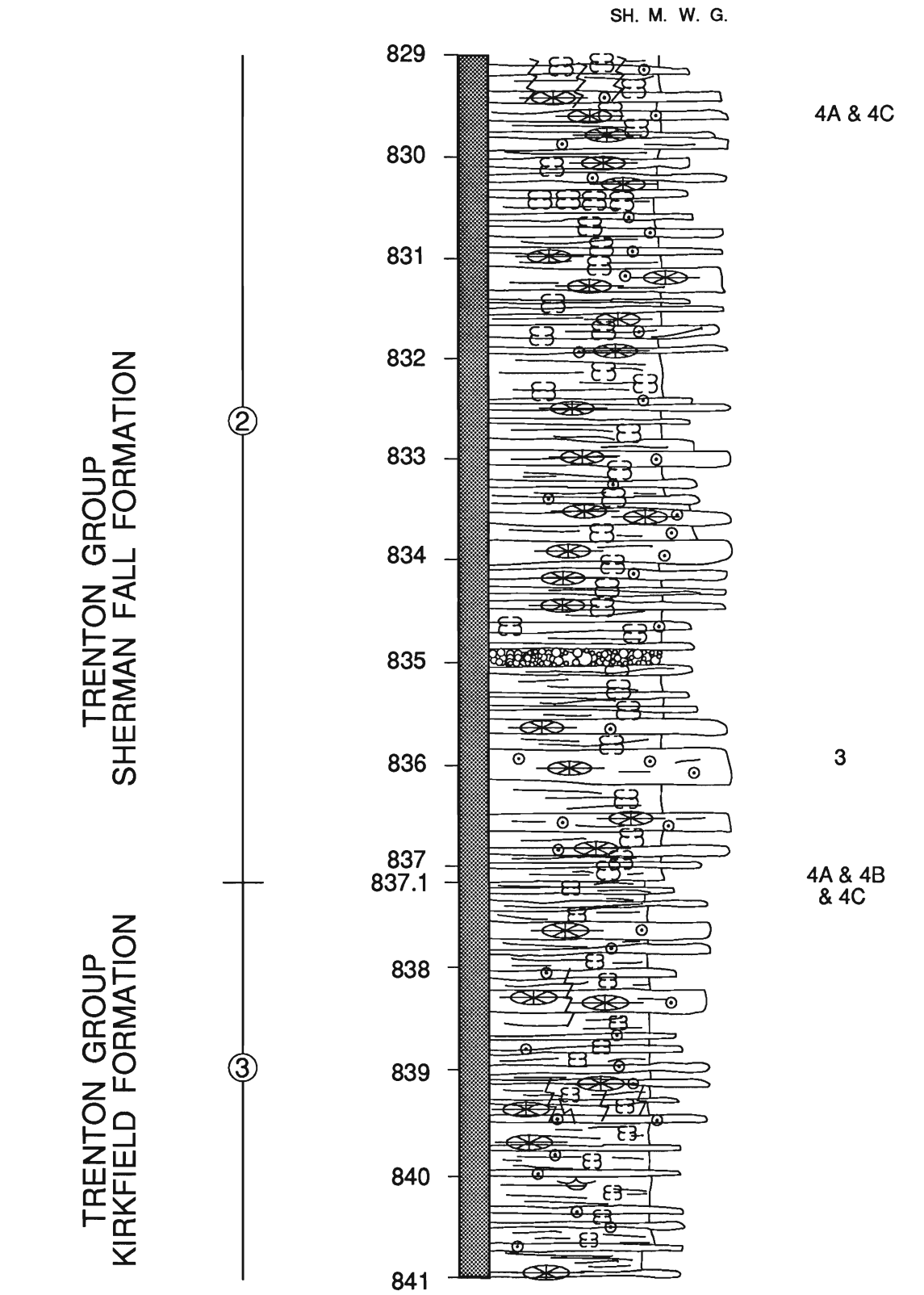

CONSUMERS' ET AL 34160 ROMNEY 5-8-11

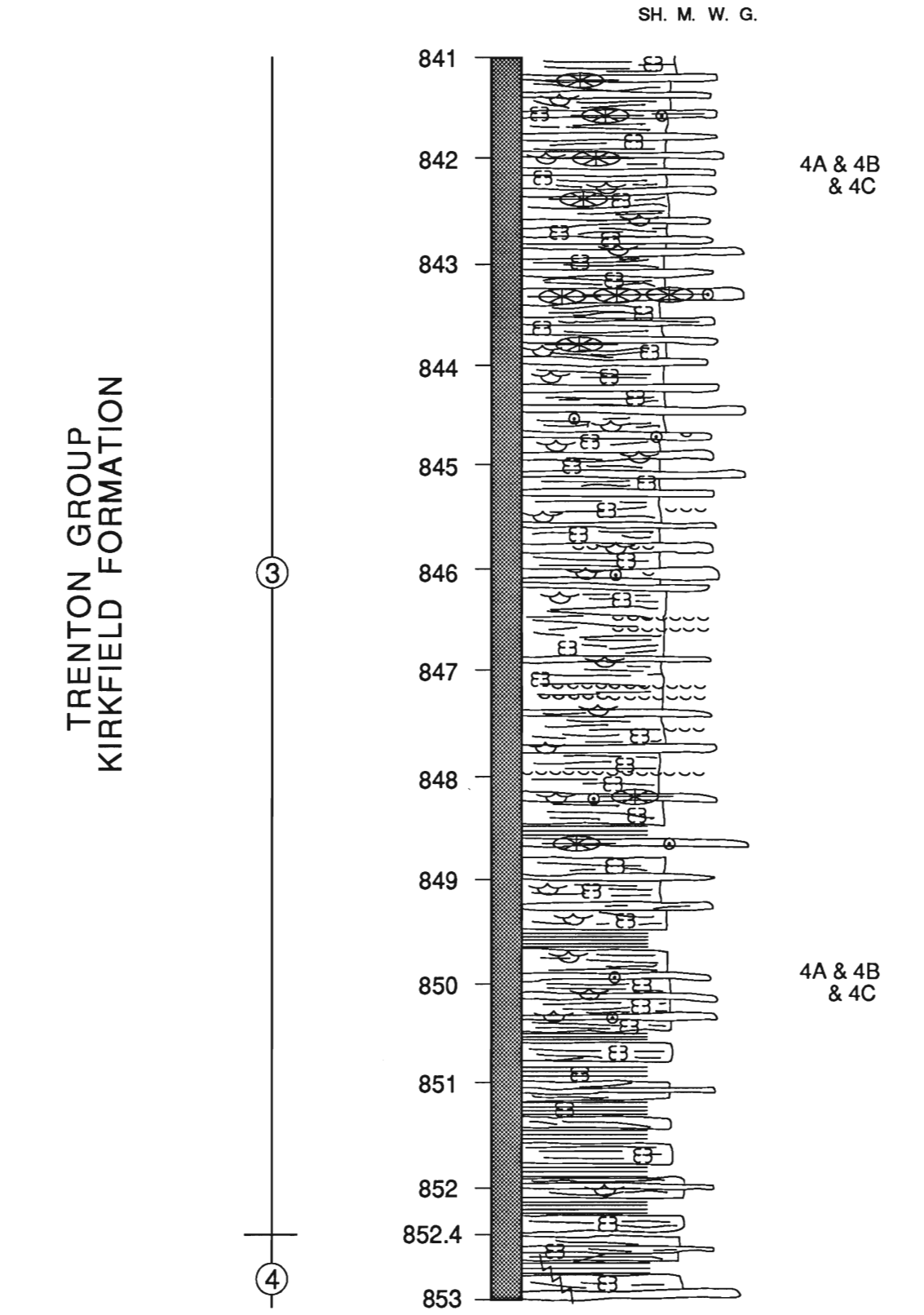

CONSUMERS' ET AL 34160 ROMNEY 5-8-II

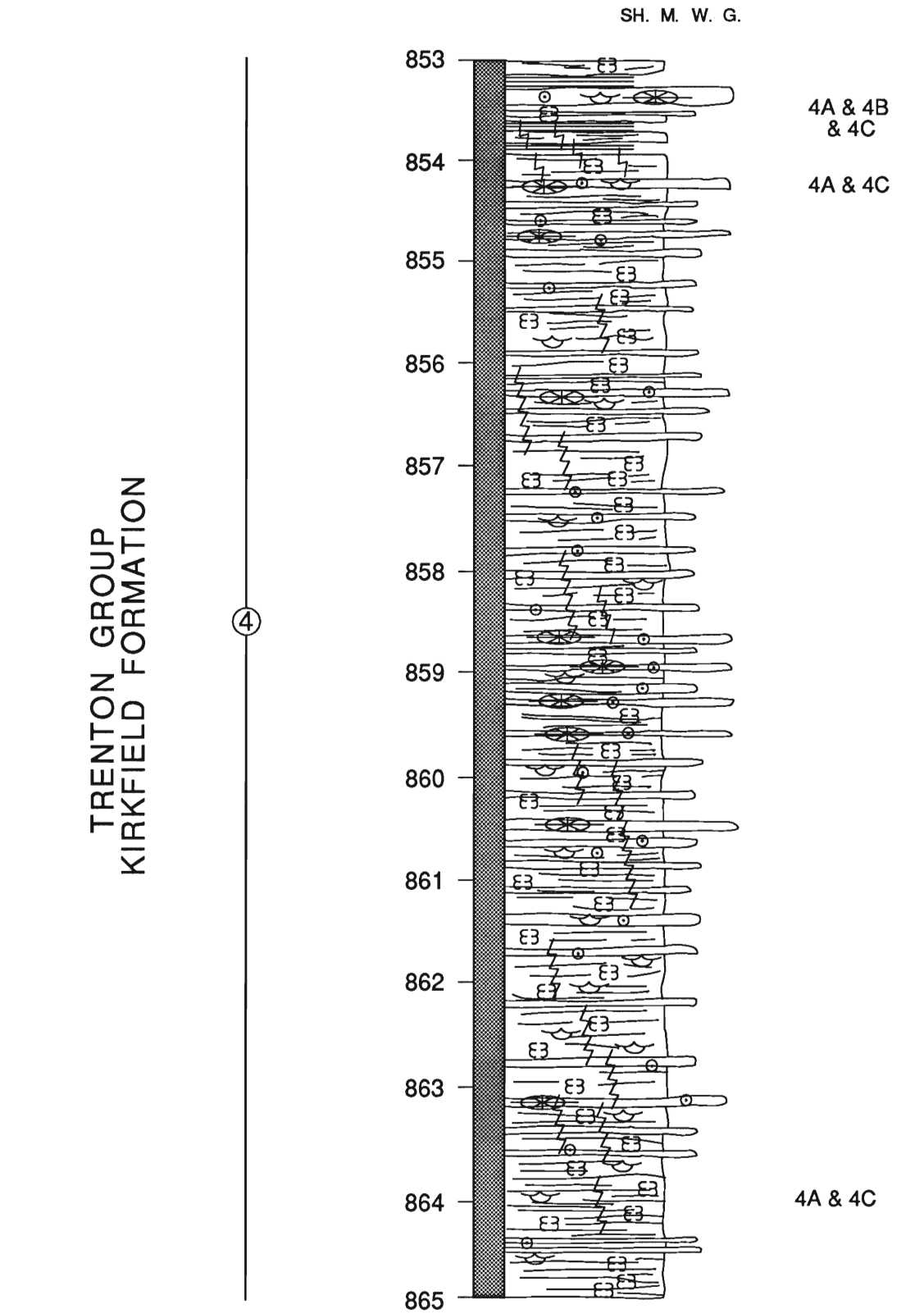

CONSUMERS' ET AL 34160 ROMNEY 5-8-II

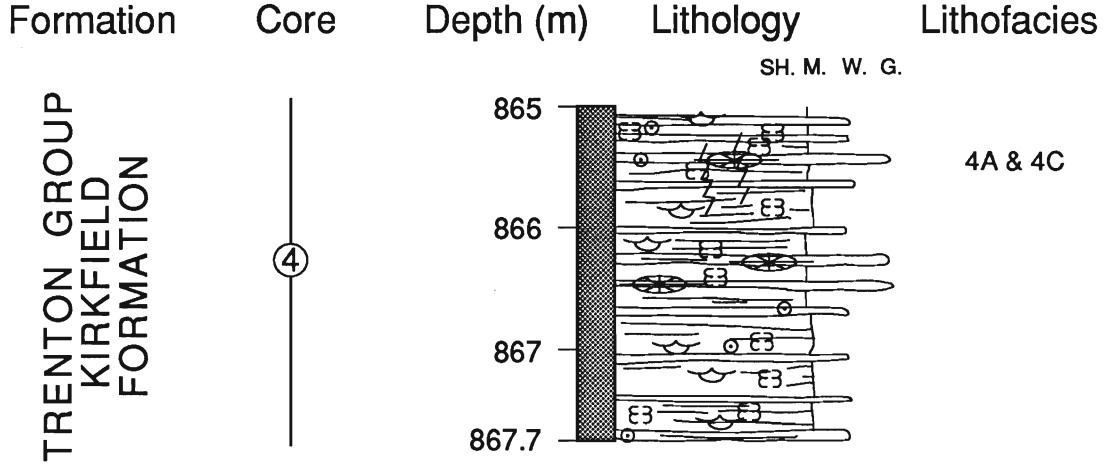

Appendix II

PETROGRAPHIC ANALYSIS
WELL NO 33821 MERSEA
3 - 12 - I

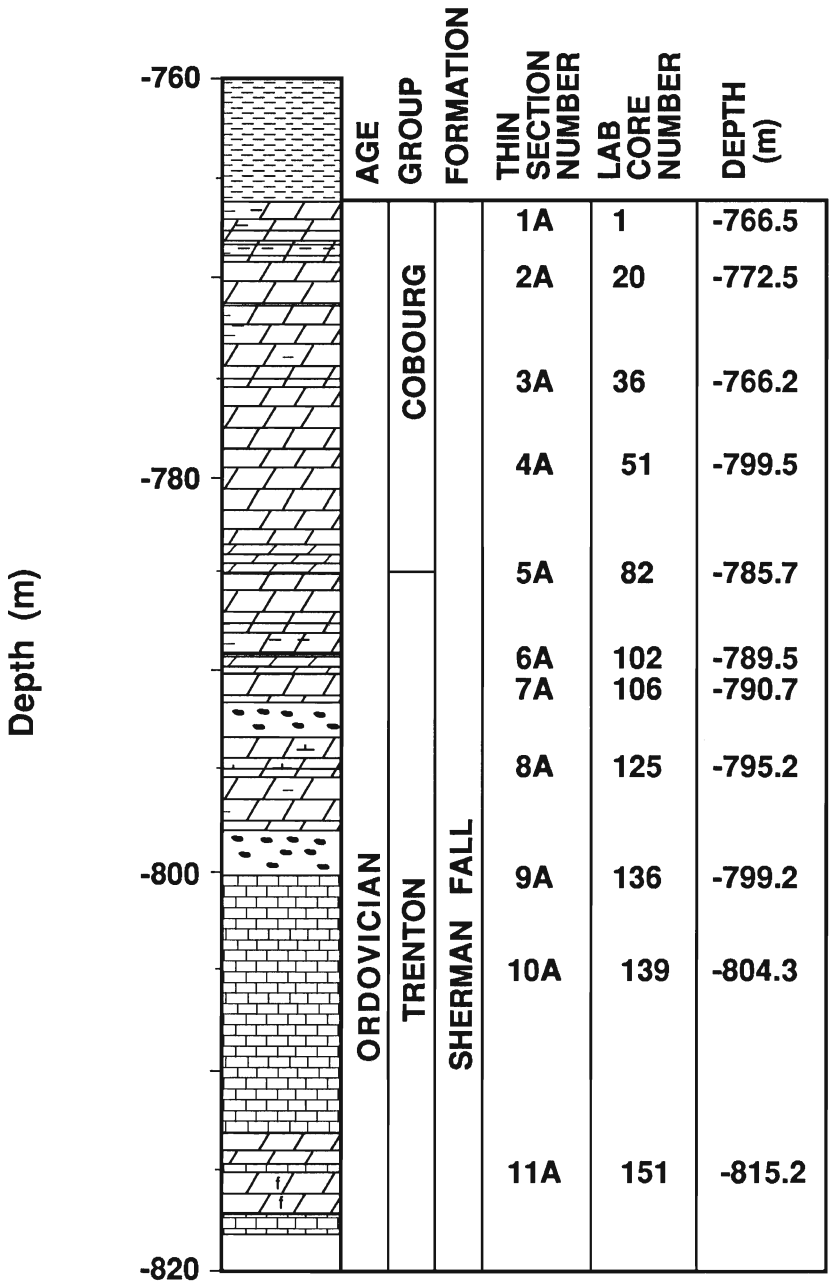

PETROGRAPHIC ANALYSIS
WELL NO 33821 - EXTENDED
MERSEA 3 - 12 - I

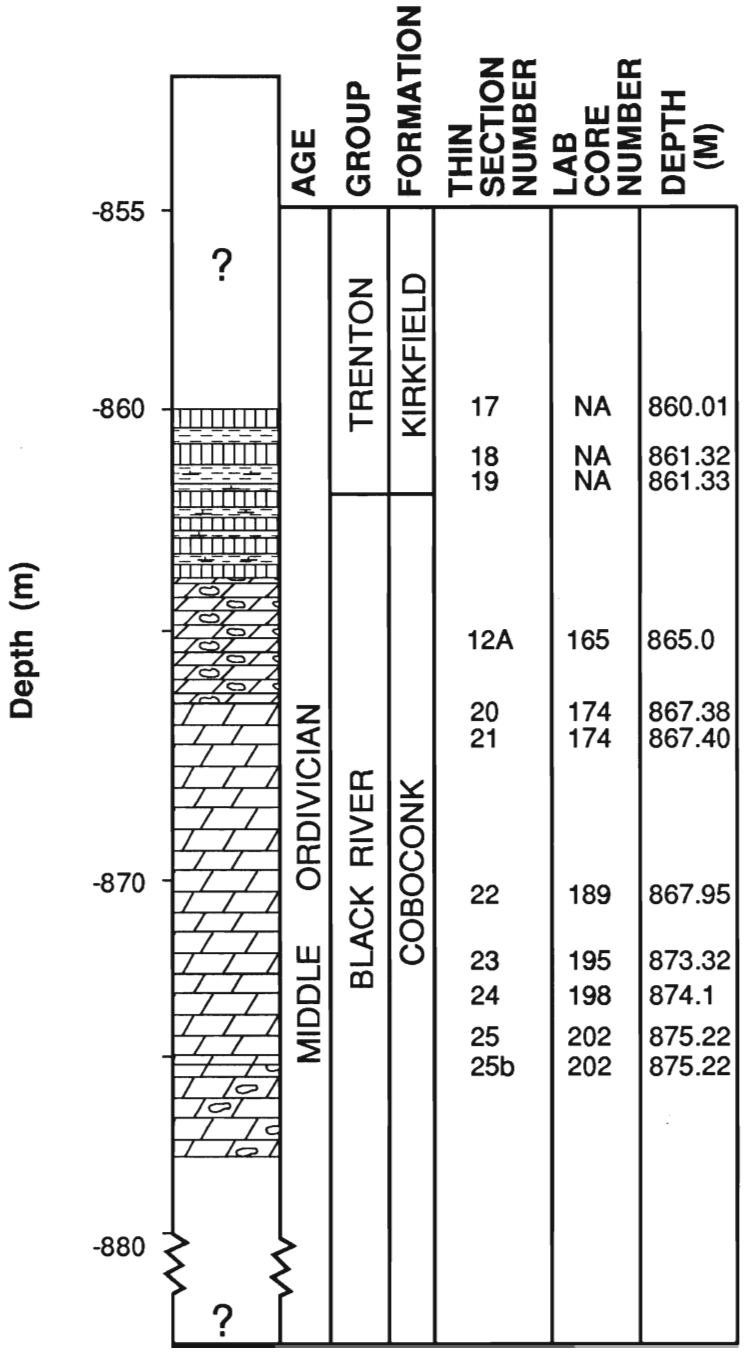

PETROGRAPHIC ANALYSIS
WELL NO 33821 - EXTENDED
MERSEA 3 - 12 - I

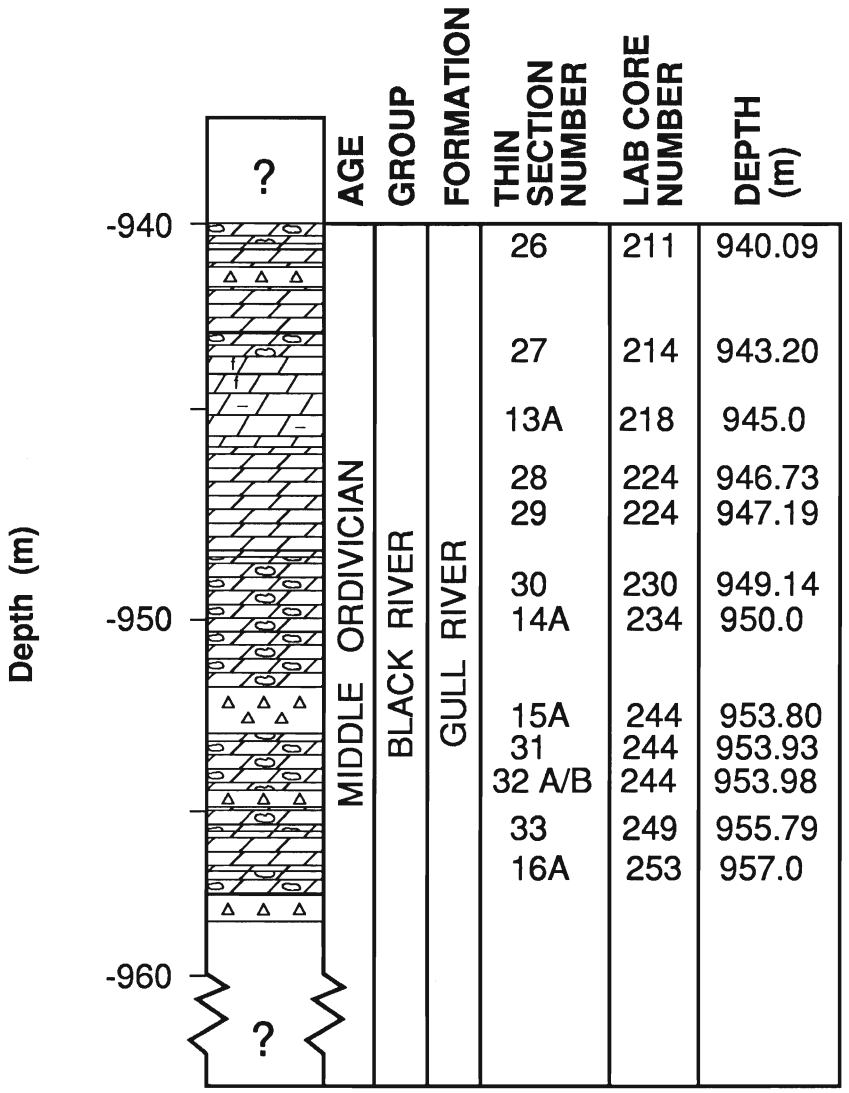

PETROGRAPHIC ANALYSIS
WELL NO 33823 MERSEA
1 - 12 - A

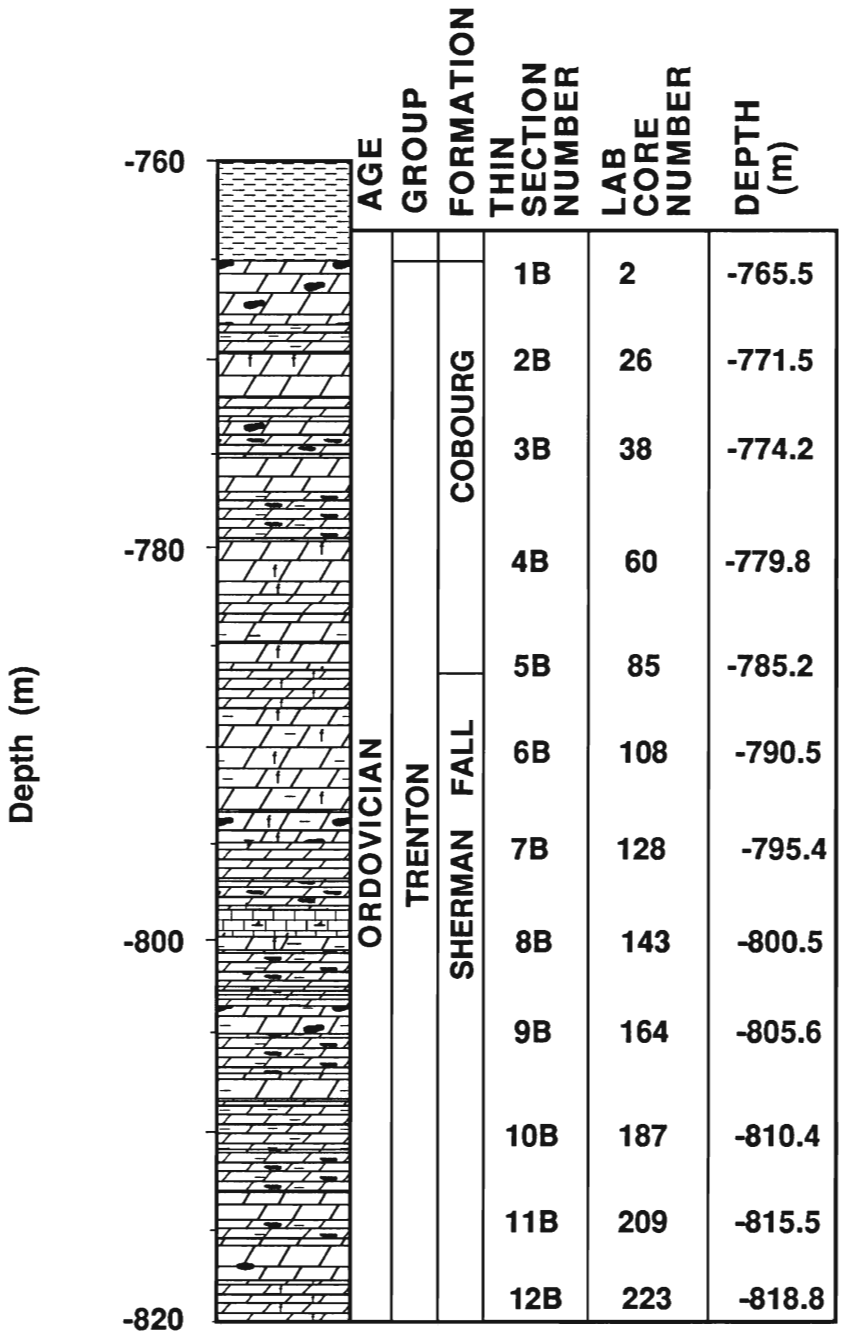

PETROGRAPHIC ANALYSIS
WELL NO 34151
MERSEA 7 - 18 - VIII

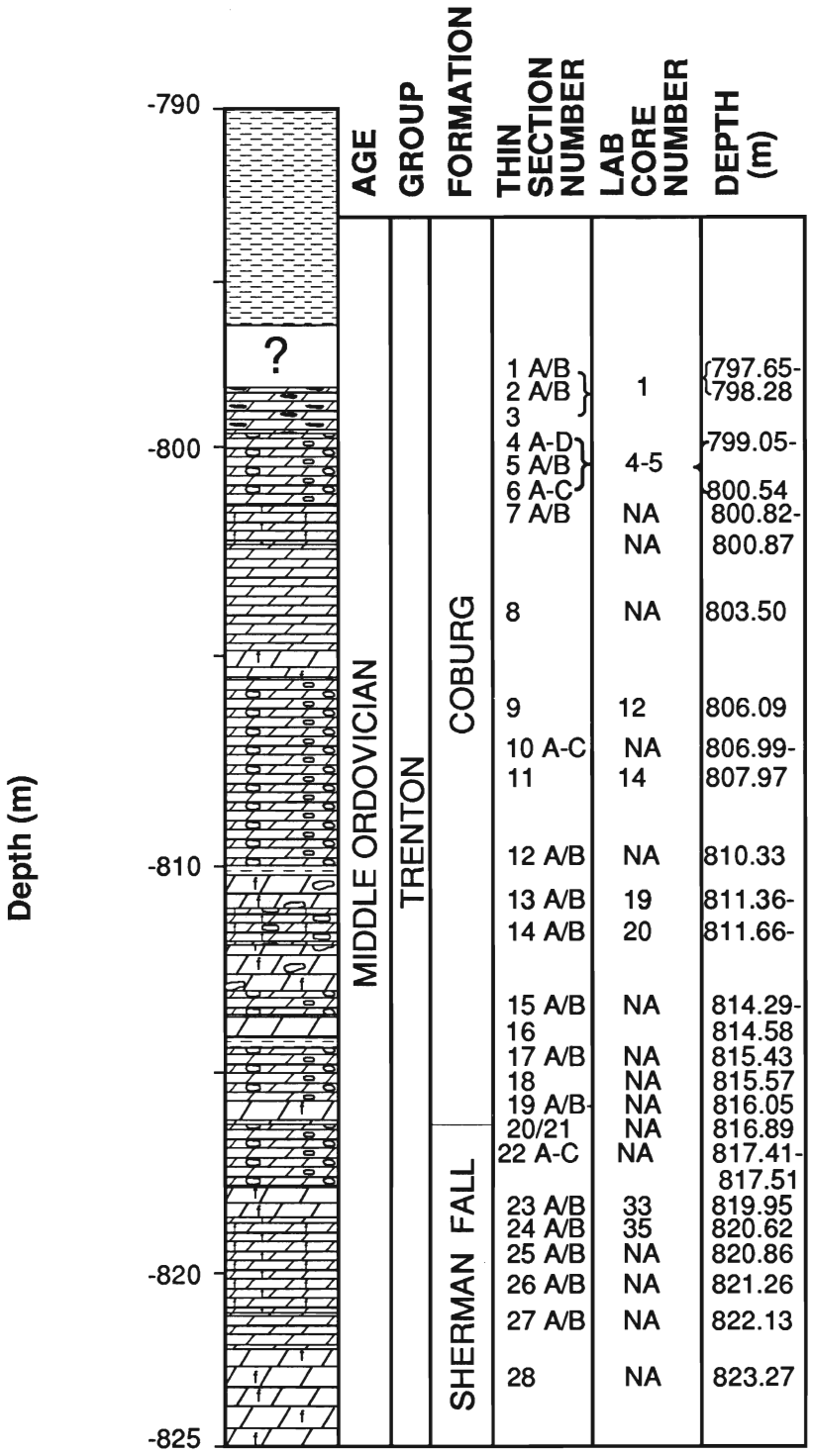

PETROGRAPHIC ANALYSIS
WELL NO 34151
MERSEA 7 - 18 - VIII

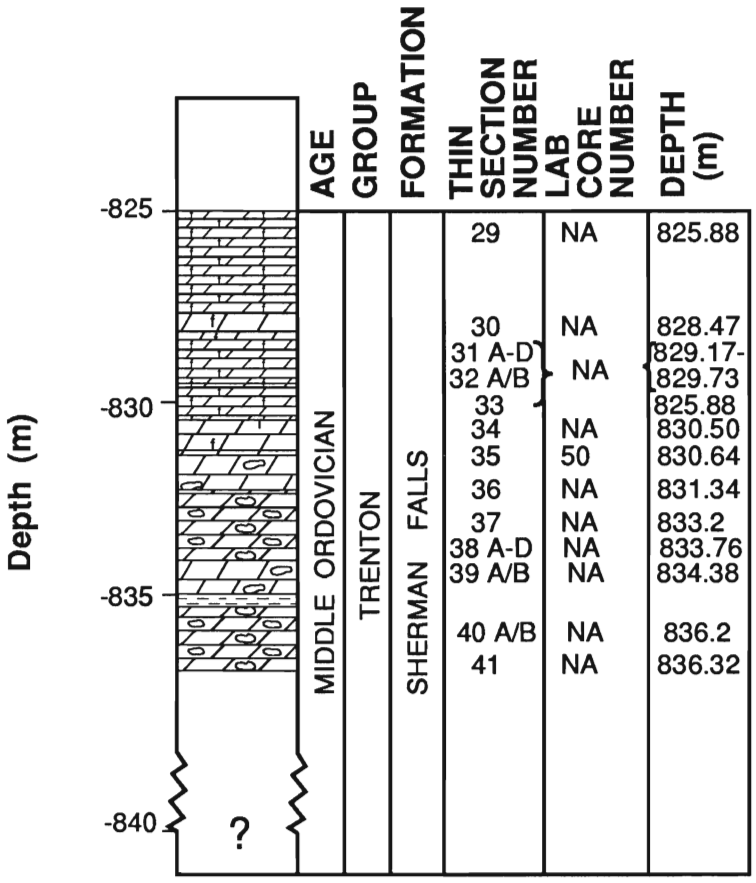

PETROGRAPHIC ANALYSIS
WELL NO 34160
ROMNEY 5 - 8 - II

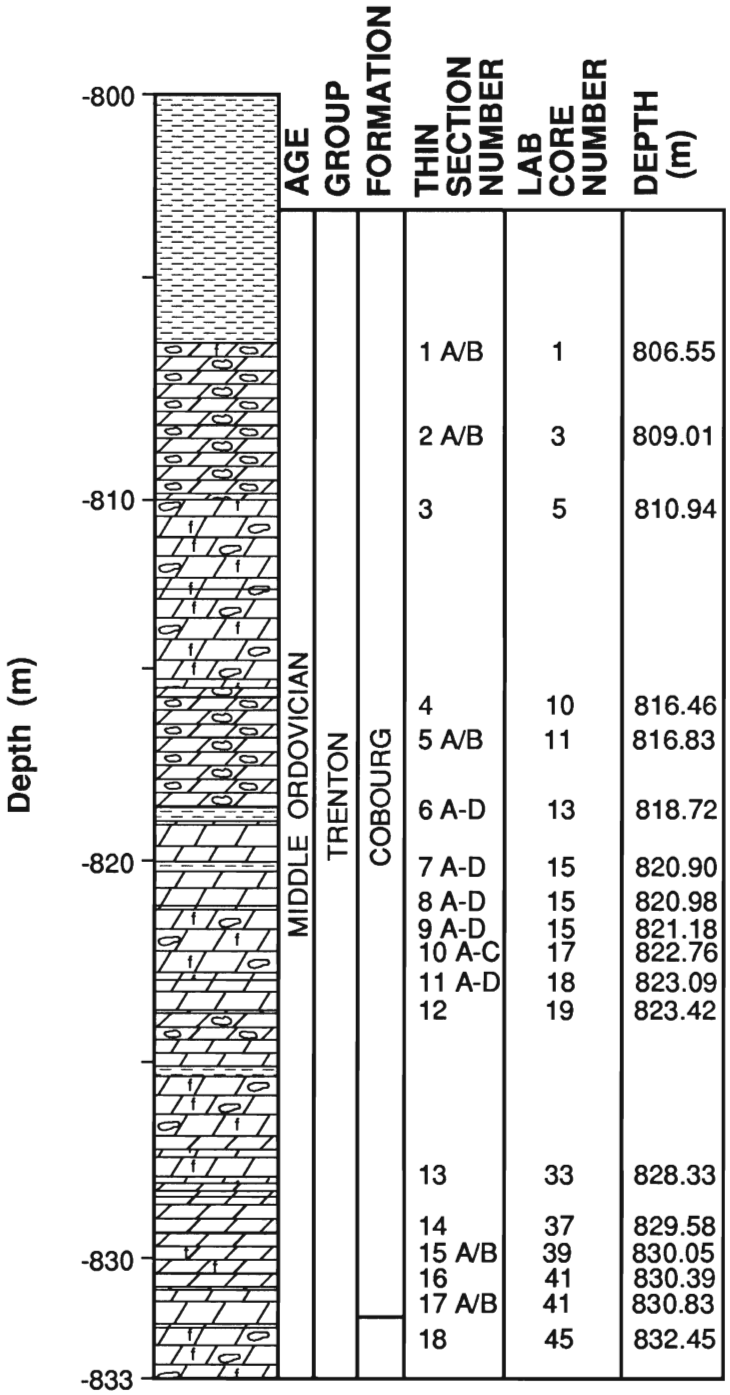

PETROGRAPHIC ANALYSIS
WELL NO 34160
ROMNEY 5 - 8 - II

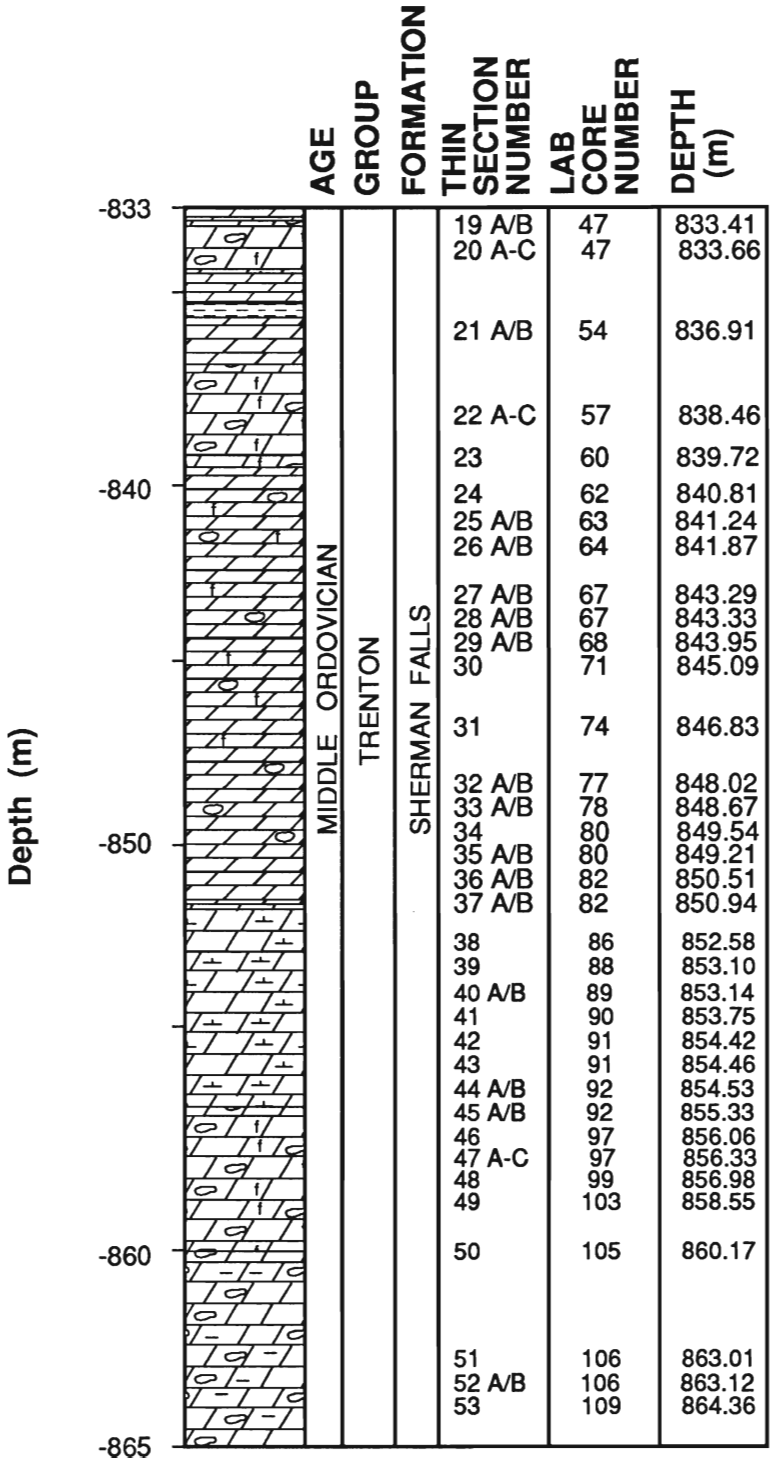

THIN SECTION NUMBER	LAB CORE NUMBER	DEPTH (m)
19 A/B	47	833.41
20 A-C	47	833.66
21 A/B	54	836.91
22 A-C	57	838.46
23	60	839.72
24	62	840.81
25 A/B	63	841.24
26 A/B	64	841.87
27 A/B	67	843.29
28 A/B	67	843.33
29 A/B	68	843.95
30	71	845.09
31	74	846.83
32 A/B	77	848.02
33 A/B	78	848.67
34	80	849.54
35 A/B	80	849.21
36 A/B	82	850.51
37 A/B	82	850.94
38	86	852.58
39	88	853.10
40 A/B	89	853.14
41	90	853.75
42	91	854.42
43	91	854.46
44 A/B	92	854.53
45 A/B	92	855.33
46	97	856.06
47 A-C	97	856.33
48	99	856.98
49	103	858.55
50	105	860.17
51	106	863.01
52 A/B	106	863.12
53	109	864.36

PETROGRAPHIC ANALYSIS
WELL NO 34160
ROMNEY 5 - 8 - II

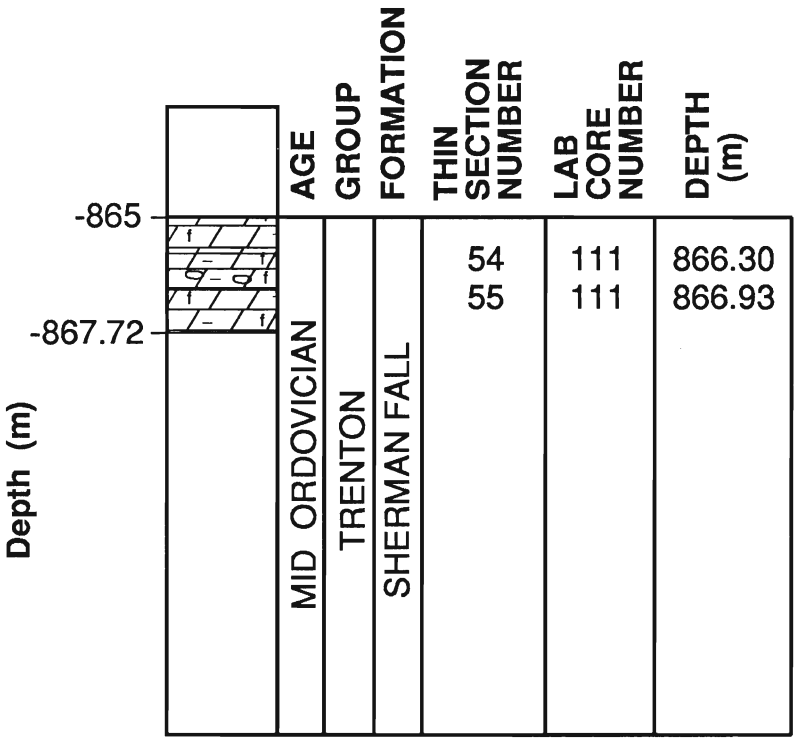

Appendix III

Equation used to derive the theoretical diagenetic fluids responsible for the alteration and precipitation of the various carbonate components (McIntire, 1963; Kinsman, 1969);

$$\frac{{}^{m}Me/{}^{m}Ca\ (s)}{{}^{m}Me/{}^{m}Ca\ (l)} = k \qquad (5)$$

${}^{m}Me/{}^{m}Ca$ (s) is calculated by computing the molar concentration of the element with respect to calcium using the results from the trace element analysis.

k represents the distribution coefficient of the element for that particular carbonate phase.

The partition coefficients used in the computation of the theoretical diagenetic fluids (summarized in Veizer, 1983) are the following;

Limestone Diagenesis:

Mg: k = 0.036 (range is 0.013 - 0.06)
Fe: k = 20 (range is $1 < x < 20$)
Mn: k = 5.4 (range is 5.4 - 30)
Na: k = 0.000025 (range is 0.00002 - 0.00003)
Sr k = 0.05 for A to dLMC, and HMC to dLMC

Onset of dolomitization:

Mg, Fe, Mn, and Na for dolomitic limestones k = as reported above
Sr: k = 0.0375 (range is 0.025 - 0.05) for dolomitic limestones

Distribution coefficients for Sr used in the computation of the ${}^{m}Sr/{}^{m}Ca$ ratio for all theoretical diagenetic fluids:

Sr: k = 0.025 for Saddle Dolomite A
Sr: k = 0.05 for Saddle Dolomite B
Sr: k = 0.13 for direct precipitation of Calcite
Sr: k = 0.025 for Dolomite
Sr: k = 0.0375 for Dolomitic Limestones
Sr: k = 0.05 for Limestones

Appendix III-Limestone Matrix

Sample No.	IR %	Ca (ppm)	Mg (ppm)	Na (ppm)	Fe (ppm)	Mn (ppm)	Cu (ppm)	Zn (ppm)	Sr (ppm)	Ni (ppm)	Pb (ppm)	V (ppm)	Well No.	Depth (m)
230.0	12.3	383028	2867	881	2638	698	0	0	315	5	3	18	33821	-801.99
233.0	12.6	380571	1771	698	1829	555	6	0	314	6	0	17	33821	-803.43
234.0	11.1	380090	1810	1000	1697	468	0	0	498	8	3	17	33821	-803.50
235.0	11.7	377828	1540	802	1244	370	6	0	646	8	9	15	33821	-806.00
237.0	10.5	406742	337	718	899	254	0	0	803	6	0	19	33821	-808.00
238.0	7.8	397059	436	623	218	192	5	0	911	4	0	16	33821	-808.52
239.0	1.3	353535	1717	493	1364	380	5	3	694	4	0	14	33821	-810.79
241.0	9.5	408040	661	463	496	267	11	0	82	4	7	16	33821	-812.12
242.0	7.1	393743	431	508	216	202	5	0	736	5	0	18	33821	-812.14
243.0	6.4	349946	429	492	214	198	5	0	702	4	0	15	33821	-813.05
245.0	11.6	357062	395	647	282	222	6	0	920	7	3	16	33821	-813.11
246.0	11.6	360953	431	480	233	212	6	0	699	5	3	16	33821	-817.15
256.0	10.9	327915	504	492	785	548	6	0	580	8	0	18	33821	-860.01
259.0	14.8	345657	352	677	469	560	6	0	439	5	0	14	33821	-861.39

Appendix III-Dol. Limestone

Sample No.	IR %	Ca (ppm)	Mg (ppm)	Na (ppm)	Fe (ppm)	Mn (ppm)	Cu (ppm)	Zn (ppm)	Sr (ppm)	Ni (ppm)	Pb (ppm)	V (ppm)	Well No.	Depth (m)
231.0	0.8	427366	6246	2036	6283	1167	10	0	455	25	43	42	33821	-801.90
47.1	7.9	286120	42480	860	5889	1051	11	15	145	5	35	26	33821	-799.15
228.0	14.6	341706	29439	963	3621	556	12	0	321	14	11	20	33821	-799.00
229.0	9.6	302460	29650	490	3337	756	11	0	253	4	0	30	33821	-800.00
251.0	15.2	319499	16667	1459	3073	427	12	12	390	21	38	15	33821	-817.10
15.2	10.9	333560	14620	410	1745	568	11	0	320	9	0	38	33823	-798.00
16.2	3.5	326140	11605	590	13495	1677	5	0	425	5	13	21	33823	-798.20
333.0	9.7	324444	3611	572	3833	807	6	0	251	6	7	17	33823	-798.50
17.2	4.5	293820	19810	380	3477	737	5	0	365	5	0	36	33823	-798.60
18.2	7.0	298900	26380	380	4221	820	5	0	300	6	0	36	33823	-798.80
19.2	7.5	306350	9280	610	4022	880	5	0	490	4	0	56	33823	-799.00
20.2	6.7	289960	47980	430	5848	1101	5	0	200	5	3	39	33823	-799.20
21.2	10.1	256440	20990	630	3125	700	6	0	210	7	0	45	33823	-799.50
22.2	9.1	258800	42740	570	5033	961	6	2	180	7	0	42	33823	-799.80
335.0	11.1	202368	9414	747	13980	1731	6	0	106	5	0	12	33823	-801.29

Appendix III-Dolomite Matrix

Sample No.	IR %	Ca (ppm)	Mg (ppm)	Na (ppm)	Fe (ppm)	Mn (ppm)	Sr (ppm)	Zn (ppm)	Cu (ppm)	Ni (ppm)	Pb (ppm)	V (ppm)	Depth (m)	Well No.
2.0	0.0	236089	89819	1330	14526	1661	277	65	30				-806.50	34160
4.0	0.0	221875	123589	514	11089	1582	89	46	30	9	6	13	-807.20	34160
5.0	14.8	244565	142995	719	12476	1915	40	105	36	0	7	13	-808.40	34160
6.0	1.2	207500	117083	659	9042	1688	69	23	10	1	6	11	-809.40	34160
8.0	4.5	204185	117275	523	12457	1871	47	65	21	13	8	10	-810.61	34160
10.0	2.9	213242	119386	566	8835	1581	47	30	21	2	5	10	-811.50	34160
12.0	16.0	230238	131905	1142	10667	1756	65	36	24	3	6	9	-812.48	34160
13.0	0.4	220885	108745	416	11327	2044	68	82	10	1	8	6	-814.42	34160
14.0	0.0	210542	118775	402	9920	1561	55	15	10	1	5	4	-814.50	34160
15.0	0.0	219737	115789	470	14615	1964	67	133	30	7	5	6	-815.11	34160
16.0	5.3	203788	124242	791	13203	1772	60	42	32	47	10	15	-815.57	34160
20.0	0.0	207724	122866	609	13100	1748	56	30	41	7	8	9	-817.50	34160
21.0	75.3	132661	65323	7710	6452	875	133	262	121	46	42	21	-819.07	34160
22.0	0.0	216975	130967	938	9856	1582	45	74	31	5	7	5	-819.53	34160
24.0	0.0	208539	123765	751	13086	1725	45	51	31	7	5	6	-819.70	34160
25.0	0.0	210306	126735	745	12245	1737	45	102	71	10	7	7	-820.57	34160
29.0	7.6	207251	120887	713	9361	1585	48	74	43	5	8	4	-821.30	34160
32.0	2.0	218182	130372	574	12304	1927	57	51	31	6	6	4	-821.45	34160
36.0	4.5	212128	122234	733	13798	2644	339	48	32	6	6	5	-821.50	34160
37.0	0.8	219355	122077	588	11290	1942	89	40	30	10	8	8	-821.60	34160
40.0	0.0	175000	103469	512	12143	2190	56	22	20	11	7	10	-822.47	34160
42.0	0.0	126749	64198	1172	8282	1239	68	32	10	16	10	9	-823.38	34160
43.0	0.0	209462	123108	589	11753	1727	44	13	20	3	6	6	-824.53	34160
44.0	7.1	218376	126389	643	14861	2048	59	25	21	8	7	6	-825.03	34160
45.0	0.0	199900	117972	748	12520	1595	44	119	20	25	7	6	-825.95	34160
50.0	3.3	199038	103312	697	12895	1781	71	60	32	8	6	5	-826.54	34160
51.0	0.0	211454	121315	459	13665	1863	55	45	30	5	7	4	-827.24	34160
52.0	0.0	212090	122951	533	12900	1828	45	58	31	9	6	4	-827.75	34160
55.0	0.4	211983	118388	555	14576	2052	45	36	52	6	7	6	-828.27	34160
57.0	0.0	209173	118347	455	12994	1883	33	19	30	13	6	10	-828.90	34160
58.0	1.6	202273	125930	712	15527	1560	45	92	31	4	5	8	-829.24	34160
59.0	0.0	215081	124494	568	17945	2151	56	94	30	4	6	5	-829.45	34160
60.0	0.0	212100	125900	612	15930	1736	44	99	40	4	6	8	-830.33	34160
61.0	0.0	211345	122892	709	18012	2143	55	43	10	5	6	7	-831.29	34160
62.0	0.8	210494	136626	996	9239	1542	45	91	10	4	5	8	-831.50	34160
63.0	4.8	203243	117364	801	16360	1728	58	69	10	8	5	4	-832.07	34160
66.0	1.2	208300	121862	588	16002	1645	45	63	10	8	4	4	-833.13	34160
67.0	1.6	209062	121562	457	17010	1836	46	89	10	5	11	4	-833.92	34160
68.0	2.9	215441	127101	559	13225	1691	35	56	11	4	6	10	-834.09	34160

Appendix III-Dolomite Matrix

Sample No.	IR %	Ca (ppm)	Mg (ppm)	Na (ppm)	Fe (ppm)	Mn (ppm)	Sr (ppm)	Zn (ppm)	Cu (ppm)	Ni (ppm)	Pb (ppm)	V (ppm)	Depth (m)	Well No.
69.0	0.0	213008	118089	496	16809	2124	22	42	10	5	5	0	-834.32	34160
70.0	0.0	205321	126707	858	15994	1815	44	0	10	10	6	0	-835.52	34160
72.0	8.4	211623	115680	868	17511	1891	84	0	11	5	6	0	-836.00	34160
74.0	0.0	206855	122883	694	14476	1749	55	5	10	4	5	0	-836.92	34160
75.0	0.4	210671	121240	743	17378	1917	45	20	10	7	5	0	-837.43	34160
76.0	0.0	209248	130894	626	16728	1735	45	0	20	5	6	0	-839.10	34160
78.0	0.8	120427	63923	569	8892	1110	34	12	0	6	3	0	-840.42	34160
79.0	0.0	213066	124588	784	15957	1817	45	0	10	11	22	5	-841.02	34160
80.0	9.5	222045	123409	1506	17943	1869	112	0	23	30	17	6	-842.52	34160
81.0	5.6	220148	123734	1508	17679	2207	93	0	11	11	14	5	-842.54	34160
82.0	6.5	219869	122817	684	18057	1924	72	20	11	10	18	4	-843.07	34160
83.0	0.8	214300	122400	696	16950	1908	44	63	10	6	14	4	-843.67	34160
84.0	0.0	215139	124104	2328	16793	1911	44	37	30	14	11	4	-844.00	34160
86.0	11.6	217647	122398	895	16833	1798	37	15	11	13	17	10	-844.41	34160
88.0	7.3	212555	120374	2459	16806	1826	48	24	11	186	13	12	-845.54	34160
90.0	53.4	193103	104741	4597	15022	1560	95	84	43	50	34	27	-845.88	34160
91.0	4.8	217782	126151	732	16977	2041	46	27	10	8	18	13	-846.20	34160
92.0	10.4	213004	121413	1021	15818	1826	62	93	11	16	15	15	-846.81	34160
93.0	23.5	220968	122715	3032	15336	1759	89	78	27	19	21	15	-847.43	34160
94.0	21.8	211053	113684	2496	14276	1654	87	34	13	17	21	14	-847.63	34160
95.0	9.4	216216	123649	851	15101	1759	37	26	11	9	14	39	-847.96	34160
96.0	2.9	211555	122059	716	15231	1778	35	69	11	7	13	44	-848.36	34160
97.0	8.6	213839	122545	1057	16529	1892	49	48	11	8	11	13	-848.92	34160
98.0	6.4	218562	129614	807	16491	1893	59	23	11	11	14	7	-849.00	34160
99.0	2.8	214627	135062	1523	13786	1675	46	58	21				-851.00	34160
101.0	3.3	216702	130000	977	14585	1823	47	18	11	31	13	6	-851.39	34160
102.0	7.0	219889	132111	832	11200	1620	37	19	11	14	18	5	-852.05	34160
103.0	2.8	214271	125208	649	14906	1829	46	5	10	22	13	4	-852.66	34160
104.0	13.1	217824	121412	1277	13171	1517	102	14	35	17	49	21	-853.00	34160
105.0	8.7	221018	127765	1004	9923	1458	61	3	0	13	27	19	-853.50	34160
106.0	8.6	240175	104476	867	18177	2049	84	3	0	13	17	18	-853.97	34160
107.0	12.3	245622	102419	1141	12684	1660	51	1	0	7	12	17	-854.49	34160
108.0	5.4	226427	122727	830	13499	1604	58	0	0	8	28	16	-856.50	34160
110.0	7.3	213399	128105	1153	13813	1638	36	4	0	9	20	16	-857.23	34160
112.0	4.4	218998	125157	752	17432	1663	34	5	0	9	11	14	-858.02	34160
113.0	2.2	218841	128986	761	14990	1580	34	2	0	8	28	17	-859.42	34160
114.0	5.4	218697	126261	1204	12206	1521	46	3	0	10	28	14	-861.06	34160
115.0	4.0	215560	124585	957	15290	1544	46	1	0	7	24	16	-861.94	34160
116.0	13.7	213164	122748	1216	11328	1536	76	15	12	14	42	18	-864.00	34160

Appendix III-Dolomite Matrix

Sample No.	IR %	Ca (ppm)	Mg (ppm)	Na (ppm)	Fe (ppm)	Mn (ppm)	Sr (ppm)	Zn (ppm)	Cu (ppm)	Ni (ppm)	Pb (ppm)	V (ppm)	Depth (m)	Well No.
118.0	3.0	217828	129406	928	6301	1199	45	10	41	11	30	14	-864.98	34160
121.0	2.2	215871	127801	1045	13060	1584	46	9	10	11	33	6	-866.00	34160
122.0	6.0	224356	126717	905	17361	1692	35	14	11	7	17	7	-866.76	34160
123.0	7.1	213232	126030	926	16518	1730	36	5	11	10	10	7	-867.00	34160
124.0	7.6	216847	119222	1947	26242	2746	36	10	11	9	10	3	-867.62	34160
125.0	4.2	213075	125209	834	18933	1789	35	6	0	6	15	6	-868.10	34160
127.0	5.8	223611	132158	770	19444	1844	35	9	11	6	18	7	-798.69	34151
128.0	10.6	222494	120490	1106	21826	1957	49	7	11	7	19	4	-799.40	34151
129.0	22.0	228165	124935	1646	17829	1868	71	12	13	17	26	4	-800.38	34151
130.0	14.0	229720	116783	1613	23193	2874	64	7	12	16	15	9	-801.40	34151
131.0	11.5	218721	118151	1132	26370	2498	50	3	0	9	34	9	-802.40	34151
133.0	7.2	222737	123491	990	18103	1966	59	14	0	7	21	7	-803.43	34151
134.0	10.5	230000	128222	998	19111	1876	49	1	0	8	23	7	-804.40	34151
135.0	10.5	235360	130293	1042	19257	1669	37	8	0	10	36	20	-805.18	34151
137.0	3.7	220842	119474	957	24000	1752	58	4	0	7	16	15	-806.48	34151
139.0	9.2	220485	122137	1026	23899	1706	48	4	0	15	10	12	-807.12	34151
140.0	7.9	224835	112857	689	26374	2393	36	0	0	5	9	11	-807.40	34151
142.0	1.0	213434	114646	680	23737	1922	44	0	0	5	15	12	-808.50	34151
143.0	23.0	223568	117839	1470	25521	1848	100	8	0	10	8	12	-808.80	34151
145.0	10.5	223423	118356	963	24662	1885	74	5	0	9	12	14	-809.60	34151
146.0	13.5	220163	117599	1157	24476	2314	51	15	0	8	12	10	-810.55	34151
149.0	2.8	216632	119854	879	26819	2193	23	6	0	8	12	11	-810.62	34151
152.0	41.9	233103	100690	2245	24828	1990	133	10	0	21	12	9	-812.50	34151
154.0	17.4	220581	121550	1196	25424	1909	40	7	0	11	12	10	-812.90	34151
156.0	11.3	218679	117882	1165	24146	1862	50	6	0	8	14	11	-813.46	34151
157.0	12.2	229792	122864	972	25058	2062	38	16	0	7	12	19	-813.84	34151
158.0	6.4	222872	127128	799	25000	2298	23	1	0	9	15	16	-814.00	34151
162.0	15.1	241920	134660	1055	24473	2016	52	5	0	9	19	15	-814.65	34151
164.0	5.0	220084	125418	932	22803	1866	46	8	0	6	15	23	-818.00	34151
166.0	4.0	219710	129668	815	22407	1683	46	1	0	17	15	15	-818.98	34151
167.0	13.1	246674	142546	1057	26950	2042	38	0	0	6	20	15	-819.26	34151
168.0	3.8	219287	126939	763	24319	1901	35	0	0	7	18	18	-820.64	34151
169.0	8.2	222876	129194	821	24401	1764	36	0	0	5	33	14	-821.84	34151
170.0	6.4	224731	130000	712	23548	1705	35	0	0	6	13	13	-822.72	34151
172.0	4.0	216042	128646	1071	20417	1704	34	0	0	3	17	28	-823.65	34151
173.0	4.2	218803	126261	979	21954	1737	35	1	0	7	4	11	-824.10	34151
174.0	10.7	239977	137838	1041	24212	1922	37	9	0	4	5	14	-824.60	34151
175.0	17.8	255474	147810	922	28102	2124	67	0	0	3	4	16	-825.10	34151
176.0	15.9	249522	143780	867	26196	2035	39	0	0	2	3	17	-825.55	34151

Appendix III-Dolomite Matrix

Sample No.	IR %	Ca (ppm)	Mg (ppm)	Na (ppm)	Fe (ppm)	Mn (ppm)	Sr (ppm)	Zn (ppm)	Cu (ppm)	Ni (ppm)	Pb (ppm)	V (ppm)	Depth (m)	Well No.
177.0	14.2	244693	136085	863	26297	1942	65	7	0	4	9	16	-826.09	34151
178.0	19.0	258867	149631	1034	21798	1914	41	2	0	4	6	41	-826.64	34151
180.0	15.1	251540	140047	917	25474	2120	52	1	0	3	7	23	-827.22	34151
182.0	6.8	228448	129849	1165	25108	1847	36	23	0	3	3	19	-827.75	34151
183.0	15.7	251190	150595	792	21429	1776	52	10	0	2	5	21	-828.14	34151
185.0	19.9	271554	141103	825	29323	2380	69	4	0	5	3	17	-830.22	34151
187.0	9.1	236222	125111	760	25778	1953	49	3	0	2	4	19	-831.79	34151
191.0	16.1	265284	122986	820	25000	2985	52	6	0	4	4	18	-832.02	34151
192.0	9.4	236918	126829	790	25610	1991	49	25	0	2	4	11	-832.25	34151
193.0	7.2	223815	122845	705	24784	1790	47	3	0	3	4	9	-832.56	34151
194.0	17.5	236098	121707	1006	25244	1972	94	9	12	10	10	11	-833.06	34151
196.0	23.5	250260	138802	914	31771	2809	43	27	0	3	13	11	-833.27	34151
197.0	25.2	245418	137601	1244	28437	2036	59	15	0	4	20	16	-833.66	34151
198.0	12.8	241183	131671	729	26798	2097	64	0	0	2	4	9	-834.75	34151
200.0	14.7	245338	132867	1101	24825	2244	64	8	0	6	4	12	-835.48	34151
209.0	19.7	376667	19298	2801	7143	383	620	26	25	16	77	23	-766.80	33821
210.0	10.1	229663	108989	1571	20225	1535	198	20	11	8	42	15	-767.00	33821
211.0	2.8	217967	119713	938	18789	1729	34	22	10	10	29	14	-767.86	33821
212.0	11.7	225973	125286	1141	18535	1839	38	25	11	7	27	12	-768.00	33821
213.0	7.8	222126	121367	1704	15184	1372	36	33	11	12	29	15	-769.00	33821
214.0	6.9	218872	118221	1168	20390	2004	48	23	11	15	25	16	-770.00	33821
215.0	8.6	222817	120852	905	19214	1869	36	19	11	13	30	15	-771.00	33821
218.0	15.0	230357	120833	1114	19286	1585	39	42	12	16	23	19	-777.68	33821
220.0	4.8	218058	116701	951	15240	1751	57	5	21	5	26	14	-782.00	33821
221.0	2.4	202245	116122	1369	15510	1610	34	12	10	16	23	10	-783.21	33821
222.0	3.6	205579	112603	1083	24483	2530	34	6	10	5	23	14	-787.04	33821
223.0	17.1	221799	77218	1591	19065	2640	53	2	12	24	38	14	-788.29	33821
225.0	4.3	212500	123199	1760	24153	2265	35	10	11	11	19	15	-790.05	33821
226.0	17.7	268382	117525	630	18382	2018	81	5	12	11	19	18	-793.92	33821
227.0	15.7	298246	140431	1024	22249	2380	39	4	12	7	24	19	-794.49	33821
228.0	14.6	341706	29439	963	3621	556	321	0	12	14	11	20	-799.00	33821
231.0	16.6	229327	131490	661	16947	1752	79	0	12	11	18	19	-802.00	33821
248.0	16.5	230723	120602	1860	16506	1869	80	0	12	12	36	19	-814.00	33821
249.0	8.6	221351	126580	858	16667	1403	48	11	11	6	16	15	-815.97	33821
250.0	13.1	237239	130742	977	22042	2295	38	9	0	9	17	17	-816.00	33821
251.0	15.2	319499	16667	1459	3073	427	390	12	12	21	38	15	-818.00	33821
254.0	5.5	221154	122436	926	17415	1483	59	15	0	7	17	15	-820.00	33821
255.0	13.8	237935	135615	776	22158	2041	38	6	0	11	22	15	-863.16	33821
262.0	14.9	230491	131659	671	25000	2254	39	2	12	7	22	13	-863.54	33821

Appendix III-Dolomite Matrix

Sample No.	IR %	Ca (ppm)	Mg (ppm)	Na (ppm)	Fe (ppm)	Mn (ppm)	Sr (ppm)	Zn (ppm)	Cu (ppm)	Ni (ppm)	Pb (ppm)	V (ppm)	Depth (m)	Well No.
266.0	12.9	235764	132060	814	24306	2029	38	6	12	17	21	13	-864.57	33821
267.0	12.8	244186	135698	729	25000	2259	38	1	0	6	24	14	-865.55	33821
268.0	11.4	220429	121558	2126	16479	1877	2644	12	11	8	22	14	-866.90	33821
270.0	15.4	233493	127512	1151	20933	1989	53	8	12	8	11	13	-867.39	33821
271.0	19.2	255693	148515	839	16460	1777	54	6	25	19	15	15	-868.00	33821
272.0	19.4	238308	139055	1900	13930	1536	41	11	12	12	15	20	-869.00	33821
273.0	14.5	242925	129835	856	18042	2574	39	8	12	22	12	14	-870.00	33821
274.0	13.1	228538	127494	966	18329	1896	38	5	12	6	14	12	-871.95	33821
275.0	17.6	247304	139338	1249	21569	2263	40	7	12	7	15	15	-873.35	33821
276.0	19.0	268123	145668	900	20297	2120	41	2	12	5	21	14	-874.10	33821
277.0	19.0	253580	144815	1133	20247	2130	41	5	12	13	15	16	-875.23	33821
278.0	20.8	259949	145791	1033	20663	1950	28	4	13	12	13	16	-876.60	33821
279.0	21.3	259794	149613	888	22552	2228	43	3	13	7	17	22	-877.60	33821
280.0	17.7	247337	131961	828	19613	2229	40	0	12	29	19	21	-940.09	33821
281.0	14.9	232009	130958	737	22430	2023	51	6	23	30	17	18	-941.95	33821
282.0	19.1	250246	144472	830	16339	1596	27	6	12	8	15	40	-946.73	33821
286.0	16.9	242086	144005	981	12830	1278	26	10	12	21	19	16	-947.19	33821
287.0	17.3	242048	149880	1171	17470	1643	27	7	12	6	17	15	-947.88	33821
288.0	17.7	227206	133578	2702	23039	2674	40	15	12	20	13	15	-947.94	33821
289.0	16.4	225359	133134	1998	19139	1837	66	12	12	10	15	12	-949.14	33821
290.0	18.9	242556	140199	1268	24442	2419	41	10	12	13	16	20	-950.58	33821
292.0	19.6	252985	143781	1057	22015	2147	55	9	12	16	24	22	-951.70	33821
293.0	19.3	221945	130424	1266	24065	2335	41	9	12	7	27	22	-952.40	33821
294.0	15.1	268444	129858	719	23341	2135	52	11	12	25	15	19	-952.78	33821
295.0	15.0	227765	127529	1104	22118	2061	52	11	12	14	12	19	-953.94	33821
297.0	10.3	213901	114686	591	26794	2471	49	7	0	3	5	13	-954.41	33821
298.0	6.7	210304	116594	678	22668	2036	48	3	0	2	10	14	-954.89	33821
300.0	11.8	226131	125113	743	20362	1887	37	6	0	4	9	12	-955.80	33821
301.0	8.0	213786	118928	824	21335	1993	24	7	0	17	10	12	-955.80	33821
331.0	6.2	210385	116381	662	21627	1954	35	10	0	8	6	10	-797.50	33823
332.0	8.6	216484	125604	731	22088	1975	36	12	0	4	4	11	-797.98	33823
340.0	8.4	216667	117215	951	21272	1870	60	14	11	14	8	8	-814.00	33823
341.0	7.3	222876	113508	914	21133	2070	72	12	0	7	5	14	-818.56	33823
342.0	21.3	244388	118878	597	24617	2602	42	15	0	8	7	16	-818.84	33823
343.0	12.8	194954	98394	1766	19725	1851	76	5	11	10	25	11	-820.20	33823
344.0	2.0	209711	105785	1279	26963	2567	46	49	42	9	23	38	-820.26	33823
345.0	14.5	211422	108042	1526	20862	2334	64	2	12	14	11	8	-820.38	33823
346.0	15.5	220881	95704	1153	19690	2395	79	4	0	12	8	6	-822.00	33823

Appendix III-Dolomite Matrix

Sample No.	IR %	Ca (ppm)	Mg (ppm)	Na (ppm)	Fe (ppm)	Mn (ppm)	Sr (ppm)	Zn (ppm)	Cu (ppm)	Ni (ppm)	Pb (ppm)	V (ppm)	Depth (m)	Well No.
1.1	6.1	220170	93230	880	22228	1710	475	11	3	4	11	17	-766.72	33821
2.1	4.9	212350	113790	425	20443	2062	60	4	5	3	18	18	-772.50	33821
3.1	5.8	208060	115800	450	20501	1820	65	2	11	5	3	19	-773.50	33821
4.1	9.5	213330	116820	615	17641	1674	65	5	6	6	0	20	-775.00	33821
5.1	5.9	210160	117240	440	17945	1838	65	5	5	4	3	17	-775.20	33821
6.1	6.4	211930	112770	480	21490	2046	90	8	5	8	0	17	-775.50	33821
7.1	5.4	209800	110470	385	25450	2121	70	10	11	8	5	19	-776.15	33821
8.1	3.9	207970	113100	360	27529	2031	85	0	10	4	0	18	-776.50	33821
9.1	6.8	210320	115540	570	20753	1965	185	6	11	4	8	17	-777.00	33821
10.1	2.8	200770	117990	415	24433	2028	60	2	10	4	14	17	-777.20	33821
11.1	9.1	206330	113670	560	26707	2222	100	3	6	5	12	18	-777.40	33821
12.1	7.2	211790	109290	750	24973	1973	90	0	5	5	0	17	-777.60	33821
13.1	7.1	243970	117070	460	21490	1860	60	0	5	5	0	17	-778.00	33821
14.1	2.7	267050	122280	420	17250	1588	40	0	5	4	7	15	-779.50	33821
15.1	9.8	239530	119530	775	15329	1395	70	0	6	6	0	19	-780.00	33821
16.1	5.4	233550	119570	505	19015	2002	55	0	11	5	0	17	-780.20	33821
17.1	5.3	197000	116300	530	24605	2519	60	2	5	5	0	18	-780.50	33821
18.1	4.5	195370	113550	510	22158	2153	60	5	16	5	0	15	-780.80	33821
19.1	2.5	203090	117060	430	19175	1932	55	7	5	5	0	15	-781.00	33821
20.1	7.6	231030	104910	1130	15173	2016	90	5	11	8	13	18	-781.50	33821
21.1	3.1	174350	98575	520	22355	2367	50	7	10	6	0	14	-783.00	33821
22.1	4.5	179800	101290	495	13880	1481	45	11	11	5	7	12	-783.50	33821
23.1	9.9	180040	97200	450	16127	1657	50	11	11	6	6	24	-784.00	33821
24.1	5.9	191900	101690	580	13723	1428	55	11	11	9	5	21	-784.20	33821
25.1	7.3	190150	102920	660	14455	1380	55	11	11	12	6	21	-784.40	33821
26.1	8.9	212000	107270	2115	17219	1692	125	11	11	13	6	21	-784.60	33821
27.1	6.5	184170	97680	935	21098	2585	80	11	11	9	6	22	-784.80	33821
28.1	8.4	188320	103970	640	16830	1542	70	11	11	9	2	21	-785.00	33821
29.1	6.2	172650	106330	460	17591	1698	55	5	5	8	4	18	-785.20	33821
30.1	6.0	182320	105640	405	19071	1861	50	5	5	9	4	17	-785.40	33821
31.1	8.8	170940	93050	470	17215	1732	65	5	5	14	3	18	-785.70	33821
32.1	6.0	173370	94260	510	15118	1631	55	5	5	8	3	18	-785.80	33821
33.1	4.3	169190	91350	400	17730	1672	50	5	5	8	4	17	-786.00	33821
34.1	6.6	162450	92920	510	17403	1584	50	5	5	9	1	18	-786.20	33821
35.1	6.9	262680	139420	710	17417	1638	75	5	5	7	4	26	-786.40	33821
36.1	4.6	163020	90995	335	18691	1718	35	5	5	5	3	15	-786.60	33821
37.1	6.2	169430	91490	415	22045	1970	55	5	5	5	3	19	-786.80	33821
38.1	4.3	164540	91610	390	22618	1987	50	10	10	5	4	16	-787.00	33821
39.1	4.8	163110	89225	470	22603	2067	60	0	5	6	0	16	-787.20	33821

Appendix III-Dolomite Matrix

Sample No.	IR %	Ca (ppm)	Mg (ppm)	Na (ppm)	Fe (ppm)	Mn (ppm)	Sr (ppm)	Zn (ppm)	Cu (ppm)	Ni (ppm)	Pb (ppm)	V (ppm)	Depth (m)	Well No.
40.1	6.4	175780	88100	530	29100	2780	45	2	11	7	17	17	-787.40	33821
41.1	3.1	170970	90515	435	18576	1663	40	0	5	4	7	17	-787.60	33821
42.1	9.4	180590	94205	700	13651	1529	70	16	17	4	53	19	-787.80	33821
43.1	4.2	175470	89170	460	21271	2800	50	15	5	4	38	18	-788.00	33821
44.1	5.4	196410	73540	445	22346	3592	65	26	11	7	39	15	-788.20	33821
45.1	24.1	180040	93890	570	18134	2302	60	19	7	9	56	21	-788.40	33821
46.1	12.3	190150	96310	660	17102	2115	70	15	11	5	50	17	-788.60	33821
47.1	7.9	286120	42480	860	5889	1051	145	15	11	5	35	26	-788.80	33821
48.1	5.6	177280	89065	570	16508	2042	50	15	11	5	43	16	-789.50	33821
49.1	5.6	203440	99640	1160	12473	1680	70	17	5	6	40	19	-790.70	33821
50.1	3.3	183440	100870	625	12422	1457	35	13	10	5	45	16	-792.00	33821
51.1	11.4	192570	101760	1080	19444	2808	85	18	11	5	54	19	-792.50	33821
52.1	16.8	239370	80860	710	17331	2543	100	2	12	6	52	21	-793.00	33821
53.1	3.8	187130	101470	500	15240	1772	45	0	5	7	38	15	-793.50	33821
54.1	11.0	223560	92035	750	13149	1834	110	0	6	5	9	24	-794.00	33821
55.1	10.5	232360	82875	720	14788	2395	100	0	6	5	7	23	-795.20	33821
56.1	15.9	226470	89000	790	15462	2323	120	5	12	5	13	22	-797.50	33821
58.1	7.8	201560	99415	615	13946	1726	80	0	11	5	5	19	-804.30	33821
59.1	10.0	202980	92195	810	20278	2979	70	0	6	4	0	20	-815.20	33821
1.2	9.6	218670	97490	450	19633	1814	175	0	11	8	6	22	-766.20	33823
2.2	5.0	190520	97760	280	19630	2086	50	2	5	5	14	20	-771.50	33823
3.2	3.8	186090	101930	380	17827	1790	40	6	10	6	8	19	-774.15	33823
4.2	6.6	195690	98260	410	19429	2205	60	0	5	5	33	21	-779.80	33823
5.2	5.9	194190	104060	395	17252	1998	50	0	5	0	35	18	-784.00	33823
6.2	12.5	227630	105550	480	19954	1975	90	0	6	6	19	23	-785.20	33823
7.2	17.4	207640	108300	650	18750	1921	70	0	6	9	32	27	-786.00	33823
8.2	6.6	227900	62385	365	13538	3020	115	0	11	5	34	29	-786.20	33823
9.2	3.9	188300	105610	470	14823	1703	50	0	5	4	11	19	-786.50	33823
10.2	12.8	191630	105840	410	1611	522	50	0	6	5	0	40	-786.80	33823
11.2	6.9	195700	86685	520	17903	1834	55	0	5	5	17	22	-787.00	33823
12.2	12.3	202740	105700	380	19129	1942	50	0	17	5	7	22	-787.20	33823
13.2	8.4	239150	62600	460	18326	1933	170	0	11	7	10	24	-787.50	33823
14.2	4.1	229510	104570	440	19727	1950	170	0	5	4	5	18	-787.80	33823
23.2	8.6	198430	97760	440	18559	1928	70	2	5	5	7	26	-800.50	33823
24.2	16.6	209440	94030	640	12185	1731	75	2	6	8	21	30	-802.00	33823
25.2	9.0	186440	106000	360	14136	1846	50	6	6	5	0	25	-803.00	33823
26.2	9.5	177250	109300	585	12376	1765	50	0	6	5	0	29	-804.00	33823
27.2	9.5	200950	99690	555	11865	1711	40	2	6	8	0	29	-804.20	33823
28.2	6.3	208470	104190	665	12594	1744	80	0	5	4	23	29	-804.50	33823

Appendix III-Dolomite Matrix

Sample No.	IR %	Ca (ppm)	Mg (ppm)	Na (ppm)	Fe (ppm)	Mn (ppm)	Sr (ppm)	Zn (ppm)	Cu (ppm)	Ni (ppm)	Pb (ppm)	V (ppm)	Depth (m)	Well No.
29.2	11.5	203600	109330	830	12713	1714	90	3	6	2	14	25	-804.80	33823
30.2	18.5	194210	97260	540	27703	3252	60	0	6	5	0	33	-805.00	33823
31.2	24.4	206580	102220	1370	15180	1911	140	2	7	10	32	41	-805.20	33823
32.2	8.1	199940	102160	745	10521	1653	70	0	5	2	13	21	-805.60	33823
33.2	19.2	203170	110600	935	12313	1689	70	2	6	6	0	34	-805.80	33823
34.2	17.8	214610	105020	1080	13808	1797	110	0	6	13	40	32	-806.00	33823
35.2	15.3	207910	106480	775	12323	1681	60	0	6	5	0	20	-806.20	33823
36.2	15.5	206280	91805	690	17933	2031	100	0	6	4	9	23	-806.50	33823
37.2	18.0	203970	105840	640	19693	2014	120	0	6	6	8	27	-806.80	33823
38.2	14.6	206810	109060	530	18331	1928	95	0	6	6	0	28	-807.00	33823
39.2	8.3	192710	91725	390	26936	2426	80	0	5	3	13	17	-807.50	33823
40.2	19.7	223590	106750	330	15816	1837	125	0	6	3	3	19	-808.00	33823
41.2	9.2	211110	86525	410	17731	2088	80	0	6	5	0	22	-809.50	33823
42.2	9.9	223870	95170	330	14111	2057	155	0	6	4	0	21	-810.40	33823
43.2	6.1	210450	71480	360	16077	1918	65	0	5	3	6	19	-812.00	33823
44.2	8.4	208520	118370	570	18880	2007	85	2	5	5	0	19	-812.50	33823
45.2	7.5	206700	103710	420	20022	2512	100	0	5	6	0	20	-813.00	33823
46.2	10.5	224640	103370	890	18339	2118	115	0	6	5	0	23	-813.50	33823
340.0	19.4	233750	96395	940	19092	2117	125	0	0	9	27	30	-814.00	33823
48.2	10.8	213280	107390	595	20773	2152	65	0	6	5	8	19	-814.50	33823
49.2	4.8	212230	102570	485	19641	2235	70	0	5	5	0	18	-815.00	33823
50.2	5.8	211190	113870	560	19893	1876	60	22	11	5	23	17	-815.50	33823
51.2	31.2	214940	103180	690	27293	2575	55	20	7	8	6	23	-816.00	33823
52.2	11.4	202460	105890	660	23874	2180	85	17	6	8	1	21	-816.50	33823
53.2	6.1	165110	112500	1035	21921	1988	40	15	5	6	1	18	-817.00	33823
54.2	14.1	218010	96445	860	15986	1725	80	18	6	6	1	28	-817.50	33823
55.2	71.0	178120	107170	6180	16034	1755	65	55	17	59	1	47	-818.00	33823
56.2	6.4	213590	78290	440	19388	1827	70	18	5	7	1	21	-818.50	33823
330.0	10.3	226906	111771	1066	20628	2031	22	56	1	8	27	14	-796.00	33823
331.0	6.2	210385	116381	662	21627	1954	32	10	1	8	6	10	-797.50	33823
332.0	8.6	216484	125604	731	22088	1975	33	12	1	4	4	11	-797.98	33823
47.2	8.4	216667	117215	951	21272	1870	11	14	55	14	8	8	-814.00	33823
341.0	7.3	222876	113508	914	21133	2070	65	12	1	7	5	14	-818.56	33823
342.0	21.3	244388	118878	597	24617	2602	38	15	1	8	7	16	-818.84	33823
343.0	12.8	194954	98394	1766	19725	1851	69	5	11	10	25	11	-820.20	33823
344.0	2.0	209711	105785	1279	26963	2567	42	49	42	9	23	38	-820.26	33823
345.0	14.5	211422	108042	1526	20862	2334	58	2	12	14	11	8	-820.38	33823
346.0	15.5	220881	95704	1153	19690	2395	72	4	0	12	8	6	-822.00	33823
307.0	10.0	227232	118527	843	20424	2113	786	4	0	4	31	60	-766.00	33823

Appendix III-Dolomite Matrix

Sample No.	IR %	Ca (ppm)	Mg (ppm)	Na (ppm)	Fe (ppm)	Mn (ppm)	Sr (ppm)	Zn (ppm)	Cu (ppm)	Ni (ppm)	Pb (ppm)	V (ppm)	Depth (m)	Well No.
308.0	7.0	223283	123391	732	15129	1812	71	2	0	4	28	28	-767.00	33823
309.0	9.4	219341	119121	1071	18681	2109	60	8	11	7	31	31	-769.00	33823
310.0	12.2	237727	116818	851	19205	2207	50	3	0	9	62	27	-770.77	33823
312.0	7.1	218547	115618	698	18113	2115	48	4	0	6	47	25	-771.50	33823
314.0	8.0	214642	109978	614	20174	2670	48	21	0	7	46	27	-772.70	33823
316.0	12.4	214064	110333	935	16303	2343	76	15	11	7	50	38	-775.50	33823
317.0	7.7	208000	110703	663	14919	2051	54	0	5	5	44	36	-777.50	33823
322.0	12.3	211970	119702	784	14548	1888	50	2	6	8	74	35	-782.00	33823
324.0	21.7	213712	113265	1160	16008	1977	70	10	6	14	93	40	-790.00	33823
325.0	6.2	210352	121451	749	13661	1886	47	3	5	5	74	38	-791.50	33823
328.0	16.3	214456	118280	911	15591	1961	53	3	6	7	79	45	-793.00	33823
329.0	4.2	210377	106289	423	16667	2123	52	6	5	6	54	37	-794.50	33823

Appendix III-Brachiopods

	Sample No.	IR %	Ca (ppm)	Mg (ppm)	Na (ppm)	Fe (ppm)	Mn (ppm)	Sr (ppm)	Ni (ppm)	V (ppm)	Locality
1	1	0	342105	926	1780	1095	277	822	12	22	33821
2	2	3	326882	559	1919	925	206	722	13	14	33821
3	3	0	336508	1127	2849	1238	322	594	10	11	33821
4	240	10	287640	4865	2803	4404	798	618	8	28	33821

Appendix III-Saddle Dolomite

Sample No.	IR %	Ca (ppm)	Mg (ppm)	Na (ppm)	Fe (ppm)	Mn (ppm)	Sr (ppm)	Zn (ppm)	Cu (ppm)	Ni (ppm)	Pb (ppm)	V (ppm)	Well No.	Depth (m)
7.0	2.42	214301	110744	468	20661	1934	114	6	11	11	5	40	34160	-810.59
15.0	1.99	210041	114097	546	22110	2041	45	4	0	6	6	10	34160	-815.11
17.0	6.37	223830	122660	527	23085	2117	35	4	0	17	22	11	34160	-816.36
18.0	3.01	223140	117149	404	16477	2076	51	4	15	3	99	8	34160	-816.39
19.0	2.22	215361	115567	211	15670	1990	34	2	5	9	66	10	34160	-816.43
23.1	2.53	227622	96677	290	14486	2191	40	1	5	2	50	10	34160	-819.20
23.2	2.50	214990	114887	478	15708	2027	51	1	5	2	63	12	34160	-819.50
27.0	2.50	223081	111873	324	14688	2012	34	1	5	2	35	9	34160	-819.86
30.0	2.81	241477	102583	356	14928	2736	159	6	5	2	26	13	34160	-821.28
35.0	2.69	221926	115676	273	13883	2546	45	3	5	2	36	12	34160	-821.43
39.0	2.90	302778	38580	403	7202	2582	192	2	10	3	0	14	34160	-821.59
48.0	2.80	256790	101029	539	17593	2520	79	17	10	5	28	20	34160	-825.41
50.0	3.11	222492	115512	277	16339	2125	40	7	10	5	373	11	34160	-825.95
53.0	2.92	209793	111813	381	17979	2402	46	10	10	3	216	16	34160	-827.28
54.0	5.13	209269	113136	543	16684	2239	35	5	5	3	88	12	34160	-827.72
56.0	2.71	208496	115448	508	16993	2300	34	12	5	3	26	5	34160	-827.77
59.0	2.45	217782	116945	467	20606	2355	35	14	11	3	32	22	34160	-829.24
61.0	4.20	218040	121794	321	15693	2143	34	4	5	2	50	6	34160	-830.33
67.0	2.31	222867	112127	311	14748	2010	57	5	5	2	23	8	34160	-833.13
77.0	2.30	213804	110941	407	16207	2120	34	6	5	2	25	6	34160	-838.50
78.0	4.22	218816	116352	433	16824	2225	58	4	5	2	28	10	34160	-839.10
80.0	2.61	215825	109381	381	17320	2203	40	4	5	3	32	7	34160	-841.02
81.0	5.73	224467	111407	396	16045	2247	35	8	11	2	21	9	34610	-842.52
85.0	5.02	220697	116790	329	15523	2118	52	2	5	2	34	8	34160	-843.67
91.0	2.52	212436	111042	299	14757	2004	45	2	0	3	22	10	34610	-845.88
123.0	6.87	228850	119957	538	18438	2416	36	4	0	5	2	13	34160	-866.76
126.0	4.20	217518	98540	428	26017	2547	218	4	5	4	23	15	34151	-798.69
132.0	3.64	235399	107143	436	19643	2655	69	11	11	4	101	26	34151	-803.48
138.0	3.32	206601	114657	449	18399	1934	51	5	5	3	353	10	34151	-807.14
141.0	6.30	205283	113127	370	17930	2042	41	537	0	3	31	9	34151	-808.70
142.0	9.04	233223	121634	944	21965	2008	49	8	11	3	204	12	34151	-808.80
143.0	3.81	205208	111042	478	17812	1889	46	18	0	2	27	9	34151	-809.60
144.0	3.72	214577	111494	437	19436	2157	40	7	5	4	113	10	34151	-810.48
147.0	3.52	203906	113854	566	20104	2479	46	4	10	2	29	9	34151	-811.73
151.0	3.25	221488	114046	845	23585	2398	35	9	10	4	51	7	34151	-812.88
155.0	2.71	203254	116116	564	15857	1867	40	6	5	8	17	9	34151	-813.75
161.0	4.69	203246	113403	555	18743	2218	40	6	5	2	49	9	34151	-817.96
164.0	3.21	198446	116477	486	17668	2074	28	6	5	2	77	8	34151	-818.98
184.0	2.81	201858	113106	535	22549	2385	34	16	5	3	14	8	34151	-830.26

Appendix III-Saddle Dolomite

Sample No.	IR %	Ca (ppm)	Mg (ppm)	Na (ppm)	Fe (ppm)	Mn (ppm)	Sr (ppm)	Zn (ppm)	Cu (ppm)	Ni (ppm)	Pb (ppm)	V (ppm)	Well No.	Depth (m)
186.0	2.81	205882	111558	488	19659	2800	57	2	5	3	16	7	34151	-831.80
189.0	5.04	241083	100425	641	18896	3056	58	105	0	3	0	5	34151	-832.24
192.0	5.81	210426	111489	434	20479	2440	47	5	5	4	71	7	34151	-832.56
193.0	2.81	218698	105372	340	18388	2393	45	11	5	3	0	6	34151	-833.06
194.0	3.63	207374	111715	534	20031	2401	46	17	10	3	14	5	34151	-833.27
195.0	4.41	213574	110377	438	19235	2512	40	18	10	2	2	6	34151	-833.31
198.0	4.11	209561	112853	379	18130	2259	40	2	5	2	49	5	34151	-835.48
266.0	4.41	228040	97170	436	15461	3053	329	4	5	4	2	6	33821	-863.54
267.0	9.84	233408	126949	736	22829	2587	416	6	0	2	0	6	33821	-864.57
269.0	2.03	223755	114315	438	18776	2400	57	60	11	3	57	37	33821	-866.05
291.0	6.67	239881	119345	372	21428	2991	33	88	0	3	12	26	33821	-950.46
294.0	15.35	258353	129594	766	25776	4021	39	18	12	169	11	20	33821	-952.40
296.1	5.20	204747	116667	666	17827	2305	29	5	21	5	38	15	33821	-952.80
296.2	4.31	203874	117487	538	18586	2542	35	5	5	4	35	15	33821	-952.80
297.0	3.70	209407	106653	582	15489	2567	63	5	10	4	34	13	33821	-953.94
299.1	5.11	207173	114873	504	17511	2909	46	8	47	7	34	14	33821	-954.72
299.2	3.41	207269	116719	492	15628	2259	29	4	5	11	48	14	33821	-954.72
302.0	4.44	230696	111814	1236	20992	2847	35	7	0	8	36	23	33821	-957.36
307.0	4.22	210377	106289	423	16667	2123	47	6	5	6	54	37	33823	-766.01
312.0	3.00	118023	113491	295	24871	2207	77	0	5	4	92	9	33823	-771.50
313.0	9.68	123996	126339	587	26562	2454	45	0	0	5	27	13	33823	-771.60
314.0	4.83	118922	115433	590	23679	2353	32	0	11	3	124	10	33823	-772.70
315.0	4.30	120010	114211	609	24556	2406	42	0	5	4	217	9	33823	-774.15
318.0	4.19	125573	101562	794	20208	1914	161	0	5	3	184	16	33823	-777.83
320.0	6.99	122288	112675	544	23792	2525	48	0	5	4	248	11	33823	-778.00
339.0	2.81	110062	128793	588	23633	2497	36	0	5	5	33	12	33823	-813.65
344.1	11.74	162844	89449	367	19725	2322	38	0	0	19	0	6	33823	-820.26
344.2	14.57	161137	93483	441	19668	2305	35	0	12	3	0	7	33823	-820.26
348.0	4.51	110084	125630	683	26943	3001	37	9	16	5	21	11	33823	-823.35

Appendix III-Calcite Cement

Sample No.	IR %	Ca (ppm)	Mg (ppm)	Na (ppm)	Fe (ppm)	Mn (ppm)	Cu (ppm)	Zn (ppm)	Sr (ppm)	Ni (ppm)	Pb (ppm)	V (ppm)	Well No.	Depth (m)
7.0	2.4	362033	208	558	1763	3122	11	0	125	10	0	29	34160	-810.59
19.1	9.6	390000	222	541	1889	3779	11	7	98	10	0	43	34160	-816.43
19.2	0.0	346154	769	936	2692	3461	19	6	85	19	0	29	34160	-816.43
23.0	1.4	167850	507	325	1623	2789	5	2	45	6	0	6	34160	-819.20
31.0	4.8	340671	524	279	2935	6237	5	0	115	3	0	15	34160	-821.25
33.0	3.1	318135	2124	370	5078	4974	10	0	319	4	0	16	34160	-821.40
34.0	3.6	331946	937	430	3278	5879	5	0	114	4	0	13	34160	-821.42
38.0	3.9	347962	209	294	2090	5590	5	0	425	7	0	15	34160	-821.57
48.0	4.3	336134	840	486	2311	3782	5	0	116	6	0	10	34160	-825.41
50.0	9.2	367550	166	365	2704	7230	6	0	134	6	0	10	34160	-825.95
52.0	2.9	379400	104	662	1501	4814	5	0	97	5	0	8	34160	-827.26
56.0	3.7	345026	366	440	2984	6963	10	0	98	5	0	10	34160	-827.77
59.0	2.0	338477	412	554	2469	5247	11	5	113	13	0	21	34160	-829.24
61.0	3.8	342767	524	499	2830	6394	0	0	150	6	0	14	34160	-830.33
67.0	3.2	343168	606	258	2702	4296	5	0	148	5	0	9	34160	-833.13
80.0	4.2	342932	576	313	2880	4817	5	0	92	9	0	9	34160	-841.02
81.0	3.6	350312	520	320	2027	2755	5	0	69	4	0	19	34160	-842.52
86.0	6.0	357602	214	431	1820	2998	11	0	82	5	0	19	34160	-844.00
89.0	1.6	346708	206	253	1954	3601	11	0	113	9	0	43	34160	-845.09
91.0	2.7	344296	462	247	1901	2312	5	0	102	4	0	18	34160	-845.88
123.0	2.5	345679	514	392	1800	2263	5	0	68	4	0	18	34160	-866.76
132.0	2.6	321281	1860	432	5062	5165	21	0	91	4	0	21	34151	-803.48
142.0	3.2	345361	619	373	3196	6392	10	0	79	6	0	21	34151	-808.80
143.1	3.5	325750	362	240	2689	5843	10	14	97	4	0	18	34151	-809.60
143.2	2.8	331109	154	334	2105	5185	21	0	119	3	0	20	34151	-809.60
144.0	3.3	339730	207	203	2178	5135	10	0	103	3	0	16	34151	-810.48
151.1	2.1	327021	154	363	2610	7216	10	0	118	5	0	19	34151	-812.88
151.2	2.8	316305	464	412	2735	6760	10	0	102	3	0	18	34151	-812.88
153.0	3.1	327657	774	301	4334	7585	5	0	131	3	6	18	34151	-813.23
159.0	3.3	319731	620	316	3977	8264	10	0	119	3	0	16	34151	-815.02
160.1	3.6	310166	1556	305	5135	6846	5	0	103	3	0	15	34151	-817.86
160.2	2.9	322831	878	342	3977	7645	10	3	108	3	0	15	34151	-817.86
163.0	3.3	323529	1135	474	3509	6914	10	0	125	3	56	18	34151	-818.98
165.0	5.1	344013	105	726	840	3099	5	4	69	3	0	18	34151	-819.13
181.0	4.0	326743	1197	494	2706	3226	5	0	63	4	0	15	34151	-828.13
190.0	3.3	344720	155	281	2795	7143	10	0	91	4	0	19	34151	-832.24
191.0	5.3	406652	150	307	2425	7081	21	51	118	7	0	41	34151	-832.24
192.0	1.4	365717	239	133	2584	5951	10	4	106	3	0	19	34151	-832.56
193.0	1.2	371574	208	226	2492	5736	5	0	106	3	0	15	34151	-833.06

Appendix III-Calcite Cement

Sample No.	IR %	Ca (ppm)	Mg (ppm)	Na (ppm)	Fe (ppm)	Mn (ppm)	Cu (ppm)	Zn (ppm)	Sr (ppm)	Ni (ppm)	Pb (ppm)	V (ppm)	Well No.	Depth (m)
195.1	2.1	380123	379	144	3509	6609	10	3	118	4	0	18	34151	-833.31
195.2	1.3	381606	163	246	3008	6758	10	0	148	17	0	17	34151	-833.31
219.0	3.0	372671	238	147	2624	4814	10	4	148	5	0	18	33821	-780.08
226.0	1.5	375510	811	306	2474	1122	5	0	174	3	0	17	33821	-793.92
262.1	0.4	384381	274	270	2546	7404	10	2	89	6	0	18	33821	-863.16
262.2	1.8	386850	229	249	2207	6116	10	0	84	4	0	18	33821	-863.16
267.0	6.4	420601	65	1170	1020	3970	11	2	1311	11	0	37	33821	-864.57
269.1	2.2	361570	1178	642	3233	2789	21	4	148	4	0	20	33821	-866.05
269.2	3.6	339027	797	224	3307	5849	10	3	575	4	0	24	33821	-866.05
291.0	0.8	279472	6494	519	12256	3354	20	3	101	5	0	24	33821	-950.46
294.0	0.0	343117	2520	1182	6184	3745	10	10	66	8	0	51	33821	-952.40
301.0	8.9	385965	948	537	4391	7950	11	0	145	4	0	19	33821	-955.80
302.0	1.9	377919	902	1765	1645	1699	21	0	82	4	0	21	33821	-957.36
314.0	6.5	375403	682	172	3534	5263	16	0	100	4	70	19	33823	-772.70
315.0	1.9	380224	173	265	2426	4842	10	0	95	4	0	16	33823	-774.15
319.0	1.8	375764	463	185	3091	5193	10	0	78	3	3	17	33823	-777.94
323.0	5.6	388653	127	251	2089	5885	11	3	117	2	0	19	33823	-785.02
347.0	1.6	226434	9314	545	15143	2459	10	13	34	12	0	16	33823	-822.07

Appendix IIIb: Precision and Accuracy Determination

Precision of the analytical method for the determination of the trace elements for the rock matrix and cements was controlled by running duplicates within separate batches to maintain precision of the analysis from batch to batch. A compilation of the trace element concentrations for each duplicate with the respective original carbonate species is presented within Appendix IIIb. The relative precision of the analysis is described within the methodology portion where the calculated precision for each element is given.

The relative accuracy of the analytical method was achieved by determining the cation concentrations of Ca, Mg, Na, Sr, Fe and Mn from acceptable geochemical standards, NBS 634 and NBS 636. Ideally the use of dolomite standards which contain elemental concentrations similar to those determined within this thesis would have provided a more absolute determination in the accuracy of the analytical method. However this does not invalidate the accuracy determination since the trace elemental concentrations were not used to represent or infer stoichiometric concentrations of the rock or cement species implicitly.

The calibration of the Atomic Absorbtion Spectometer is achieved by preparing stock solutions over a range of detectable limits for the specific element. This calibrates the AAS to detect the concentrations expected to be found within the diluted solutions from the dissolved rock or cement samples. Every ten samples the AAS is recalibrated with a 'reslope' which contains the concentration of the median reference solution.

The following tables include the expected and measured values for a variety of trace elements used in the accuracy determination:

International Standard NBS 634 (Weight of 0.2030 g)

Cation Measured	Expected Value (+/- 10 %) (ppm)	Measured Value (ppm)	Accuracy (%)
Calcium	446 688	448 522	0.4
Magnesium	19 899	20 197	1.5
Strontium	1 014	910	10.3
Sodium	1 113	1 169	5.0
Iron	19 863	15 616	21.4
Manganese	1 949	1 653	15.2

International Standard NBS 636 (Weight of 0.2030 g)

Cation Measured	Expected Value (+/- 10 %) (ppm)	Measured Value (ppm)	Accuracy (%)
Calcium	453 834	466 995	2.9
Magnesium	23 517	23 399	0.5
Strontium	338	347	2.7
Sodium	816	864	5.9
Iron	11 260	9 729	13.6
Manganese	835	714	14.5

App. IIIb-Precision Analysis

Sample No.	IR %	Ca (ppm)	Mg (ppm)	Na (ppm)	Fe (ppm)	Mn (ppm)	Cu (ppm)	Zn (ppm)	Sr (ppm)	Ni (ppm)	Pb (ppm)	V (ppm)	Type	Species
12.0	16.8	228812	125090	998	13986	1687	18	7	79	7	15	69	Duplicate	Dolomite matrix
12.0	16.0	230238	131905	1142	10667	1756	24	36	65	3	6	9	Original	Dolomite matrix
24.0	3.1	218595	122417	712	19060	1682	10	12	45	4	0	55	Duplicate	Dolomite matrix
24.0	0.0	208539	123765	751	13086	1725	31	51	45	7	5	6	Original	Dolomite matrix
69.0	4.4	221324	116282	381	19800	2083	5	3	35	3	0	56	Duplicate	Dolomite matrix
69.0	0.0	213008	118089	496	16809	2124	10	42	22	5	5	0	Original	Dolomite matrix
85.0	13.0	227867	118349	639	19381	1723	11	3	44	6	0	67	Duplicate	Dolomite matrix
85.0	11.6	217647	122398	895	16833	1798	11	15	37	13	17	10	Original	Dolomite matrix
152.0	40.9	245501	100340	1481	20034	2188	0	6	140	11	1	52	Duplicate	Dolomite matrix
152.0	41.9	233103	100690	2245	24828	1990	17	10	133	21	36	9	Original	Dolomite matrix
174.0	4.2	217782	120607	509	20607	1843	10	5	40	5	11	56	Duplicate	Dolomite matrix
174.0	7.2	239977	137838	1041	24212	1922	0	9	38	4	5	14	Original	Dolomite matrix
187.0	16.1	228332	117985	496	23727	1992	11	6	37	5	0	56	Duplicate	Dolomite matrix
187.0	17.8	236222	125111	760	25778	1953	0	3	37	2	4	19	Original	Dolomite matrix
39.0	3.3	284213	38406	362	6988	2664	10	4	148	3	0	65	Duplicate	Saddle Dolomite
39.0	4.2	302778	38580	403	7202	2582	10	2	192	3	0	20	Original	Saddle Dolomite
77.0	2.6	222732	116701	366	21907	2132	10	3	40	4	20	61	Duplicate	Saddle Dolomite
77.0	3.1	213804	110904	407	16207	2120	5	6	34	2	25	6	Original	Saddle Dolomite
147.0	2.4	220633	117671	465	25843	2436	10	4	39	4	26	65	Duplicate	Saddle Dolomite
147.0	1.8	203906	113854	566	20104	2479	10	4	46	2	29	9	Original	Saddle Dolomite
184.0	3.1	207461	116269	535	29378	2436	10	1	40	4	0	61	Duplicate	Saddle Dolomite
184.0	2.0	201858	113106	535	22549	2385	5	16	34	3	14	8	Original	Saddle Dolomite
297.0	2.5	217953	110494	483	21399	2632	5	0	45	4	0	65	Duplicate	Saddle Dolomite
297.0	2.3	209407	106653	582	15489	2567	10	5	63	4	34	13	Original	Saddle Dolomite
31.0	2.6	382645	508	259	2841	6715	10	1	108	4	0	48	Duplicate	Calcite cement
31.0	3.1	340671	524	278	2935	6237	5	0	115	3	0	15	Original	Calcite cement
144.0	2.7	386097	207	197	2168	5510	10	0	102	4	0	47	Duplicate	Calcite cement
144.0	2.8	339730	192	203	2178	5135	10	0	103	3	0	16	Original	Calcite cement
192.0	3.1	392427	216	161	2578	6276	10	0	91	2	0	44	Duplicate	Calcite cement
192.0	4.3	336134	239	133	2584	5951	10	4	106	3	1	15	Original	Calcite cement
226.0	2.3	384892	504	312	2492	1285	10	1	174	3	0	42	Duplicate	Calcite cement
226.0	3.3	375510	811	306	2474	1122	5	0	174	3	0	18	Original	Calcite cement
323.0	4.6	392339	92	267	2043	5873	10	0	112	3	0	48	Duplicate	Calcite cement
323.0	3.0	388653	127	251	2089	5885	11	3	117	2	0	19	Original	Calcite cement

Appendix IV-Shales

Sample No.	Ca (ppm)	Mg (ppm)	Na (ppm)	Fe (ppm)	Mn (ppm)	Cu (ppm)	Zn (ppm)	Sr (ppm)	Ni (ppm)	Pb (ppm)	V (ppm)	Well No.	Depth (m)
26	1852	1350	2280	27400	191	38	41	122	148	1	353	34160	-819.84
29	5192	2755	1924	27800	461	25	28	118	8	6	268	34160	-820.55
46	555	1275	2018	25350	131	18	34	50	60	10	323	34160	-825.18
47	595	1212	2061	29850	139	18	31	40	38	14	278	34160	-825.31
73	922	1422	1732	26700	138	18	20	98	64	9	264	34160	-835.80
117	6528	3280	1626	25300	511	30	20	75	77	4	245	34160	-862.41
146	9908	5045	1591	22150	766	10	15	122	53	9	126	34151	-810.61
171	2590	1588	1591	24350	172	802	15	152	76	1	189	34151	-823.98
199	11622	6065	1202	22700	882	12	1	110	65	12	102	34151	-835.61
202	2150	1585	1844	32300	326	25	52	82	154	1	194	33821	-765.40
205	3662	1195	1816	74300	354	170	52	150	372	1	286	33821	-766.07
207	1045	1540	1822	30200	250	20	44	70	69	1	269	33821	-766.70
224	2458	1835	2760	21100	318	15	1	132	13	1	189	33821	-788.31
242	26052	2142	908	5200	334	15	1	490	19	21	52	33821	-812.12
244	26818	1538	772	3350	283	8	1	988	3	19	40	33821	-812.80
247	24832	1588	980	5950	325	12	1	478	33	19	50	33821	-813.11
257	5220	1870	1791	22550	246	12	12	108	70	14	140	33821	-860.28
260	10005	1705	2000	23300	206	12	29	260	69	3	135	33821	-862.88
261	5108	1928	2114	30150	190	20	20	145	54	8	146	33821	-863.01
264	6890	2000	1974	26800	263	18	32	132	100	10	130	33821	-863.32
268	5658	2840	1145	9100	476	12	7	48	35	8	10	33821	-865.55
304	2422	1622	1600	34300	302	45	38	98	124	7	199	33823	-764.30
306	1470	1515	1756	31000	268	25	55	80	111	25	221	33823	-765.40
337	17442	8162	682	16300	1086	15	21	125	60	9	76	33823	-810.00

Appendix V-Brines

Well No.	Ca (ppm)	Mg (ppm)	Na (ppm)	Fe (ppm)	Mn (ppm)	Cu (ppm)	Zn (ppm)	Sr (ppm)	Ni (ppm)	Pb (ppm)	V (ppm)	∂18-O (SMOW)	∂2-H
33823	33570	5300	49720	9	5	0.26	1.20	346	2	421	1	-3.44	-41.93
34310	15260	2700	33950	3	6	0.21	0.29	295	1	1	1	-3.22	-47.03
33817	26250	5630	48050	3	3	0.24	0.41	613	1	2	1	-1.81	-38.42
34103	27910	6170	51150	3	3	0.25	0.41	691	1	15	1	-1.89	-31.63
34100	31420	6770	43650	3	5	0.73	0.77	598	1	16	1	-2.23	-27.25
34105	24400	7690	57100	93	51	0.34	1.04	635	6	20	1	-1.75	-36.44
33825	25530	5440	40350	4	4	0.24	0.40	588	1	11	1	-2.18	-44.72
33821	29640	6200	42800	3	4	0.25	0.41	768	5	105	1	-2.41	-48.93
34102	27710	5890	34650	3	4	0.24	0.50	773	2	141	1	-2.44	-33.62
33775	24260	5040	46950	4	5	0.28	0.51	717	6	101	1	-2.26	-35.17
33824	23420	4910	46700	3	4	0.33	0.55	747	3	20	1	-2.24	-30.98
34281	26780	4640	42800	4	4	0.30	0.45	694	2	73	1	-2.28	-31.24
34011	29440	5590	50450	4	5	0.24	0.39	562	2	1	1	-2.84	-21.66
34150	29020	6190	45100	44	27	0.38	0.73	432	2	31	1	-2.69	-44.75
33818	34230	7190	45150	39	64	0.24	0.49	769	3	1	1	-2.50	-32.93
34106	21730	4530	47200	3	4	0.22	0.49	669	2	1	1	-2.45	-36.59
33822	26390	5790	46500	6	19	0.29	0.58	706	2	33	1	-2.53	
34340	28220	5120	44050	3	5	0.26	0.79	644	2	63	1	-2.21	-29.00
34313	18770	3850	30900	3	4	0.19	0.36	442	1	1	1		

Appendix VI-Oils

Well No.	Ni (ppm)	V (ppm)	Hillman/Klymer	Hillman TR. 2	Renwick	Gold/Wheatly
33823	177	1378	6			
33817	230	1036	5			
34103	230	1185	2			
34100	274	220	10			
34105	219	928	9			
33825	179	1067	3			
33821	144	843		2		
34102	177	941		3		
33775	252	1071	7			
33824	201	1020	4			
34281	280	381			1	
34011	171	546				2
34150	198	421				3
33818	179	1386		1		
34106	178	1498	1			
33822	276	772	8			
34340	214	1265				1
34349	169	1555			2	

Appendix VII-C/S

Depth (m)	TOC	Leco Sulphur	C/S Ratio	Well No.	Rock Type
-764.30	1.89	1.19	1.59	33821	Shale
-765.60	1.89	1.10	1.72	33821	Shale
-766.44	2.13	6.04	0.35	33821	Shale
-767.00	0.31	0.71	0.44	33821	Dolomite
-770.00	0.58	0.05	11.60	33821	Dolomite
-775.00	0.92	0.13	7.08	33821	Dolomite
-779.50	0.45	0.06	7.50	33821	Dolomite
-781.50	2.20	0.70	3.14	33821	Dolomite
-784.60	1.90	0.24	7.92	33821	Dolomite
-785.00	1.10	0.11	10.00	33821	Dolomite
-785.70	0.89	0.16	5.56	33821	Dolomite
-786.40	0.66	0.11	6.00	33821	Dolomite
-787.20	0.54	0.05	10.80	33821	Dolomite
-788.80	1.90	0.45	4.22	33821	Limestone
-789.50	0.56	0.08	7.00	33821	Dolomite
-792.50	0.20	0.04	5.00	33821	Dolomite
-795.20	1.10	0.08	13.75	33821	Dolomite
-799.15	1.50	0.28	5.36	33821	Limestone
-803.50	0.36	0.11	3.27	33821	Limestone
-804.00	1.30	0.30	4.33	33821	Dolomite
-810.15	0.22	0.08	2.75	33821	Dol. Limestone
-812.00	3.20	0.72	4.44	33821	Limestone
-814.00	0.48	0.11	4.36	33821	Dolomite
-818.00	0.22	0.04	5.50	33821	Dolomite
-820.00	0.14	0.84	0.17	33821	Dolomite
-863.35	1.47	1.14	1.29	33821	Shale
-866.90	0.22	0.04	5.50	33821	Dolomite
-873.35	0.10	0.02	5.00	33821	Dolomite
-940.09	0.12	0.03	4.00	33821	Dolomite
-949.14	0.10	0.05	2.00	33821	Dolomite
-955.80	0.20	0.02	10.00	33821	Dolomite
-764.19	2.35	1.06	2.22	33823	Shale
-764.98	2.11	5.86	0.36	33823	Shale
-768.00	0.11	0.18	0.61	33823	Dolomite
-771.50	0.89	0.08	11.12	33823	Dolomite
-777.60	0.42	0.10	4.20	33823	Dolomite
-779.80	0.81	0.06	13.50	33823	Dolomite
-785.20	0.90	0.20	4.50	33823	Dolomite
-786.20	0.31	0.10	3.10	33823	Dolomite
-791.85	0.01	0.04	0.25	33823	Dolomite
-794.50	1.60	0.33	4.85	33823	Limestone
-798.00	0.96	0.15	6.40	33823	Limestone
-799.00	0.72	0.31	2.32	33823	Dol. Limestone
-799.50	1.20	0.29	4.14	33823	Dol. Limestone
-803.00	1.60	0.18	8.89	33823	Dolomite
-805.20	3.60	0.54	6.67	33823	Dolomite
-806.00	2.50	0.58	4.31	33823	Dolomite
-807.50	0.70	0.07	10.00	33823	Dolomite
-809.50	0.96	0.14	6.86	33823	Dolomite
-812.00	2.00	0.47	4.26	33823	Dolomite
-814.00	0.32	0.08	4.00	33823	Dolomite
-820.20	1.69	0.23	7.35	33823	Dolomite
-800.38	0.26	0.16	1.62	34151	Dolomite
-806.48	0.13	0.09	1.44	34151	Dolomite
-810.55	0.10	0.09	1.11	34151	Dolomite
-814.00	0.15	0.09	1.67	34151	Dolomite

Appendix VII-C/S

Depth (m)	TOC	Leco Sulphur	C/S Ratio	Well No.	Rock Type
-820.64	0.04	0.01	4.00	34151	Dolomite
-825.55	0.01	0.01	1.00	34151	Dolomite
-831.75	0.07	0.04	1.75	34151	Dolomite
-834.75	0.41	0.13	3.15	34151	Dolomite
-806.55	0.06	0.19	0.32	34160	Dolomite
-810.69	0.19	0.04	4.75	34160	Dolomite
-814.42	0.20	0.12	1.67	34160	Dolomite
-821.50	0.15	0.04	3.75	34160	Dolomite
-826.54	0.11	0.03	3.67	34160	Dolomite
-831.55	0.03	0.02	1.50	34160	Dolomite
-835.35	0.36	0.79	0.46	34160	Dolomite
-840.42	0.11	0.02	5.50	34160	Dolomite
-845.54	1.16	1.25	0.93	34160	Dolomite
-850.98	2.07	0.62	3.34	34160	Dolomite
-855.89	1.20	0.34	3.53	34160	Dolomite
-864.67	8.05	1.77	4.55	34160	Dolomite
-866.76	0.97	0.11	8.82	34160	Dolomite
-843.87	0.21	0.06	3.50	34428	Limestone
-845.10	0.06	0.01	6.00	34428	Limestone
-845.77	0.21	0.14	1.50	34428	Limestone
-846.93	0.01	0.01	1.00	34428	Limestone
-847.91	0.16	0.04	4.00	34428	Limestone
-848.57	0.13	0.09	1.44	34428	Limestone
-849.64	0.18	0.06	3.00	34428	Limestone
-849.97	0.18	0.15	1.20	34428	Limestone
-850.95	0.18	0.07	2.57	34428	Limestone
-851.76	0.21	0.07	3.00	34428	Limestone
-852.48	0.19	0.04	4.75	34428	Limestone
-853.23	0.12	0.03	4.00	34428	Limestone
-854.48	0.07	0.01	7.00	34428	Limestone
-855.12	1.01	0.56	1.80	34428	Limestone
-855.92	0.31	0.11	2.82	34428	Limestone
-856.75	0.65	0.44	1.48	34428	Limestone
-857.94	0.13	0.11	1.18	34428	Limestone
-858.73	0.19	0.12	1.58	34428	Limestone
-859.98	0.08	0.02	4.00	34428	Limestone
-861.05	0.28	0.13	2.15	34428	Limestone
-861.42	0.57	0.44	1.30	34428	Limestone
-862.88	0.83	1.07	0.78	34428	Shale
-863.49	0.06	0.02	3.00	34428	Limestone
-864.05	0.13	0.14	0.93	34428	Limestone
-864.60	0.39	0.21	1.86	34428	Limestone
-865.73	0.29	0.12	2.42	34428	Limestone
-866.55	0.29	0.11	2.64	34428	Limestone
-867.02	0.65	0.31	2.10	34428	Limestone
-867.98	0.31	0.15	2.07	34428	Limestone
-868.68	0.93	0.84	1.11	34428	Shale
-869.11	0.33	0.14	2.36	34428	Limestone
-869.85	0.16	0.14	1.14	34428	Limestone
-870.49	0.27	0.12	2.25	34428	Limestone
-871.38	0.53	0.42	1.26	34428	Limestone
-872.07	0.49	0.27	1.81	34428	Limestone
-872.75	0.45	0.23	1.96	34428	Limestone
-873.70	0.35	0.22	1.59	34428	Limestone
-1095.13	0.08	0.41	0.20	7	Limestone
-1096.07	0.20	0.13	1.54	7	Limestone

Appendix VII-C/S

Depth (m)	TOC	Leco Sulphur	C/S Ratio	Well No.	Rock Type
-1097.12	0.18	0.08	2.25	7	Limestone
-1098.10	0.12	0.08	1.50	7	Limestone
-1098.67	0.09	0.06	1.50	7	Limestone
-1099.54	0.09	0.05	1.80	7	Limestone
-1100.31	0.08	0.03	2.67	7	Limestone
-1101.30	0.10	0.08	1.25	7	Limestone
-1102.34	0.14	0.09	1.56	7	Limestone
-1103.40	0.04	0.03	1.33	7	Limestone
-1104.28	0.06	0.04	1.50	7	Limestone
-1105.13	0.09	0.05	1.80	7	Limestone
-1106.37	0.35	0.36	0.97	7	Limestone
-1107.22	0.06	0.07	0.86	7	Limestone
-1108.86	0.14	0.13	1.08	7	Limestone
-1109.60	0.13	0.11	1.18	7	Limestone
-1110.62	0.16	0.15	1.07	7	Limestone
-1111.22	0.17	0.22	0.77	7	Limestone
-1112.08	0.06	0.08	0.75	7	Limestone
-1113.08	0.15	0.42	0.36	7	Limestone
-1114.28	0.08	0.07	1.14	7	Limestone
-1115.29	0.21	0.59	0.36	7	Limestone
-1116.33	0.23	0.85	0.27	7	Limestone
-1117.48	0.20	0.27	0.74	7	Limestone
-1118.36	0.09	0.09	1.00	7	Limestone
-1119.04	0.18	0.08	2.25	7	Limestone
-1120.09	0.36	0.14	2.57	7	Limestone
-1121.26	0.17	0.09	1.89	7	Limestone
-1122.28	0.10	0.07	1.43	7	Limestone
-1123.17	0.07	0.09	0.78	7	Limestone
-1124.17	0.17	0.08	2.12	7	Limestone
-1125.30	0.08	0.15	0.53	7	Limestone
-1126.31	0.20	0.11	1.82	7	Limestone
-1127.37	0.05	0.15	0.33	7	Limestone
-1128.38	0.29	0.24	1.21	7	Limestone
-1128.68	1.07	2.02	0.53	7	Limestone
-1129.73	0.65	0.27	2.41	7	Limestone
-1130.05	0.27	2.60	0.10	7	Shale
-1130.61	0.05	0.12	0.42	7	Limestone

Appendix VIII-SI Data

Sample No.	Dol. ∂18-O	Dol. ∂13-C	Depth (m)	Well No.	Sample No.	Sad. Dol. ∂18-O	Sad. Dol. ∂13-C	Depth (m)	Well No.	Sample No.	Calcite ∂18-O	Calcite ∂13-C	Depth (m)	Well No.
209.0	-8.55	-0.23	-766.50	33821	219.0	-9.67	0.78	-780.08	33821	218.0	-7.60	-0.65	-779.65	33821
210.0	-8.76	-0.54	-766.50	33821	220.0	-9.33	0.34	-781.00	33821	219.0	-8.04	-0.55	-780.08	33821
213.0	-7.67	0.29	-769.00	33821	267.0	-9.26	0.19	-864.57	33821	224.0	-7.60	-0.65	-788.40	33821
4.1	-8.35	0.42	-775.00	33821	294.0	-9.35	-0.05	-952.40	33821	226.1	-10.77	-0.51	-793.00	33821
219.0	-9.06	0.52	-780.08	33821	312.0	-9.47	0.83	-771.50	33823	226.2	-12.18	-1.18	-793.00	33821
19.1	-8.56	0.69	-781.00	33821	314.0	-9.09	0.12	-772.70	33823	226.3	-8.14	0.25	-793.50	33821
26.1	-7.50	0.76	-784.60	33821	322.0	-9.25	0.49	-784.00	33823	227.1	-9.33	-0.20	-794.00	33821
45.1	-7.89	0.63	-788.40	33821	323.0	-9.07	0.60	-785.02	33823	227.2	-11.05	-0.28	-797.50	33821
49.1	-8.67	-0.12	-792.00	33821	339.1	-9.35	0.59	-813.00	33823	267.0	-8.40	-2.17	-864.57	33821
49.1	-8.24	-0.26	-792.00	33821	339.2	-9.66	0.38	-813.50	33823	294.0	-8.44	-1.16	-952.40	33821
51.1	-9.79	0.05	-793.00	33821	340.0	-10.51	0.45	-816.00	33823	311.0	-8.56	-0.30	-770.10	33823
52.1	-8.12	0.51	-793.50	33821	126.0	-10.08	-1.34	-798.69	34151	314.0	-8.35	-0.74	-772.70	33823
53.1	-8.96	0.25	-794.00	33821	142.0	-10.24	-0.53	-808.80	34151	323.0	-8.15	-0.77	-785.02	33823
55.1	-9.20	0.36	-797.50	33821	151.0	-9.04	-0.70	-812.88	34151	340.2	-9.22	0.63	-815.00	33823
229.0	-9.23	-0.38	-800.00	33821	163.0	-9.34	-0.70	-818.98	34151	142.0	-7.95	-1.15	-808.80	34151
59.1	-8.30	0.62	-815.20	33821	189.0	-9.07	-0.53	-832.24	34151	151.1	-8.55	-1.32	-812.88	34151
255.0	-10.79	0.05	-820.00	33821	7.0	-10.30	-0.82	-810.59	34160	151.2	-8.25	-1.35	-812.88	34151
267.0	-10.50	0.67	-864.57	33821	15.0	-10.29	-0.56	-815.11	34160	164.0	-8.67	-1.48	-818.98	34151
273.0	-10.52	1.02	-869.00	33821	23.0	-10.14	-0.55	-819.20	34160	181.0	-7.83	-2.94	-828.13	34151
277.0	-10.03	0.47	-874.10	33821	34.0	-9.41	-0.34	-821.43	34160	190.0	-8.40	-1.35	-832.24	34151
281.0	-10.65	-0.51	-940.09	33821	48.0	-10.21	-0.46	-825.41	34160	191.0	-7.57	-1.95	-832.24	34151
287.0	-10.64	0.40	-947.19	33821	67.0	-10.22	-0.08	-833.13	34160	7.0	-7.97	-1.85	-810.59	34160
294.0	-10.39	-0.20	-952.40	33821	78.0	-9.83	-0.43	-839.11	34160	15.0	-7.97	-1.64	-815.11	34160
301.0	-10.35	-0.10	-955.80	33821	91.0	-10.00	-0.91	-845.88	34160	23.0	-7.68	-1.20	-819.20	34160
1.2	-10.91	-0.65	-765.50	33823	123.0	-9.92	0.21	-866.76	34160	33.0	-8.28	-0.91	-821.40	34160
311.0	-10.08	-0.06	-770.10	33823						34.0	-8.17	-1.01	-821.42	34160
311.0	-10.41	0.11	-770.10	33823						48.0	-8.12	-1.23	-825.41	34160
312.0	-10.77	-0.02	-771.50	33823						67.0	-8.31	-0.58	-833.13	34160
314.0	-11.60	-1.04	-772.70	33823						91.0	-7.97	-0.03	-845.88	34160
317.0	-9.65	0.63	-777.50	33823						123.0	-9.63	-0.89	-866.76	34160
321.0	-9.45	-0.37	-779.92	33823										
5.2	-10.16	0.56	-784.00	33823										
323.0	-10.77	0.33	-785.02	33823										
8.2	-8.03	-0.60	-786.20	33823										
8.2	-10.45	0.35	-786.20	33823										
324.0	-10.23	0.48	-790.00	33823										
334.0	-10.32	0.26	-800.00	33823										
338.0	-9.52	0.45	-810.08	33823										
45.2	-10.21	0.25	-813.00	33823										
16.2	-10.37	0.20	-813.50	33823										
49.2	-10.55	0.04	-815.00	33823										
50.2	-10.40	0.40	-816.00	33823										
126.0	-9.67	-0.56	-798.69	34151										
128.0	-10.21	-0.68	-800.38	34151										
133.0	-10.63	-0.91	-804.40	34151										
142.0	-10.99	-0.76	-808.80	34151										

Appendix VIII-SI Data

Sample No.	Limestone ∂18-O	Limestone ∂13-C	Depth (m)	Well No.	Sample No.	LMC ∂18-O	LMC ∂13-C	Depth (m)	Well No.
225.0	-7.34	1.01	-788.40	33821	1.0	-5.80	0.98	-800.22	33821
230.0	-9.74	0.97	-802.00	33821	2.0	-6.06	1.00	-803.41	33821
234.0	-3.44	5.23	-806.00	33821	240.0	-7.97	0.21	-810.20	33821
238.0	-4.96	0.75	-810.00	33821	117.0	-9.46	0.32	-862.41	34160
243.0	-4.65	0.64	-812.14	33821	120.0	-9.77	0.25	-864.67	34160
252.0	-6.73	-0.51	-817.15	33821					
256.0	-4.37	2.26	-860.01	33821					
331.0	-9.71	0.82	-797.50	33823					
336.0	-7.88	1.00	-805.00	33823					

Sample No.	Dol. ∂18-O	Dol. ∂13-C	Depth (m)	Well No.
152.0	-9.75	-0.72	-812.90	34151
164.0	-9.93	-0.12	-818.98	34151
172.0	-10.07	0.08	-824.10	34151
182.0	-9.90	-0.40	-828.14	34151
191.0	-9.33	-0.56	-832.25	34151
197.0	-10.81	-0.56	-834.75	34151
1.0	-8.98	-1.29	-806.55	34160
8.0	-10.62	-0.88	-810.61	34160
15.0	-10.56	-1.11	-815.11	34160
22.0	-10.51	-0.21	-819.07	34160
36.0	-10.29	-0.04	-821.45	34160
49.0	-11.00	-0.75	-825.45	34160
59.0	-10.92	-0.24	-829.24	34160
67.0	-11.11	-0.30	-833.13	34160
78.0	-11.47	0.16	-839.10	34160
91.0	-11.13	0.10	-845.88	34160
102.0	-11.39	0.10	-851.39	34160
110.0	-10.53	-0.13	-856.50	34160
115.0	-10.97	-0.10	-861.06	34160
123.0	-10.56	0.19	-866.76	34160

Appendix IX

Table IX.1: Results of Factor Analysis -- Limestones
Orthogonal Transformation Solution-Varimax

Element	Factor 1	Factor 2	Factor 3	Communality
log IR	---	---	-.827	.716
log Ca	-.797	---	---	.834
log Mg	.940	---	---	.930
log Na	---	.836	---	.730
log Fe	.931	---	---	.900
log Mn	.928	---	---	.866
log Sr	-.434	---	.651	.905
log Cu	---	.691	---	.718
log Ni	---	.905	---	.828
log V	.666	---	---	.562

Factor	Eigenvalue	Pct. of Variation	Diagnosis
1	4.162	49.0	Burial Diagenesis Dolomitization
2	2.316	30.2	Enrichment in ionic substitution
3	1.513	20.7	Leaching

Table IX.2: Results of Factor Analysis -- Dolomites
Orthogonal Transformation Solution-Varimax

Element	Factor 1	Factor 2	Factor 3	Factor 4	Communality
log IR	---	.774	---	---	.789
log Ca	---	---	-.674	---	.562
log Mg	.863	---	---	---	.765
log Na	---	.826	---	---	.749
log Fe	.816	---	---	---	.851
log Mn	.881	---	---	---	.797
log Sr	-.608	---	---	---	.603
log Cu	---	---	.693	---	.601
log Zn	---	---	.693	---	.564
log Pb	---	---	---	.854	.797
log Ni	---	---	---	---	.611
log V	---	---	---	.670	.657

Factor	Eigenvalue	Pct. of Variation	Diagnosis
1	3.242	32.9	Dolomitization
2	2.437	23.9	Leaching
3	1.612	24.8	Substitution for Ca
4	1.057	18.4	low concentrations low variability

Table IX.3: Results of Factor Analysis -- Saddle Dolomite Cement

Orthogonal Transformation Solution-Varimax

Element	Factor 1	Factor 2	Factor 3	Factor 4	Communality
log IR	.814	---	---	---	.737
log Ca	---	---	.852	---	.791
log Mg	---	.755	---	---	.811
log Na	.799	---	---	---	.689
log Fe	---	.858	---	---	.856
log Mn	---	.832	---	---	.807
log Sr	---	---	---	-.730	.760
log Cu	---	---	---	---	.938
log Zn	---	---	.785	---	.646
log Pb	---	---	---	.871	.842
log Ni	.710	---	---	---	.626
log V	.800	---	---	---	.772

Factor	Eigenvalue	Pct. of Variation	Diagnosis
1	3.088	27.7	Leaching
2	2.132	27.0	Preferred Substitution
3	1.63	16.8	Preferred substitution
4	1.412	16.8	low concentrations low variability
5	1.014	11.8	low concentrations for Cu-low variability

Table IX.4: Results of Factor Analysis – Calcite Cements

Orthogonal Transformation Solution-Varimax

Element	Factor 1	Factor 2	Factor 3	Factor 4	Communality
log IR	---	---	---	.906	.873
log Ca	-.625	---	---	---	.675
log Mg	.949	---	---	---	.911
log Na	---	---	.718	.496	.784
log Fe	.879	---	---	---	.894
log Mn	---	---	-.799	---	.663
log Sr	---	.837	---	---	.736
log Ni	---	---	.529	---	.330
log V	---	.852	---	---	.782

Factor	Eigenvalue	Pct. of Variation	Diagnosis
1	2.343	32.8	Preferred Substitution during precipitation
2	1.673	25.3	low concentrations
3	1.579	24.2	Preferred substitution
4	1.055	17.7	low concentrations low variability

Appendix X: Lopatin Basin Modelling considerations and assumptions.

(1) Reconstruction of the sedimentary burial history is based on present day thicknesses taken from a columnar stratigraphic section representative of the Paleozoic section within southwestern Ontario, compiled by Telesis Oil and Gas Ltd.

(2) Estimates of the time and duration of deposition for the stratigraphic units within southwestern Ontario came from the North American chronostratic scales and correlations in Harland et al. (1982), p. 14 to 26.

(3) Geothermal gradient is an estimated temperature gradient that must have existed during the maturation of the rocks. This was determined by calculating the burial history curves, for different geothermal gradients, until a minimum TTI of 15 (equivalent to CAI's of 1.5-2.0) was reached for the Middle Ordovician strata of southwestern Ontario.

(4) Surface temperatures are estimates based on reconstructions of the study area throughout geologic time by Zeigler et al., (1977) and Morel and Irving (1978).

Time = in millions of years (Ma)

Ts = Surface temperature in degrees Celsius (°C)

TTI = Time Temperature Index

CAI = Colour Alteration Index

Rock layer parameters:

Layer:	Formation	Time at top	Time at bottom	Thickness m	Ts C
1 :	Drift	0.0	144.0	30	20.0
2 :	Unconformity	144.0	238.0	-200	20.0
3 :	Miss/Penn/P/T	238.0	360.0	200	25.0
4 :	Unconformity	360.0	374.0	0	25.0
5 :	Devonian	374.0	384.0	100	30.0
6 :	Unconformity	384.0	408.0	0	30.0
7 :	Silurian	408.0	436.0	390	25.0
8 :	Unconformity	436.0	438.0	0	25.0
9 :	Ord. Shales	438.0	456.0	260	25.0
10 :	Disconformity	456.0	460.0	0	25.0
11 :	Trenton/Bl.Riv.	460.0	468.0	225	25.0
12 :	Unconformity	468.0	505.0	0	25.0
13 :	Cambrian	505.0	525.0	50	25.0

Geothermal Gradients:

# :	Time	Leg 1
1 :	0.0	4.50 (C/100 m)

Formation summary:

Layer:	Formation	Top Bottom m	Temperature C	TTI
1 :	Drift	0	20.0	0.0
		30	21.3	0.4
5 :	Devonian	30	21.3	1.6
		130	25.8	2.2
7 :	Silurian	130	25.8	2.3
		520	43.4	8.1
9 :	Ord. Shales	520	43.4	8.1
		780	55.1	18.4
11 :	Trenton/Bl.Riv.	780	55.1	18.4
		1005	65.2	37.1
13 :	Cambrian	1005	65.2	37.3
		1055	67.5	43.6

Calculation interval: 6.0 m.y.

Top of oil window (at TTI= 15): 716 m.
Bottom of oil window (at TTI=160): not reached.